

**CUSTOM ISOELECTRIC CHROMATOFOCUSING:
ADVANCED MODELS AND METHODS FOR HIGH-
RESOLUTION PROTEIN PURIFICATION**

by

Derek Yau Chung Choy

B.A.Sc., The University of British Columbia, 2004

**A THESIS SUBMITTED IN PARTIAL FULFILMENT OF THE
REQUIREMENTS FOR THE DEGREE OF**

DOCTOR OF PHILOSOPHY

in

THE FACULTY OF GRADUATE AND POSTDOCTORAL STUDIES

(Chemical and Biological Engineering)

**THE UNIVERSITY OF BRITISH COLUMBIA
(Vancouver)**

September 2013

© Derek Yau Chung Choy, 2013

Abstract

Isoelectric chromatofocusing (ICF), a mode of chromatography by which proteins are separated based on changes in their charge with pH, is widely used at analytical scales, but its use in bio-product manufacturing has been limited. This is partly due to poor knowledge about operating ICF at scale, lack of understanding of its elution mechanisms, and the use of complex, costly buffers. Work presented in this thesis focuses on advancing ICF at both analytical and preparative scales.

A method for generating pH gradients in ICF is developed using simple low-molecular-weight buffers. On anion and cation exchange media, linear gradients spanning more than six pH units are generated through isocratic or gradient interchange of loading and elution phases. The buffers used are selected to satisfy cost constraints and for compatibility with detection by UV absorption at 280 nm and mass spectrometry.

A new surface-reaction/chemical-equilibria model is derived and solved by computer-aided simulations to predict pH and ionic strength profiles generated on anion and cation exchange columns. The model can be used for *in silico* design of custom-shaped elution profiles to improve separation performance. The method is used to achieve high purity and process throughput of a desired isoform of recombinant N-lobe of human transferrin produced by *Pichia pastoris* using custom isocratic ICF on preparative media. Gradient sculpting methods are used to enhance ICF as the first dimension in a multidimensional

separation platform used for the detection and analysis of O-linked N-acetylglucosamine modified proteins within the proteome of differentiated C2C12 mouse myoblast cells.

Finally, a model of protein transport and binding in ICF is developed and used to show that elution is not dictated solely by a protein's isoelectric point (pI), but is instead multi-modal in nature with Donnan equilibria, ion-exchange, and ion-displacement effects at work. The model predicts how simultaneous modulation of ionic strength and pH during elution can greatly improve the separation of proteins with similar pI 's; elution characteristics including retention time, peak width and resolution can likewise be improved. By coupling mathematical relationships describing these elution mechanisms to the solution of the continuity equation, protein elution times are accurately predicted.

Preface

A version of Chapter 2 of this dissertation has been accepted with revisions to *Biotechnology and Bioengineering* for publication as: Choy DYC, Haynes CA. Versatile Chromatofocusing on Strong Anion Exchange Media Via a New Model that Custom Designs Mobile Phases using Simple Buffers. I designed and prepared all mobile phases used and performed all chromatographic separations shown in that chapter. I also wrote and executed all program code that was required (see Appendix A). As first author, I prepared the manuscript with subsequent editing from C.A. Haynes.

A version of Chapter 3 will be submitted as: Choy DYC, Chan C, Haynes CA. Development of a Gradient Formulation Model for Isoelectric Chromatofocusing on a Strong Cation Exchange Column. As first author, I formulated the research strategy under the guidance of the principle investigator C.A. Haynes and designed all mobile phases used in the chapter. As a research assistant, C. Chan prepared mobile phases and performed chromatographic separations shown in this chapter. Mass spectrometry was performed by the Centre for High-Throughput Biology Proteomics Core Facility at the University of British Columbia. I conducted all other sample analyses, performed all model simulations (see Appendix B) and prepared the manuscript with subsequent editing from C.A. Haynes.

A version of Chapter 4 has been submitted as: Choy DYC, Haynes CA. A Novel Mixed-Mode Model for Interpreting and Predicting Protein Elution during Isoelectric Chromatofocusing. I designed and prepared all mobile phases used, and performed all chromatographic separations shown in this chapter. I also conceived the adsorption isotherm based on experimental observations and related work found in literature. Finally, I wrote and executed all program code that was required (see Appendix C). As first author, I prepared the manuscript with subsequent editing from C.A. Haynes.

A version of Chapter 5 will be submitted for publication as: Choy DYC., Haynes CA. Chromatofocusing Design for Preparative Isocratic Purification of Proteins: Separating Isoforms of the N-Lobe of Human Transferrin Produced in Recombinant *Pichia pastoris*. As first author, I formulated the research strategy and designed all mobile phases used in the chapter. I carried out all fermentations with the help of the Michael Smith Laboratories Pilot Plant at the University of British Columbia. I also planned and performed all sample preparation procedures and chromatographic separations shown in this chapter. Mass spectrometry was performed by the Centre for High-Throughput Biology Proteomics Core Facility at the University of British Columbia. Finally, I prepared the manuscript with subsequent editing from C.A. Haynes.

A version of Chapter 6 will be submitted for publication as: Choy DYC, Lam EWK, Kast J, Haynes CA. Custom Development of a Liquid Chromatography Based Platform for the Detection and Identification of O-GlcNAc Modified Proteins in the C2C12 Mouse Myoblast Proteome. As collaborators, E.W.K. Lam and I designed the research strategy together under the guidance of principle investigators J. Kast and C.A. Haynes. I performed all chromatographic separations and E.W.K. Lam performed all gel separations and mass spectrometry shown in this chapter. I prepared the manuscript together with E.W.K. Lam with subsequent editing from C.A. Haynes.

Table of Contents

Abstract.....	ii
Preface.....	iv
Table of Contents.....	vii
List of Tables.....	xii
List of Figures	xiv
Nomenclature.....	xx
Acknowledgements	xxviii
Dedication.....	xxx
Chapter 1: Introduction	1
1.1 Introduction to Liquid Chromatography for Protein Separation	1
1.1.1 Liquid chromatography applied to proteins.....	1
1.1.2 Size exclusion chromatography	4
1.1.3 Reversed phase chromatography and hydrophilic interaction chromatography	5
1.1.4 Hydrophobic interaction chromatography	7
1.1.5 Affinity chromatography	8
1.1.6 Ion exchange chromatography.....	9
1.2 Isoelectric Chromatofocusing.....	14
1.2.1 History.....	14
1.2.2 Commercial chromatofocusing systems	16
1.2.3 Major developments in chromatofocusing.....	16
1.2.3.1 Anion-exchange based chromatofocusing without polyampholyte buffers	17
1.2.3.2 Cation-exchange based chromatofocusing without polyampholyte buffers	19

1.2.3.3	Predicting pH gradient shape.....	19
1.2.3.4	Understanding and predicting protein elution in chromatofocusing	20
1.2.4	Challenges in chromatofocusing application and theory	22
1.3	Thesis Objectives	23
Chapter 2:	Versatile Chromatofocusing on Strong Anion Exchange Media via a New Model that Custom Designs Mobile Phases using Simple Buffers.....	25
2.1	Background	25
2.2	Experimental	29
2.2.1	Materials for analytical studies	29
2.2.2	Materials for chromatofocusing studies.....	29
2.2.3	Column packing.....	30
2.2.4	Chromatography design and procedures.....	31
2.2.5	pH electrode calibration.....	32
2.2.6	Gel electrophoresis procedures	32
2.2.7	Mass spectrometry	33
2.3.	Theory	33
2.3.1	Governing equations.....	34
2.3.2	Equilibrium relations	35
2.3.3	Binding of buffer components to the stationary phase	39
2.3.4	Model solution to predict elution gradient profiles	42
2.4	Results and Discussion.....	43
2.4.1	Buffer selection.....	43
2.4.2	Stationary phase properties.....	45
2.4.3	Linear pH gradient prediction, buffer formulation and application.....	52
2.4.4	Creation of custom pH gradient profiles using the model.....	57
2.4.5	Isolation of the N-lobe of human transferrin using a preparative matrix	62
2.5	Concluding Remarks	65

Chapter 3: Model Development for Custom Gradient Formulation for Isoelectric Chromatofocusing on a Strong Cation Exchange Column.....	66
3.1. Background	67
3.2. Experimental	68
3.2.1 Materials	68
3.2.2 Chromatography column operation	70
3.2.3 pH electrode calibration	71
3.2.4 Mass spectrometry	71
3.2.5 UV-visible spectrometry	71
3.2.6 Circular dichroism	72
3.3 Theory	72
3.4 Results and Discussion	76
3.4.1 Development of buffer formulations	76
3.4.2 Model-based buffer formulation	78
3.4.3 Chromatofocusing of proteins on a strong cation exchange column	81
3.5 Concluding Remarks	88
Chapter 4: A Novel Mixed-Mode Model for Interpreting and Predicting Protein Elution during Isoelectric Chromatofocusing.....	89
4.1 Background	89
4.2 Experimental	92
4.2.1 Materials	92
4.2.2 Chromatography	93
4.2.3 pH electrode calibration	94
4.2.4 Characteristic charge measurement	94
4.3 Known and Putative Mechanisms for Protein Elution in Chromatofocusing	95
4.4 Model Structure and Equations	99
4.4.1 Protein transport and binding	100
4.4.2 Donnan effect	103
4.4.3 Solution algorithm	104
4.5 Results and Discussion	105

4.5.1 Isoelectric chromatofocusing as a mixed-mode separation	105
4.5.2 Predicting protein elution in ICF	108
4.5.3 Model-based interpretation of the isoelectric chromatofocusing of proteins	113
4.5.4 Ion-displacement effects on protein retention and resolution.....	117
4.6 Concluding Remarks	119
Chapter 5: Chromatofocusing Design for Preparative Isocratic Purification of Proteins: Separating Isoforms of the N-Lobe of Human Transferrin Produced in Recombinant <i>Pichia Pastoris</i>.....	121
5.1 Background	121
5.2 Experimental	124
5.2.1 Materials for analytical studies	124
5.2.2 Materials for preparative ICF studies	124
5.2.3 Fermentations.....	125
5.2.4 Sample preparation for chromatography	126
5.2.5 pH electrode calibration.....	126
5.2.6 Chromatography	127
5.2.7 Gel electrophoresis.....	128
5.2.8 Mass spectrometry	128
5.3 Results and Discussion.....	129
5.3.1 Recombinant protein production.....	129
5.3.2 Comparing gradient and isocratic isoelectric chromatofocusing	130
5.3.3 Simple strategy for optimizing ICF operating under isocratic elution.....	132
5.4 Concluding Remarks	138
Chapter 6: Application of Custom Gradient Chromatofocusing to Detection and Identification of O-GlcNAc Modified Proteins in C2C12 Mouse Myoblasts.....	139
6.1 Background	140
6.2 Experimental	146
6.2.1 Cell culture.....	146
6.2.1.1 Insulin/streptozotocin/glucose treatment.....	147

6.2.1.2 Untreated and alloxan treatment.....	147
6.2.2 Sample preparation for chromatography	147
6.2.3 Isoelectric chromatofocusing	148
6.2.4 Initial dot-blot screen	149
6.2.5 Electrophoresis.....	150
6.2.6 Western gels.....	151
6.2.7 In-gel digestion and mass spectrometric analysis.....	151
6.3 Results and Discussion.....	153
6.3.1 ICF of lysate-derived proteomes of differentiated C2C12 mouse myoblasts	153
6.3.2 Insulin/streptozotocin/glucose treated sample	160
6.3.2 Untreated sample	164
6.3.4 Using proteomics data to validate proposed ICF elution mechanisms.....	167
6.4 Concluding Remarks	170
Chapter 7: Conclusions and Recommendations for Future Work	172
7.1 Motivation for and Advances Provided by this Work.....	172
7.2 Recommendations for Future Work	175
References.....	178
Appendices.....	189
Appendix A: Description of the Program for Sculpting Buffer Compositions through the Calculation of pH and Ionic Strength Profiles in an Anion Exchange Column	189
Appendix B: Description of the Program for Sculpting Buffer Compositions through the Calculation of pH and Ionic Strength Profiles in a Cation Exchange Column	211
Appendix C: Description of the Program for the Prediction of Protein Elution from an Anion Exchange Column during Isoelectric Chromatofocusing.....	234

List of Tables

Table 1.1:	Common buffers for AEX chromatography across various pH ranges	11
Table 1.2:	Common buffers for CEX chromatography across various pH ranges.....	12
Table 2.1:	<i>pK</i> values of buffer ions at 25 °C and 0 M ionic strength	44
Table 2.2:	Regressed binding constants and maximum binding capacity for acetate and lactate on the Mono Q strong anion exchange matrix at 25 °C.....	47
Table 2.3:	Regressed lumped linear-isotherm constants for non-specific binding of imidazole and piperazine on the Mono Q strong anion exchange matrix at 25 °C.....	48
Table 2.4:	Model-derived buffer species concentrations (mM) in various formulations of buffer A/buffer B pairs used for AEICF sample loading and gradient elution.....	48
Table 3.1:	<i>pK</i> values of buffer ions at 25 °C and 0 M ionic strength.....	69
Table 3.2:	Model-derived buffer species concentrations (mM) in various formulations of buffer A/buffer B pairs used for CEICF sample loading and gradient elution.....	69
Table 3.3:	Measured stationary phase equilibrium binding constants for buffer species having a specific affinity for the Mono S strong cation exchange matrix	79
Table 4.1:	pH, ionic strength (mM) and buffer species concentrations (mM) in various formulations of buffer A/buffer B pairs used for sample loading and gradient elution.....	92
Table 4.2:	Column parameters used for all modeling	94
Table 5.1:	pH, ionic strength (mM) and buffer species concentrations (mM) in various formulations of buffer A/buffer B pairs used for ICF separation of recombinant <i>Pichia pastoris</i> supernatants.....	124
Table 6.1:	pH, ionic strength (mM) and buffer species concentrations (mM) in model-sculpted formulations of buffer A/buffer B pairs used for ICF fractionation of differentiated C2C12 mouse myoblast samples.....	148

Table 6.2:	Benchmark proteins identified in selected SDS-PAGE bands derived from alloxan-inhibited differentiated C2C12 mouse myoblast samples.....	160
Table 6.3:	Proteins identified as O-GlcNAc positive in aligned western/SDS-PAGE gels derived from insulin/STZ/glucose treated differentiated C2C12 mouse myoblasts [§]	163
Table 6.4:	Proteins identified as O-GlcNAc positive in aligned western/SDS-PAGE gels derived from untreated differentiated C2C12 mouse myoblasts [§]	166
Table A-1:	List of species tracked by MATLAB script file “ICFM.m” for the calculation of pH and ionic strength profiles during AEICF.....	190
Table B-1:	List of species tracked by MATLAB script file “ICFM.m” for the calculation of pH and ionic strength profiles during CEICF.....	212
Table C-1:	Input data files and variables used in MATLAB script file “solver.m” for the prediction of protein elution during AEICF.....	234

List of Figures

- Figure 2.1:** Comparison of pH profiles generated at 25 °C and a mobile phase flow rate of 1 mL min⁻¹ using buffer formulation 1003 with (blue) and without (red) the Mono Q HR10/10 strong anion exchange column present in the flow field. Dashed lines provided to define linearity of gradient..... 45
- Figure 2.2:** Proton titration curve for the Mono Q HR10/10 strong anion exchange column from pH 12.0 to 2.0. Data show that the buffering capacity of the stationary-phase matrix is negligible between pH 10.0 to 3.5. 46
- Figure 2.3:** On-column speciation diagram at 25 °C of pH-dependent concentrations of bound chloride, acetate, and lactate, and of free acetic acid and lactic acid when buffer formulation 1003 is applied. All species concentrations computed from the combined multiple-chemical-equilibria/surface-adsorption model (Equations 2.1 to 2.17). All species concentrations are normalized by the total concentration of each species in the system, which changes throughout the pH gradient generated using buffer formulation 1003..... 49
- Figure 2.4:** Comparison of pH profiles generated using buffer formulation 1003 on the following columns at the specified flowrates: A) Mono Q HR10/10 column (1 mL min⁻¹), B) Q Sepharose Fast Flow XK16/15 column (5 mL min⁻¹), C) Capto Q XK16/14 column (5 mL min⁻¹), D) Q Ceramic HyperD 20 HR10/10 column (25 mL min⁻¹), and E) Accell Plus QMA HR10/10 column (25 mL min⁻¹). All columns operated at 25 °C..... 51
- Figure 2.5:** Comparison of predicted and experimental pH profiles generated at 25 °C using buffer formulation 1003 at a mobile-phase flow rate of 1 mL min⁻¹ A) in the absence of a column, B) in the presence of the Mono Q HR10/10 strong anion exchange column and accounting for interactions of buffer species with the stationary phase in the model prediction, C) in the presence of the Mono Q HR10/10 strong anion exchange column but ignoring buffer-matrix interactions in the model prediction. 52
- Figure 2.6:** A) Elution chromatogram for a mixture containing purified fractions of myoglobin, carbonic anhydrase, α -lactalbumin, bovine serum albumin, ovalbumin, β -amylase and trypsin inhibitor, as well as crude (mixed isoform) conalbumin injected as a 500 μ L pulse onto a Mono Q HR10/10 column at 25 °C and a mobile-phase (buffer formulation 1003, linear gradient at -0.1 pH mL⁻¹) flow rate of 1 mL min⁻¹. B) Elution chromatogram for the same mixture of proteins (with a 20-fold decrease of conalbumin concentration) injected as a 500 μ L pulse onto a Mono Q

HR10/10 column at 25 °C and a mobile-phase (buffer formulation 1003, shallow linear gradient at -0.05 pH mL⁻¹) flow rate of 1 mL min⁻¹. Significantly improved resolution is achieved with the shallower pH gradient..... 55

Figure 2.7: Isoelectric focusing (IEF) gel for 10 µL individual protein solution (10 mg mL⁻¹) samples of myoglobin, carbonic anhydrase, conalbumin, bovine serum albumin, ovalbumin, β-amylase, trypsin inhibitor, β-lactoglobulin A, β-lactoglobulin B and α-lactalbumin (lanes 2 to 11). Samples were loaded onto a ReadyGel IEF pH 5-8 and electrophoresed in a Mini-Protean III unit. IEF protein standards (3 µL) containing cytochrome C (*pI* = 9.6), lentil lectin (*pI*'s = 7.80, 8.00 and 8.20), human hemoglobin C (*pI* = 7.5), human hemoglobin A (*pI* = 7.1), equine myoglobin (*pI*'s = 6.8 and 7.0), human carbonic anhydrase (*pI* = 6.5), bovine carbonic anhydrase (*pI* = 6.0), β-lactoglobulin B (*pI* = 5.1) and phycocyanin (*pI*'s = 4.45, 4.65 and 4.75) were loaded to lanes 1 and 12 for reference. 56

Figure 2.8: Comparison of predicted and experimental pH profiles generated using model-designed buffer formulations A) 0301, B) 0302, C) 0303 and D) 0304 on a Mono Q HR10/10 strong anion exchange column operated at a mobile phase flow rate of 1 mL min⁻¹ and 25 °C..... 57

Figure 2.9: Comparison of elution chromatograms for native human blood plasma injected as a 200 µL pulse onto a Mono Q 10/100GL strong anion exchange column operated at 25 °C and a mobile-phase flow rate of 1 mL min⁻¹: chromatogram generated using A) buffer formulation 1003, or B) buffer formation 0305 that was custom optimized using the model to maximize resolution of the 12 dominant proteins in plasma 59

Figure 2.10: Comparison of elution chromatograms for a mixture of 1.21 mg mL⁻¹ myoglobin, 1.00 mg mL⁻¹ of β-lactoglobulin B and 0.75mg mL⁻¹ glucose oxidase injected as a 500 µL pulse onto a Mono Q HR10/10 strong anion exchange column operated at 25 °C and a mobile-phase flow rate of 1 mL min⁻¹; chromatogram generated using A) buffer formulation 1003, or B) 0303 that was custom optimized using the model to maximize resolution of the three proteins and their minor isoforms 61

Figure 2.11: Comparison of chromatograms for clarified supernatant from a recombinant *Pichia pastoris* Mut^S fermentation producing four unique isoforms of human transferrin differentiated by their charge state. Both runs conducted on a Q Ceramic HyperD 20 HR10/10 strong anion exchange column at a mobile phase flow rate of 25 mL min⁻¹ and 25 °C. A) elution by A) standard linear-gradient ion exchange (60 mL elution gradient from 0 to 1 M NaCl; 10 mM DAP at pH 10.0), and by B) gradient isoelectric chromatofocusing (buffer formulation 1003, standard linear gradient) 64

Figure 3.1:	Comparison of pH profiles generated using buffer formulation 2101 at ionic strengths of A) 100 mM and B) 150 mM on a Mono S HR10/10 strong cation exchange column at a mobile phase flow rate of 1 mL min ⁻¹ at 25 °C.....	77
Figure 3.2:	Comparison of predicted and actual pH profiles generated using buffer formulation 1021 on a Mono S HR10/10 strong cation exchange column at a mobile phase flow rate of 1 mL min ⁻¹ at 25 °C.....	80
Figure 3.3:	Comparison of predicted and actual pH profiles generated using model-derived buffer formulations A) 2101, B) 2102 and C) 2103 on a Mono S HR10/10 strong cation exchange column operated at a mobile phase flow rate of 1 mL min ⁻¹ at 25 °C.....	81
Figure 3.4:	Elution chromatogram for a mixture containing trypsin inhibitor, insulin, ribonuclease A, chymotrypsinogen A, bovine cytochrome C, equine cytochrome C and lysozyme and injected as a 500 µL pulse onto a Mono S HR10/10 strong cation exchange column at 25 °C and a mobile phase (buffer formulation 1021, standard gradient method) flow rate of 1 mL min ⁻¹	82
Figure 3.5:	Comparison of elution chromatograms generated using buffer formulations having buffer species, each at 10 mM, and an ionic strength of 100 mM, 150 mM, 200 mM, 250 mM, 300 mM, 400 mM, 500 mM or 750 mM. Each model-derived buffer formulation was designed to generate a linear pH gradient from 2.0 to 11.0. The sample is comprised of a mixture of 1 mg mL ⁻¹ bovine cytochrome C and 1 mg mL ⁻¹ equine cytochrome C. It was injected as a 500 µL pulse onto a Mono S column operated at 25 °C and a mobile phase flow rate of 1 mL min ⁻¹	84
Figure 3.6:	Elution chromatograms for separation of isoforms of A) 1 mg mL ⁻¹ bovine cytochrome C and B) 1 mg mL ⁻¹ equine cytochrome C injected as a 500 µL pulse onto a Mono S HR10/10 column operated at 25 °C and a mobile phase (buffer formulation 1021, <i>I</i> = 200 mM) flow rate of 1 mL min ⁻¹	85
Figure 3.7:	UV-visible absorption traces of Fraction 1 (red) and Fraction 2 (yellow) isolated through the resolution of bovine cytochrome C (Figure 3.6A). Also shown and superimposed are the corresponding spectra for Fraction 1 (blue) and Fraction 2 (light blue) isolated through the resolution of equine cytochrome C (Figure 3.6B).....	86
Figure 3.8:	Circular dichroism traces of A) Fraction 1 (red) and Fraction 2 (yellow) isolated through the resolution of bovine cytochrome C (Figure 3.6A), and B) Fraction 1 (blue) and Fraction 2 (light blue) of resolved equine cytochrome C (Figure 3.6B).....	87

Figure 4.1:	Model-based estimates of the magnitude of the elution pH shift away from the <i>pI</i> caused by the Gouy-Chapman, Donnan and chromatofocusing effects as a function of ionic strength.....	106
Figure 4.2:	Comparison of elution chromatograms generated using buffer formulation 1003 adjusted to ionic strengths of 105 mM, 125 mM, 150 mM, 175 mM and 200 mM. Each model-derived formulation generates a linear pH gradient from 10.0 to 3.5 and was used to resolve a mixture of 2.5 mg mL ⁻¹ β-lactoglobulin A and 2.5 mg mL ⁻¹ of β-lactoglobulin B injected as a 500 μL pulse onto a Mono Q HR10/10 column at 25 °C and a mobile phase flow rate of 1 mL min ⁻¹ . Dotted lines indicate elution volumes at which the measured pH equals 5.3 and 5.1.....	107
Figure 4.3:	Comparison of predicted and actual chromatograms for the elution of β-lactoglobulin A using a linear pH gradient from pH 10.0 to 3.5 at approximate ionic strengths of 105 mM (A), 125 mM (B), 150 mM (C), 175 mM (D), 200 mM (E), 250 mM (F) and 500 mM (G) on a Mono Q HR10/10 column operated at a mobile phase flow rate of 1 mL min ⁻¹ at 25 °C.....	109
Figure 4.4:	Comparison of predicted and actual chromatograms for the elution of β-lactoglobulin B using a linear pH gradient from pH 10.0 to 3.5 at approximate ionic strengths of 105 mM (A), 125 mM (B), 150 mM (C), 175 mM (D), 200 mM (E), 250 mM (F) and 500 mM (G) on a Mono Q HR10/10 column operated at a mobile phase flow rate of 1 mL min ⁻¹ at 25 °C.....	110
Figure 4.5:	Characteristic charge vs. pH data for β-lactoglobulin A (<i>pI</i> = 5.1) and β-lactoglobulin B (<i>pI</i> = 5.3) on the Mono Q HR10/10 strong anion exchange matrix	111
Figure 4.6:	Predicted elution pH vs. conductivity for β-lactoglobulin A (red), β-lactoglobulin B (blue), α-lactalbumin (green) and trypsin inhibitor (purple) compared to experimental results for ICF on the Mono Q HR10/10 strong anion exchange column at 25 °C.....	112
Figure 4.7:	Reduced peak width (V_w / V_R) vs. elution pH for β-lactoglobulin A resolved by ICF on a Mono Q HR10/10 strong anion exchange column at 25 °C.....	114
Figure 4.8:	Comparison of elution chromatograms generated using buffer formulation 0203 adjusted to ionic strengths of 30 mM, 50 mM, 75 mM, 100mM, 125 mM, 150 mM and 175 mM to generate a linear pH gradient from 10.0 to 3.5 and elute 0.2 mg mL ⁻¹ FLAG® Peptide injected as a 500 μL pulse onto a Mono Q HR10/10 column at 25°C and a mobile phase flow rate of 1 mL min ⁻¹	115

- Figure 4.9:** Comparison of elution chromatograms generated using buffer formulation 1093 adjusted to ionic strengths of 75 mM, 125 mM, 150 mM, 175 mM and 225 mM. The resulting linear pH gradient from 9.0 to 3.5 is used to resolve a mixture of 2.5 mg mL⁻¹ α-lactalbumin and 2.5 mg mL⁻¹ of trypsin inhibitor injected as a 500 μL pulse onto a Mono Q HR10/10 column at 25°C and a mobile phase flow rate of 1 mL min⁻¹..... 117
- Figure 4.10:** Comparison of elution chromatograms generated using buffer formulations 1093, 2093 and 4093. Each linear pH gradient from 9.0 to 3.5 is used to resolve a mixture of 2.5 mg mL⁻¹ β-lactoglobulin A and 2.5 mg mL⁻¹ of β-lactoglobulin B injected as a 500 μL pulse onto a Mono Q HR10/10 column at 25°C and a mobile phase flow rate of 1 mL min⁻¹. The range of ionic strength at which the two proteins elute is indicated. 119
- Figure 5.1:** Changes in dry cell weight and hTf/2N concentrations throughout fermentation of recombinant *Pichia pastoris* Mut^S at 30 °C, 40% (v/v) of saturation DO concentration, pH 4.5, and 1% (v/v) methanol. Induction was initiated 24 hours after culture inoculation (batch fermentation from 0 h < Elapsed Fermentation Time (EFT) < 6 h; culture was batch-fed with 50% (w/v) glycerol at 18 mL h⁻¹ from 6 h < EFT < 24 h; then fed with 50% (w/v) glycerol at 11 mL h⁻¹ from 24h < EFT < 67 h). 129
- Figure 5.2:** Comparison of A) gradient isoelectric chromatofocusing (labeled with the intact masses of four distinguishable hTf/2N isoforms) and B) isocratic isoelectric chromatofocusing of recombinant *Pichia pastoris* Mut^S fermentation broth on a Q Ceramic HyperD 20 HR10/10 strong anion exchange column at a mobile phase (buffer formulation 1003) flow rate of 25 mL min⁻¹ at 25 °C..... 131
- Figure 5.3:** Elution pH vs. conductivity for major protein components resolved using ICF on the Q Ceramic HyperD 20 HR10/10 strong anion exchange column. Dotted black line represents approximate changes in ionic strength during ICF separations with buffer formulation 1005C..... 133
- Figure 5.4:** Customized pH gradient for the isolation of the desired hTf/2N isoform (collected in eight 1 mL fractions) from three undesired isoforms using the Q Ceramic HyperD 20 HR10/10 strong anion exchange column at a mobile phase (buffer formulation 1005C) flow rate of 25 mL min⁻¹ at 25 °C..... 136
- Figure 5.5:** SDS-PAGE gel separation of raw culture supernatant (Lane 1), isometrically pure transferrin peak collected from ICF (Lanes 2 to 9) and SeeBlue Plus2 Pre-Stained Standard (Lane 12) 137
- Figure 6.1:** A) Concave pH gradient (buffer formulation 03CC) and B) shallow pH gradient (buffer formulation 1003, linear gradient at -0.05 pH mL⁻¹) ICF fractionation of the proteome (16 mg) of insulin/STZ/glucose treated

differentiated C2C12 mouse myoblast cell lysate loaded as a 10 mL pulse onto a Mono Q HR10/10 strong anion exchange column at a mobile phase flow rate of 1 mL min⁻¹ at 25 °C; 900 µL eluent fractions were collected. 155

Figure 6.2: Overlay of chromatograms of linear gradient ICF fractionations of the proteomes of insulin/STZ/glucose treated (red), untreated (green) and alloxan-inhibited (blue) differentiated C2C12 mouse myoblast cell lysate samples loaded as a 10 mL pulse onto a Mono Q HR10/10 strong anion exchange column at a mobile phase flow rate of 1 mL min⁻¹ at 25 °C; 900µL eluent fractions were collected. 156

Figure 6.3: Dot-blot (12 µL) of each fraction collected by linear gradient ICF (Figure 6.2) of the proteomes of A) insulin/STZ/glucose treated, B) untreated, and C) alloxan-inhibited differentiated C1C12 mouse myoblasts on a PVDF membrane blocked with a 5% BSA solution and probed with CTD110.6..... 158

Figure 6.4: SDS-PAGE (10%) gel separation of selected fractions from ICF separation of the proteome of alloxan-inhibited differentiated C2C12 mouse myoblast cell lysate; red outlined bands on the SDS-PAGE gel were excised for mass analysis. 159

Figure 6.5: A) SDS-PAGE (10%) gel separation of selected fractions from ICF separation of the proteome of insulin/STZ/glucose treated differentiated C2C12 mouse myoblast cell lysate and B) western gel of the corresponding fractions probed with the CTD110.6 antibody; outlined bands on the SDS-PAGE gel were excised for mass analysis. 161

Figure 6.6: A) SDS-PAGE (10%) gel separation of selected fractions from ICF separation of the proteome of untreated differentiated C2C12 mouse myoblast cell lysate, and B) western gel of the corresponding fractions probed with the CTD110.6 antibody; red outlined bands on the SDS-PAGE gel were excised for mass analysis. 165

Figure 6.7: Difference between elution pH and *pI* plotted against the molecular weight of benchmark C2C12 mouse myoblast cell lysate proteins reveals a roughly logarithmically inverse relationship..... 169

Nomenclature

A	total anionic species	mol m^{-3}
A_i	anionic species i	mol m^{-3}
B_i	buffer i	mol m^{-3}
c	mobile phase protein concentration	mol m^{-3}
C_i	mobile phase concentration of buffer species i	mol m^{-3}
C_i^0	initial mobile phase concentration of buffer species i	mol m^{-3}
C_i^{feed}	feed mobile phase concentration of buffer species i	mol m^{-3}
D	Debye-Hückel component of β	--
D_{axi}	axial dispersion coefficient for species i	$\text{m}^2 \text{s}^{-1}$
e	electron charge	C
e_{matrix}	matrix porosity	--
H	height equivalent of a theoretical column plate	m
ΔH^0	formation constant at 25 °C	J mol^{-1}
I	ionic strength	M
K	protein equilibrium binding constant	--
k	Boltzmann's constant	J K^{-1}
K_{bi}	equilibrium binding constant of buffer i	$\text{m}^3 \text{mol}^{-1}$
K_{i1}	first equilibrium constant of buffer i	--
K_{i1}^*	first concentration-based equilibrium constant of buffer i	$\text{m}^3 \text{mol}^{-1}$
K_{i2}	second equilibrium constant of buffer i	--

K_{i2}^*	second concentration-based equilibrium constant of buffer i	$\text{m}^3 \text{mol}^{-1}$
L	column length	m
m	characteristic charge	--
P	Stern equation proportionality constant	--
Pe	Peclet number	--
pH_{bulk}	bulk mobile phase pH	--
pH_{surf}	matrix surface pH	--
pK_{i1}	logarithm of first protonation constant of buffer i	--
pK_{i2}	logarithm of second protonation constant of buffer i	--
q	stationary phase protein concentration	mol m^{-3}
Q_i	stationary phase concentration of buffer species i	mol m^{-3}
Q_i^{max}	matrix maximum binding capacity for buffer species i	mol m^{-3}
S	surface charge density	C m^{-2}
S_T	matrix ionic capacity	mol m^{-3}
t	time	s
T	temperature	K
T_{Bi}	total concentration of all forms of buffer i	mol m^{-3}
TC_i	total mobile phase concentration of buffer i	mol m^{-3}
u	superficial mobile phase velocity	m s^{-1}
V_R	elution volume	mL
V_W	elution bandwidth	mL
z, z_i	ion valence (of species i)	--
Z	axial position	m

Greek Symbols

β	lumped Debye-Hückel non-coulombic association constant	--
β'	non-coulombic association constant	--
β_{i1}	formation constant of monoprotonated state of buffer i	mol m^{-3}
β_{i2}	formation constant of diprotonated state of buffer i	$\text{mol}^2 \text{m}^{-6}$
γ_i	activity coefficient for species i	--
δ	Stern layer thickness	nm
ε	column void fraction	--
ε'	solvent dielectric constant	--
ε_0	permittivity of free space	F m^{-1}
θ	bound protein fraction	--
κ	Debye-Hückel constant	m^{-1}
λ_{De}	Debye length	m
π	circle circumference to diameter ratio	--
ρ	surface free-charge density	C m^{-2}
ρ_0	solvent density	kg m^{-3}
σ	steric factor	--
ϕ	non-coulombic adsorption potential	J
Ψ	electrical potential	V
$\Psi_0, \Psi(0)$	matrix surface potential	V

Abbreviations

1D	one dimension(al)
2D	two dimension(al)
2DGE	two dimensional gel electrophoresis
3D	three dimension(al)
ACE	acetic acid
AEICF	anion exchange isoelectric chromatofocusing
AEX	anion exchange
AMP	adenosine monophosphate
BCN, BICINE	2-(Bis(2-hydroxyethyl)amino)acetic acid
BMGY	buffered glycerol-complex medium
BRC	Biomedical Research Centre
BSA	bovine serum albumin
BTS, bis-tris	2-[Bis(2-hydroxyethyl)amino]-2-(hydroxymethyl)propane-1,3-diol
CEICF	cation exchange isoelectric chromatofocusing
CEX	cation Exchange
CHBE	Chemical and Biological Engineering
CHS, CHES	2-(cyclohexylamino)ethanesulfonic acid
CPS, CAPS	3-(cyclohexylamino)-1-propanesulfonic acid
CV(s)	column volume(s)
DAP	Propane-1,3-diamine (1,3 diaminopropane)
DCW	dry cell weight
DEA	2,2'-Iminodiethanol (diethanolamine)

DEAE	diethylaminoethyl
DMEM	Dulbecco's Modified Eagle Medium
DNA	deoxyribonucleic acid
DO	dissolved oxygen
DSP	downstream processing
DTT	DL-dithiothreitol
<i>E. coli</i>	<i>Escherichia coli</i>
ECL	enhanced chemiluminescence
EFT	elapsed fermentation time
eNOS	endothelial nitric oxide synthase
FOR	formic acid
FPLC	fast protein liquid chromatography
GE	General Electric
GFAT	glutamine-fructose-6-phosphate amido-transferase
GTP	guanosine triphosphate
HBP	hexosamine biosynthesis pathway
HCP(s)	host cell protein(s)
HIC	hydrophobic interaction chromatography
HILIC	hydrophilic interaction chromatography
HPS, HEPES	2-[4-(2-hydroxyethyl)piperazin-1-yl]ethanesulfonic acid
HRP	horseradish peroxidase
hTf/2N	N-lobe of human transferrin
ICF	isoelectric chromatofocusing

IDA	iminodiacetic acid
IEC	ion exchange chromatography
IEF	isoelectric focusing
IgA	immunoglobulin A
IgG	immunoglobulin G
IgM	immunoglobulin M
IMAC	immobilized metal affinity chromatography
IMI	1 <i>H</i> -imidazole (imidazole)
IPG	immobilized pH gradient
IRS	insulin receptor substrate
LAC	2-Hydroxypropanoic acid (lactic acid)
LC	liquid chromatography
LDS	lithium dodecyl sulfate
mAb	monoclonal antibody
MAL	propanedioic acid (malonic acid)
MALDI	matrix assisted laser desorption/ionization
MDLC	multidimensional liquid chromatography
MEM α	Minimum Essential Medium Eagle, Alpha Modifications
MES	2-(<i>N</i> -morpholino)ethanesulfonic acid
MFFP	Multi-user Facility for Functional Proteomics
MS	mass spectrometry
MS/MS	tandem mass spectrometry
MSO, MOPSO	3-[<i>N</i> -morpholino]-2-hydroxypropanesulfonic acid

MW	molecular weight
mTOR	mammalian target of rapamycin
NP40	Tergitol-type NP-40
NTA	nitrilotriacetic acid
NTUs	number of transfer units
O-GlcNAc	O-linked N-acetylglucosamine
<i>P. pastoris</i>	<i>Pichia pastoris</i>
PAGE	polyacrylamide gel electrophoresis
PBS	phosphate buffer saline
PBS-T	phosphate buffer saline with Tween 20 detergent
pH	logarithm of the reciprocal of hydrogen ion activity
<i>pI</i>	isoelectric point
<i>pK</i>	logarithm of protonation constant
<i>pK^{0*}</i>	logarithm of protonation constant at 25 °C and 0 M ionic strength
PIP	Piperazine
PTM(s)	post-translational modification(s)
PTM ₁	<i>Pichia</i> trace metals
PVDF	polyvinylidene difluoride
Q	quaternary Amine
QSAR	quantitative structure-activity relationship
QSRR	quantitative structure-retention relationship
RPLC	reverse phase chromatography
RPM	revolutions per minute

S	sulphonyl group
SDS	sodium dodecyl sulfate
SEC	size exclusion chromatography
SMA	steric mass action
Sp1	specificity protein 1
STZ	streptozotocin
TOF	time of flight
TRS, tris	2-amino-2-hydroxymethylpropane-1,3 diol
UBC	University of British Columbia
UDP-GlcNAc	uridine diphosphate N-acetylglucosamine
UV	ultraviolet

Acknowledgements

Firstly, I would like to thank my supervisor Dr. Charles Haynes for providing a supportive and open research environment for me to explore new ideas in. Knowledgeable and highly experienced, he guided me through the completion of my dissertation and challenged me to become a more mature engineer and scholar.

Similarly, I would like to thank Dr. Louise Creagh for her valuable advice and unwavering support. In addition I thank her for providing opportunities for me to learn and apply new skills while working for the CHBE undergraduate and graduate teaching laboratories.

I would like to express my gratitude to Suzanne Perry, Gary Lesnicki, Dr. Adriana Cajiao, Dr. Grant Mauk, Dr. Dana Devine, Dr. Ross MacGillivray, Dr. Juergen Kast and Jason Rogalski for graciously offering the use of their lab equipment and providing guidance.

I would also like to thank the countless past and present staff, students and faculty members at Michael Smith Laboratories, Centre for Blood Research, Biomedical Research Centre and in the Chemical and Biological Engineering department for their assistance and encouragement. Special thanks to Dr. Patrick Francis for his valuable advice, and to Dr. Edgar Lam for the productive and enjoyable research collaboration.

I would like to acknowledge the funding sources that made my work possible, particularly the National Science and Engineering Research Council of Canada.

I am grateful to all my friends, including many who were already mentioned above, for cheering me through my greatly extended career as a graduate student. A very special thanks goes to my girlfriend Elaine Kwan, who was always understanding, loyal and caring. Finally, I am indebted to my family, especially my parents, for offering immeasurable support that empowered me to complete my research.

Dedication

To my family

Chapter 1

Introduction

1.1 Introduction to Liquid Chromatography for Protein Separation

1.1.1 Liquid chromatography applied to proteins

The first use of liquid chromatography dates back to the early 20th century, when it was applied to the separation of plant pigments [1]. Since then, significant progress has been made in the development of powerful modes of chromatography, as well as theories and models that permit mechanistic understanding, optimization and scale-up of those operations [2-6]. Today, the term liquid chromatography encompasses a broad range of separation methods applicable to many classes of analytes in amounts ranging from analytical (nanograms to grams) to preparative (kilograms to tons).

Proteins must be isolated before they can be subjected to detailed structural or functional studies, or marketed as a pharmaceutical product. Challenging these separation processes is the fact that all proteins are comprised of combinations of the same 20 amino acids and, in the case of globular proteins, are of similar sizes based on their Stokes radii (~ 1 nm to at most a few tens of nanometres). The requirements for separating mixtures of proteins are therefore somewhat akin to those for chemicals having very similar volatilities and molecular weights by distillation. A key difference, however, is the

limited range of operating conditions that can be applied to protein mixtures due to their labile nature. Chromatography is the most widely applied unit operation for separating complex protein mixtures because it has the capacity to offer a very large number of theoretical (equilibrium) plates, but at conditions (temperature, pressure, pH) and in solvents that preserve the fold and function of the complex molecules being purified [7].

Liquid chromatography is generally operated in cylindrical beds packed with spherical porous particles into which the analytes to be separated may partition and possibly adsorb. Feed and processing solutions (loading, wash and elution buffers) are applied at the top of the column, and fluid exiting the column is monitored (for properties such as UV absorption, conductivity and pH) to detect changes in composition. A number of amino acids, especially the aromatic amino acids phenylalanine, tryptophan and tyrosine, absorb ultraviolet light. Therefore, eluting proteins and peptides in liquid chromatography are often detected by measuring UV absorbance at 280 nm, a wavelength at which all three aromatic amino acids exhibit a reasonably high extinction coefficient.

Separation is achieved through differences in the partitioning and retention of components within the stationary phase, which effectively removes those components from axial mobile-phase flow. The mechanically stable and functional matrices required for liquid chromatography are typically produced through chemical cross-linking of polymers or inorganic glasses. Those matrices may bear functional ligands prior to cross-linking or casting, or ligands may be introduced following synthesis of the base matrix

through surface modification. The chemistry (such as radical polymerization or living polymerization) and conditions (such as monomer, initiator and cross-linking agent concentrations, temperature, and solvents) employed determine the final properties of the stationary phase. Nominal diameters of beaded media typically range from 1 μm to 20 μm for analytical columns, and up to about 300 μm for lower-pressure preparative applications. Pore diameters typically range from 5 nm to 200 nm, with many chromatographic media exhibiting a range of different pore sizes. Finally, media used for preparative applications typically offer an accessible surface area between 100 $\text{m}^2 \text{g}^{-1}$ and 500 $\text{m}^2 \text{g}^{-1}$ of stationary phase [8].

The modes of liquid chromatography most often used to purify proteins in their native states generally separate on the basis of one or a few physico-chemical properties, including differences in protein size, in net or regional protein charge provided by acidic (aspartic acid, Asp - D; glutamic acid, Glu - E) and basic (Lysine, Lys - K; Arginine, Arg - R; Histidine, His - H) amino acids present at the solvent-exposed surface, in protein-surface hydrophobicity/hydrophilicity, and/or in the ability to chelate transition-metal ions. In addition, many proteins have a strong and specific affinity for particular (bio-)chemical species, including metabolites and other bio-macromolecules (such as proteins and DNA) that are, for instance, substrates in reactions catalyzed by the protein or designated targets as part of a signaling pathway or immune response; these selective “affinity” interactions can be used to specifically capture and purify a target protein of interest [9]. A number of liquid chromatography techniques most commonly

used to purify peptides and proteins, particularly at preparative scales, are briefly discussed below.

1.1.2 Size exclusion chromatography

Pioneered in the 1950s [10, 11], size exclusion chromatography (SEC) separates proteins primarily based on their size, or more specifically based on their Stokes radii [12]. When applied at industrial scales, SEC columns are usually cylindrical beds packed under moderate pressure with beads of a porous polymer gel offering a distribution, sometimes broad, of pore sizes that can be controlled by the method and degree of polymerization [13]. Transport within the stationary phase is typically dominated by diffusion, while transport in the interstitial volume is dominated by convection. Differences in the partitioning of proteins with different Stokes radii between the mobile and stationary phases therefore provide the mechanism of separation.

SEC is a mode of elution chromatography, with the sample loaded as a liquid plug of volume generally no more than 15% (v/v) that of the column. The mobile phase composition typically remains constant in an SEC separation, so elution is isocratic (constant mobile-phase composition). The technique does not require the use of specific types of mobile phases, but when applied to biologic mixtures it is common to use a low-ionic-strength aqueous buffer of defined pH away from the isoelectric point (pI) of the target protein. Large proteins too big to enter any of the pores elute from the column first. Smaller proteins enter pores of the stationary phase at a rate limited by diffusion and typically do not convectively migrate through the column while in that phase. Thus,

the smallest proteins with access to the most pore volume elute last. Since salt molecules and other contaminants are usually much smaller than proteins, SEC is a popular technique for sample desalting. It is also applied industrially as a desalting or product polishing step typically aimed at removing unwanted oligomeric forms of the product [14].

1.1.3 Reversed phase chromatography and hydrophilic interaction chromatography

Reversed phase liquid chromatography (RPLC) was developed in the 1970s as a means to achieve high resolution separations [15]. It is likely the most widely-used mode of chromatography for analytical applications, due in part to the many different adsorption mechanisms in play, which can include hydrophobic, London/van der Waals dispersion, $\pi - \pi^*$ and ion-pairing interactions, providing great flexibility with respect to tuning separations to achieve high purities and excellent peak capacities. As a result, a very large number of high quality RPLC matrices are available, including porous and non-porous beaded surfaces bearing a uniform brush of aliphatic chains ranging from C₆ to C₁₈ in length. Resin hydrophobicity is proportional to the length and density of the attached chains. RPLC is an adsorptive mode of chromatography, and proteins are usually loaded as a column-sub-saturating pulse (linear isotherm region) in an aqueous mobile phase of sufficient ionic strength to promote binding, particularly in the presence of an added acid such as trifluoroacetic or formic acid [16]. Binding is driven in part by the hydrophobic effect, an entropically favorable process at near-ambient temperatures that results in dehydration and close association of hydrophobic surfaces on the protein and the sorbent; however, as noted above, other secondary driving forces are known to

contribute as well. A high-resolution separation of the bound mixture may then be achieved through sequential elution using a linear or nonlinear gradient in mobile phase organic solvent content that is generated through the incremental replacement of the aqueous loading buffer with an organic eluent such as acetonitrile or methanol. To a first approximation, bound proteins elute and partition back into the mobile phase in accordance with their degrees of surface hydrophobicity [8].

A related mixed-mode separation, hydrophilic interaction chromatography (HILIC), was developed based on the recognition that many association reactions between biological analytes (such as proteins and nucleic acids) involve combinations of coulombic, hydrogen-bonding/polar, and London/van der Waals dispersion forces. HILIC therefore exploits stationary phases bearing charged hydrophilic ligands to adsorb and separate proteins through both short-range and ion-exchange interactions [17]. Unlike RPLC, HILIC uses a hydrophilic stationary phase modified with a selection of functional groups, such as amide, diol, cyano, polysuccinimide, sulfoalkylbetaine, and cyclodextrin moieties [18]. Samples are often frontally loaded on the column using a mobile phase consisting mostly of an organic solvent such as acetonitrile, with a small amount of water adjusted to a pH value selected so as to make the net charge of the target protein(s) of interest opposite in sign to that of the matrix surface. The column is designed such that the small amount of water in the mobile phase adsorbs onto the polar stationary phase; charged polar analytes partition favorably into this aqueous layer and bind to the oppositely charged stationary phase. Selective elution can then be achieved through the use of a decremental organic solvent gradient and/or an incremental ionic strength

gradient. Though the low solubility of many salts in the organic mobile phase is a limiting factor, HILIC has proven especially useful for purifying certain classes of molecules, including those that do not bind to RPLC columns under traditional loading conditions. RPLC and HILIC generally achieve very high resolution separations, but the required use of an organic phase is problematic, as it can irreversibly denature proteins, making the method unsuitable for many applications, often including therapeutic protein manufacturing [19].

1.1.4 Hydrophobic interaction chromatography

Hydrophobic interaction chromatography (HIC) is designed to avoid or at least abate protein denaturation during processing by employing an aqueous mobile phase to load, elute and separate proteins based primarily on differences in their degree of solvent-exposed hydrophobicity [20]. Like RPLC, HIC uses a stationary phase bearing hydrophobic ligands, but in this case those ligands (such as phenyl groups or C₃ to C₆ aliphatic chains) are smaller in size and thus present a much lower specific hydrophobic surface area. In HIC, proteins are typically frontally loaded in an aqueous mobile phase containing a kosmotropic salt such as ammonium sulfate at a concentration of at least 1 M. The presence of the kosmotrope reduces the solubility of proteins in water, causing them to associate with the stationary phase surface, often in the form of aggregates or a precipitate. As the mobile phase salt concentration is reduced in a decremental gradient, bound proteins are resolubilized and elute from the column, to a first approximation, in order of increasing hydrophobicity [21].

1.1.5 Affinity chromatography

Affinity chromatography takes advantage of the ability of certain molecules, such as antibodies, to selectively bind to specific proteins or epitopic targets [22]. Immobilized metal affinity chromatography (IMAC) represents one example, where the presence, at the matrix surface, of a transition metal ion (such as Cu^{2+} or Ni^{2+}) with an unfilled d or higher orbital permits strong and selective binding of His/Cys-rich proteins or chimeric proteins bearing a poly-His tail, as well as peptides capable of strongly chelating the metal [23]. Surface-anchored ligands used to fix the transition metal ion to the matrix include iminodiacetic acid (IDA) and nitrilotriacetic acid (NTA). For example, the NTA ligand is tetradentate, complexing with the Ni^{2+} ion such that two coordination sites are available for binding the imidazole rings of available histidine residues on the peptide.

Many other examples of affinity chromatography exist, and the importance of the method to industry has led to extensive studies that compare different immobilization chemistries and define ways to increase ligand density and improve ligand utilization. The most frequently applied form of affinity chromatography is immobilized *Staphylococcus aureus* Protein A (and its protein family, *SpA* Ig-binding domains, variants) for the capture and purification of monoclonal antibody (mAb) products from cell culture. The performance of protein A and engineered protein A (*e.g.* MabSelect) resins have therefore been exhaustively studied with the aim of improving binding capacity, protein mass transfer, host cell protein removal and virus clearance [24]. When compared to other modes of chromatography, affinity chromatography is typically more expensive,

but those cost requirements can be offset when dense loading and extremely high levels of product purity are achieved, as in the case of mAb purification.

1.1.6 Ion exchange chromatography

Developed in the 1940s for the separation of rare earth metals [25-28], ion exchange chromatography (IEC) is now the most widely used technique for the separation of small charged organic molecules in analytical and preparative quantities. Moreover, it is the most widely used method for purifying proteins at the preparative scale [29]. IEC uses an aqueous mobile phase, along with a stationary phase carrying a moderate to very high density of fixed surface charge. Common ligands used to introduce positive surface charge on the matrix include quaternary amines such as anchored trimethylamine (Q anion exchange media) and tertiary diethylaminoethyl (DEAE anion exchange media) groups; carboxyl and sulfoxyl groups are most often employed as charged ligands when a negative surface charge density (cation exchange) is required. The basic quaternary amines (*e.g.* Q Sepharose) and DEAE groups most often used to functionalize anion exchange (AEX) media are characterized by a high to very high pK , giving the matrix a positive charge density below pH 10, where AEX separations are typically conducted. Net negatively charged analytes, including proteins in environments above their pI , bind to an AEX matrix through ion exchange reactions. Modern AEX media used by industry for preparative protein purifications can bind up to 270 mg of protein per millilitre (mL) of resin, making them very economical and well suited for throughput-intensive steps like initial product capture from culture supernatants. Typically, AEX column loading is performed using a buffered mobile phase having a pH between *ca.* 5 and 9. Step, multi-

step or programmed gradient changes in mobile phase salt (*e.g.* NaCl) concentration up to *ca.* 1 M are then applied for elution. The anion of the salt competes for binding sites at the stationary phase surface and releases each protein from its bound state at a characteristic ionic strength. Proteins separate primarily because the amount of salt needed for displacement varies with the external net charge of the protein, though other forces including dispersion and $\pi - \pi^*$ interactions can also influence binding and elution.

The simplicity, versatility, high capacity, and good resolving power of AEX chromatography have together served to make this mode of chromatography one of the most widely employed in the biotech industry. It is routinely applied to product capture, concentration, purification and polishing, as well as to the removal of negatively-charged endotoxin from protein preparations [2, 4, 7, 9, 30]. If the purification of a particular protein from a complex mixture is the goal of an AEX separation, the loading-phase pH is usually set 1 to at most 3 pH units above the *pI* of the target protein. One or more of a variety of available buffering molecules (Table 1.1), each characterized by a unique *pK*, may be used to control the mobile phase pH.

The acidic sulfoxyl and carboxyl groups are used in cation exchange (CEX) media. CEX chromatography is not applied quite as often industrially as AEX, in part because most proteins carry a net negative charge at physiological pH. Nonetheless, it is a powerful separation modality, offering peak and binding capacities equivalent to its AEX sibling. Moreover, applications of CEX are growing, including its use in mAb capture and

purification from cell culture [31-33], as well as in the initial capture and concentration of proteins produced under acidic conditions, such as in recombinant cultures of the yeast *P. pastoris* [34-38]. Typically, CEX chromatography is performed with a buffered mobile phase (Table 1.2) at a pH between *ca.* 3 and 7, with increasing salt concentration again serving as the method for elution. As with AEX, uses of CEX generally include initial capture, clean-up and concentration of protein products, as well as intermediate purification and final polishing of the target.

Table 1.1: Common buffers for AEX chromatography across various pH ranges [39, 40]

pH Range	Buffer	<i>pK</i> *
11.9 - 12.9	Phosphate	12.35 / 7.198 / 2.148
10.6 - 11.6	Piperidine	11.12
10.2 - 11.2	Triethylamine	10.72
10.1 - 11.1	1,3-Diaminopropane	10.55
9.2 - 10.2	Piperazine	9.731 / 5.333
9.0 - 10.0	Ethanolamine	9.498
8.4 - 9.4	Diethanolamine	8.883
8.4 - 9.4	1,3-Diaminopropane	8.88
8.0 - 9.0	<i>N</i> -Methyl-diethanolamine	8.52
7.6 - 8.6	Tris	8.072
7.3 - 8.3	Triethanolamine	7.762
6.5 - 7.5	Imidazole	6.993
6.2 - 7.2	Bis-tris propane	9.10 / 6.65
6.0 - 7.0	Bis-tris	6.484
5.6 - 6.6	L-Histidine	9.43 / 6.07 / 1.5
4.8 - 5.8	Piperazine	9.731 / 5.333
4.3 - 5.3	<i>N</i> -Methyl piperazine	4.75

*In water at 298.15 K, an ionic strength = 0 M, and a pressure = 0.1 MPa

Table 1.2: Common buffers for CEX chromatography across various pH ranges [39, 40]

pH Range	Buffer	<i>pK</i> *
1.4 - 2.4	Maleic acid	1.92 / 6.27
2.4 - 3.4	Malonic acid	2.88 / 5.68
2.6 - 3.6	Citric acid	3.128 / 4.761 / 6.396
3.4 - 4.4	Lactic acid	3.86
3.7 - 4.7	Butaneandioic acid	4.21
4.3 - 5.3	Acetic acid	4.756
5.3 - 6.3	Methyl malonic acid	5.76
5.8 - 6.8	MES	6.270
6.3 - 7.3	ACES	6.847
6.7 - 7.7	Phosphate	2.148 / 7.198 / 12.35
7.1 - 8.1	HEPES	3.0 / 7.564
7.5 - 8.5	HEPPS	7.957
7.5 - 8.5	HEPPSO	8.042
7.8 - 8.8	BICINE	2.0 / 8.334
7.9 - 8.9	TAPS	8.44
8.9 - 9.9	CHES	9.394
10.0 – 11.0	CAPS	10.499

*In water at 298.15 K, an ionic strength = 0 M, and a pressure = 0.1 MPa

Matrices displaying strongly basic groups such as the quaternary amine are positively charged at all pH values tolerated by the matrix and are classified as strong anion exchangers, while those presenting strongly acidic ligands such as the sulfoxyl group are classified as strong cation exchangers. The DEAE and carboxyl groups, with *pK* values of *ca.* 10 and 4 respectively, form weak anion and cation exchangers. Common counter-ions used to generate ionic strength during elution are chloride, acetate or formate for anion exchange, and sodium, potassium or lithium for cation exchange.

Separation performance of ion exchange columns is generally determined by the properties of the key interacting species driving adsorption and desorption: the ligands on the stationary phase, the protein(s) to be separated, as well as the pH, ionic strength and binding contributions of constituents in the mobile phase. Depending on their mechanical stability, ion exchange media can be applied at low, medium or high pressure, permitting both preparative purification of high-value protein therapeutics and high-resolution analytical separation of complex protein or proteomic samples. In certain cases, the application of IEC to protein mixtures using a step change or gradient in ionic strength for elution can result in exceptional resolution and purity. For example, complete resolution of isoforms differing by as little as a single charged group has been achieved for several proteins [41, 42]. However, satisfactory separations using conventional AEX or CEX are not realized in all cases, and this has motivated the development of alternative strategies for operating IEC columns in a manner that maintains product biological activity while improving yield and resolution. One of these strategies involves the selective elution of proteins bound to an IEC column through the continuous addition of displacer molecules that compete for binding sites on the matrix; this approach, known as displacement chromatography, results in the formation of a “train” of eluting protein species, sorted by their relative affinity to the IEC media, that moves through the column as a series of “boxcars” (high-purity plug-flow zones). It is best applied to the purification of a single target protein from a complex feedstock, where it can sometimes offer truly exceptional purities and yields [43-55]. Largely due to cost and complexity concerns, displacement chromatography has not found significant traction in industry despite its power and fundamental elegance. Another idea, which has

found significant use in industry, is to operate an IEC column in flow-through mode with respect to the product of interest. Often applied to the clean-up of mAb products, this strategy is particularly effective in cases where the total load of contaminants is low, so that column cycle times and lifetimes are maximized [56, 57].

A third strategy, which is the focus of this thesis, is to elute bound proteins by changing the pH of a low ionic strength mobile phase. Like traditional IEC, this method, known as Isoelectric Focusing Chromatography or Isoelectric Chromatofocusing (ICF), can offer exceptional resolving power. Its history and scientific underpinnings are described in the next section.

1.2 Isoelectric Chromatofocusing

1.2.1 History

Chromatofocusing was pioneered by Sluyterman *et al.* in 1978 [58-64]. It has historically been performed on a weak anion exchange column equilibrated with a high pH, low ionic strength buffer (the load and wash buffer) prior to sample loading. Following frontal loading of sample in the same buffer, a pH gradient can be generated within the column through isocratic or gradient switching of the mobile phase to a low pH (and usually low ionic strength) elution buffer. Proteins that are net-negatively-charged at the pH of the loading buffer are initially bound to the stationary phase; traditional ICF theory suggests that each bound protein then elutes when the mobile phase pH becomes equal (or at least sufficiently close) to the protein's *pI* [58, 59]. Eluted

proteins migrate through the column as a self-sharpening peak, since those proteins traveling faster than the peak mean move up the pH gradient and thereby regain the negative charge that drives binding; proteins dispersed behind the peak mean move down the pH gradient, causing them to carry a larger net positive charge that results in greater repulsion from the stationary phase (lower partition coefficient). In theory, this electrostatically driven focusing of the eluting protein can serve to counteract band broadening caused by axial dispersion, resulting in improved peak capacity when compared to conventional ion exchange. In principle, chromatofocusing can also be carried out on a cation exchange column, but its application in that modality has received almost no attention in the literature.

Polyampholyte buffers are most often used to generate the required pH gradient. Those buffers are comprised of large (bio-)macromolecules presenting multiple functional groups, each of which offers a unique pK value such that buffering capacity is maintained across a wide range of pH. Due to their chemical complexity, polyampholytes are relatively expensive to manufacture, which in part explains the currently low interest from industry in this mode of chromatography as a tool for preparative separations. In addition, the polyampholytes available are chemically heterogeneous, making their buffering characteristics difficult to predict. They can also bind to analytes during the separation. This, along with the fact that the molecular weight of the polyampholytes used may be commensurate to that of the proteins being separated, makes their removal from the eluent stream more challenging [65, 66].

1.2.2 Commercial chromatofocusing systems

While not currently applied at preparative scales, chromatofocusing is used quite extensively analytically. GE Healthcare Life Sciences produces and markets two proprietary polyampholyte buffers [67]: Polybuffer 74, which provides buffering capacity between pH 7 and 4, and Polybuffer 96, which provides buffering capacity between pH 9 and 6. These polyampholyte buffers are designed to generate quasi-linear pH gradients on several weak anion exchange resins marketed by that company, including Mono P, Polybuffer Exchanger PBE94 and Polybuffer Exchanger PBE118. The latter two media are designed specifically for chromatofocusing applications, as the weak anionic functional groups on the resins, together with the matched polyampholyte buffer, provide the buffering capacity required to generate a stable quasi-linear elution pH gradient.

In 2005, Beckman Coulter entered the chromatofocusing arena by introducing a multidimensional liquid chromatography (MDLC) platform, called the ProteomeLab PF2D, that implements chromatofocusing as the first separation dimension for proteome fractionations [68]. The chromatofocusing column uses Polybuffer 74 and a proprietary weak AEX stationary phase. Eluents from the first separation dimension are subjected to a second dimension RPLC separation, followed by mass spectrometry of a type appropriate for the proteomic study of interest.

1.2.3 Major developments in chromatofocusing

Since the invention of chromatofocusing by Sluyterman *et al.* [58-63], researchers have worked to advance the method by focusing (primarily) on three aspects of development:

the generation of useful pH gradients without the use of polyampholyte buffers, the prediction of pH gradient profiles, and understanding the mechanism(s) of protein elution.

1.2.3.1 Anion-exchange based chromatofocusing without polyampholyte buffers

In principle, the buffering capacity of polyampholyte buffers can be replaced with a mixture of simple monoprotic or diprotic buffers. Each such simple buffer provides buffering capacity across a narrow pH range. Due to their small sizes and simple chemistries, monoprotic or diprotic buffers have stable, predictable and reproducible buffering characteristics, and can be easily separated from proteins using diafiltration (buffer exchange) or size exclusion chromatography. Simple buffer cocktails can therefore be created for application to a weak ion exchange stationary phase so as to take advantage of the intrinsic buffering capacity of that matrix.

Based on this concept, various attempts have been made to generate quasi-linear pH gradients capable of resolving protein mixtures on weak anion exchangers. The gradient is typically created by first loading the sample using a mobile phase containing one set of simple buffers, and then eluting by step switching of flow to an isocratic elution phase containing a different mixture of buffers that serves to create a decreasing pH gradient. Frey and coworkers were among the first to explore this idea and show that a pH gradient can be generated in an anion exchange column using anionic buffers [69-73]. The anionic buffer species are expected to bind the oppositely charged stationary phase during equilibration at high pH, and then protonate and desorb as the low-pH elution buffer is

introduced, so as to provide a steady source of buffering capacity. Frey also demonstrated that ICF pH gradients can be generated in a weak anion exchanger using simple cationic buffers [66, 74, 75]. That latter approach proved effective in separating proteins within a clarified *E. coli* cell lysate through the generation of a concave elution gradient over the pH range of 4.7 to 3.7 [76]. Logan *et al.* pursued a similar idea, generating a quasi-linear pH gradient from pH 9.5 to 5.0 using a loading phase, as well as an isocratic elution phase, that each contained only two simple buffering species. Their strategy was to first select buffers with multiple protonation states, and then select a weak anion exchange stationary phase with complementary buffering characteristics [77].

Programmed gradient elution has also been demonstrated using simple buffers. Anderson *et al.* equilibrated a weak anion exchanger with cationic buffers at high pH, and then created an elution gradient using a mixture of cationic and anionic buffers; a concave pH gradient from pH 7.5 to 3.0 was achieved [65, 78, 79]. Calling this technique gradient chromatofocusing, they used it to resolve fibrinogen degradation products [80]. An attractive and very high-resolution separation mode at analytical scales, gradient chromatofocusing has been applied to various proteomics applications. For example, Greibrokk *et al.* created a MDLC platform comprised of gradient chromatofocusing and RPLC [81], and have since applied it to the analytical separation of various complex proteomes followed by protein identification using mass spectrometry [81-85].

1.2.3.2 Cation-exchange based chromatofocusing without polyampholyte buffers

Research on chromatofocusing on a cation exchange stationary phase is limited [86, 87], due in part to the additional challenge of controlling the binding of protons to the negatively-charged stationary phase. Adsorption and desorption of protons strongly affects mobile phase pH, making the creation of smooth pH profiles more difficult. The method was first described by Hearn and Lytle [86, 87], and advanced by Frey *et al.*, who generated pH gradients on weak cation exchange columns using mobile phase formulations containing polyampholyte buffers as well as formulations containing simple buffers [88, 89]. The pH gradients created were of limited range, all falling between pH 4 and 6.

1.2.3.3 Predicting pH gradient shape

As described above, the challenge in defining and controlling elution pH profiles using monoprotic and diprotic buffers remains a central factor limiting the use of polyampholyte buffers and the acceptance of preparative ICF by industry. Some efforts have therefore been directed toward developing models that improve understanding of gradients produced using simple buffers. Frey and coworkers used acid-base theory to understand at a qualitative level pH profiles formed on weak anion exchange resins [69-73, 90]. That model permitted the reformulation of buffer components to eliminate those that can specifically interact with the stationary phase, allowing Frey *et al.* to design isocratic elution formulations offering concave or quasi-linear pH gradient shapes [66, 74, 75].

Anderson *et al.* proposed a method to estimate pH gradients formed during gradient chromatofocusing [78] by dividing the column into 10 discrete sections and calculating the pH in each section over time based on local mobile-phase buffer composition. In their model, buffers and protons are passed to subsequent sections and to the outlet of the column based purely on the linear velocity (interstitial convection). A number of anionic buffers were employed in the loading and elution phases. As with the model of Frey and coworkers, estimated pH gradients were in qualitative agreement with experiment.

1.2.3.4 Understanding and predicting protein elution in chromatofocusing

In pioneering chromatofocusing, Sluyterman *et al.* posited that, to a first approximation, elution from the charged stationary-phase matrix occurs at a pH equal to or near the *pI* of the desorbing protein. However, more recent studies have shown that a protein often elutes at a mobile-phase pH away from its *pI*. This is true irrespective of the method by which the *pI* of the protein is determined: popular methods include calculation based on amino acid sequence, and measurement using isoelectric focusing (IEF) gel electrophoresis [88, 91, 92]. This could simply reflect that none of the methods used for *pI* determination provide a protein's *pI* under the solution conditions used during chromatofocusing. Indeed, protein post-translational modifications can significantly shift a protein's *pI* away from its calculated value by up to several units [92], and some proteins are known to resonate between conformations and isoforms (charge states), effectively blurring the concept of a single *pI* value [93]. Moreover, amphoteric amino acids in a protein may be located in regions with varying degrees of solvent accessibility or in the proximity of other chemical groups that influence their titration behavior and

thus the protein's pI . Finally, IEF operates at voltages significantly higher than the redox potential of water. As a result, both conformational changes and chemical modifications can and often do occur in proteins during IEF [56, 94-99]. The definition of pI , at least as an unequivocally measured and/or calculated property of a native-state protein, is therefore not clear.

However, these uncertainties in the definition of pI do not explain the fact that protein elution during chromatofocusing is known to exhibit a complex, nonlinear dependence on column operating conditions and mobile phase compositions. Anderson *et al.* found that protein elution time is strongly affected by buffer concentration in the mobile phase [79, 91], and, based on this observation, hypothesized that elution in gradient chromatofocusing is governed by both pH and ionic strength [91]. Although they did not advance this hypothesis in terms of theory development, they did show that separation characteristics (peak width and resolution) can be altered through changes in buffer concentrations.

Frey *et al.* also found that elution pH values in chromatofocusing are inconsistent with expected pI values [76]. They developed the first theory to account for this effect [100] by assuming that the shift in elution pH is related to the differential change in protein charge with pH near the pI of the protein, $(dz / dpH)_{pI}$. Their model represents a significant advance, but is nevertheless only valid for elution pH values that fall near the expected pI of the protein. For four proteins whose elution behavior satisfies that

condition, they reported accurate prediction of retention times, a noteworthy achievement.

1.2.4 Challenges in chromatofocusing application and theory

Although chromatofocusing using simple buffers can provide outstanding resolving power for many protein-containing feedstocks, it has nevertheless not received significant use, particularly in preparative applications, due to a number of contributing factors. Control of pH gradient shape and length has proven difficult operationally and, to date, truly linear gradients have only been achieved using polyampholyte buffers. Thus, a much deeper fundamental understanding must be established as to how mobile phases comprised of simple monoprotic and diprotic buffers can best be designed and used to control protein retention and elution. Moreover, most chromatofocusing systems that have been characterized to date use weak anion exchange media designed for analytical applications. This has restricted scale-up and process-development efforts by industry, where use of preparative stationary phase media is required. Finally, chromatofocusing separations are typically designed to elute proteins at a pH near their pI , where protein solubility is generally at a minimum or nearly so. The high protein loads applied during preparative separations therefore raise concerns over protein (and potentially column) loss by precipitation during loading and elution. As a result, protein loads may need to be reduced to ensure process robustness, eliminating the potential of exploiting the full capacity of the column.

While chromatofocusing has enjoyed widespread use in analytical applications, most notably as the first dimension of MDLC platforms (*e.g.* Beckman ProteomeLab PF2D) for proteomic fractionations, polyampholyte buffers are usually employed, obviating the ability to sculpt the shape of the pH gradient to improve peak capacity. The use of simple buffering species could address this limitation, but current challenges to their implementation must be solved, including the compatibility of these buffer formulations with various analytical downstream processes and detectors such as mass spectrometry.

The issues cited above therefore represent critical barriers to the expanded application of chromatofocusing to analytical separations, as well as to its adoption by industry for the preparative separation of proteins.

1.3 Thesis Objectives

Recognizing those factors that currently limit the fundamental understanding and application of isoelectric chromatofocusing, the goal of the present work is to provide the following technical and theoretical advances:

- The development of a method for formulating mobile phases comprised of monoprotic and diprotic buffers that permit the generation of broad and stable pH gradients from pH 9 (or above) to below pH 5 for chromatofocusing on anion exchange matrices (Chapter 2).

- The development of a method for formulating mobile phases comprised of monoprotic and diprotic buffers that permit the generation of broad and stable pH gradients from pH 3 (or below) to above pH 8 for chromatofocusing on cation exchange matrices (Chapter 3). In both methods, the goal is to identify and utilize buffering species compatible with common protein detection modes, such as UV absorption at 280 nm, and mainstream analytical detection platforms, such as gel electrophoresis and mass spectrometry.
- The development of a robust model to quantitatively predict pH gradient profile as a function of the compositions of the loading and elution phases, and to sculpt pH gradient profiles to maximize separation performance (Chapters 2 and 3).
- The establishment of an improved understanding of the mechanisms governing protein binding and elution in chromatofocusing, and the application of that theoretical knowledge to the development of a new model for predicting elution profiles as a function of column operating conditions and compositions of the loading and elution phases (Chapter 4).
- The application of those advances to representative analytical and preparative protein separations (Chapters 5 and 6).

Chapter 2

Versatile Chromatofocusing on Strong Anion Exchange Media via a New Model that Custom Designs Mobile Phases using Simple Buffers

A method is described for using simple monoprotic and diprotic buffers to create stable mobile phases for sample loading and for achieving an elution pH gradient of desired shape covering any pH range from pH 10.0 to pH 3.5. The method is shown to provide a versatile platform for optimizing and conducting isoelectric chromatofocusing of protein mixtures on strong anion exchange media. The method utilizes a new model, developed here, that combines multiple-chemical and adsorption-equilibria theory to permit *in silico* tailoring of elution pH profiles using mixtures of simple buffers.

2.1 Background

In the chromatofocusing of protein mixtures, an anion exchange column is typically utilized to take advantage of the fact that the *pI* of most proteins falls below physiological pH. To date, weak AEX media has almost always been employed to take advantage of the fact that the buffering capacity of these matrices can help stabilize pH profiles generated within the column in the pH range near the *pK*(s) of the anchored cationic surface ligands. Column equilibration with a moderate to high pH buffer is followed by sample loading in that buffer, which historically has been comprised of polyampholytes offering a diversity of titratable groups. Isocratic or programmed gradient elution is then

applied. Very high peak capacities and tight elution bands can be achieved [81-85, 101-103] due, in part, to the strong band-focusing effect [104].

While increasingly used for analytical separations, chromatofocusing using AEX media has not found significant use in preparative downstream processing (DSP) due to a number of factors. Polyampholytes are chemically complex, expensive, difficult to fully characterize, and known to bind to biologics, making their removal more difficult and increasing the possibility of product contamination [65, 66]. The effects of residual polyampholyte loads on the performance and life cycle of both the AEX media and subsequent DSP operations is also a concern that has not been well studied to date. Efforts have therefore been made to identify ways to replace polyampholytes with mixtures of simple monovalent and divalent buffers, with most of that work focused on controlling the elution pH gradient on weak AEX columns packed with analytical to at most semi-preparative (*e.g.* Mono P) media. Frey and coworkers have made among the most significant contributions [69, 70, 105-107]. On Mono P columns, they demonstrated that simple buffers could be used to create by step (isocratic) elution a quasi-linear elution gradient spanning a fairly narrow range of pH [89]. On that same matrix, they also demonstrated that simple buffers could be used to create a concave elution gradient from pH 4.7 to 3.7 to resolve proteins in clarified *E. coli* cell lysate [76]. Others have made important contributions as well; primarily working with analytical-grade weak AEX media, Anderson *et al.* showed that non-linear gradients spanning a modest range of acidic pH values (7.5 to 3.0) could be achieved using combinations of simple cationic buffers and weak acids [65, 78, 80].

In contrast, work towards using preparative media for chromatofocusing is limited, with the only major study provided by Logan *et al.*, who, quite impressively, generated a quasi-linear pH gradient from pH 9.5 to 5.0 on DEAE Sepharose Fast Flow, a weak AEX column, to purify a recombinant protein product from bacterial periplasmic extract [77]. While weak AEX media is employed in manufacturing, strong ion exchange media is used more often to take advantage of the higher loading capacities provided. Regrettably, work on how best to apply simple buffers to conduct chromatofocusing on strong AEX media is extremely sparse [81-84, 108], with no studies reported to date on preparative media.

Important questions related to how best to implement chromatofocusing at the preparative scale therefore remain and must be addressed to permit more reliable and widespread use of the method. At the top of that list is the need to develop methods 1) to precisely design the composition and pH of the mobile phase used to equilibrate and load sample onto a strong AEX column (buffer A), and 2) to precisely design the composition of the elution phase (buffer B) to stably control the span, shape and slope of the pH gradient so as to maximize purification factor and yield with minimal solvent usage and cost. This is a significant challenge, as to date the seemingly straightforward task of using combinations of simple buffers to generate a truly linear elution gradient spanning a wide pH range has proven difficult to realize [77] (see Chapter 1).

Here, multiple-chemical-equilibria theory is combined with Langmuir-adsorption theory, known and measured column properties, and pK data for a wide range of simple

monoprotic and diprotic buffers to establish an improved model for tailoring the compositions of the load and elution phases so as to create elution pH profiles of defined and stable shape within columns packed with strong AEX media. Since proteins are typically unstable and reactive at pH extrema, the model is designed to permit the creation of stable loading conditions and gradient profiles of any desired shape over the pH range of 3.5 to 10.0. Only simple buffering species that do not produce significant UV responses at 280 nm during the separation are utilized, thereby facilitating protein elution band quantitation. As a demonstration, the model is used to generate stable loading conditions at pH 10.0 and a linear pH gradient from pH 10.0 to 3.5 in a HR10/10 column packed with Mono Q, a semi-preparative strong AEX matrix. These conditions represent true extremes for conducting protein chromatofocusing on a strong AEX column, and are explored here to define the full range over which our method can be reliably applied. The robustness and flexibility of the technique is then demonstrated by creating gradients of pre-designed shape and slope over a range of pH, flow rates, and buffer concentrations. Finally, the method is used to optimize the separation of blood plasma proteins and mixtures of model proteins having a broad range of isoelectric points, as well as to the very high-throughput purification, on a column packed with preparative AEX media, of the recombinant N-lobe of human transferrin from the clarified supernatant of *Pichia pastoris* culture.

2.2 Experimental

2.2.1 Materials for analytical studies

ReadyGel IEF pH 5-8 (Cat. No. 161-1184), IEF 10x cathode buffer (Cat. No. 161-0762), IEF 10x anode buffer (Cat. No. 161-0761), IEF Sample Buffer (Cat. No. 161-0763), IEF Standards pH 4.45 - 9.6 (Cat. No. 161-0310), and Coomassie Brilliant Blue R-250 (Cat. No. 161-0400) were purchased from BioRad Inc. Crocein scarlet (Cat. No. C8822) was purchased from Sigma. 2-propanol (Cat. No. A451-1) and methanol (Cat. No. A412P-4) were obtained from Fisher. The IEF staining solution consisted of 27% (v/v) 2-propanol, 10% (v/v) acetic acid, 0.04% (v/v) Coomassie Blue R-250 and 0.05% (v/v) crocein scarlet in nanopure water, while the destaining solution consisted of 40% (v/v) methanol and 10% (v/v) acetic acid in nanopure water.

2.2.2 Materials for chromatofocusing studies

All buffer solutions used as mobile phases for column equilibration and sample loading/elution were prepared with nanopure water, adjusted to the desired pH with concentrated HCl, and then filtered through a 0.22 μm Durapore[®] PVDF membrane (Millipore) and vacuum degassed. 1,3-Diaminopropane (Cat. No. D23602), diethanolamine (Cat. No. D83303), trizma hydrochloride (Cat. No. T3253), imidazole (Cat. No. I0125), bis-tris (Cat. No. 156663), piperazine (Cat. No. P7003) and lactic acid (Cat. No. L6661) were obtained from Sigma. Glacial acetic acid (Cat. No. A38P-212), hydrochloric acid (Cat. No. A144-225) and potassium phosphate monobasic (Cat. No. P285) were obtained from Fisher.

The prepacked Mono Q HR10/10 strong anion exchange column (void fraction $\varepsilon = 0.36$; porosity $e_{matrix} = 0.64$) was obtained from GE Healthcare Life Sciences, as was the Mono Q 10/100GL (void fraction $\varepsilon = 0.36$; porosity $e_{matrix} = 0.64$) strong anion exchange column. Q Sepharose Fast Flow and Capto Q strong anion exchange media were kindly provided by GE Healthcare Life Sciences. Q Ceramic HyperD 20 strong anion exchange media was kindly provided by Pall Life Sciences. Accell Plus QMA strong AEX media (300 Å average pore size) was obtained from Waters Corporation. Empty columns XK16/20 (Cat. No. 18-8773-01), and HR10/10 (Cat No. 19-7464-01, 18-1541-01, 18-1542-01) were obtained from GE Healthcare Life Sciences. Myoglobin (Cat. No. M1882), carbonic anhydrase (Cat. No. C7025), conalbumin (Cat. No. A0755), α -lactalbumin (Cat. No. L6010), bovine serum albumin (Cat. No. A7906), ovalbumin (Cat. No. A2512), β -amylase (Cat. No. A8781), trypsin inhibitor (Cat. No. T9003), and β -lactoglobulin B (Cat. No. L8005) were obtained from Sigma. Glucose oxidase (Cat No. 49180) was obtained from Fluka. All analyte solutions were prepared in nanopure water to achieve a final concentration of 5 mg mL⁻¹, unless otherwise stated. Prior to the studies reported here, each model protein was purified by chromatofocusing and then stored at 4 °C until use.

2.2.3 Column packing

An AKTAexplorer100 (GE Healthcare Life Sciences), an integrated FPLC system consisting of two LC pumps, a pH flow cell, 3-channel UV detector, conductivity detector, and fraction collector (FRAC-950) was used for all chromatofocusing studies. The system was controlled using the Unicorn 4.12 (Build 213) software. Q Sepharose

Fast Flow and Capto Q media were washed and resuspended in nanopure water containing 0.5 M NaCl, then loaded into XK16/20 columns by inclined pouring to bed heights of 15 cm (Q Sepharose Fast Flow) and 14 cm (Capto Q) at a constant pressure of 0.5 MPa using 10 column volumes (CVs) of mobile phase to ensure stable packing. Q Ceramic HyperD 20 media was packed in a similar manner into a HR 10/10 column (10 CVs of 0.1 M potassium phosphate, 0.5 M sodium chloride mobile phase at pH 6.8; 2.0 MPa packing pressure; 10 cm column height). Accell Plus QMA Anion Exchange Media was suspended in methanol to form a slurry containing 25% (v/v) resin, loaded to a bed height of 10 cm on a HR 10/10 column with the outlet connected to a water aspirator, then washed with 5 CVs of 1 M NaCl and 10 CVs of loading buffer at a constant back-pressure of 2.5 MPa.

2.2.4 Chromatography design and procedures

Proteins were manually injected using a 500 μL sample loop and detected upon elution at 280 nm. A 2 mL in-line mixer was used to mix the two buffers A (the column equilibration and sample loading buffer) and B (the buffer required for isocratic or gradient elution). For eluent pH profile experiments in the absence of a column, the system was first equilibrated with buffer A at a flow rate of 10 mL min^{-1} followed by a programmed linear gradient from 0% (v/v) to 100% (v/v) buffer B at a flow rate of 1 mL min^{-1} . After each run, the system was washed with 5 mL of 20% (v/v) ethanol at a flow rate of 1 mL min^{-1} . For runs involving a column, the column was first equilibrated with 5 CVs to 10 CVs of buffer A, followed by a linear gradient of buffer B, at fixed flow rates of 1 mL min^{-1} (Mono Q HR10/10 and Mono Q 10/100GL), 5 mL min^{-1} (Q

Sepharose Fast Flow XK16/15 and Capto Q XK16/14) or 25 mL min⁻¹ (Q Ceramic HyperD 20 HR10/10 and Accell Plus QMA HR10/10). After each run, the column was washed with 1 CV of 1 M NaCl followed by 5 CVs of 20% (v/v) ethanol at a flow rate of either 0.5 mL min⁻¹ (Mono Q HR10/10 and Mono Q 10/100GL), 2.5 mL min⁻¹ (Q Sepharose Fast Flow XK16/15 and Capto Q XK16/14) or 10 mL min⁻¹ (Q Ceramic HyperD 20 HR10/10 and Accell Plus QMA HR10/10).

2.2.5 pH electrode calibration

Buffer pH values were measured with a pH/Ion Analyzer 350 from Corning, calibrated with standard buffers of pH 4.00 (Cat No. B00765), 7.00 (Cat No. B00813) and 10.00 (Cat No. B00801) from Radiometer Analytical. To eliminate observed flow effects on measured pH values, the pH electrode in the AKTAexplorer100 was adjusted at flow within the column-free system to the static pH values of the starting and elution buffers measured off-line using the calibrated pH/Ion Analyzer.

2.2.6 Gel electrophoresis procedures

The Mini-Protean III electrophoresis unit from BioRad was used to perform gel IEF on each model protein studied. Protein samples were prepared in nanopure water and IEF sample buffer to yield final concentrations of 10 mg mL⁻¹ protein and 5% (w/v) glycerol. Each gel lane was loaded with either 10 µL of a protein sample or 3 µL of IEF standard mixture. Electrophoresis was performed at 100 V for 60 minutes, and then at 250 V for 60 minutes using a Power Station 300 power supply from Labnet International Inc. A final migration at 500 V for 30 minutes using a FB500 power supply from Fisher Biotech

was then conducted. The focused gel was stained with IEF staining solution for 30 minutes and destained overnight with IEF destaining solution.

2.2.7 Mass spectrometry

Protein tryptic digestion, mass spectrometry and database searching were completed in collaboration with The University of British Columbia Laboratory of Molecular Biophysics Proteomics Core Facility (UBC LMB PCF). Aliquots of 0.2 μL of protein fractions collected from chromatofocusing eluents were lyophilized using a SC110A vacuum concentrator and UVS400 vacuum system from Thermo Electron Corp. and then reconstituted in nanopure water. Intact protein mass analysis was performed on a Voyager-DE STR Workstation MALDI-TOF from Applied Biosystems. Protein identification was performed by tryptic digestion followed by analysis on an API Q STAR PULSARi Hybrid LC/MS/MS from LC Packings and Applied Biosystems. A MASCOT database search was performed for protein identification.

2.3. Theory

Temporal and axial prediction of total proton concentrations, as well as prediction of pH values (free proton concentrations) within a chromatofocusing column require accounting for all local speciation in the mobile phase, all buffering capacity provided by the stationary phase, and all adsorption reactions occurring at the stationary phase that influence local proton concentration in the mobile phase. These connected reactions can be collectively modeled using multiple-chemical equilibria theory to treat mobile-phase

speciation, column titration data to treat specific stationary-phase buffering capacity, and Langmuir-type theory to treat sorbate adsorption equilibria.

2.3.1 Governing equations

At any axial position within a uniformly packed cylindrical chromatography column, the temporal change in concentration of a chemical species i within the mobile phase can be described by the continuity equation:

$$\frac{\partial C_i}{\partial t} = D_{ax} \frac{\partial^2 C_i}{\partial Z^2} - \left(\frac{u}{\varepsilon} \right) \frac{\partial C_i}{\partial Z} - \left(\frac{1-\varepsilon}{\varepsilon} \right) \frac{\partial Q_i}{\partial t} \quad (2.1)$$

where C_i and Q_i are the mobile phase and stationary phase concentrations of i , respectively, at time t and axial column position Z . Radial and angular gradients are ignored, and band broadening within the interstitial volume is treated using an (apparent) axial dispersion coefficient D_{ax} for species i . The superficial mobile phase velocity is u and column void fraction is ε . In the special case of studies conducted in the absence of the column, equation 2.1 may be simplified by setting $\varepsilon = 1$, $D_{ax} = 0$ and u equal to the linear velocity within the tubing.

In chromatofocusing on a strong AEX column, equation 2.1 is applied to each negatively charged species (such as acetate, lactate and chloride ions) present in the mobile phase and able to bind to the positively charged resin. When applied to neutral or positively charged species, or to all species in the absence of the stationary phase, equation 2.1 may be simplified to:

$$\frac{\partial C_i}{\partial t} = \frac{\partial}{\partial Z} \left[D_{ax} \frac{\partial C_i}{\partial Z} - \left(\frac{u}{\varepsilon} \right) C_i \right] \quad (2.2)$$

Molecular diffusivities of the monovalent and divalent buffers used in this study in water are known [109] and fall between $6 \times 10^{-10} \text{ m}^2 \text{ s}^{-1}$ and $10^{-11} \text{ m}^2 \text{ s}^{-1}$. Plate analysis of elution peaks under non-binding conditions show that D_{ax} is on average larger by an order of magnitude for these small buffer species, falling near $10^{-9} \text{ m}^2 \text{ s}^{-1}$ based on the relation $D_{ax} = (Hu / 2)$, where H is the height equivalent of a theoretical column plate computed from the Knox equation. The Peclet number (Lu / D_{ax}) is therefore larger than 50 (and in most cases many orders of magnitude larger) at every flow condition used in this study. In addition, elution in chromatofocusing involves application of relatively shallow axial gradients in the concentration of each buffer species, such that $\partial C_i / \partial Z$ is small. For the purposes of predicting the local pH at position Z , it is therefore reasonable to neglect the axial dispersion term in equations 2.1 and 2.2, which greatly simplifies tracking the concentrations of both adsorbing and nonadsorbing buffer species during gradient elution.

2.3.2 Equilibrium relations

In the Brønsted formalism, all buffers are treated as weak acids. Acid-base equilibria for each buffer species B_i within the mobile phase during gradient elution are described by:

$$K_{i1} = \frac{\{(HB_i)^{z+1}\}}{\{H^+\}\{B_i^z\}} = \frac{\gamma_{(HB_i)^{z+1}}}{\gamma_{H^+}\gamma_{B_i^z}} \frac{[(HB_i)^{z+1}]}{[H^+][B_i^z]} = \frac{\gamma_{(HB_i)^{z+1}}}{\gamma_{H^+}\gamma_{B_i^z}} K_{i1}^* \quad (2.3)$$

$$K_{i2} = \frac{\{(H_2B_i)^{z+2}\}}{\{H^+\}\{(HB_i)^{z+1}\}} = \frac{\gamma_{(H_2B_i)^{z+2}}}{\gamma_{H^+}\gamma_{(HB_i)^{z+1}}} \frac{[(H_2B_i)^{z+2}]}{[H^+][(HB_i)^{z+1}]} = \frac{\gamma_{(H_2B_i)^{z+2}}}{\gamma_{H^+}\gamma_{(HB_i)^{z+1}}} K_{i2}^* \quad (2.4)$$

where z is the valence of B_i in its fully deprotonated state, K_{i1} is the first equilibrium constant and K_{i2} is the second equilibrium constant for successive protonation of a diprotic buffer B_i . Quantities in $\{\}$ and in $[\]$ in equations 2.3 and 2.4 are the activities and concentrations, respectively, of the species defined within the bracket. As activities are not convenient units to work with in the laboratory, the last equalities in equations 2.3 and 2.4 define concentration-based equilibrium constants (K_{ij}^*), which are related to their corresponding K_{ij} values through a ratio of ion activity coefficients γ_i . For any monoprotic buffer, $K_{i2} = 0$ and only equation 2.3 is required.

Concentration-based equilibrium constants are related to tabulated protonation constants (pK_i 's) for each buffering species by:

$$pK_{i1} = -\log K_{i1}^* \quad (2.5)$$

$$pK_{i2} = -\log K_{i2}^* \quad (2.6)$$

and for the buffers used in this study, they are reported in Table 2.1 at a temperature of 298.15 K and an extrapolated hypothetical ionic strength of 0 M [39, 40].

The concentrations of all species present in the mobile phase at any axial position Z may be computed through the application of these equilibrium relationships to the total mass balance for each fully deprotonated buffering component B_i^z . This is most conveniently achieved by defining species equilibria in terms of concentration-based formation constants of the form:

$$\beta_{ij}^* = \frac{[(H_j B_i)^{z+j}]}{[B_i^z][H^+]^j} \quad (2.7)$$

where, for example, β_{11}^* is the formation constant for the monoprotonated state of buffer 1 (see Table 2.1), and β_{31}^* is the formation constant for the monoprotonated state of buffer 3 (note that in this formalism $\beta_{i1}^* = K_{i1}^*$ and $\beta_{i2}^* = K_{i1}^* K_{i2}^*$). In equation 2.7, a negative value for the stoichiometric coefficient j indicates the presence and number of hydroxyl ions in the complex.

The concentration of each protonated species is constrained by the total mass balances for the corresponding buffer component B_i and the proton H^+ . These mass balances are given by:

$$T_{B_i} = [B_i^z] + \sum_j [(H_j B_i)^{z+j}] \quad (2.8)$$

$$T_{H^+} = [H^+] + \sum_i \sum_j j [(H_j B_i)^{z+j}] = 10^{-pH} + \sum_i \sum_j j [(H_j B_i)^{z+j}] \quad (2.9)$$

where T_{B_i} represents the total molar concentration of buffer B_i and there are j protons in each protonated species $H_j B_i$ carrying charge $z+j$. These results can be rewritten in terms of the free proton concentration and the concentration of each fully deprotonated species through application of equation 2.7. For example:

$$T_{B_i} = [B_i^z] + \sum_i \sum_j \beta_{ij}^* [B_i^z] [H^+]^j \quad (2.10)$$

where in our studies the indices i sum over all buffers reported in Table 2.1 (note that $z = 0$ for each cationic buffer used), and indices j sum over all protonated states of each buffer B_i .

Finally, it is well known that protonation constants depend on temperature [110]. As suggested by equations 2.3 and 2.4, they also depend on ionic strength I since the ratio of activity coefficients depends on I . Comprehensive theories, such as the specific ion interaction theory of Guggenheim and Turgeon [111], have been established to compute these ionic-strength and associated ion-activity-coefficient corrections to pK . But, as the ionic strength remains low in chromatofocusing (< 0.2 M), the correction can be made by

computing required γ_i values for all ionic species using the ion activity coefficient model of Davies [112]:

$$\ln \gamma_i = -1.82 \times 10^6 (\epsilon' T)^{-3/2} z^2 \left(\frac{\sqrt{I}}{1 + \sqrt{I}} - 0.2I \right) \quad (2.11)$$

where ϵ' is the solvent dielectric constant at temperature T , z is the ion valence, and I is the ionic strength ($I = 0.5 \sum_i C_i z_i^2$). Activity coefficient corrections are ignored (assumed equal to 1) for all uncharged components/species.

2.3.3 Binding of buffer components to the stationary phase

In the chromatofocusing systems under study, the hydroxyl ion OH^- , the chloride ion Cl^- , and each buffer species carrying a negative charge number (*e.g.* lactate and acetate) are expected to bind to the positively-charged resin as described by the multicomponent monovalent binding isotherm for ion exchange:

$$Q_i = \frac{Q_i^{\max} K_{b_i} C_i}{[\text{Cl}^-] + \sum_j K_{b_j} C_j} \quad (2.12)$$

where K_{b_i} is the equilibrium constant for the surface exchange reaction:



Here A_i represents any chloride-ion-displacing monovalent anionic species, and Q_i^{max} is the maximum binding capacity of the matrix for component A_i . Application of equation 2.12 tacitly assumes that each adsorbing monovalent anion occupies a single ligand-binding site on the stationary phase without steric overlap with adjacent binding sites. The utility of this assumption is the avoidance of having to use more complex implicit isotherm models, such as the steric mass action model [113], to describe binding of the small, similarly-sized, monovalent buffering components.

In our system, each A_i (chloride ion, lactate ion, acetate ion) carries a charge number of $z = -1$ and the general total mass balance for each of these binding species is given by:

$$T_{A_i} = [A_i^z] + Q_i + \sum_i \sum_j \beta_{ij}^* [A_i^z] [H^+]^j \quad (2.14)$$

$$T_{Cl^-} = [Cl^-] + Q_{Cl^-} \quad (2.15)$$

Equation 2.14 is used in place of equation 2.10 for each binding species A_i .

Finally, due to their ring structure and more hydrophobic nature relative to the other buffer species used, imidazole and piperazine exhibit weak affinity to a relatively small number of secondary (uncharged) binding sites present on the Mono Q. At pH 10.0, imidazole is exclusively present in its deprotonated ($z = 0$) state, while both the $z = 0$ and $z = 1$ piperazine species ($pK = 9.7$) are present. In standard on-column depletion studies, all three species were found to bind to the matrix through a mechanism that did not

involve ion-pairing with the quaternary amines on the stationary phase surface (no observed change in column ion capacity). Binding of all three species was therefore treated as independent of the dominant ion exchange equilibria in the system (equation 2.12), and a standard competitive Langmuir isotherm was used to model this minor secondary process:

$$Q_i = \frac{Q_i^{\max} K_{b_i} C_i}{1 + \sum_j K_{b_j} C_j} \quad (2.16)$$

where the total mass balance on either imidazole or piperazine is given by equation 2.14 with Q_i computed by the linearized form of equation 2.16 since the second term in the denominator is far less than unity under all column operating conditions employed here.

Global regression of the model to a limited set of linear and non-linear pH gradients measured at the column outlet was used to estimate Q_i^{\max} and K_{b_i} values for each adsorbing anion, as well as the lumped $Q_i^{\max} K_{b_i}$ parameter for the binding of imidazole or piperazine. The nonlinear regression was based on minimizing the total sum of squared residuals in pH values computed (equation 2.9) by the model relative to the corresponding measured elution pH data sets.

The new model developed here for predicting and sculpting chromatofocusing elution gradients therefore identifies and accounts for a number of unique mechanisms that influence buffering capacity within a strong AEX column, including the buffers used,

their concentrations and possible protonation states, the dependence of those protonation states on temperature and ionic strength, the release of hydroxyl ions and chloride ions initially bound to the stationary phase, and the binding of specific buffer species, most importantly those carrying a negative charge number of $z = -1$.

The model as derived is designed for prediction of pH gradient profiles on a strong AEX column. In particular, the protonation state of the surface ligands of a strong AEX column is unchanged during normal chromatofocusing operation. This is not the case for weak AEX columns. Nevertheless, due to its general structure, the model can be applied to that class of columns by including the buffering capacity of the column in equations 2.9 and 2.12. Here, however, the focus is on strong AEX columns.

2.3.4 Model solution to predict elution pH gradient profiles

Temporal elution pH values were computed from equation 2.9 through numerical solution of the set of coupled transport (equations 2.1 and 2.2), multiple-chemical-equilibria (equations 2.3 to 2.11), and adsorption-equilibria equations (equations 2.12 to 2.16) using a finite difference iteration scheme written in MATLAB 6.1. Initial and boundary conditions for solution of the continuity equation are:

$$\begin{aligned}
 C_i &= C_i^o & t = 0, & \quad 0 \leq Z \leq L \\
 C_i &= C_i^{feed} & Z = 0, & \quad 0 < t \\
 \frac{\partial C_i}{\partial Z} &= 0 & Z = L, & \quad t \geq 0
 \end{aligned}
 \tag{2.17}$$

where C_i^o is the mobile phase concentration of component i in a column equilibrated with buffer A, and C_i^{feed} is the mobile phase concentration of i in the mixture of buffers A and B being fed into the column to create the elution gradient.

Time and space domains are discretized using a Crank-Nicolson scheme to approximate differentials by a central difference in time and an average central difference in space. The column was meshed in the Z dimension at a density equal to or greater than that required to make solution of the model independent of mesh number. This discretization of the transport/reaction-equilibria equations yields a set of tridiagonal linear algebraic equations that were solved for 1000 time increments.

2.4 Results and Discussion

2.4.1 Buffer selection

Creation of pH profiles of desired shape, length and pH range for isocratic or programmed gradient elution of proteins adsorbed to ion exchange media requires careful control of total buffering capacity along the entire pH range of the gradient. The first goal of this study was to select a set of simple monoprotic and diprotic buffers that together have the potential to provide the necessary buffering capacity across the pH range of 10.0 to *ca.* 3.5 to 4.0. Table 2.1 lists the buffers ultimately selected along with their pK values and a description of the dependence of those values on temperature and ionic strength. Buffers were selected that together offer pK values approximately one unit apart.

Table 2.1: *pK* values of buffer ions at 25 °C and 0 M ionic strength [39, 114]

Number	Buffer	Type	<i>pK</i> ^{0*}
1	1,3 Diaminopropane (DAP)	Cationic	10.55/8.88 ²
2	Diethanolamine (DEA)	Cationic	8.883 ¹
3	Tris (TRS)	Cationic	8.072 ¹
4	Imidazole (IMI)	Cationic	6.993 ²
5	Bis-tris (BTS)	Cationic	6.484 ¹
6	Piperazine (PIP)	Cationic	9.731/5.333 ¹
7	Acetic acid (ACE)	Anionic	4.756 ¹
8	Lactic acid (LAC)	Anionic	3.86 ²

*Dependence on temperature derived from the Van't Hoff Equation: $dpK^0/dT = -\Delta H^0/(19.12 T^2)$

Dependence on ionic strength derived from the Debye-Hückel Equation when $I \leq 100$ mM: $pK = pK^0 + 0.509 (2z + 1) I^{0.5} / (1 + 1.6 I^{0.5})$

Dependence on ionic strength derived by Davies when $100 \text{ mM} \leq I \leq 500$ mM: $pK = pK^0 + 0.509 (2z + 1) (I^{0.5} / (1 + I^{0.5}) - 0.2 I)$

where water is the solvent, $-\Delta H^0$ is the enthalpy of the specific buffer dissociation reaction at 25 °C (J mol⁻¹), T is the temperature (K), z is the net charge of the buffer in its protonated form, and I is the ionic strength (M).

¹ Goldberg, R. N., N. Kishore, and R. M. Lennen. Thermodynamic Quantities for the Ionization Reactions of Buffers. 2002, Biotechnology Division, National Institute of Standards and Technology: Gaithersburg MD, United States of America.

² Instructions 71-5017-89 AE: Mono Q 10/100GL and Mono S 10/100GL Ion Exchange Columns. 2006, GE Healthcare Bio-Sciences AB: Uppsala, Sweden.

The use of cationic buffering species, which are neutrally charged in their deprotonated state and positively charged when protonated, was preferred because those species do not bind the cationic ligands presented on an AEX column. However, a limited number of anionic buffers were required in the elution buffer (buffer B) to maintain buffering capacity at lower pH. No anionic buffers were included in buffer A to insure that the maximum binding capacity of the matrix is maintained during sample loading. Finally, monoprotic buffers were favored over diprotic buffers so as to achieve more facile control of pH gradient profiles through independent changes in the concentration of each buffer used.

Figure 2.1 shows that the simple buffers reported in Table 2.1 can be used to construct a loading buffer (buffer A)/elution buffer (buffer B) pair that generates a linear gradient

(blue line) from pH 10.0 to pH 3.5 within a Mono Q HR10/10 column. This is the first reported demonstration of a stable linear gradient over such a wide pH range using simple buffering agents operating within an AEX column. As detailed below, it was achieved using the buffer-design model derived and described in this work.

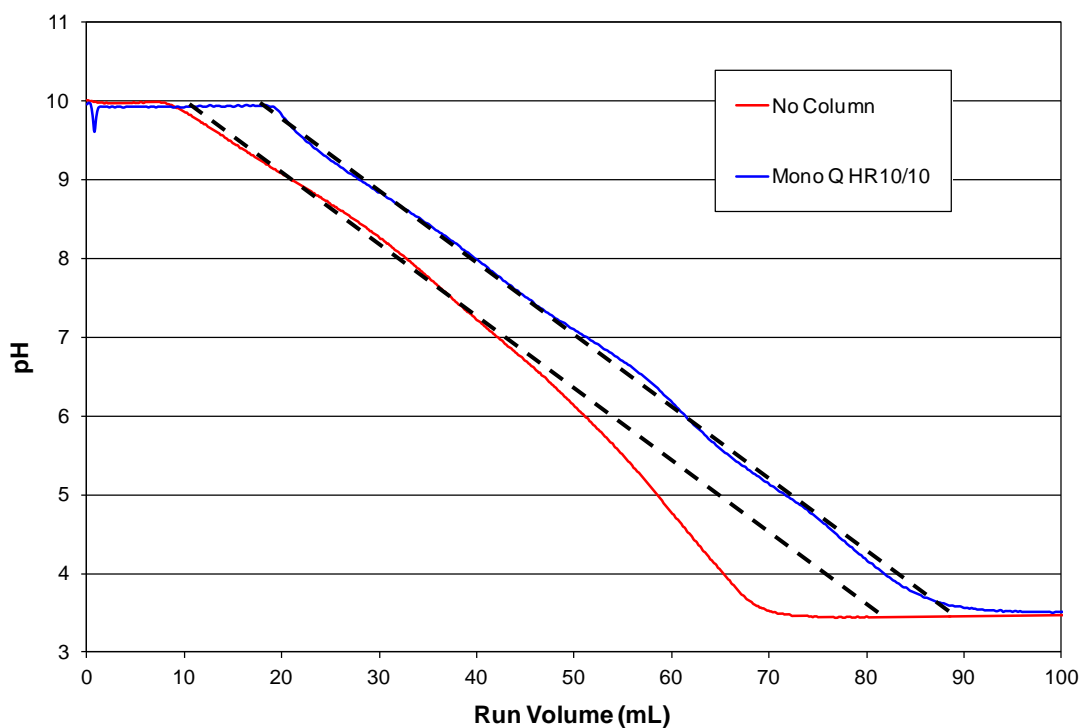


Figure 2.1: Comparison of pH profiles generated at 25 °C and a mobile phase flow rate of 1 mL min⁻¹ using buffer formulation 1003 with (blue) and without (red) the Mono Q HR10/10 strong anion exchange column present in the flow field. Dashed lines provided to define linearity of gradient.

2.4.2 Stationary phase properties

While weak AEX matrices, such as the Mono P traditionally used for chromatofocusing, are thought to provide some buffering capacity within the permissible pH range of AEX column operation (*ca.* 10.0 > pH > 3.5) [22], the strong AEX media Mono Q does not.

Figure 2.2 shows a titration curve for an 8 mL Mono Q HR10/10 column generated by flow of 0.01 M HCl (1 M NaCl, pH 2.0) through the column pre-equilibrated to pH 12.0 with 0.01 M NaOH (1 M NaCl). The data show that all of the strong quaternary ammonium ligands present within the column are titrated above pH 10.0 (Figure 2.2), so that the column itself has no appreciable buffering capacity between pH 10.0 and 3.5.

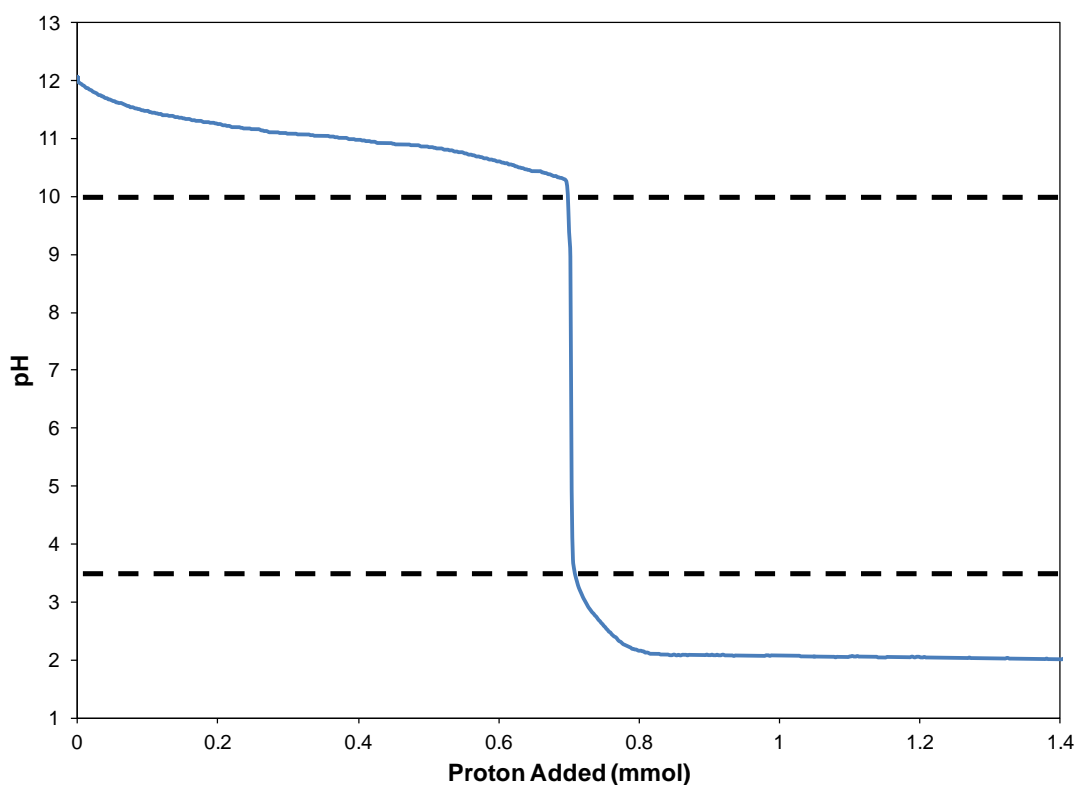


Figure 2.2: Proton titration curve for the Mono Q HR10/10 strong anion exchange column from pH 12.0 to 2.0. Data show that the buffering capacity of the stationary-phase matrix is negligible between pH 10.0 to 3.5.

Although its composition was varied in these studies, buffer A, the equilibration and loading buffer, always contained at least 10 mM of Cl^- . As a result, $[\text{Cl}^-] \gg [\text{OH}^-]$ at all

column operating conditions. Ion exchange reactions at the pre-equilibrated stationary phase surface were therefore modeled based on displacement of the Cl^- ion. This permitted simplification of equation 2.12 to:

$$Q_i = \frac{Q_i^{max} K_{bi} C_i}{[Cl^-] + \sum_j K_{bj} C_j} \quad (2.18)$$

where K_{bi} now represents the dimensionless affinity constant for the exchange of Cl^- with anion i at quaternary amines on the resin surface. For the Mono Q matrix, Table 2.2 reports regressed Q_i^{max} and K_{bi} values for each adsorbing anion, while Table 2.3 reports the regressed lumped $Q_i^{max} K_{bi}$ parameter for imidazole and piperazine species binding to secondary binding sites on Mono Q. The importance of including the binding of these species to the stationary phase is made clear by comparing the gradients produced in the absence and presence of the Mono Q HR10/10 column when the same buffers A and B (given by buffer formulation 1003 in Table 2.4) and the same gradient flow program are employed. The lag time in detecting the gradient when the column is present simply reflects the added void volume of the column and system.

Table 2.2: Regressed binding constants and maximum binding capacity for acetate and lactate on the Mono Q strong anion exchange matrix at 25 °C

Anion	Q_i^{max} (mol m ⁻³)	K_{bi}
Acetate	320 ± 10	3.42 ± 0.01
Lactate	320 ± 10	1.28 ± 0.01

Table 2.3: Regressed lumped linear-isotherm constants for non-specific binding of imidazole and piperazine on the Mono Q strong anion exchange matrix at 25 °C

Buffer	Molecular Formula	$Q_i^{max} K_{bi}$ (m ³ mol ⁻¹)
Imidazole	C ₃ H ₄ N ₂	7.0 ± 0.2
Piperazine	C ₄ H ₁₀ N ₂	1.1 ± 0.3
Piperazine H ⁺	C ₄ H ₁₀ N ₂ H ⁺	5.2 ± 0.3

Table 2.4: Model-derived buffer species concentrations (mM) in various formulations of buffer A/buffer B pairs used for AEICF sample loading and gradient elution.

Buffer		pH	DAP	DEA	TRS	IMI	BTS	PIP	ACE	LAC
1003	Starting	10.0	10	10	10	10	10	10	0	0
	Elution	3.5	10	10	10	10	10	10	10	10
0301	Starting	10.0	2	2	2	2	2	2	0	0
	Elution	3.5	10	10	10	10	10	10	10	10
0302	Starting	10.0	10	10	10	10	10	10	0	0
	Elution	3.5	2	2	2	2	2	2	2	2
0303	Starting	10.0	2	45	2	2	2	2	0	0
	Elution	3.5	2	45	2	2	2	2	45	45
0304	Starting	10.0	2	2	2	45	45	2	0	0
	Elution	3.5	2	2	2	45	45	2	2	2
0305	Starting	10.0	2	2	2	2	2	35	0	0
	Elution	3.5	2	2	2	2	2	35	10	10

The key difference then is that the shapes of the two gradients produced under otherwise identical operating conditions are not the same: conditions producing a nonlinear gradient in the absence of the column (red line) produce a linear gradient (blue line) in the presence of the column. Gradient nonlinearity in the column-free system arises due to the absence of acetic acid and lactic acid in buffer A, which reduces their respective

buffering capacities as buffer B is mixed with buffer A. When the column is present, that reduction is compensated by the binding and accumulation of acetate and lactate anions to the stationary phase as soon as buffer B is introduced, which serves to increase the total and local concentration of each of these species within the column when the mobile phase pH nears their pK' s. As shown in the corresponding on-column speciation diagram (Figure 2.3), a surplus of buffering capacity is thereby created within the column through the protonation and release of acetic and lactic acids back into the mobile phase as the pH

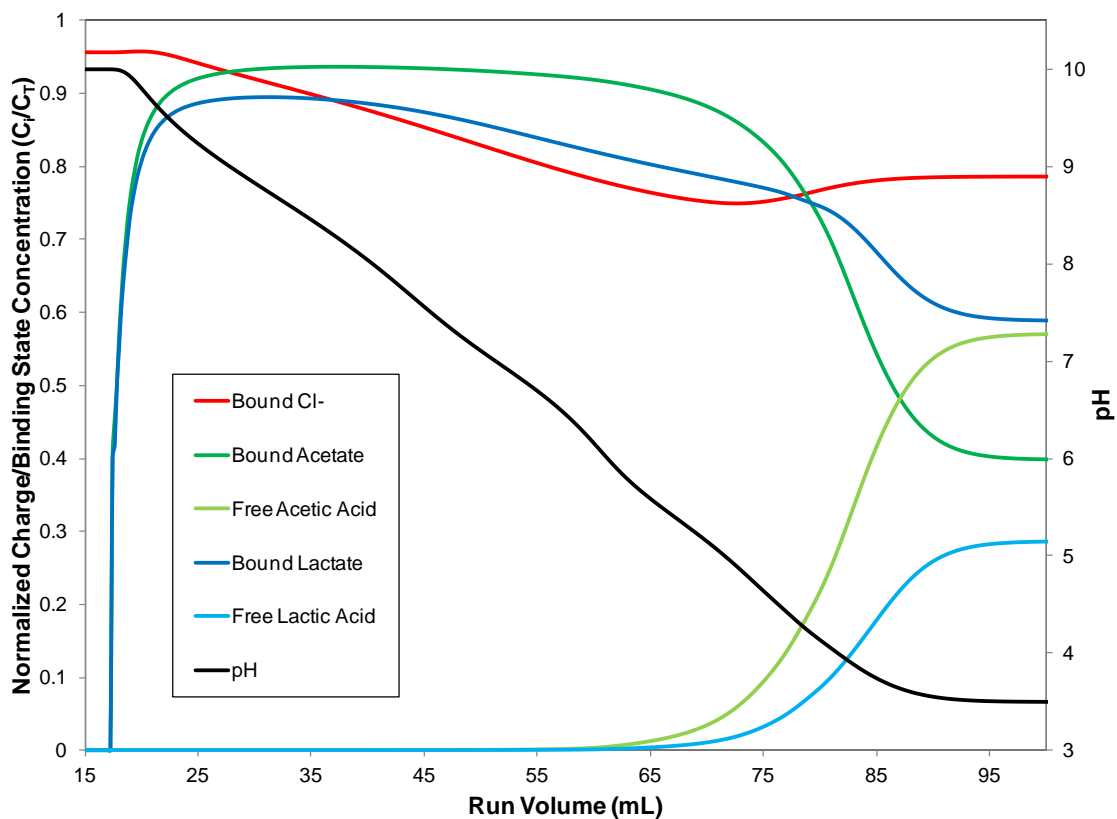


Figure 2.3: On-column speciation diagram at 25 °C of pH-dependent concentrations of bound chloride, acetate, and lactate, and of free acetic acid and lactic acid when buffer formulation 1003 is applied. All species concentrations computed from the combined multiple-chemical-equilibria/surface-adsorption model (Equations 2.1 to 2.17). All species concentrations are normalized by the total concentration of each species in the system, which changes throughout the pH gradient generated using buffer formulation 1003.

is lowered. Significantly smaller contributions are provided by the binding and release of imidazole and piperazine species; those data are not shown to avoid graphical clutter.

These results reported for the Mono Q matrix serve to highlight the challenge in fully understanding and modeling pH profiles formed within AEX columns. That complexity is related, in part, to the nature and extent of weak acid (lactate and acetate) uptake, as well as imidazole and piperazine uptake by the stationary phase matrix, which are dependent on the chemistry of the matrix. As shown in Figure 2.4, buffer formulation 1003 (Table 2.4), which creates a linear elution pH gradient on the Mono Q column, does not do so on other strong AEX media. Though not dramatic, the differences in gradient shape on the different AEX columns are significant, particularly at lower pH where more pronounced departures from linearity are observed on the Q Sepharose FF, Capto Q and Q Ceramic HyperD 20. The Q Sepharose FF and Capto Q resins exhibit stronger binding of anionic buffering species relative to that measured for the Mono Q, resulting in pH gradients that extend across a larger total volume of eluent. Q Ceramic HyperD 20 exhibits increased binding of imidazole and piperazine, resulting in deviations at high pH due to the higher pK values of those species. In contrast, the less often used Accell Plus QMA matrix shows relatively little binding of any of these analytes, allowing pH gradient profiles to be accurately predicted without appreciable adjustment for buffer binding effects within the model. To better understand the influence of these adsorption processes, their effect on the model-based prediction and sculpting of elution pH gradients on the Mono Q column was explored in greater detail.

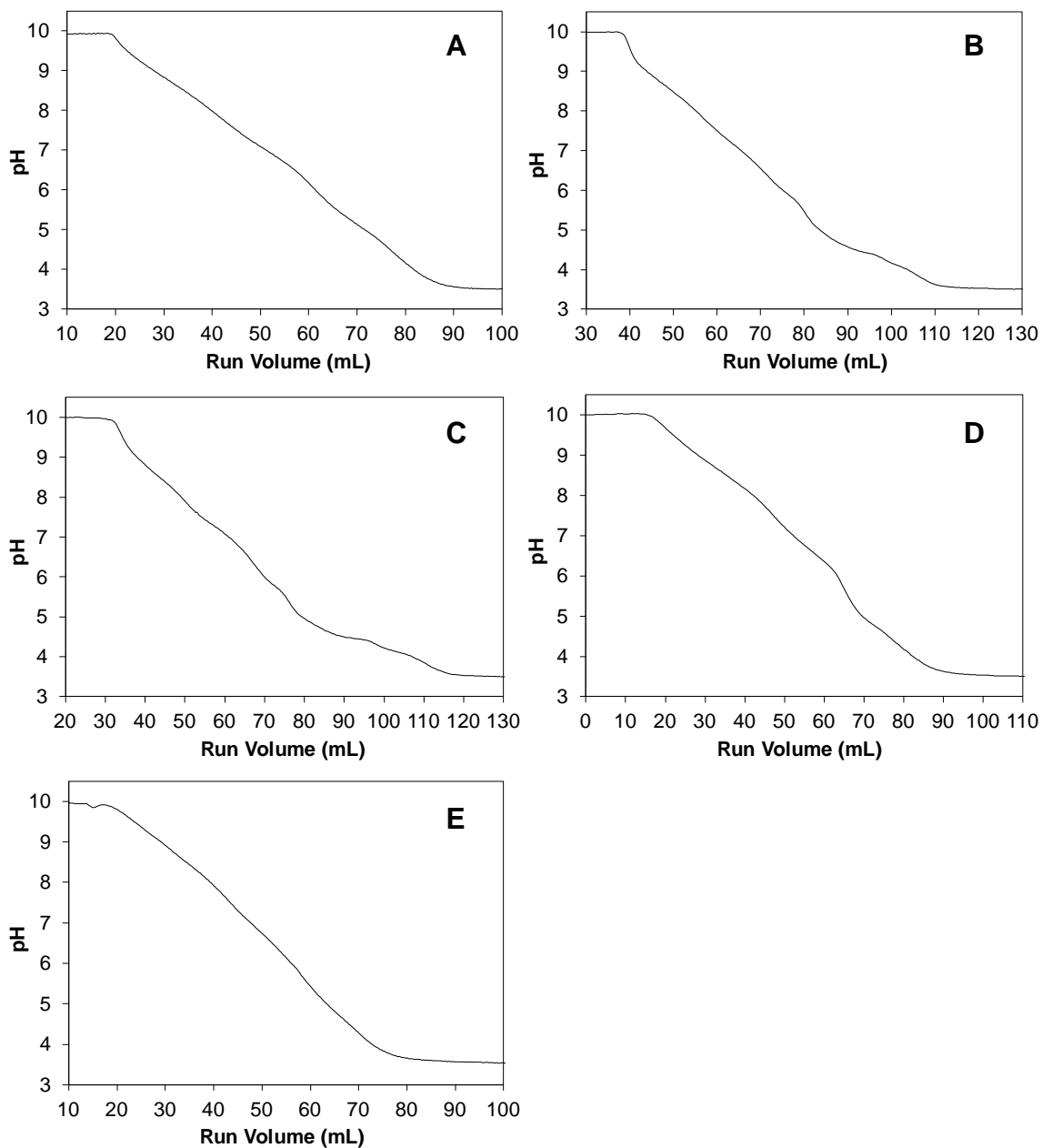


Figure 2.4: Comparison of pH profiles generated using buffer formulation 1003 on the following columns at the specified flow rates: A) Mono Q HR10/10 column (1 mL min⁻¹), B) Q Sepharose Fast Flow XK16/15 column (5 mL min⁻¹), C) Capto Q XK16/14 column (5 mL min⁻¹), D) Q Ceramic HyperD 20 HR10/10 column (25 mL min⁻¹), and E) Accell Plus QMA HR10/10 column (25 mL min⁻¹). All columns operated at 25 °C.

2.4.3 Linear pH gradient prediction, buffer formulation and application

The programmed linear gradient achieved on the Mono Q HR10/10 column was created by using the model embodied in equations 2.1 to 2.18 to formulate the required compositions of buffers A and B. In the absence of a column, the model predicts that buffer formulation (1003 in Table 2.4) will produce a convex gradient spanning pH 10.0 to 3.5. The model-predicted column-free gradient is in quantitative agreement with experiment (Figure 2.5A). When the column is present and the optimized formulation

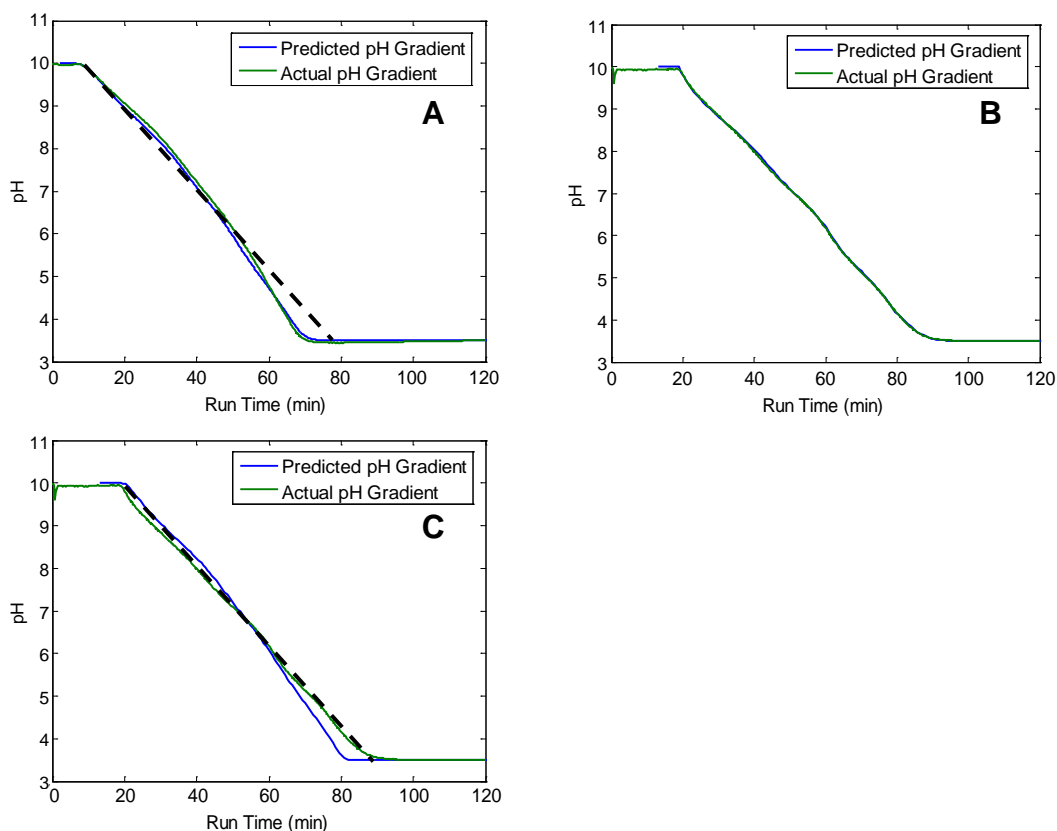


Figure 2.5: Comparison of predicted and experimental pH profiles generated at 25 °C using buffer formulation 1003 at a mobile-phase flow rate of 1 mL min⁻¹ A) in the absence of a column, B) in the presence of the Mono Q HR10/10 strong anion exchange column and accounting for interactions of buffer species with the stationary phase in the model prediction, C) in the presence of the Mono Q HR10/10 strong anion exchange column but ignoring buffer-matrix interactions in the model prediction.

1003 is again used, a linear pH gradient is predicted by the model, as observed experimentally (Figure 2.5B). The use of the model to formulate the buffer compositions needed to achieve a linear pH gradient requires inclusion of those equations describing adsorption of specific buffering components to the stationary phase. Without those contributions, errors in gradient prediction are observed due to a lack of accounting of the added buffering capacity of the retained buffering species (Figure 2.5C).

In the Mono Q column, model simulations show that the generation of a linear pH profile can be achieved by creating near even buffering capacity across the entire gradient. Moreover, due both to the ability to independently control the buffering capacity of each added buffer species and to the lack of buffering capacity of the strong quaternary amines on the column, facile control of the slope of the linear pH gradient is straightforward and robust using the model. This result is not possible (or at least not easily achieved) using conventional polyampholyte buffers since independent adjustment of the abundance and activities of each of the different types of titratable groups is not possible. Moreover, previous attempts to adjust the slope of linear gradients created using cocktails of simple buffers covering a much smaller pH range have resulted in significant nonlinear changes to gradient shape and a reduction in the useful elution pH range [65].

In chromatography, longer gradients (elution times) generally result in band broadening and product dilution. While this is also true in chromatofocusing, the degree of dilution is reduced by the relatively strong band-focusing effect, a feature that can be leveraged to improve separations. As an example, Figure 2.6 reports ICF chromatograms for the

fractionation of a mixture of eight proteins comprising of a wide range of isoelectric points; the Mono Q HR10/10 column and buffer formulation 1003 were used. Under an elution gradient of -0.1 pH mL^{-1} (Figure 2.6A), most of the proteins are either fully or partially separated. Peak widths of approximately 1 mL to 2 mL are typically recorded, which equates to dilution factors of approximately 2 to 4. The coarse fraction of conalbumin is an exception, as it contains a number of different isoforms distinguishable by their intact and tryptic-fragment molecular masses. Conalbumin was included in the feed and resulting chromatogram to illustrate the fact that the resolving power of chromatofocusing causes each isoform to bind and elute at a unique elution volume. The result is consistent with an IEF gel, where conalbumin appears as a smeared zone as opposed to a tightly focused band (Figure 2.7). The somewhat larger bandwidth for bovine serum albumin likewise agrees with its behavior on an IEF gel. In chromatofocusing, we therefore find that the loading of a mixture of protein isoforms can result in broad elution peaks that may or may not be Gaussian in shape, while that for a single protein isoform results in elution as a concentrated tight peak that shows relatively little increase in band broadening with increased elution time.

No significant separation of α -lactalbumin from bovine serum albumin (BSA) is observed in Figure 2.6A. Here, further exploitation of the focusing effect is particularly beneficial, as a reduction in the slope of the gradient to *ca.* -0.05 pH mL^{-1} results in complete separation of α -lactalbumin and BSA without a significant increase in protein dilution. For the same reason, improved separation of carbonic anhydrase and myoglobin, and ovalbumin and β -amylase is also achieved.

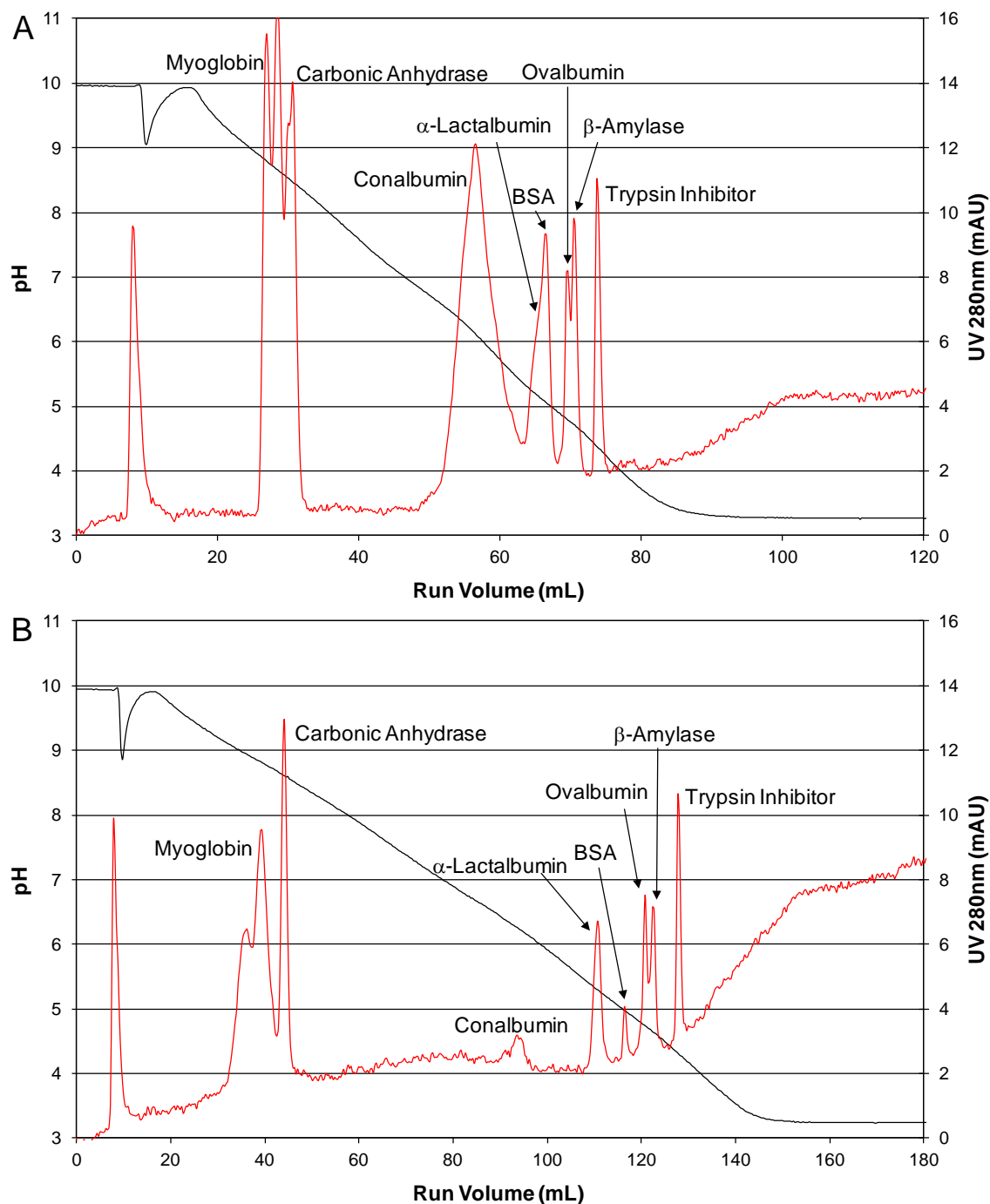


Figure 2.6: A) Elution chromatogram for a mixture containing purified fractions of myoglobin (pI 's = 6.8 and 7.0), carbonic anhydrase (pI = 6.0), α -lactalbumin (pI = 4.2 to 4.5), bovine serum albumin (pI = 5.1), ovalbumin (pI = 4.8), β -amylase (pI = 4.7) and trypsin inhibitor (pI = 4.6), as well as crude (mixed isoform) conalbumin (pI = 6.0 to 6.6) injected as a 500 μ L pulse onto a Mono Q HR10/10 column at 25 $^{\circ}$ C and a mobile-phase (buffer formulation 1003, linear gradient at -0.1 pH mL $^{-1}$) flow rate of 1 mL min $^{-1}$. B) Elution chromatogram for the same mixture of proteins (with a 20-fold decrease of conalbumin concentration) injected as a 500 μ L pulse onto a Mono Q HR10/10 column at 25 $^{\circ}$ C and a mobile-phase (buffer formulation 1003, shallow linear gradient at -0.05 pH mL $^{-1}$) flow rate of 1 mL min $^{-1}$. Significantly improved resolution is achieved with the shallower pH gradient.

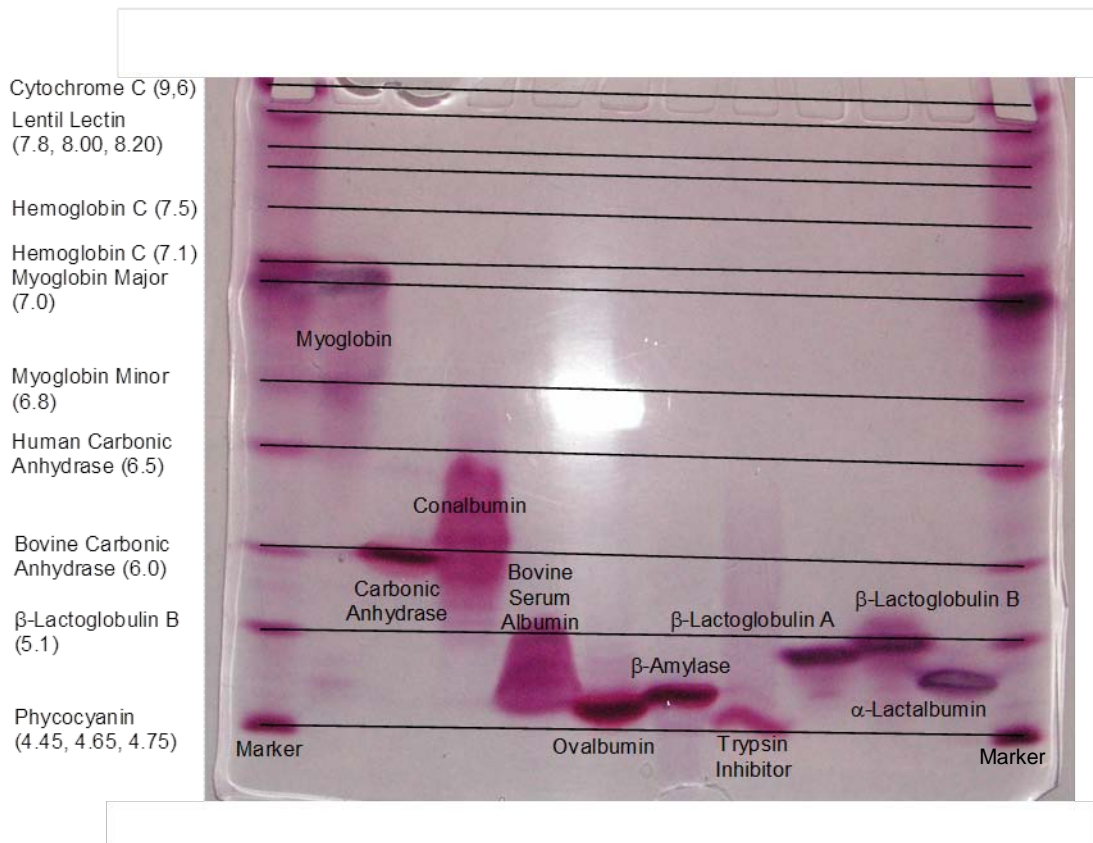


Figure 2.7: Isoelectric focusing (IEF) gel for 10 μL individual protein solution (10 mg mL^{-1}) samples of myoglobin, carbonic anhydrase, conalbumin, bovine serum albumin, ovalbumin, β -amylase, trypsin inhibitor, β -lactoglobulin A, β -lactoglobulin B and α -lactalbumin (lanes 2 to 11). Samples were loaded onto a ReadyGel IEF pH 5-8 and electrophoresed in a Mini-Protean III unit. IEF protein standards (3 μL) containing cytochrome C ($pI = 9.6$), lentil lectin (pI 's = 7.80, 8.00 and 8.20), human hemoglobin C ($pI = 7.5$), human hemoglobin A ($pI = 7.1$), equine myoglobin (pI 's = 6.8 and 7.0), human carbonic anhydrase ($pI = 6.5$), bovine carbonic anhydrase ($pI = 6.0$), β -lactoglobulin B ($pI = 5.1$) and phycocyanin (pI 's = 4.45, 4.65 and 4.75) were loaded to lanes 1 and 12 for reference.

An important final observation is that isoelectric chromatofocusing on a strong AEX column typically elutes proteins in an order that is consistent with their theoretical or reported isoelectric points. However, in general, elution often does not occur at the expected pI , and may in fact occur at a pH significantly removed from the pI , suggesting that chromatofocusing operates as a mixed-mode separation.

2.4.4 Creation of custom pH gradient profiles using the model

The results in Figure 2.6 show that improved peak separation can be achieved through the use of a shallower gradient over the pH range where overlapping peaks elute. To improve throughput, steeper pH gradients may be employed in other zones where a high efficiency separation is not required. This suggests that there could be significant value in using the model to custom-design the span and shape of the elution pH gradient by tailoring the compositions of buffers A and B. Figure 2.8 shows that the model can indeed be used to generate gradients of desired shape, with predicted shapes quantitatively matching experiment across the entire span of the pH gradient. The model-

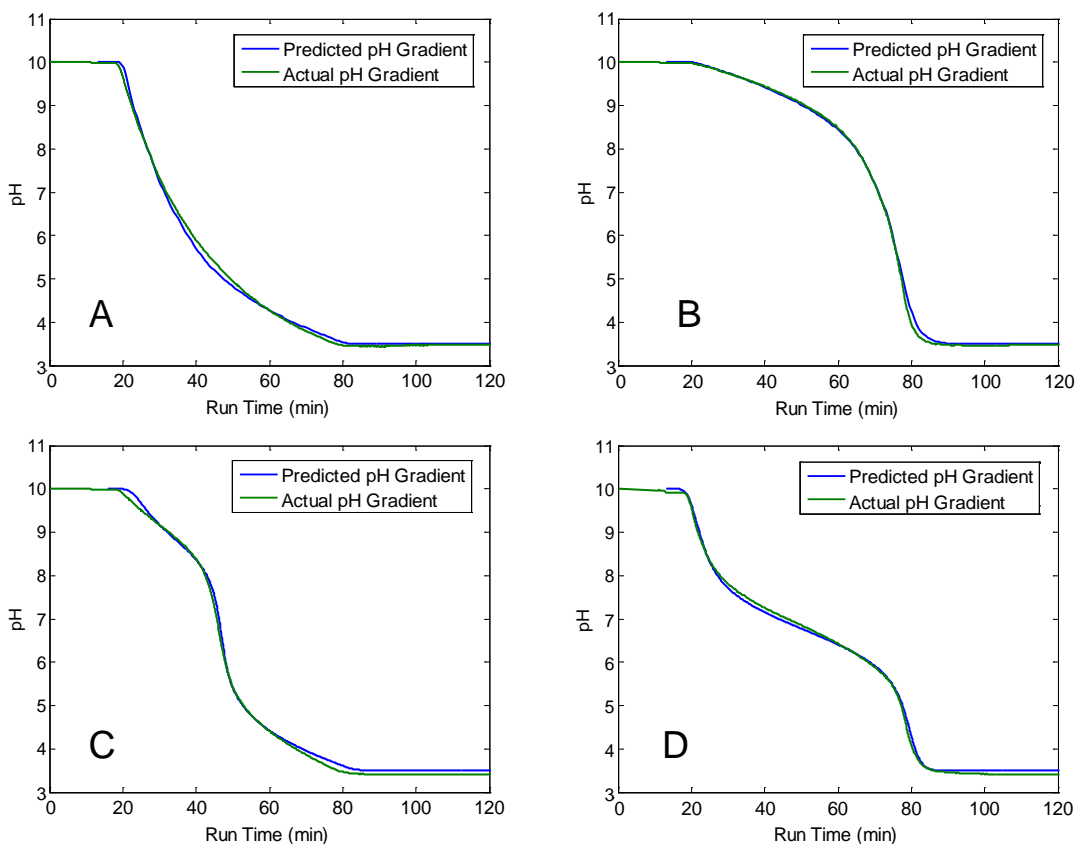


Figure 2.8: Comparison of predicted and experimental pH profiles generated using model-designed buffer formulations A) 0301, B) 0302, C) 0303 and D) 0304 on a Mono Q HR10/10 strong anion exchange column operated at a mobile phase flow rate of 1 mL min^{-1} and $25 \text{ }^\circ\text{C}$.

optimized buffer formulations used to generate each elution profile are reported in Table 2.4. Through proper tailoring of buffer compositions, concave (Figure 2.8A; formulation 0301) or convex (Figure 2.8B; formulation 0302) elution profiles can be generated to improve resolution at low and high pH, respectively. More complex shapes (Figures 2.8C and 2.8D) can also be generated in cases where a shallower or steeper gradient is required in two or more distinct elution pH zones. Again, model predictions match experiment quantitatively.

These custom pH elution profiles should provide improved fractionation of complex samples containing two or more sets of proteins, each characterized by a tight cluster of isoelectric points. An example is provided in Figure 2.9, which compares chromatograms for human blood plasma loaded on the Mono Q column and then eluted using either a linear (Figure 2.9A) or custom non-linear (Figure 2.9B) pH gradient. Peaks in both chromatograms include the twelve most abundant blood proteins (serum albumin, immunoglobulins G, A and M, haptoglobin, α 1-antitrypsin, fibrinogen, α 2-macroglobulin, α 1-acid glycoprotein, transferrin, apolipoprotein AI and apolipoprotein AII) [115], which elute in two distinct pH zones based on their isoelectric points. In the linear gradient, the two most abundant high-*pI* immunoglobulins, IgG and IgA, elute as an unresolved broad peak within elution volumes of 30 mL to 50 mL; relatively poor separation of the major low-*pI* blood proteins is also observed, such that a distinct peak maximum for each is not clearly identified. By sculpting the gradient, a significant improvement in peak capacity (*ca.* 2-fold) is achieved, resulting in the identification of an elution peak for IgG, IgA, and each of the dominant low-*pI* plasma proteins.

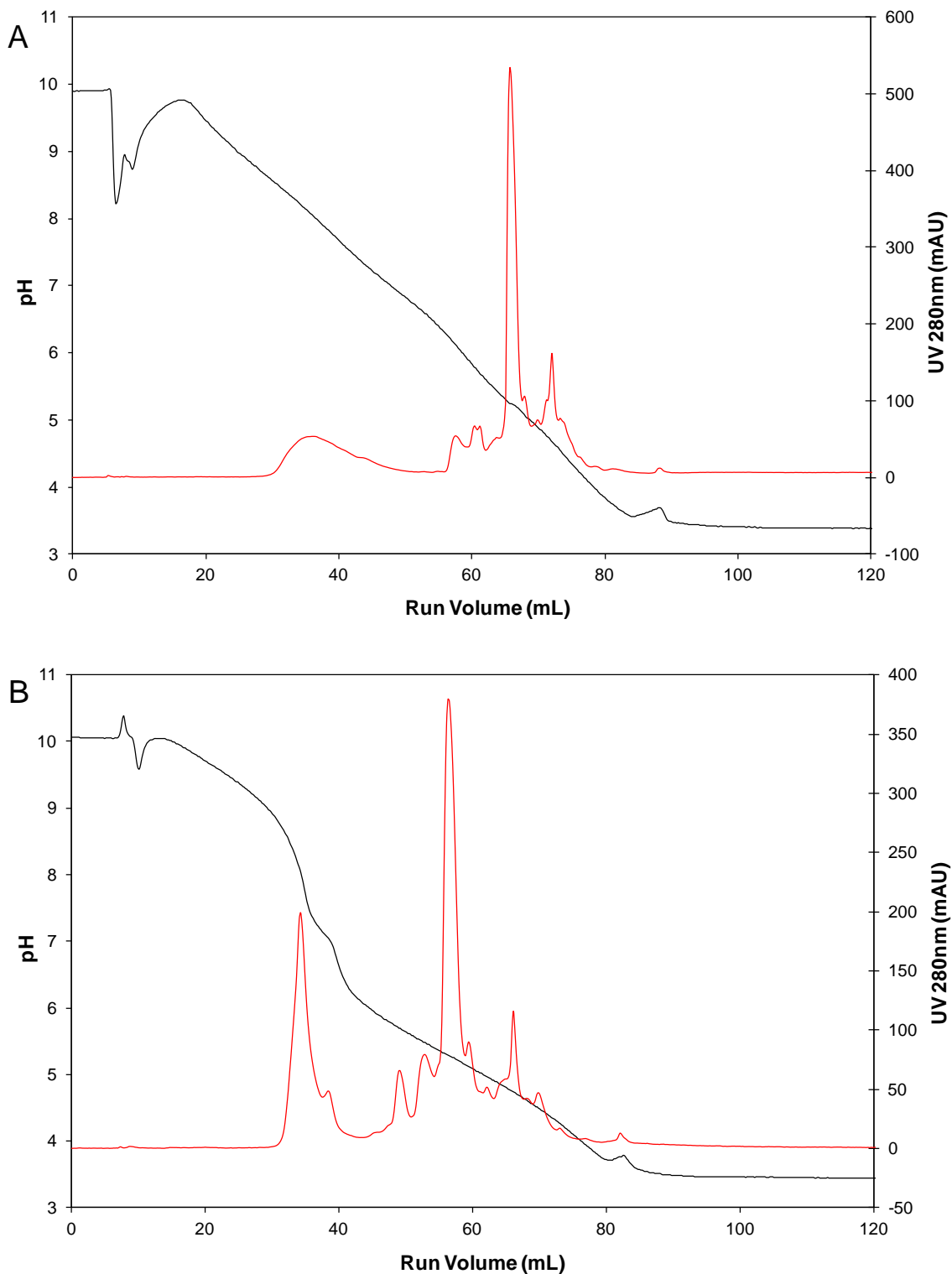


Figure 2.9: Comparison of elution chromatograms for native human blood plasma injected as a 200 μL pulse onto a Mono Q 10/100GL strong anion exchange column operated at 25 $^{\circ}\text{C}$ and a mobile-phase flow rate of 1 mL min^{-1} : chromatogram generated using A) buffer formulation 1003, or B) buffer formation 0305 that was custom optimized using the model to maximize resolution of the 12 dominant proteins in plasma

The model was also used to sculpt a gradient that provides complete separation of a mixture of myoglobin, β -lactoglobulin B and glucose oxidase. Again as a benchmark, the sample was first resolved using a linear pH gradient generated by buffer formulation 1003 (Figure 2.10A). Incomplete separation of β -lactoglobulin B and glucose oxidase is observed. As demonstrated in section 2.4.3, complete separation of these proteins may be achieved by employing a shallower pH gradient. That approach, however, has the disadvantage of increasing column cycle time. A more attractive strategy is therefore to custom design a pH gradient that fully separates all components while maintaining or possibly improving throughput.

One such gradient, generated by model-optimized buffer formulation 0303, is shown in Figure 2.10B along with the resulting chromatogram for the ternary mixture. A β -lactoglobulin B/glucose oxidase peak resolution of 0.95 is achieved, along with improved throughput (glucose oxidase elution peak reaches baseline at 62 minutes, as opposed to 73 minutes in the linear gradient system). In principal, throughput can be improved further by designing and employing a steeper pH gradient. However, the use of buffer formulation 0303 results in the separation of a number of minor myoglobin isoforms that elute as a cluster of small peaks (within elution volumes 32 mL to 42 mL of Figure 2.10B) immediately following that of the dominant myoglobin isoform. A steep gradient between pH 8.5 and 5.0 would therefore need to be designed with care so as to avoid contamination of β -lactoglobulin B with the minor myoglobin isoforms.

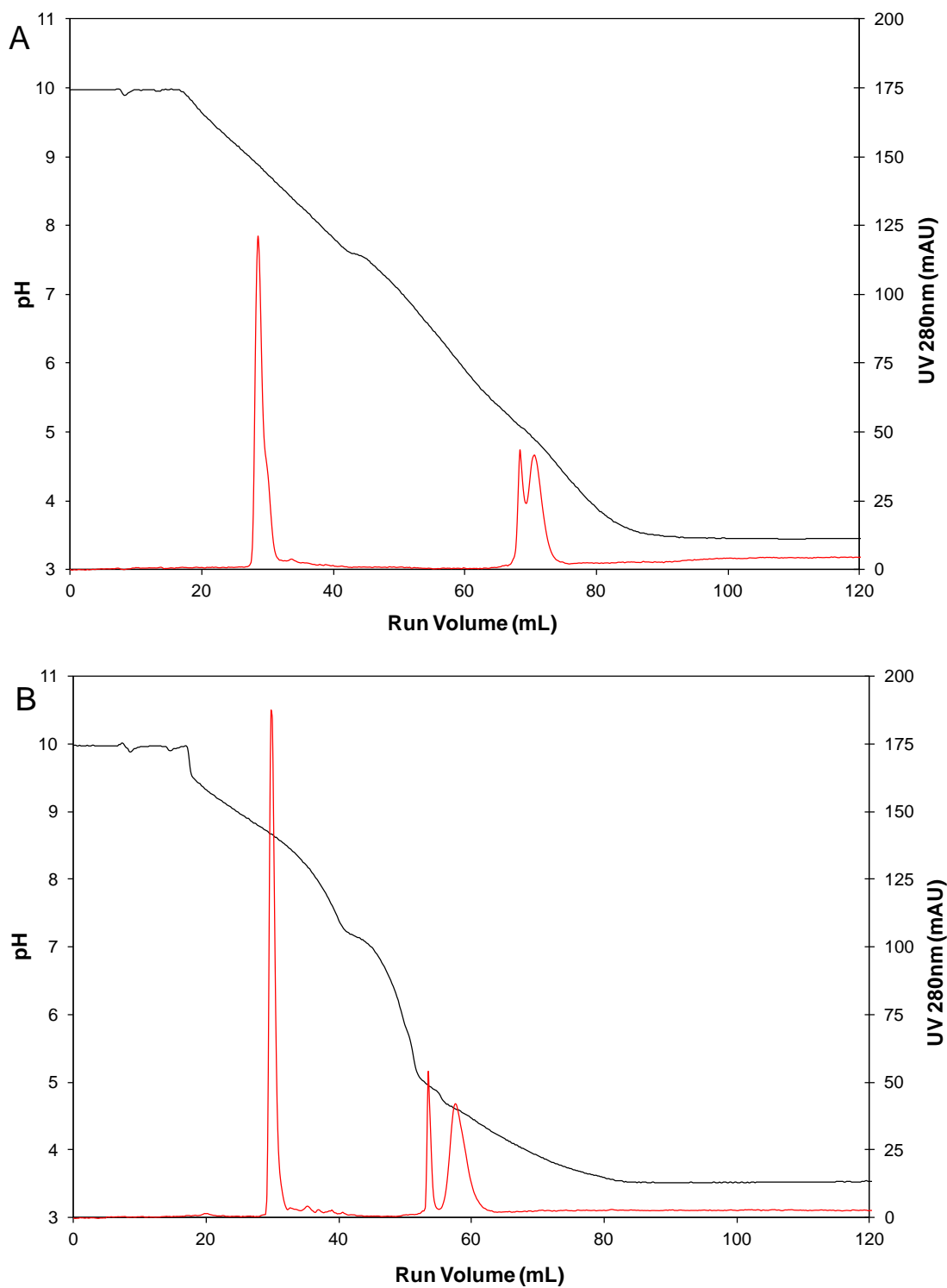


Figure 2.10: Comparison of elution chromatograms for a mixture of 1.21 mg mL⁻¹ myoglobin, 1.00 mg mL⁻¹ of β -lactoglobulin B and 0.75mg mL⁻¹ glucose oxidase injected as a 500 μ L pulse onto a Mono Q HR10/10 strong anion exchange column operated at 25 °C and a mobile-phase flow rate of 1 mL min⁻¹; chromatogram generated using A) buffer formulation 1003, or B) 0303 that was custom optimized using the model to maximize resolution of the three proteins and their minor isoforms

Here, a gradient covering a large pH range was purposely applied. However, the crafting of a gradient covering a narrow pH range is also possible using the model (it is in fact easier), and could and should be used to resolve any mixture in which the *pI* of all proteins lies within a single narrow pH range.

2.4.5 Isolation of the N-lobe of human transferrin using a preparative matrix

While studies on the Mono Q were used to refine and validate the buffer formulation/gradient-design model, one stated goal was to apply that tool to design and refine chromatofocusing of proteins and protein mixtures on preparative strong AEX matrices. As a first step towards that goal, the methods described here were applied to the isolation, from the clarified supernatant of *Pichia pastoris* Mut^S fermentation broth, of the isoform of recombinant N-lobe of human transferrin (hTf/2N) known to exhibit high binding affinity to its cognate transferrin receptor. In this high-density recombinant culture, the final culture supernatant primarily contains hTf/2N with a few host-cell protein or media impurities present. However, the strain produces and secretes at least four unique isoforms of hTf/2N, each possessing a unique molecular mass and/or charge state as determined by tandem mass spectrometry on the isolated intact and tryptic-digested isoforms. As the four isoforms are extremely similar in both sequence and structure, their resolution from culture represents a significant test of the separating power that can be achieved by various modes of strong AEX chromatography, including chromatofocusing.

A HR10/10 column packed with Q Ceramic HyperD 20 media, an ultra fast-flow preparative media, was used. The column was operated at a very high linear velocity, 1.3 cm s^{-1} (25 mL min^{-1}), allowing a complete column cycle, including programmed ionic strength or pH gradient elution, to be completed in less than 5 minutes. Clarified supernatant loaded at pH 10.0 (10 mM DAP), and eluted by standard ion exchange using a 60 mL linear salt gradient (NaCl) from 0 M to 1 M resulted only in modest fractionation of the hTf/2N isoforms, with the dominant and functionally preferred isoform eluting as the first peak centered at an elution volume of *ca.* 32 mL (Figure 2.11A).

In comparison, application of buffer formation 1003 to chromatofocus the same sample on the same column results in significantly greater peak separation, with the dominant and preferred hTf/2N isoform eluting as the last isoform in a nearly pure peak centered at 62 mL (Figure 2.11B). This considerable improvement in separation performance was achieved without significantly increasing total separation time or mobile phase consumption, indicating that custom chromatofocusing on a preparative strong AEX matrix can be used to isolate desired protein isoforms and can compete with or even outperform classic ion-exchange for some separations. Moreover, the target protein elutes into a mobile phase of very low ionic strength: a fraction of the ionic strength into which the protein elutes during ion-exchange. Finally, the entire separation is achieved in approximately 4.5 minutes on the scaled-down column, indicating the potential to achieve high throughputs in preparative ICF separations.

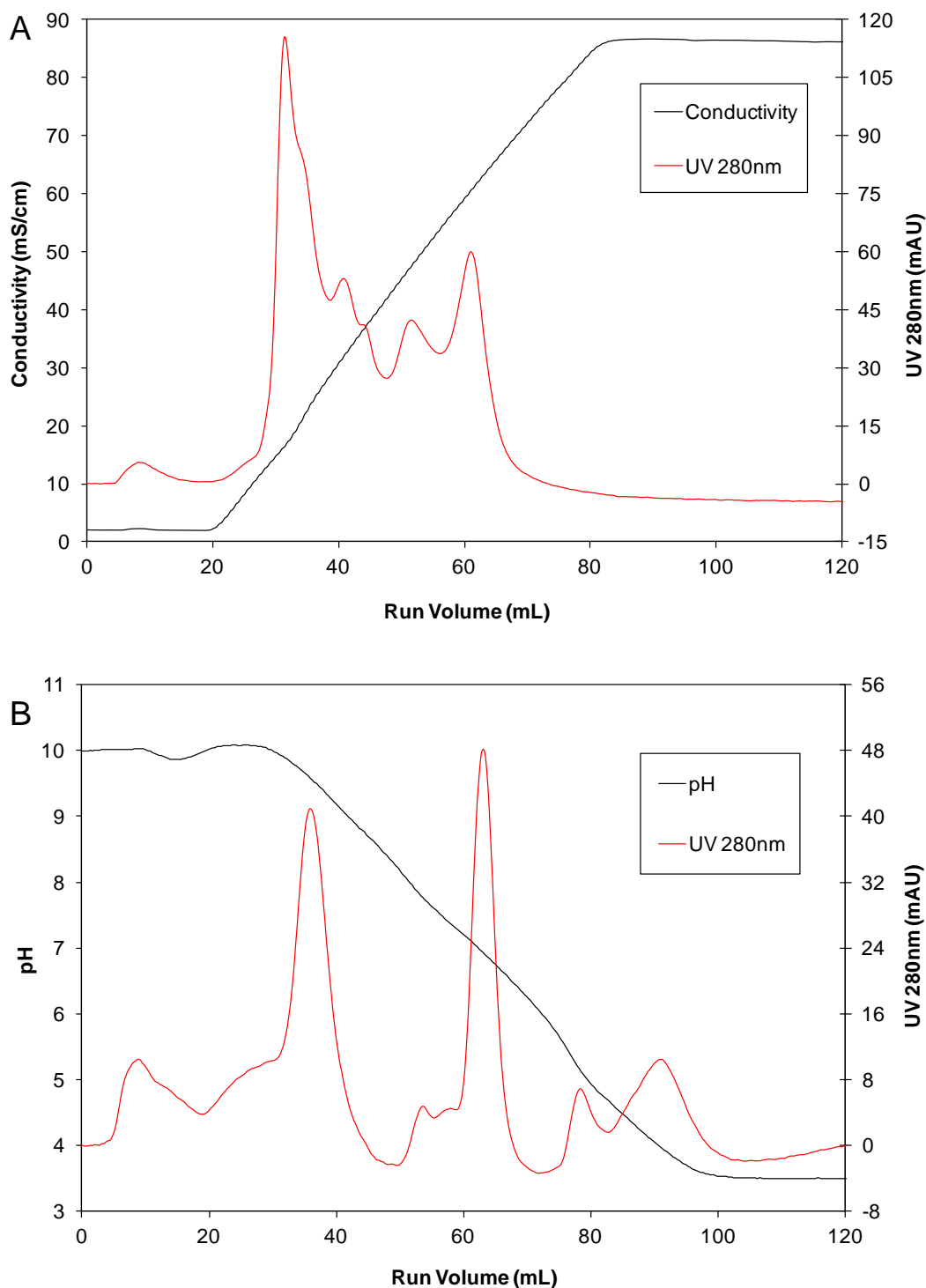


Figure 2.11: Comparison of chromatograms for clarified supernatant from a recombinant *Pichia pastoris* Mut^S fermentation producing four unique isoforms of human transferrin differentiated by their charge state. Both runs conducted on a Q Ceramic HyperD 20 HR10/10 strong anion exchange column at a mobile phase flow rate of 25 mL min⁻¹ and 25 °C. A) elution by A) standard linear-gradient ion exchange (60 mL elution gradient from 0 to 1 M NaCl; 10 mM DAP at pH 10.0), and by B) gradient isoelectric chromatofocusing (buffer formulation 1003, standard linear gradient)

2.5 Concluding Remarks

A novel isoelectric chromatofocusing technique has been presented and tested that permits sculpting of desired pH gradients between pH 10.0 and 3.5 using simple buffering species that do not interfere with downstream procedures such as UV detection and mass spectrometry. The technique is highly flexible and robust, as conditions such as flow rate and pH gradient slope can be varied in the design without compromising gradient shape and span. The method can be applied to a variety of AEX media, including preparative media. The ability to sculpt custom-pH gradient profiles for the isoelectric chromatofocusing of proteins is a valuable tool that can be used to improve the overall peak capacity of complex protein fractionations without increasing separation time. A new and comprehensive model has been developed to permit robust design and optimization of pH gradient profiles that can resolve closely related isoforms of a recombinant protein within a clarified culture supernatant. Key features of the model include terms describing all chemical equilibria and binding equilibria in the system.

Chapter 3

Model Development for Custom Gradient Formulation for Isoelectric Chromatofocusing on a Strong Cation Exchange Column

Methods are presented that extend the model described in Chapter 2 to the design and optimization of buffer formulations and operating conditions for separating complex biological mixtures on a strong cation exchange column. Loading and elution phases containing simple monoprotic and diprotic weak acids are tailored so as to generate linear or sculpted pH gradients over or within the range pH 2.0 to 11.0. A non-buffering salt (sodium chloride) is added to the mobile phase to modulate effects on pH gradient shape resulting from the interaction between free protons and the stationary phase. The solution of a system of partial differential equations describing the change in concentration of all titratable species in the mobile phase is shown to provide good predictions of elution pH gradients. The model also permits *in silico* design of mobile phase compositions for tailoring pH gradient profiles to enhance resolution. Load and elution buffers are designed to resolve mixtures of model proteins with differing isoelectric points. Mobile phase buffers and total ionic strength are also model-adjusted to permit the separation of isoforms of cytochrome C.

3.1. Background

In pioneering isoelectric chromatofocusing (ICF), Sluyterman and Wijdenes focused exclusively on anion exchange media as the stationary phase. However, they acknowledged that the separation technique could also employ a cation exchange column [59]. Nevertheless, virtually all research and commercial applications of the technique reported to date employ anion exchangers as separation media, with only a small number of largely preliminary attempts at cation-exchange-based chromatofocusing having been reported [86-89]. Polyampholyte buffers are not available for use on cation exchange columns, and attempts to use simple monoprotic and diprotic buffers have advanced only to the generation of coarse gradients covering a very narrow, near neutral, pH range [65, 66]. As a result, the basic capabilities needed to permit general use of this potentially powerful separation mode by industry and analytical laboratories are missing.

Building on the methods and model reported in Chapter 2, the aim of the present work is to develop useful gradient design methods when a cation exchange column is employed. A model is developed to tailor pH gradients of desired shape and span within the pH range 2.0 to 11.0. Mobile phases containing only simple weak acids are employed, and terms are added to the model described in Chapter 2 to account for the binding (and desorption) of protons at the stationary phase, a process that can contribute significantly to the pH profile generated under certain column operating conditions. Gradient profiles are predicted by solving a system of equations that include the continuity equations describing the temporal and positional change in the concentration of the free proton and

each titratable mobile phase component i within the column. That set of partial differential equations is coupled with equations describing multiple chemical equilibria within the mobile phase, and species adsorption/desorption at the stationary phase. The model is used to design mobile phase formulations and associated pH gradients capable of resolving mixtures of proteins with isoelectric points spanning a wide range. The model is then applied to the generation of a gradient that permits resolution of isoforms of cytochrome C with the aim of demonstrating an ability to alter separation characteristics so as to improve the performance of difficult separations.

3.2. Experimental

3.2.1 Materials

Malonic acid (Cat. No. M1750), MES (Cat. No. M8250), MOPSO (Cat. No. M8389), HEPES (Cat. No. H3375), BICINE (Cat. No. B3876), CHES (Cat. No. C2885) and CAPS (Cat. No. 2632) were obtained from Sigma. Formic acid (Cat. No. 147930010) was obtained from Acros Organics. Glacial acetic acid (Cat. No. A38P-212), hydrochloric acid (Cat. No. A144-225), sodium hydroxide (Cat. No. S318-500) and sodium chloride (Cat. No. S671-3) were obtained from Fisher. The pK values of buffers used are shown in Table 3.1. Model-derived buffer formulations are shown in Table 3.2.

All buffer solutions were prepared with nanopure water, and adjusted to the desired pH with concentrated HCl, then filtered through a 0.22 μm Durapore[®] PVDF membrane (Millipore) and vacuum degassed.

Table 3.1: *pK* values of buffer ions at 25 °C and 0 M ionic strength [39, 114]

Number	Buffer	Type	<i>pK</i> [*]
1	Malonic Acid (MAL)	Anionic	2.830/5.690 ¹
2	Formic Acid (FOR)	Anionic	3.750 ¹
3	Acetic Acid (ACE)	Anionic	4.756 ²
4	MES (MES)	Anionic	6.270 ²
5	MOPSO (MSO)	Anionic	0.060/6.900 ²
6	HEPES (HPS)	Anionic	~3.000/7.564 ²
7	BICINE (BCN)	Anionic	~2.000/8.334 ²
8	CHES (CHS)	Anionic	9.394 ²
9	CAPS (CPS)	Anionic	10.499 ²

*Dependence on temperature derived from the Van't Hoff Equation: $dpK^0/dT = -\Delta H^0/(19.12 T^2)$

Dependence on ionic strength derived from the Debye-Hückel Equation when $I \leq 100$ mM: $pK = pK^0 + 0.509(2z + 1)I^{0.5}/(1 + 1.6I^{0.5})$

Dependence on ionic strength derived by Davies when $100 \text{ mM} \leq I \leq 500$ mM: $pK = pK^0 + 0.509(2z + 1)(I^{0.5}/(1 + I^{0.5}) - 0.2I)$

where water is the solvent, $-\Delta H^0$ is the enthalpy of the specific buffer dissociation reaction at 25 °C (J mol⁻¹), T is the temperature (K), z is the net charge of the buffer in its protonated form, and I is the ionic strength (M).

¹ Serjeant, E. P., and B. Dempsey. Ionization Constants of Organic Acids in Aqueous Solution. 1979, Pergamon Press: Oxford.

² Goldberg, R. N., N. Kishore, and R. M. Lennen. Thermodynamic Quantities for the Ionization Reactions of Buffers. 2002, Biotechnology Division, National Institute of Standards and Technology: Gaithersburg MD, United States of America.

Table 3.2: Model-derived buffer species concentrations (mM) in various formulations of buffer A/buffer B pairs used for CEICF sample loading and gradient elution.

Buffer		pH	MAL	FOR	ACE	MES	MSO	HPS	BCN	CHS	CPS	NaCl
1021	Starting	2.0	10	10	10	10	10	10	10	10	10	150
	Elution	11.0	10	10	10	10	10	10	10	10	10	50
2101	Starting	2.0	10	10	10	10	10	10	10	10	10	150
	Elution	11.0	2	2	2	2	2	2	2	2	2	100
2102	Starting	2.0	2	2	2	2	2	2	2	2	2	200
	Elution	11.0	10	10	10	10	10	10	10	10	10	50
2103	Starting	2.0	50	2	2	2	2	2	2	50	50	175
	Elution	11.0	50	2	2	2	2	2	2	50	50	75

The prepacked Mono S HR10/10 strong anion exchange column (void fraction $\varepsilon = 0.36$; porosity $e_{matrix} = 0.64$) was obtained from GE Healthcare Life Sciences. Trypsin inhibitor (Cat. No. T9003), insulin (Cat. No. I2643), equine cytochrome C (Cat. No. C2867), bovine cytochrome C (Cat. No. C2037) and lysozyme (Cat. No. L4631) were obtained from Sigma and applied without further purification unless otherwise stated. Ribonuclease A (Cat. No. 17-0442D) and chymotrypsinogen A (Cat. No. 17-0442B) were obtained from GE Healthcare Life Sciences and used without further purification.

3.2.2 Chromatography column operation

An AKTAexplorer 100 from GE Healthcare Life Sciences consisting of two LC pumps, a pH flow cell, a three-channel UV detector with a 2 mm path length, and a conductivity detector, was used. The system was coupled to a FRAC-950 fraction collector from GE Healthcare Life Sciences and controlled using Unicorn 4.11 software. Samples were manually loaded into a 500 μL sample loop and eluted proteins and absorbing buffers were detected at 280 nm. A 2 mL mixing chamber was used to mix loading (buffer A) and elution (buffer B) buffers for gradient formation. The column was first equilibrated with 5 or more column volumes of buffer A (40 mL or more). All runs were performed at a flow rate of 1 mL min^{-1} unless otherwise stated, and sample was loaded in a 2 mL injection cycle followed either by a 60 mL gradient from 0% (v/v) to 100% (v/v) of buffer B then 60 mL of 100% (v/v) buffer B (standard gradient method), or a 120 mL gradient from 0% (v/v) to 100% (v/v) of buffer B then 120 mL of 100% (v/v) buffer B (double gradient method). After each run, the column was washed with 12.5 mL of 1 M NaCl followed by 40 mL of 20% (v/v) ethanol at a flow rate of 0.5 mL min^{-1} .

3.2.3 pH electrode calibration

Buffer pH values were measured with a pH/Ion Analyzer 350 from Corning, calibrated with standard pH buffers 4.00 (Cat No. B00765), 7.00 (Cat No. B00813) and 10.00 (Cat No. B00801) purchased from Radiometer Analytical. To eliminate flow effects on pH, the pH electrode in the AKTAexplorer was calibrated as described in Chapter 2.

3.2.4 Mass spectrometry

Aliquots of protein fractions collected from isoelectric chromatofocusing runs were lyophilized using a SVC 100H centrifugal evaporator (Savant Inc.) and reconstituted in alpha-cyano-4-hydroxycinnamic acid. Intact protein mass analysis was performed on a 4700 Proteomics Analyzer MALDI-TOF/TOF from Applied Biosystems operated in TOF mode.

3.2.5 UV-visible spectrometry

Elution chromatograms for sample mixtures and corresponding null separations were collected in 96 fractions of equal 0.9 mL volume along the pH gradient. Sample and null fractions were matched according to pH equivalence, with the null fraction used as a blank during spectral absorbance analysis. For each normalized sample, absorbance was measured on a Cary 1E UV-Visible spectrophotometer (Varian) over the wavelength range 190 nm to 900 nm. Quartz cuvettes with a path length of 1 cm were used for the blank and sample.

3.2.6 Circular dichroism

Spectropolarimetric analyses of eluted proteins (0.2 mL) were carried out on a J810 circular dichroism spectropolarimeter (Jasco) over the wavelength range 370 nm to 450 nm at a speed of 50 nm min⁻¹ and a response time of 5 seconds. Fractions collected during the null chromatofocusing separation, each matched to the pH of the corresponding eluted protein fraction, were again used as blanks. Quartz cuvettes with a path length of 2 mm were used for all measurements.

3.3 Theory

As noted, theory development for pH gradient design on cation exchangers builds on the concepts and model equations presented in Chapter 2. Positional and temporal changes in the concentration of each mobile species i during column operation are described by the first-order one-dimensional form of the continuity equation for liquid chromatography:

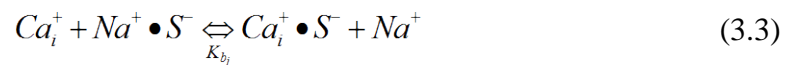
$$\frac{\partial C_i}{\partial t} = -\left(\frac{u}{\varepsilon}\right)\frac{\partial C_i}{\partial Z} - \left(\frac{1-\varepsilon}{\varepsilon}\right)\frac{\partial Q_i}{\partial t} \quad (3.1)$$

where C_i and Q_i are the mobile-phase and stationary-phase concentrations of i , respectively, at time t and axial column position z . Parameters include the superficial mobile phase velocity u and the column void fraction ε . The second-order axial dispersion term has been eliminated from the continuity equation based on the Peclet number values and arguments presented in Chapter 2. Any forward band spreading of

buffer components is therefore assumed to have a negligible effect on pH gradients formed within the column. The value of ε is set to 1 in the absence of a column; in that case, no binding of analyte i occurs and the superficial mobile phase velocity is equal to the linear (interstitial) velocity v . In chromatofocusing using a cation exchange column, equation 3.1 is applied to all solute species present in the mobile phase, including all anionic buffer species and their counter-ions (the sodium ion in this case), as well as the proton. Stern's model [116] is imposed for the stationary phase surface and the liquid layer within half an ion radii of that charged surface (Stern layer). The Gouy-Chapman treatment of the diffuse double-layer [117, 118] is then applied to define ion distributions and the distance away from the surface where the condition of electroneutrality can be applied. Binding at the stationary phase is modeled in terms of exchange reactions with sodium ions pre-bound during equilibration of the stationary phase. Binding of the proton and all other positively charged species (see below) to the negatively charged resin is therefore described by a multicomponent ion exchange binding isotherm:

$$Q_i = \frac{Q_i^{\max} K_{b_i} C_i}{[Na^+] + \sum_j K_{b_j} C_j} \quad (3.2)$$

where K_{b_i} is the binding constant (unitless) for the surface exchange reaction:



Ca_i represents any monovalent cationic species i , and Q_i^{max} is the maximum binding capacity of the stationary phase for component Ca_i . Based on results presented in Chapter 2, local equilibrium is assumed at all column positions for these low molecular weight buffering species. For each neutral or negatively charged solute species present in the mobile phase, or for all solutes in the absence of stationary phase, the final term in equation 3.1 can be neglected.

Though they each carry unit negative charge when fully deprotonated, the weak acids MOPSO, HEPES, and BICINE possess a second low- pK protonation state below which they each carry unit positive charge (Table 3.1). Along with the proton, these species (denoted $MOPSO(H_2)^+$, $HEPES(H_2)^+$ and $BICINE(H_2)^+$) can potentially bind to the negatively charged ligands of the Mono S strong cation exchange matrix. Measured elution pH profiles for a set of formulations of buffers A and B, each producing a unique gradient shape at a unique total ionic strength, were used to globally regress a K_{bi} value for the cationic $HEPES(H_2)^+$ and $BICINE(H_2)^+$ species assuming that Q_i^{max} is a constant given by the ion capacity of the matrix ($135 \pm 10 \text{ mol cm}^{-3}$). Though weak binding of the $MOPSO(H_2)^+$ cationic species can also occur in principal, the pK for protonation of the neutral $MOPSO(H)$ state is too low to observe the $MOPSO(H_2)^+$ species under normal column operating conditions used for ICF of proteins (*i.e.* pH 2.0 to 10.0). A K_{bi} for $MOPSO(H_2)^+$ was therefore not regressed and that species is not considered in the model.

As before, each buffer species B_i that does not bind to the stationary phase is treated as a weak acid in the Brønsted sense, and its positional acid-base equilibrium in the mobile

phase of the column is described by equations 2.3 to 2.11. For each weak acid species A_i used, protonation constants in the form of pK_i values are available in the literature [39] and are reported in Table 3.1.

Because HEPES(H_2)⁺ and BICINE(H_2)⁺ bind to the Mono S matrix, the total mass balance for either HEPES or BICINE must account for the bound mass of their univalent cationic species. The same is true for the Na^+ ion, so that:

$$T_{A_i^-} = [A_i^-] + Q_{i2^+} + \sum_i \sum_j \beta_{ij}^* [A_i^-] [H^+]^j \quad (3.4)$$

$$T_{Na^+} = [Na^+] + Q_{Na^+} \quad (3.5)$$

Equation 3.4 therefore replaces equation 2.10 for each buffer species A_i^- that can bind to the matrix in its fully protonated cationic state. Lastly, the proton may also bind to the stationary phase, so that its total mass balance is given by:

$$T_{H^+} = [H^+] + Q_{H^+} + \sum_i \sum_j j \beta_{ij}^* [A_i^-] [H^+]^j \quad (3.6)$$

Unlike for the anion exchange systems described in Chapter 2, static binding studies show that none of the buffering species selected in this study show an affinity for the Mono S matrix in their uncharged (monoprotonated) state. But that is not to say that modeling of chromatofocusing on cation exchange columns is straightforward. It is different from (and overall more challenging than) modeling chromatofocusing on anion

exchangers due to the fact that binding of protons to the stationary phase must be temporally and spatially quantified to properly track local pH throughout the loading and elution processes.

Solution of the model followed the algorithm and used the initial and boundary conditions described in section 2.3.4.

3.4 Results and Discussion

3.4.1 Development of buffer formulations

As noted above, the use of weak acid buffering species that are neutrally-charged in their monoprotonated state and unit negatively-charged when fully deprotonated was preferred because these species do not bind to the Mono S cation exchange matrix. To ensure even buffering capacity across the pH range of 2.0 to 11.0, a single diprotic buffer, malonic acid, was also required. Together, the set of buffering species offer pK values approximately one unit apart. If a linear gradient was desired, they could therefore be incorporated into a buffer cocktail at near equal or equal concentrations to maintain approximately equal buffering capacity over the entire pH range. The diprotic buffer used was selected so as to offer pK values sufficiently far apart such that the buffering characteristics approximate those of two independent monoprotic buffers applied at equimolar concentration.

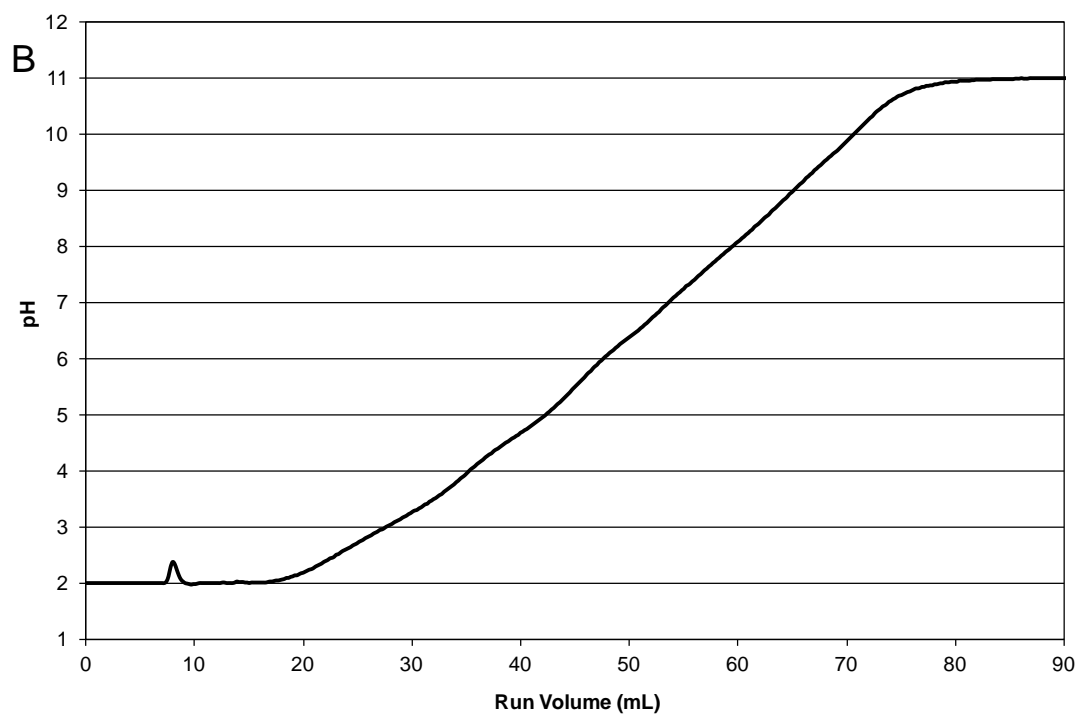
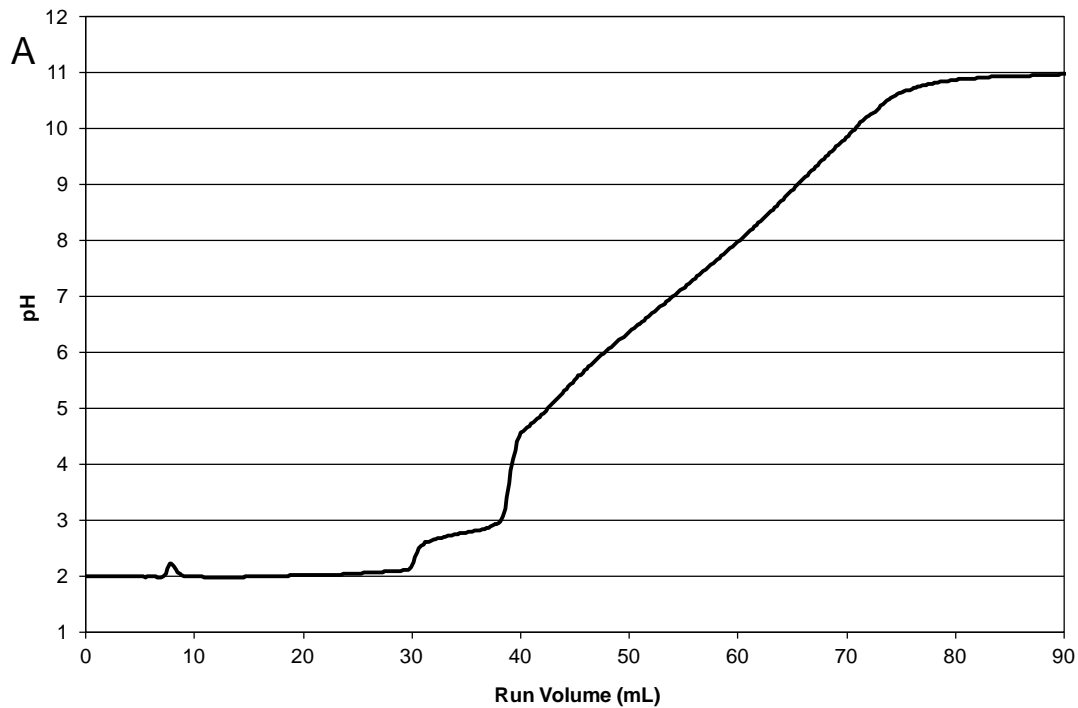


Figure 3.1: Comparison of pH profiles generated using buffer formulation 2101 at ionic strengths of A) 100 mM and B) 150 mM on a Mono S HR10/10 strong cation exchange column at a mobile phase flow rate of 1 mL min⁻¹ at 25 °C.

Due to its negative surface charge density, a cation exchange matrix such as Mono S will bind protons, which can have a direct impact on pH gradient profiles generated within the mobile phase. This is shown in Figure 3.1A, where the release of protons from the Mono S surface upon addition of the high-pH elution buffer B results in a complex non-monotonic and shallow pH profile between pH 2.0 and 3.0 in what is otherwise a linear pH gradient. This result is observed when a column equilibrated with a low-pH starting buffer A retains a relatively large mass of protons that desorb as the higher pH elution buffer B (or a binding protein) is increasingly introduced. Proper accounting of both free and bound proton concentrations in each volume element of the column is therefore absolutely necessary for accurate prediction and tailoring of elution pH gradients. In addition, the model described in this chapter can be used to show that the mass of bound protons and its effect on elution pH gradients can be modulated by changing (*e.g.* increasing) the concentration of another cation, such as the sodium ion, in buffer A. For a Mono S column operated in chromatofocusing mode (starting pH > 2), a sodium ion concentration of 150 mM or greater will typically reduce the initial retention of protons to a level where proton release does not significantly affect pH gradient profile shape, as shown in Figure 3.1B.

3.4.2 Model-based buffer formulation

Equilibrium binding constants for cationic species present above pH 2.0 and having a specific affinity for the Mono S strong cation exchange matrix are reported in Table 3.3.

Table 3.3: Measured stationary phase equilibrium binding constants for buffer species having a specific affinity for the Mono S strong cation exchange matrix

Cation	K_{bi}
H ⁺	1.2 ± 0.1
MOPSO(H ₂) ⁺	N/A*
HEPES(H ₂) ⁺	1.3 ± 0.2
BICINE(H ₂) ⁺	1.1 ± 0.2

* Though binding of MOPSO(H₂)⁺ can occur, that species is not present in the mobile phase under normal column operating conditions (pH 2.0 to 11.0). All values regressed to on-column elution pH profiles assuming Q_i^{max} is given by the ion-capacity of the column ($135 \pm 10 \text{ mol cm}^{-3}$).

Those parameters were used with the model to tailor the compositions of buffers A and B so as to generate a linear gradient from pH 2.0 up to pH 11.0 in a Mono S HR10/10 strong cation exchange column. The predicted gradient for that buffer formulation (1021, Table 3.2) is linear (Figure 3.2) and matches essentially quantitatively with the measured gradient produced by formulation 1021, indicating that the model can serve as a useful tool for rapid *in silico* design of elution conditions for protein chromatofocusing on strong cation exchange columns.

To further illustrate this, several additional buffer formulations were created using the model so as to generate various pH gradient profiles (Figure 3.3), each with distinguishing features that may be useful in improving separation performance. Concave (Figure 3.3A; formulation 2101 in Table 3.2) and convex (Figure 3.3B; formulation 2102 in Table 3.2) profiles were created. In each case, the measured gradient produced on column agrees well with model calculations on which the buffer formulation

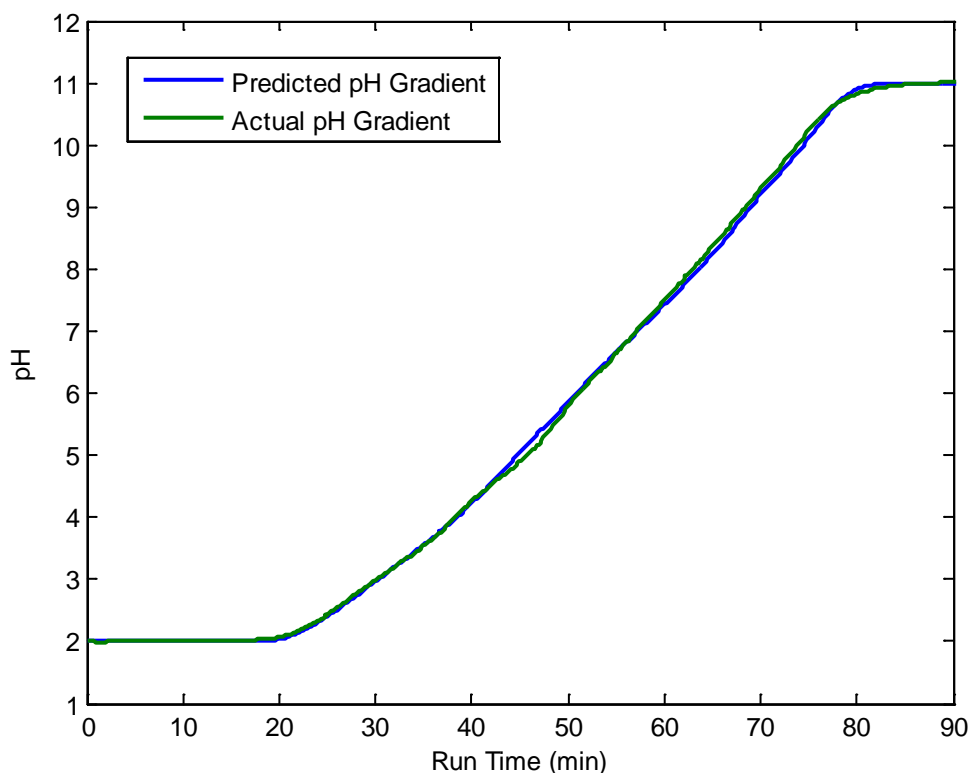


Figure 3.2: Comparison of predicted and actual pH profiles generated using buffer formulation 1021 on a Mono S HR10/10 strong cation exchange column at a mobile phase flow rate of 1 mL min⁻¹ at 25 °C.

was based. Gradients offering a more complex pH profile were also achieved (*e.g.* Figure 3.3C) through the model-based tailoring of a suitable buffer formulation (2103 in Table 3.2). For this profile displaying multiple concavities, the predicted gradient again agrees very well with experiment, showing that the model can be used to create gradients of any desired shape. The ability to customize gradient profiles across a wide pH range should greatly enhance the ability of practitioners to optimize chromatofocusing on a cation exchange column for the purpose of either purifying a single biologic from a complex feedstock, where a shallow and typically linear gradient over a narrow pH can

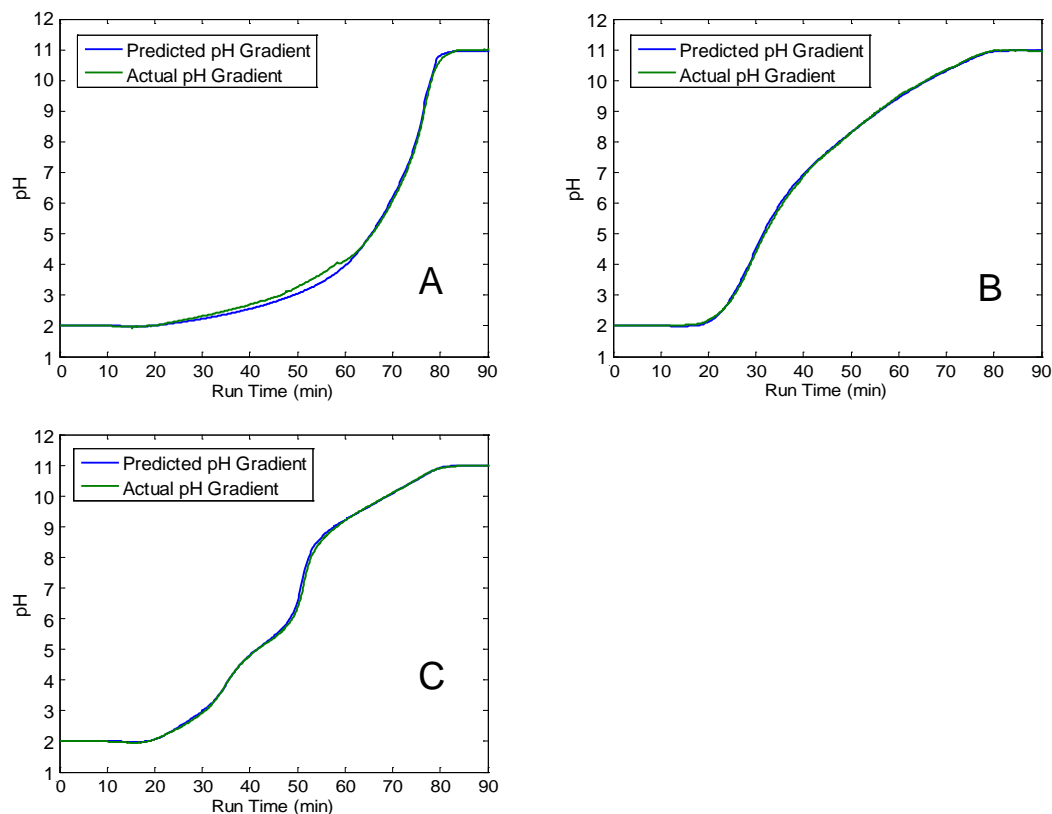


Figure 3.3: Comparison of predicted and actual pH profiles generated using model-derived buffer formulations A) 2101, B) 2102 and C) 2103 on a Mono S HR10/10 strong cation exchange column operated at a mobile phase flow rate of 1 mL min⁻¹ at 25 °C.

be employed, or fractionating a complex mixture into its individual components, where a complex gradient covering a wide pH range may be required.

3.4.3 Chromatofocusing of proteins on a strong cation exchange column

To demonstrate the ability of the proposed gradient-sculpting technique to facilitate the fractionation of complex samples, a mixture of seven proteins covering a wide range of isoelectric points was ICF separated by linear pH gradient elution on a Mono S column using model-derived buffer formulation 1021 (Figure 3.4). All proteins are resolved well

with the exception of bovine and equine cytochrome C, which fail to separate. These two orthologs of cytochrome C differ in charged amino acid composition by a single lysine, present in equine cytochrome C but substituted with guanine in bovine cytochrome C. The two orthologs are therefore highly homologous. In addition, each ortholog is known to be comprised of two distinct conformational isoforms under physiological conditions [93]. In either ortholog, these conformational variants are distinguished by a small change in the relative positions of Lys79 and Met80 that may serve to alter the solvent exposure of basic amino acid residues and thereby result in a small difference in the isoelectric points of the two variants.

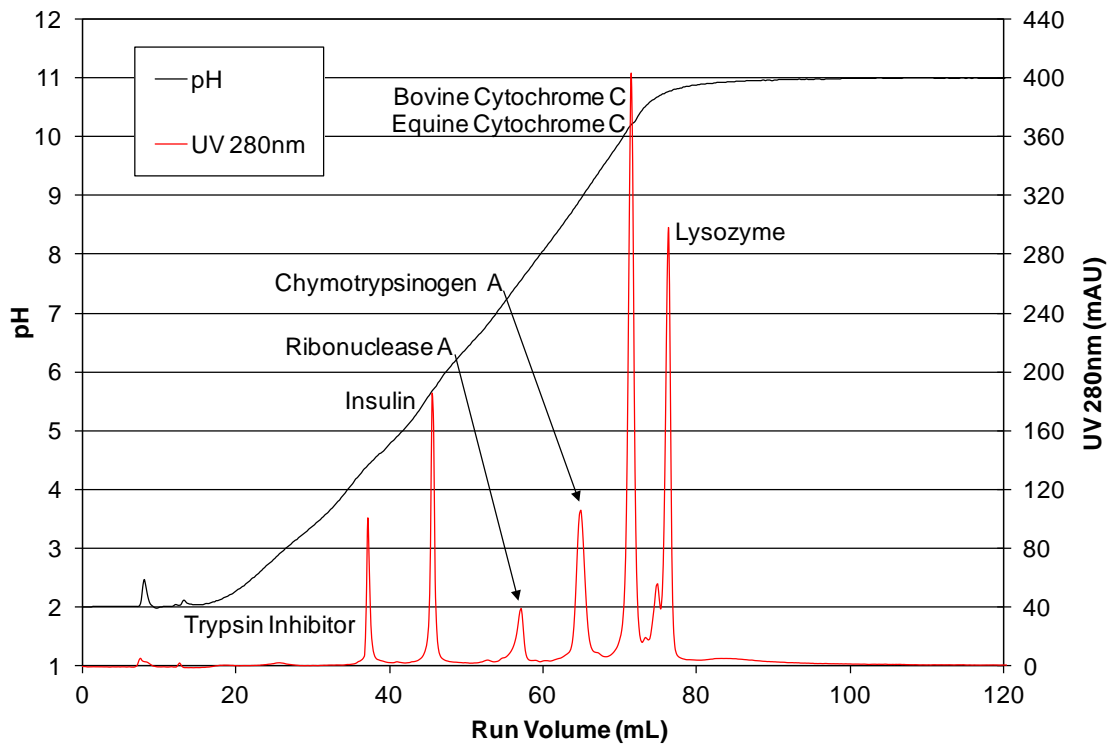


Figure 3.4: Elution chromatogram for a mixture containing trypsin inhibitor ($pI = 4.6$), insulin ($pI = 5.8$), ribonuclease A ($pI = 9.6$), chymotrypsinogen A ($pI = 8.8$ to 9.6), bovine cytochrome C ($pI = 9.6$), equine cytochrome C ($pI = 10.3$) and lysozyme ($pI = 11.0$) and injected as a $500 \mu\text{L}$ pulse onto a Mono S HR10/10 strong cation exchange column at 25°C and a mobile phase (buffer formulation 1021, standard gradient method) flow rate of 1 mL min^{-1} .

As an extreme test of separation refinement, an attempt was made to specifically improve the resolution of the two cytochrome C isoforms from either host source by using the model to design a set of shallow linear gradients from pH 2.0 to 11.0, each operating at a nearly constant ionic strength through adjustment of the total NaCl concentrations in buffers A and B (Figure 3.5). As ionic strength is increased, improved separation of the cytochrome C isoforms is recorded, and at an ionic strength of 200 mM complete peak separation of the two variants can be observed along with partial separation of the orthologs.

As separation of isoforms is a common concern in bioprocessing while that of orthologs is almost never required, each ortholog was loaded separately onto the Mono S column and eluted under the model-derived gradient at 200 mM ionic strength to confirm that complete separation of variants is achieved for either cytochrome C ortholog (Figure 3.6). The ability to realize such a challenging separation illustrates the value of model-based gradient design.

All eluting peaks recorded in Figure 3.6 were collected for mass spectrometry analysis, which confirmed identical masses and sequence for the two isoforms of bovine cytochrome C (Figure 3.6A). Similarly, the two variants of equine cytochrome C were identical in mass and sequence (Figure 3.6B). In addition, the isoforms were subjected to analysis by UV-visible spectrometry (Figure 3.7), with the spectral absorption behavior of the early eluting isoform (Fraction 1) of bovine and equine cytochrome C being similar and consistent with that reported for native yeast cytochrome C, while those of the later

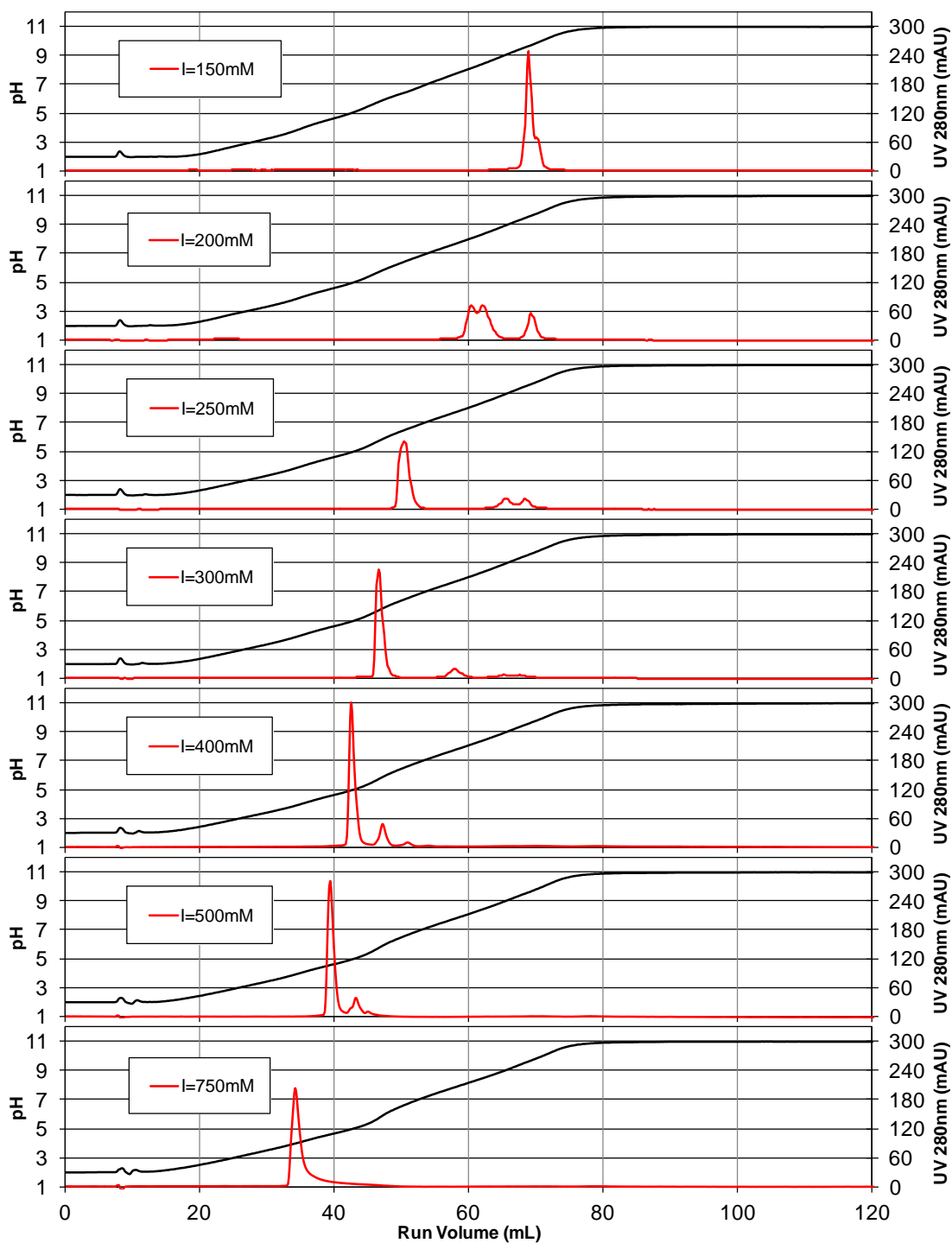


Figure 3.5: Comparison of elution chromatograms generated using buffer formulations having buffer species, each at 10 mM, and an ionic strength of 100 mM, 150 mM, 200 mM, 250 mM, 300 mM, 400 mM, 500 mM or 750 mM. Each model-derived buffer formulation was designed to generate a linear pH gradient from 2.0 to 11.0. The sample is comprised of a mixture of 1 mg mL⁻¹ bovine cytochrome C and 1 mg mL⁻¹ equine cytochrome C. It was injected as a 500 μ L pulse onto a Mono S column operated at 25 °C and a mobile phase flow rate of 1 mL min⁻¹.

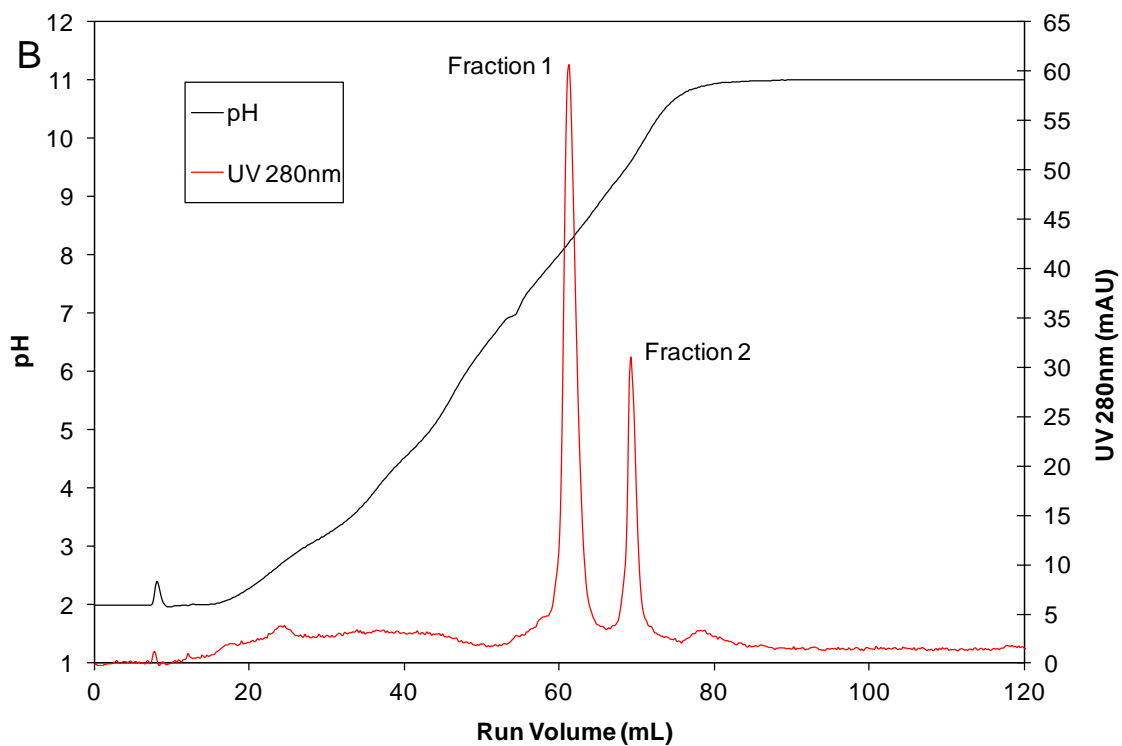
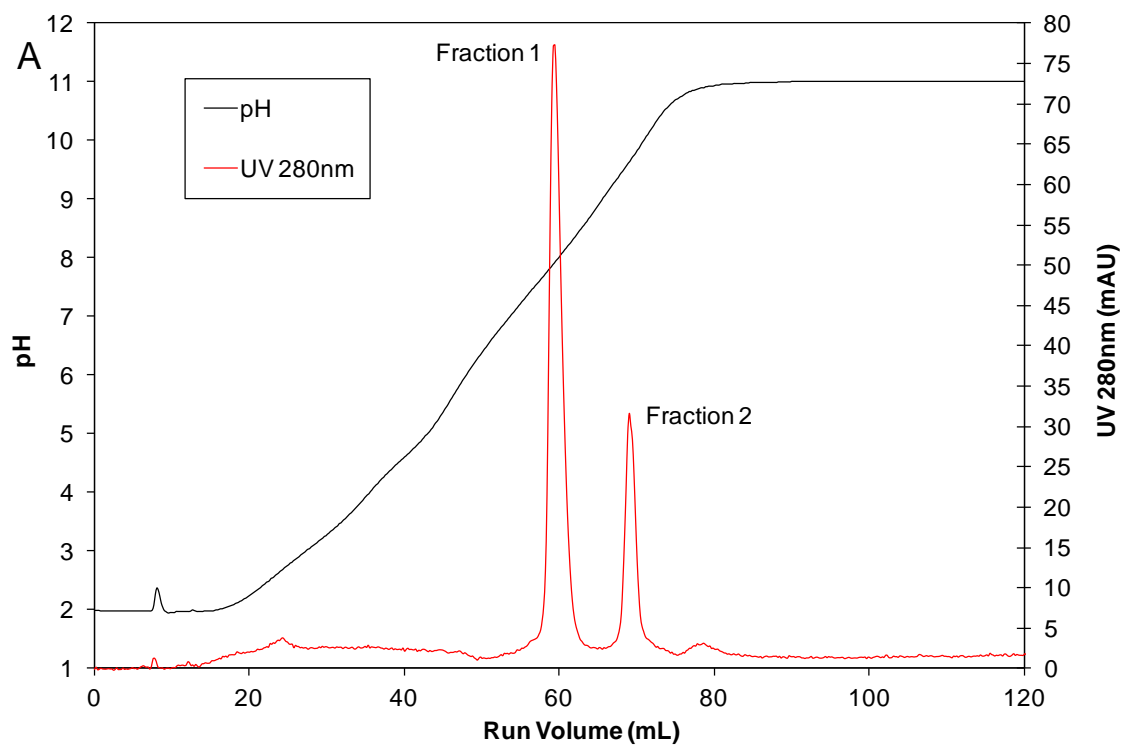


Figure 3.6: Elution chromatograms for separation of isoforms of A) 1 mg mL^{-1} bovine cytochrome C and B) 1 mg mL^{-1} equine cytochrome C injected as a $500 \text{ }\mu\text{L}$ pulse onto a Mono S HR10/10 column operated at $25 \text{ }^\circ\text{C}$ and a mobile phase (buffer formulation 1021, $I = 200 \text{ mM}$) flow rate of 1 mL min^{-1} .

eluting isoforms (Fraction 2) being consistent with the absorbance spectra reported for the alkaline isoform of yeast cytochrome C [93]. This was further confirmed through circular dichroism analysis of the fractions (Figure 3.8), indicating the ability to use the model to define gradients capable of achieving otherwise very challenging separations, including the separation of structurally similar isoforms of a given protein.

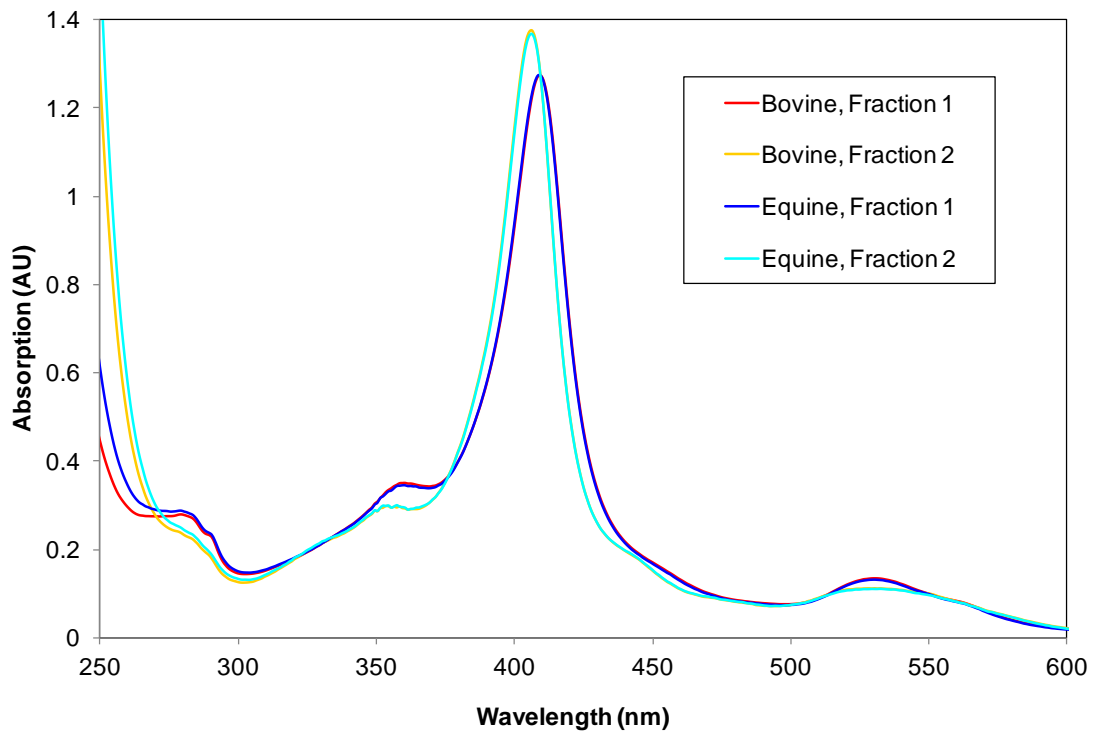


Figure 3.7: UV-visible absorption traces of Fraction 1 (red) and Fraction 2 (yellow) isolated through the resolution of bovine cytochrome C (Figure 3.6A). Also shown and superimposed are the corresponding spectra for Fraction 1 (blue) and Fraction 2 (light blue) isolated through the resolution of equine cytochrome C (Figure 3.6B).

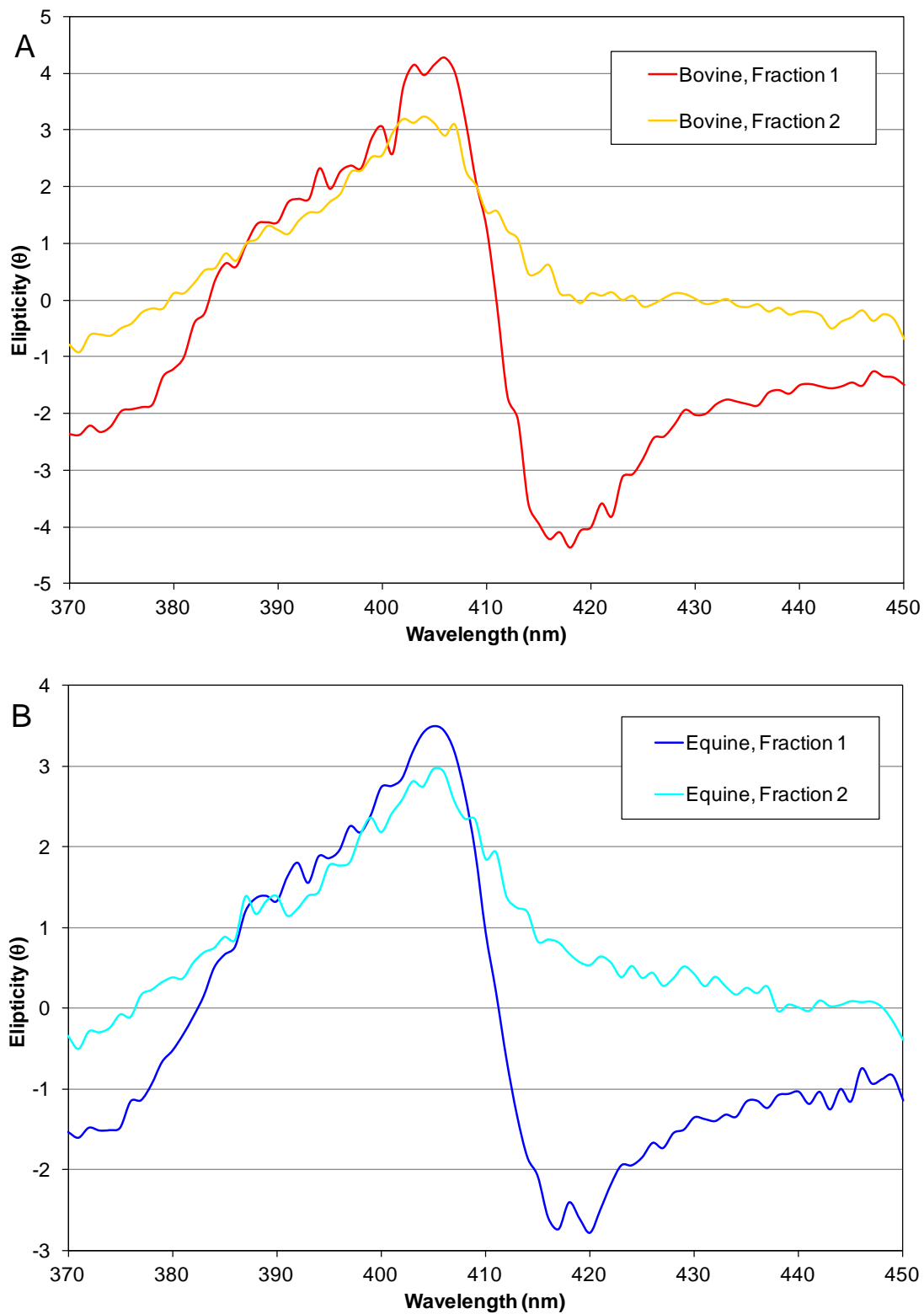


Figure 3.8: Circular dichroism traces of A) Fraction 1 (red) and Fraction 2 (yellow) isolated through the resolution of bovine cytochrome C (Figure 3.6A), and B) Fraction 1 (blue) and Fraction 2 (light blue) of resolved equine cytochrome C (Figure 3.6B).

3.5 Concluding Remarks

Although recognized as applicable by Sluyterman and Wijdenes upon their invention of chromatofocusing, cation exchange columns have received little attention as stationary phases for this mode of chromatography. As a result, necessary tools for designing and optimizing chromatofocusing separations on cation exchange columns are not available. Here, a novel model for tailoring elution pH gradients between or within pH 2.0 and 11.0 using simple weak acids is derived and validated. A computer simulation implementing a finite difference strategy is used to solve the resulting system of partial differential equations describing mass transport and all chemical and adsorption equilibria within the column. The model provides an *in silico* means to optimize compositions of load and elution buffers so as to create a desired gradient shape at a desired ionic strength. The ability to define pH gradient profiles for the isoelectric chromatofocusing of proteins is a valuable tool that can be used to increase the overall peak capacity of specific separations without increasing separation time. Similar to isoelectric chromatofocusing on anion exchange stationary phases, changes in ionic strength and buffer concentrations may be used to modulate both the shape of the gradient and the retention behavior of proteins, permitting otherwise difficult separations to be achieved.

Chapter 4

A Novel Mixed-Mode Model for Interpreting and Predicting Protein Elution during Isoelectric Chromatofocusing

The primary mechanisms influencing protein retention and elution during isoelectric chromatofocusing are defined. Those fundamental findings are used to derive a new model to predict elution times of proteins. The model uses a modified form of the steric mass action (SMA) isotherm to account for both ion exchange and isoelectric focusing contributions to protein partitioning. The dependence of partitioning on pH is accounted for through the characteristic charge parameter m of the SMA isotherm and the application of Gouy-Chapman theory to define the dependence of the equilibrium binding constant K_{bi} on both m and ionic strength. Finally, the effects of changes in matrix surface pH on protein retention are quantified through a Donnan equilibrium type model. By accounting for isoelectric focusing, ion binding and exchange, and surface pH contributions to protein retention and elution, the model is shown to accurately capture the dependence of protein elution times on column operating conditions.

4.1 Background

Since the initial development of isoelectric chromatofocusing (ICF) by Sluyterman *et al.* [58-63] in the late 1970s, chromatographers have reported differences between the ICF elution pH of a protein and the expected isoelectric point (pI) of the protein defined by

isoelectric focusing (IEF) gel electrophoresis. These differences range from less than one pH unit to up to several pH units, either above or below the expected isoelectric point. To date, these differences have proven difficult to predict or even fully understand using available chromatographic theory [88, 91, 92]. Anderson *et al.* reported a correlation between buffer concentration and elution time for various proteins, but did not define the possible mechanisms responsible for this observation [91]. Frey *et al.* investigated the relationship between elution behavior and the sensitivity of the protein's net charge to mobile phase pH near its *pI* [100]. That theory, which is arguably the most advanced to date, is valid for separations where the elution pH of the protein is near its *pI*. Finally, in studies that focused on classical ion exchange chromatography, not ICF, Tsonev *et al.* reported a strategy for qualitatively estimating retention factors from isocratic elution data, and suggested that the method may be of use in estimating the salt concentration at which a protein will elute when the pH of the mobile phase is invariant [119]. While each of these studies has or can be used to advance our general understanding of chromatofocusing, they also make clear that further developments in the fundamental understanding and prediction of protein elution during chromatofocusing are needed. In particular, though strides toward improving ICF have been made over the past several decades, especially in the areas of separation resolution, robustness and cost [65, 66, 74, 76-78], the technique has yet to be adopted by industry, due in part to the unsatisfied need to elucidate, and ultimately control the complex mechanisms that govern protein binding and elution. Achieving that goal will require a more comprehensive understanding of the fundamental underpinnings of ICF and the development of models to predict and tailor both elution gradients and protein elution times.

Here, experimental data are reported and used to define dominant mechanisms of protein binding and elution during chromatofocusing. In addition to the expected and well documented contribution from isoelectric focusing, protein retention is found to depend on ion exchange and Donnan equilibrium effects, the latter of which serve to alter the pH of solution in close proximity to the charged stationary phase to values that differ from the pH of the bulk mobile phase. Depending on the magnitudes of these effects, deviations in the elution pH of a protein away from its pI of up to several pH units in either direction can be predicted. A modified steric mass action (SMA) type isotherm is proposed as a means of capturing both ion exchange and isoelectric focusing contributions to protein binding and elution, while the pH of solution directly adjacent to the charged stationary phase is calculated using an appropriate form of the Donnan equation. Gouy-Chapman theory is used to derive a useful fundamental relationship between the equilibrium binding constant K_{bi} of a protein macro-ion i , the pH-dependent characteristic charge m of the macro-ion, and the mobile phase ionic strength I . As the difference between mobile phase pH and stationary phase surface pH is also related to the ionic strength, a complex dependence of protein elution time on m and I is predicted and observed experimentally. Finally, the model is used to estimate retention times of β -lactoglobulins A and B, trypsin inhibitor and α -lactalbumin on a Mono Q HR10/10 strong anion exchange column operated in ICF mode.

4.2 Experimental

4.2.1 Materials

1,3 Diaminopropane (Cat. No. D23602), diethanolamine (Cat. No. D83303), imidazole (Cat. No. I0125), bis-tris (Cat. No. 156663), piperazine (Cat. No. P7003) and lactic acid (Cat. No. L6661) were obtained from Sigma. Tris (Cat No. BP152), glacial acetic acid (Cat. No. A38P), hydrochloric acid (Cat. No. A144) and sodium chloride (Cat. No. S271) were obtained from Fisher. All ICF loading and elution mobile phase formulations used in this study were designed using the model reported in Chapter 2 and are listed in Table 4.1. Ionic strength adjustments to all mobile phases, when required, were achieved through the addition of sodium chloride.

Table 4.1: pH, ionic strength (mM) and buffer species concentrations (mM) in various formulations of buffer A/buffer B pairs used for sample loading and gradient elution.

Formulation		pH	I	DAP	DEA	TRS	IMI	BTS	PIP	ACE	LAC
0203	Starting	10.0	2	2	2	2	2	2	2	0	0
	Elution	3.5	29	2	2	2	2	2	2	2	2
1003	Starting	10.0	12	10	10	10	10	10	10	0	0
	Elution	3.5	102	10	10	10	10	10	10	10	10
1093	Starting	9.0	13	0	10	10	10	10	10	0	0
	Elution	3.5	72	0	10	10	10	10	10	10	10
2093	Starting	9.0	27	0	20	20	20	20	20	0	0
	Elution	3.5	134	0	20	20	20	20	20	20	20
4093	Starting	9.0	54	0	40	40	40	40	40	0	0
	Elution	3.5	257	0	40	40	40	40	40	40	40

Abbreviations: I – ionic strength (mM); DAP – 1,3 diaminopropane; DEA – diethanolamine; TRS – tris; IMI – imidazole; BTS – bis-tris; PIP – piperazine; ACE – acetic acid; LAC – lactic acid

All buffer solutions were prepared with nanopure water, then adjusted to the desired pH using concentrated HCl, filtered through a 0.22 μm Durapore[®] PVDF membrane (Millipore), and vacuum degassed.

The prepacked Mono Q HR10/10 strong anion exchange column (void fraction $\varepsilon = 0.36$; porosity $e_{matrix} = 0.64$) was obtained from GE Healthcare Life Sciences. β -lactoglobulin A (Cat. No. L7880), β -lactoglobulin B (Cat. No. L8005), α -lactalbumin (Cat. No. L6010), trypsin inhibitor (Cat. No. T9003) and FLAG[®] Peptide (Cat. No. F3290) were obtained from Sigma. All analyte solutions were prepared in nanopure water.

4.2.2 Chromatography

The AKTAexplorer100 (GE Healthcare Life Sciences) described in detail in previous chapters was used for all chromatofocusing studies. Protein samples were manually injected into a 500 μL sample loop and detected upon elution at 280 nm. A 2 mL in-line mixer was used to blend the two buffers A (the column equilibration and sample loading buffer) and B (the isocratic or gradient elution buffer) prior to introduction into the column. Standard operation of the column began with equilibration using 5 CVs to 10 CVs of buffer A. All runs were performed at a flow rate of 1 mL min^{-1} , with the sample injected in a 5 mL injection cycle, followed by a 60 mL gradient from 0% (v/v) to 100% (v/v) of buffer B and then 60 mL of 100% (v/v) buffer B. After each run, the column was washed with 12.5 mL of 1 M NaCl followed by 5 CVs of 20% (v/v) ethanol at a flow rate of 0.5 mL min^{-1} .

4.2.3 pH electrode calibration

Buffer pH values were measured with a pH/Ion Analyzer 350 from Corning, calibrated with standard pH buffers 4.00 (Cat No. B00765), 7.00 (Cat No. B00813) and 10.00 (Cat No. B00801) purchased from Radiometer Inc. To eliminate observed flow effects on measured pH values, the pH electrode in the AKTAexplorer100 was calibrated under flow as described in Chapter 2.

4.2.4 Characteristic charge measurement

The characteristic charge m of β -lactoglobulin A and β -lactoglobulin B on the Mono Q matrix was estimated as a function of pH through global regression of the general rate model of chromatography [120] employing the SMA isotherm [113] to a set of elution times for each protein measured using four different isocratic elutions (eluent of pH 6.0, 5.0, 4.0, and 3.0), as well as elution using a nonlinear pH gradient from pH 9.0 to 2.0 at six different background NaCl concentrations (50 mM to 500 mM). The m parameter was regressed at different pH values by minimizing the residual between the full set of predicted and experimental retention times. Measured (ionic capacity) or vendor supplied column parameters used for all modeling studies are reported in Table 4.2.

Table 4.2: Column parameters used for all modeling

Matrix Ionic Capacity (mol m^{-3})	320 ± 10
Column Void Fraction	0.36
Matrix Porosity	0.64
Column Length (m)	0.10
Column Radius (m)	0.005

4.3 Known and Putative Mechanisms for Protein Elution in Chromatofocusing

In traditional ion exchange chromatography, the mobile phase pH during sample loading is set so that retained proteins have a net charge sign opposite that of the stationary phase; proteins having a net negative charge will thereby bind to an anion exchange matrix, while those carrying a net positive charge bind to a cation exchange matrix. Classic and currently adopted chromatofocusing theory then assumes that a bound protein will elute as it nears net charge neutrality either through protonation (anion exchange chromatofocusing) or deprotonation (cation exchange chromatofocusing) of titratable solvent-exposed amino acids. Elution would therefore be expected when the mobile phase pH equals or nears the protein's *pI*. As elution is by pH (isocratic step or gradient), any diffusion ahead of the elution band will cause the protein to enter a region where the pH of the mobile phase induces a change in the net charge of the protein to a sign opposite to that of the matrix, resulting in further retention that brings those protein molecules back to/near the first moment of the elution band. Diffusion of the protein behind the elution band induces a net charge of same sign to that of the matrix, causing protein repulsion away from the matrix. This phenomenon, known as the focusing effect [104], is well described in the literature and is known to be responsible for the high peak capacities and tight elution bands that can be achieved using ICF.

But as chromatofocusing is conducted on ion exchange matrices at various mobile phase ionic strengths and pH ranges, other binding and elution mechanisms can and likely do contribute to the separation. Stern's modification to Gouy-Chapman theory [116]

provides a basic understanding of how a change in mobile phase ionic strength affects ion or macro-ion (protein) adsorption at a charged surface. That theory assumes that adsorption of a protein macro-ion (away from its pI) to a charged surface is driven by a combination of coulombic (electrostatic) and non-electrostatic forces. The introduction of a Stern layer addresses a significant short-coming of Gouy-Chapman theory by relaxing the assumption that ions behave as point charges and therefore that there is no physical limit for the ions in their approach to the surface. In particular, Stern's theory treats ions as having finite size, so they cannot approach the surface closer than a few nanometers. As a result, no charge accumulation occurs within a distance δ away from the surface, usually taken as the hydrated radius of the adsorbing ion; this is the Stern layer. Gouy-Chapman theory is then applied to the diffuse part of the ionic double layer, which exists at separation distances somewhat greater than δ and is defined by that region where the change in concentration of the counter ions near the charged surface follows a Boltzmann distribution. Within this diffuse double layer, the electrostatic potential and concentration of ions are low enough to justify treating the ions as point charges.

When cast in a form analogous to Langmuir adsorption theory, Stern's modification to Gouy-Chapman theory can be used to predict that the fraction θ of binding sites occupied by a protein macro-ion:

$$\frac{\theta}{1-\theta} = P \exp \left[\frac{z_i e \psi + \phi}{kT} \right] \quad (4.1)$$

is determined by a binding free energy having both electrostatic ($z_i e \psi / kT$) and chemical (ϕ / kT) contributions. In equation 4.1, P is a scaling constant and the electrical potential $\psi(r)$ is given by the solution of Poisson's equation:

$$\nabla^2 \psi = -\frac{\rho}{\epsilon_0 \epsilon'} \approx \frac{\kappa^2}{4\pi \epsilon_0} \psi \quad (4.2)$$

where:

$$\kappa^2 = \frac{4\pi e^2}{\epsilon' kT} \sum_i n_i z_i^2 = \frac{8\pi e^2}{\epsilon' kT} I \quad (4.3)$$

In equations 4.1 to 4.3, ϕ is the chemical (non-coulombic) adsorption potential of macro-ions at the boundary of the Stern layer, k is Boltzmann's constant, T is the temperature, ϵ_0 is the permittivity of free space, ϵ' is the solvent dielectric constant, and I is the ionic strength of the liquid phase containing the free macro-ion. Solution of equations 4.1 to 4.3 leads to the well-known result of either Gouy-Chapman or Debye-Hückel theory, stating that coulombic contributions to protein adsorption diminish rapidly and nonlinearly with increasing I .

The specific binding of charged species (including buffer ions) present in the mobile phase to stationary phase ligands can also promote protein elution. Therefore, unless chromatofocusing is conducted in the complete absence of added electrolyte(s), including

background salts and buffer species, protein elution will depend not only on those effects typically connected with chromatofocusing (*e.g.* elution is expected near a protein's pI due to changes in protein net charge with pH), but also on the diffuse double layer and associated shielding effects that dominate ion exchange chromatography. In this work, chromatofocusing is therefore treated as a mixed-mode separation. The treatment accounts for the fact that ICF is conducted at a non-zero ionic strength environment through the development of a model that explains why changes in ionic strength, and additional ancillary effects to be described, can cause a bound protein to elute at a pH far removed from its pI .

Along with describing the ionic strength dependence of macro-ion binding to a charged surface, Stern's modification to Gouy-Chapman theory may be used to describe the influence of the charged stationary phase on free proton concentration, and thus the pH, within the diffuse double layer. The concentration of protons near the surface of a positively-charged anion exchange matrix is predicted by that theory to be lower than the free proton concentration in the mobile phase due to coulombic repulsion, resulting in a surface pH that is lower than the measured bulk pH. Similarly, the surface pH near a negatively-charged cation exchange matrix is predicted to be higher than the bulk pH due to electrostatic attraction of protons. This difference between the surface pH and bulk pH is known as the Donnan effect, and may be predicted by Donnan equilibrium theory.

Proteins bound to a stationary phase will reside in an environment where the protonation states of their titratable groups are determined by the surface pH. As a result, the

desorption of a bound protein from the stationary phase is dictated by the surface pH, while the charge state of proteins in the mobile phase is determined by the pH of the bulk phase. The Donnan effect will therefore cause a protein to elute at a measured bulk pH lower than its pI in anion exchange isoelectric chromatofocusing (AEICF), or at a measured pH greater than its pI in cation exchange isoelectric chromatofocusing (CEICF); this serves to shift a protein's elution pH. That shift is in a direction opposite to the shift provided by classic ion exchange mechanisms. In particular, though the magnitudes of these opposing effects are both a function of ionic strength, their dependencies on I are inverted. Displacement of a bound protein macro-ion by co-ions increases with increasing ionic strength, while the Donnan effect is reduced. On an anion exchange column, protein elution during chromatofocusing will therefore occur earlier (higher mobile phase pH) with increasing ionic strength. A comprehensive theory of protein chromatofocusing must quantitatively capture these various mechanisms of binding elution. Below, a novel theory that attempts to do this is presented. The model equations presented are specific to AEICF, but the fundamental concepts also apply to ICF on cation exchange media.

4.4 Model Structure and Equations

The mechanistic arguments presented above suggest that prediction of protein elution in chromatofocusing requires proper accounting of changes in the free and bound concentrations of all charged solutes, as well as bulk and surface pH, as a function of time and position within the column. The proposed model therefore combines the

multiple-chemical and adsorption equilibria theory presented in Chapter 2, which may be used to compute mobile phase concentrations and bound concentrations of all buffer counter-ions and co-ions, with equations describing the effect of those ions on protein partitioning. The one-dimensional continuity equation is applied to each protein macro-ion, with the amount of protein retained by the stationary phase in a given column volume element given by a modified form of the SMA isotherm model that includes a binding constant K_{bi} that depends on both local ionic strength and surface pH. As the intent is to establish a model that defines the mechanism(s) of separation at play in ICF and accurately estimate elution times and order, the stationary phase is treated as a homogeneous sink in this model, and all intraparticle diffusion and film mass-transfer effects are lumped into the axial dispersion coefficient D_{ax} . The model is therefore of the classic equilibrium-dispersion form, and is capable of qualitative but likely not quantitative prediction of elution peak shape.

4.4.1 Protein transport and binding

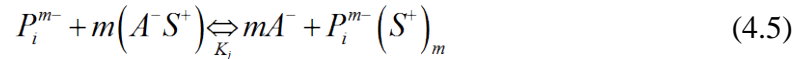
The change in mobile phase concentration of any protein macro-ion i at any time and column position is described by the continuity equation for liquid chromatography:

$$\frac{\partial c_i}{\partial t} + \frac{(1-\varepsilon)}{\varepsilon} \frac{\partial q_i}{\partial t} = -u \frac{\partial c_i}{\partial Z} + D_{ax} \frac{\partial^2 c_i}{\partial Z^2} \quad (4.4)$$

where c_i is the mobile phase concentration of the protein macro-ion i and q_i is its stationary phase concentration at time t and column axial position z . Band broadening

within the interstitial volume is treated using an (apparent) axial dispersion coefficient D_{ax} . The superficial mobile phase velocity is u and column void fraction is ε .

The general binding reaction of a protein macro-ion on an ion exchange matrix is modeled in general accordance with SMA theory:



where P_i is the protein macro-ion having a characteristic charge of m^- , S is a unit of free stationary phase carrying a single ligand of unit positive charge, and A^- is any univalent anion (co-ion) with access to the stationary phase. The equilibrium-binding isotherm for this reaction can be derived and expressed in the following form:

$$K_{b_i} = \frac{q_i [A^-]^m}{c_i (S_T - mq_i - \sigma q_i)^m} \quad (4.6)$$

where S_T is the ionic capacity of the stationary phase, σ is the steric factor, and $[A^-]$ is the total mobile phase anion concentration, which includes salt co-ions (anions) as well as buffer anions. Equation 4.6 is similar to the steric mass action (SMA) isotherm proposed by Cramer *et al.* for conventional ion exchange chromatography [113]; it differs through the use of the pH-dependant total anion concentration $[A^-]$ in place of the standard salt concentration term. In conventional ion exchange chromatography at constant pH, changes in $[A^-]$ are directly proportional to changes in the background salt concentration

(*e.g.* [NaCl]) since no changes in the concentration(s) of buffer anion(s) typically occur. In chromatofocusing, however, the contribution of changes in the concentrations of buffering anions to $[A^-]$ is significant since the concentration of the background salt stays low and the concentrations and protonation states of the buffer anions change within the gradient. Finally, as this represents a first step toward developing a comprehensive model for protein elution in chromatofocusing, the model is restricted to chromatograms in which the column has been loaded far below its maximum capacity. The steric factor term in equation 4.6 can therefore be neglected without error.

Application of equation 4.6 requires values for K_{bi} and the characteristic charge m , the latter of which is expected to depend on the local pH within the binding environment and can be determined from experimental data using, for example, the method described in [42]. However, K_{bi} also depends on m and knowledge of that relation is therefore required. Here, Stern's modification to Gouy-Chapman theory has been used to derive that relation:

$$K_{b_i} = \exp\left[\frac{\beta'(m+1)}{D\sqrt{I}}\right] \approx \exp\left[\frac{\beta m}{\sqrt{I}}\right] \quad (4.7)$$

where I is the local ionic strength within the column and the constant D is given by Debye-Hückel theory as:

$$D = \frac{1}{2.303} \left(\frac{e}{\sqrt{\epsilon_0 \epsilon' kT}} \right) \sqrt{2\pi\rho_0} \quad (4.8)$$

where ρ_0 is the solvent density. The constant β' defines the affinity (binding constant) of the protein in its hypothetical uncharged state to the stationary phase matrix at zero ionic strength. It is related to ϕ , the chemical (non-coulombic) adsorption potential (see equation 4.1) and its value is therefore protein specific. Equation 4.7 is fundamental in nature, but is arguably overly simplistic in its treatment of protein adsorption due in part to the severity of the basic assumptions of Gouy-Chapman theory when applied to a protein macro-ion (spherical uniform macro-ion of net charge z_i and characteristic charge m located at the center of the macro-ion i). β may therefore be viewed as an adjustable parameter having a value that is expected to depend on the protein's physical structure, surface hydrophobicity, and orientation during binding. In this work, β is globally fitted to protein elution times for a set of elution gradients. The value of equation 4.7 therefore lies in its prediction that K_{bi} is exponentially related to m , and that that dependence diminishes with the inverse square root of ionic strength, in accordance with the shielding effect of the ionic atmosphere predicted by Debye-Hückel theory [121].

4.4.2 Donnan effect

As noted above, Donnan theory predicts that the pH near a charged surface ($pH_{surface}$) may differ from the pH of the bulk aqueous phase (pH_{bulk}) due to electrostatic interactions between protons and the charged surface [122]:

$$pH_{surface} = pH_{bulk} + 2.303 \left(\frac{e\psi_0}{kT} \right) \quad (4.9)$$

where the surface potential ψ_0 is affected by the local ionic atmosphere according to Gouy-Chapman theory. It can be related to the charge density S of the stationary phase through the Grahame equation (a classic result derived from the Stern modification to Gouy-Chapman theory) [123] and the condition of electroneutrality, which states that the total charge of the double layer must be equal to the negative of the surface charge:

$$S = \frac{\varepsilon_0 \varepsilon' \psi_0}{\lambda_{De}} \quad (4.10)$$

The ionic strength dependence then enters through the Debye length λ_{De} , given by:

$$\lambda_{De} = \sqrt{\frac{\varepsilon_0 \varepsilon' kT}{\sum_j n_j q_j^2}} = \sqrt{\frac{\varepsilon_0 \varepsilon' kT}{2I}} \quad (4.11)$$

For each protein i , equations 4.4 to 4.11 must be solved together since the value of $pH_{surface}$ determines the characteristic charge m of the macro-ion.

4.4.3 Solution algorithm

Equations 4.4 to 4.11 were solved for each protein i using the ordinary differential equation solver in MATLAB. Values of the characteristic charge (m) and the equilibrium binding constant (K_{bi}) in each volume and time element were computed from predictions

of the local ionic strength and $pH_{surface}$. The mobile-phase pH and ionic strength in the column were therefore first calculated as model inputs using the method and associated algorithm described in Chapter 2. As the protein is infinitely dilute in the system, its presence is assumed to not affect either quantity within the model.

4.5 Results and Discussion

4.5.1 Isoelectric chromatofocusing as a mixed-mode separation

The model described in sections 4.3 and 4.4 assumes that the mechanism of protein retention and elution during ICF is mixed-mode and more complex than previously described. Though the model embraces the classic concept that the pI of the protein is a determinant of elution, it predicts that the mobile phase pH at which elution is observed also depends on I and gradients in I , which influence in different ways the relative magnitudes of two additional contributions to elution behavior: ion-shielding/ion-exchange (Gouy-Chapman) contributions and surface-pH (Donnan) contributions. These two contributions work in opposite directions to move the elution pH away from the protein's pI . The magnitude of the Donnan contribution is predicted by the model to decrease with increasing ionic strength, while that due to ion-shielding/ion-exchange effects is expected to increase (Figure 4.1). To verify these model predictions, ICF separations of a β -lactoglobulin A and β -lactoglobulin B mixture were performed on a Mono Q HR10/10 column using linear pH gradients from 10.0 to 3.5 generated with buffer formulation 1003 and adjusted to various total ionic strengths using NaCl (Figure 4.2). Each experiment was conducted such that I was kept approximately constant

throughout the separation. However, small changes in I occur during each separation, particularly at low NaCl concentrations, due to the complex multiple chemical equilibria and associated speciation occurring throughout the gradient (see Chapters 2 and 3).

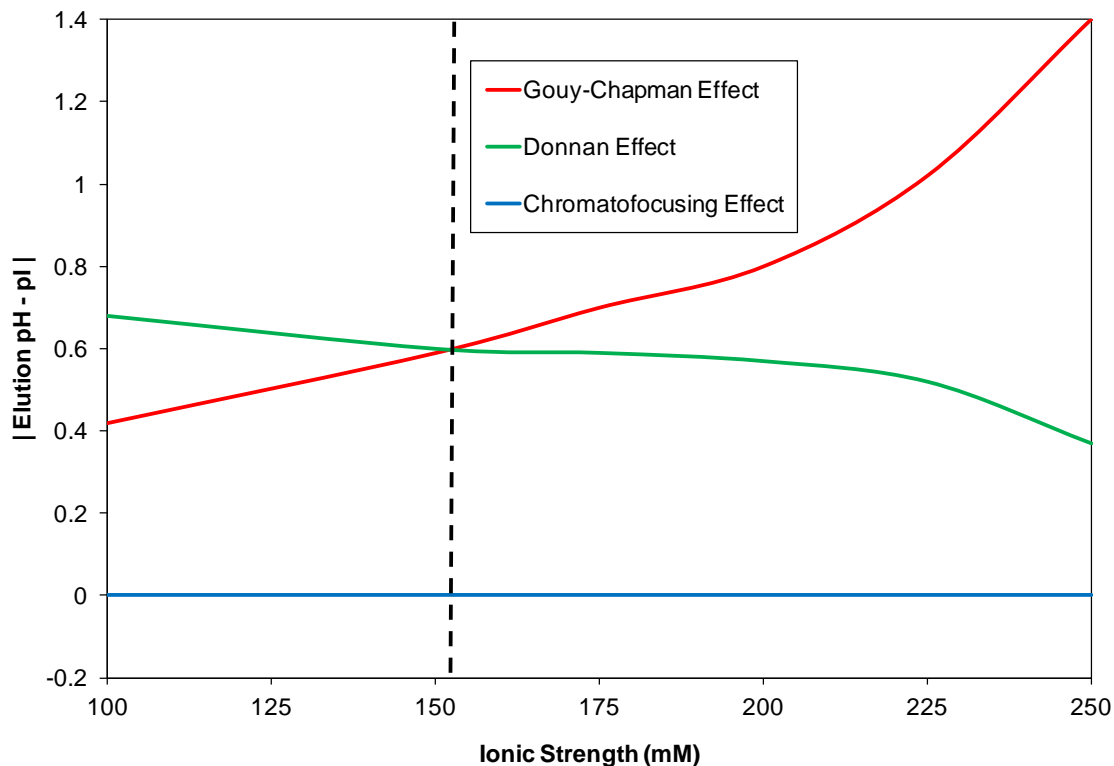


Figure 4.1: Model-based estimates of the magnitude of the elution pH shift away from the pI caused by the Gouy-Chapman, Donnan and chromatofocusing effects as a function of ionic strength.

The pH gradients generated by the different formulations are virtually identical, indicating that buffer pK values are relatively insensitive to I over the range of ionic strengths tested. For reference, the isoelectric points of β -lactoglobulin A and β -lactoglobulin B, determined by gel isoelectric focusing, are 5.1 and 5.3, respectively, as indicated by the dashed vertical lines in Figure 4.2. At an ionic strength below 150 mM,

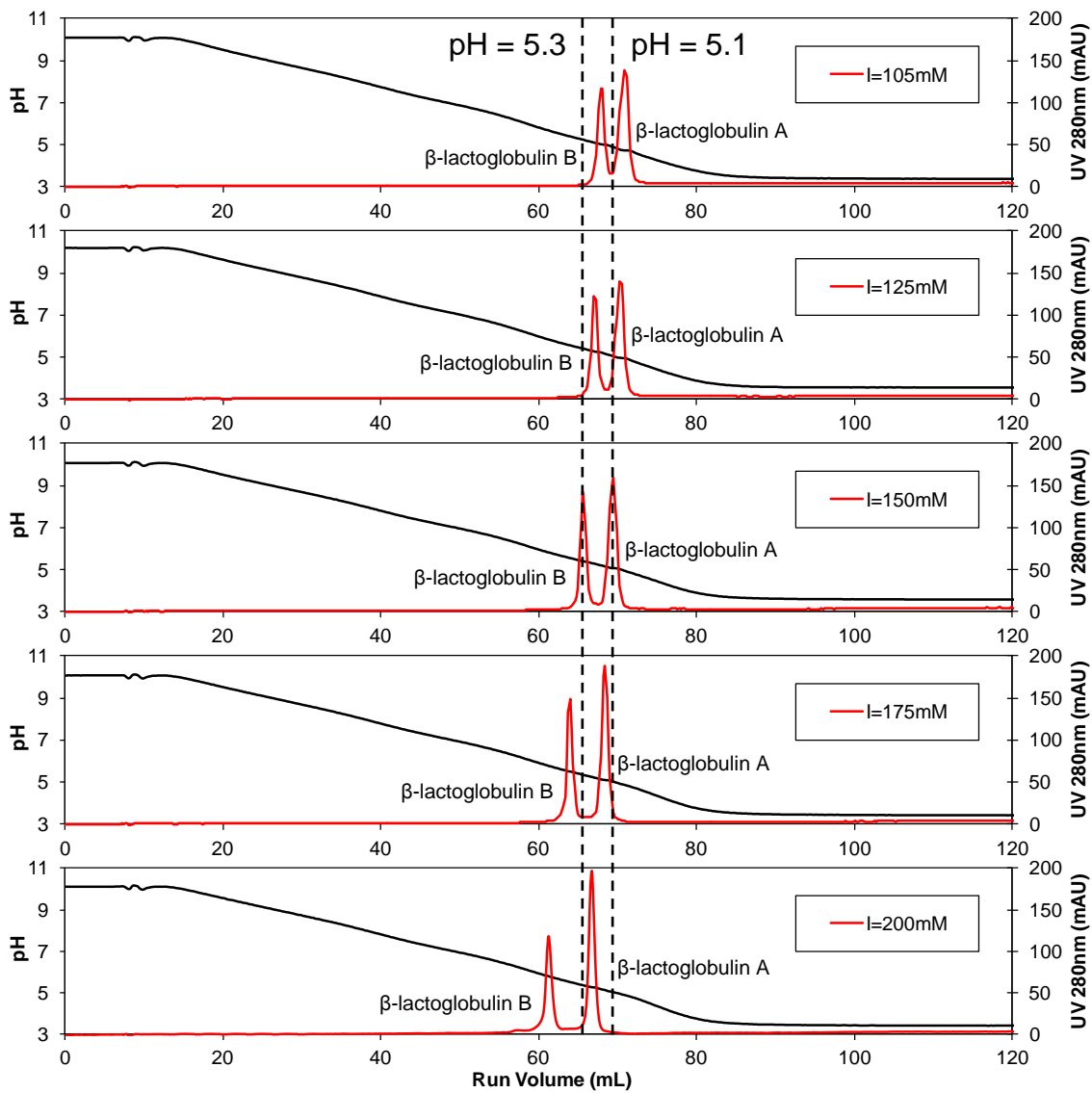


Figure 4.2: Comparison of elution chromatograms generated using buffer formulation 1003 adjusted to ionic strengths of 105 mM, 125 mM, 150 mM, 175 mM and 200 mM. Each model-derived formulation generates a linear pH gradient from 10.0 to 3.5 and was used to resolve a mixture of 2.5 mg mL^{-1} β -lactoglobulin A and 2.5 mg mL^{-1} of β -lactoglobulin B injected as a $500 \text{ }\mu\text{L}$ pulse onto a Mono Q HR10/10 column at $25 \text{ }^\circ\text{C}$ and a mobile phase flow rate of 1 mL min^{-1} . Dotted lines indicate elution volumes at which the measured pH equals 5.3 and 5.1.

each protein elutes at a pH lower than its pI , in accordance with the model, which predicts that Donnan effects dominate ion-shielding/ion-exchange effects at low ionic strengths (Figure 4.1). At an ionic strength of approximately 150 mM, the contributions of the opposing Gouy-Chapman and Donnan effects balance, and each protein elutes

its pI . At higher ionic strengths, Gouy-Chapman effects dominate the Donnan effect, as predicted by the model, and proteins elute at a pH above their respective pI .

4.5.2 Predicting protein elution in ICF

Further validation of the model was achieved by comparing model-derived elution peaks to experiment for the linear gradient elution of β -lactoglobulin A (Figure 4.3) and β -lactoglobulin B (Figure 4.4) at various ionic strengths. In all experiments, the proteins were loaded at concentrations far below the capacity of the column, so that independent elution behavior is expected. For β -lactoglobulin A, the shift in elution volume (and consequently elution pH) with increasing ionic strength is captured quantitatively by the model, including for the case where loading is at an ionic strength (500 mM) where protein binding does not occur. At these high ionic strengths, Gouy-Chapman effects dominate protein-partitioning behavior in the column. Conductivity data are also reported to show that I is nearly constant in each study. Since proteins are dissolved in nanopure water in the sample pulse, a dip in conductivity is observed in each chromatogram at an elution volume corresponding to the void plus dead volume of the instrument and column assembly. Good agreement of the model with experiment is also observed for β -lactoglobulin B. However, at an ionic strength of 250 mM, the predicted elution profile for β -lactoglobulin B does not match the primary elution peak recorded (Figure 4.4F). Here, careful analysis of the experimental chromatogram reveals that although the primary β -lactoglobulin B peak elutes earlier than the predicted peak, a low intensity peak having a first moment that matches the elution volume of the predicted peak is also observed. It is possible at this elevated ionic strength that the protein

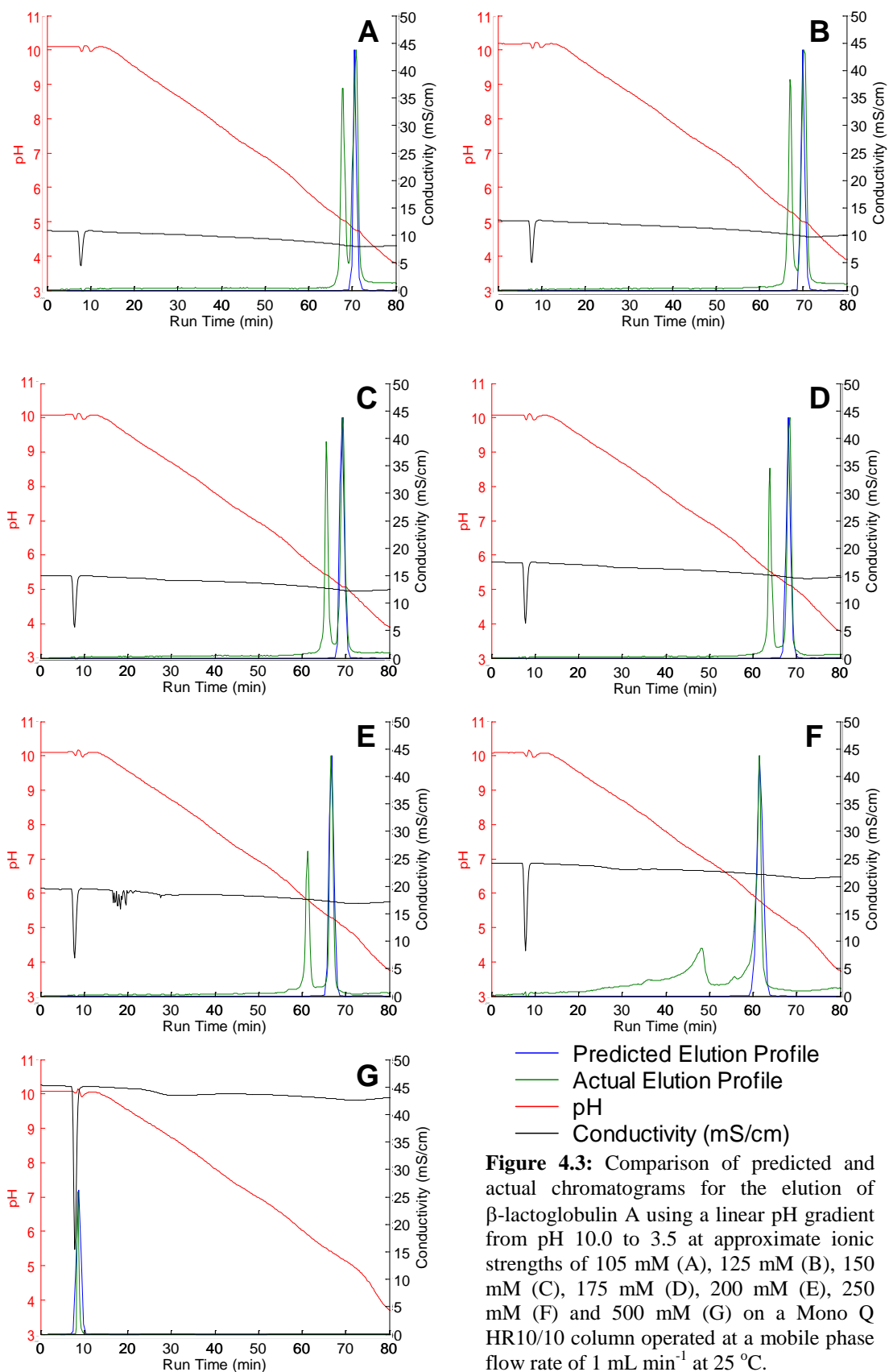


Figure 4.3: Comparison of predicted and actual chromatograms for the elution of β -lactoglobulin A using a linear pH gradient from pH 10.0 to 3.5 at approximate ionic strengths of 105 mM (A), 125 mM (B), 150 mM (C), 175 mM (D), 200 mM (E), 250 mM (F) and 500 mM (G) on a Mono Q HR10/10 column operated at a mobile phase flow rate of 1 mL min⁻¹ at 25 °C.

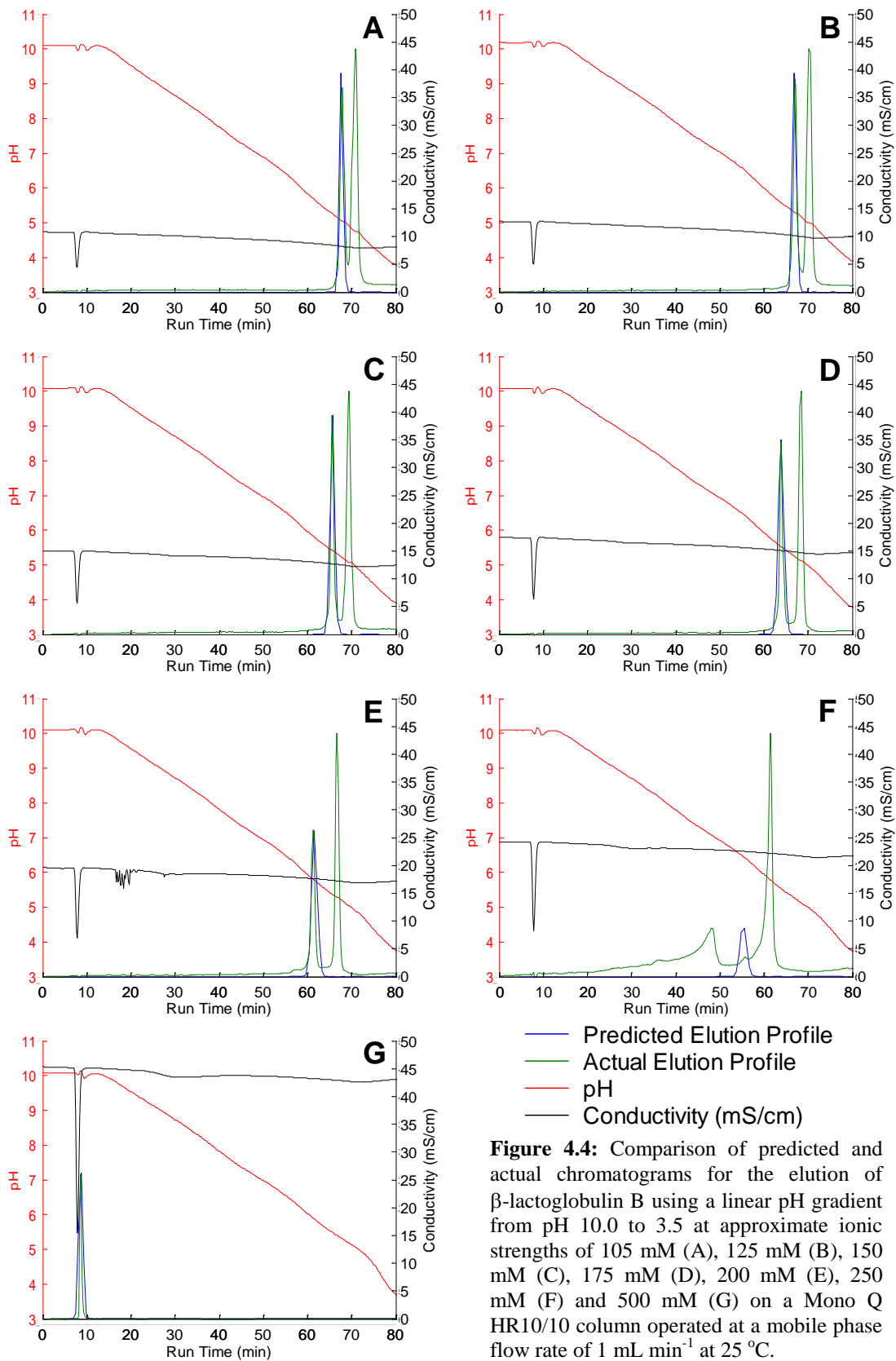


Figure 4.4: Comparison of predicted and actual chromatograms for the elution of β -lactoglobulin B using a linear pH gradient from pH 10.0 to 3.5 at approximate ionic strengths of 105 mM (A), 125 mM (B), 150 mM (C), 175 mM (D), 200 mM (E), 250 mM (F) and 500 mM (G) on a Mono Q HR10/10 column operated at a mobile phase flow rate of 1 mL min⁻¹ at 25 °C.

associates with the stationary phase in multiple isoforms or orientation(s), some of which are inconsistent with the β and/or characteristic charge values used to calculate the equilibrium binding constant. Additional studies, not a part of this thesis, would need to be carried out to test that possible explanation.

The regressed β value (1.8) is the same for β -lactoglobulin A and B, consistent with the fact that these two proteins are very similar in size, sequence and structure. For the same reason, the measured characteristic charge vs. pH curves for the two proteins are similar as well (Figure 4.5). Two important points can be made here. First, for both proteins, the measured m versus pH curve for binding to the Mono Q matrix qualitatively resembles

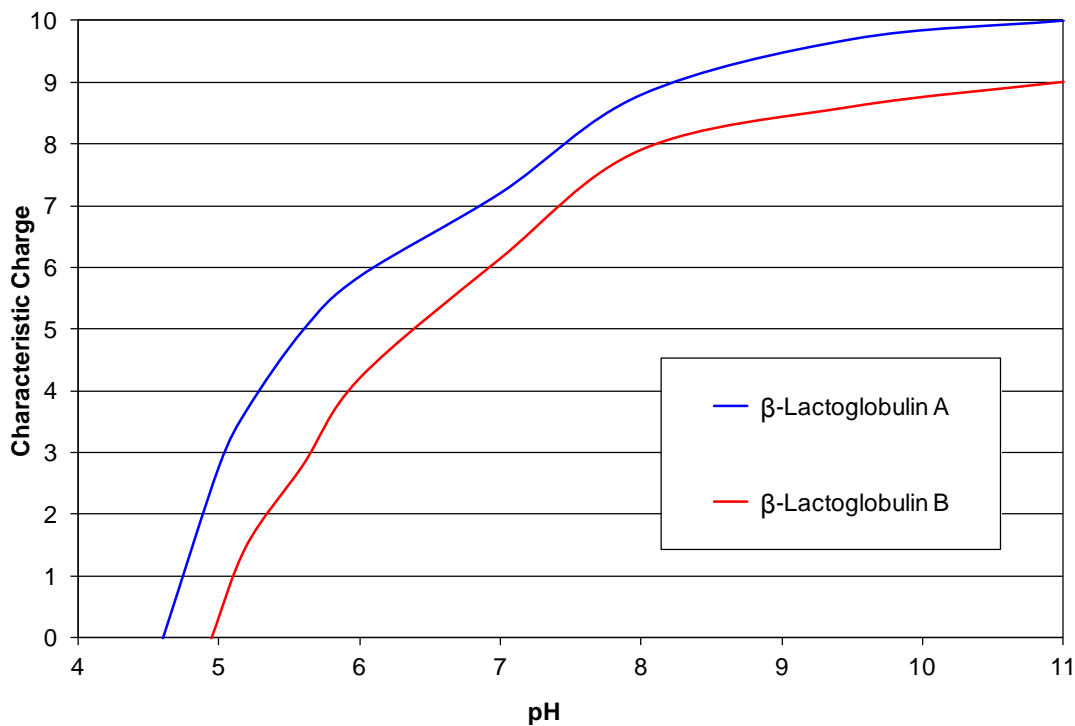


Figure 4.5: Characteristic charge vs. pH data for β -lactoglobulin A ($pI = 5.1$) and β -lactoglobulin B ($pI = 5.3$) on the Mono Q HR10/10 strong anion exchange matrix.

that reported by Yamamoto and Takashi for binding of the same proteins to a different anion exchange matrix (Resource Q) [42], suggesting that the binding orientation and contact-site arrangement is similar in the two systems. Second, and more importantly, in both systems (Mono Q and Resource Q), the characteristic charges of β -lactoglobulin A and β -lactoglobulin B are not zero when the bulk pH equals the pI of each respective protein. Adsorption to the positively-charged stationary phase surface therefore shifts pK values of proximal amino acid residues not complexed with the matrix. This may explain, at least in part, the failure of previous attempts to correlate protein pI and elution pH in chromatofocusing.

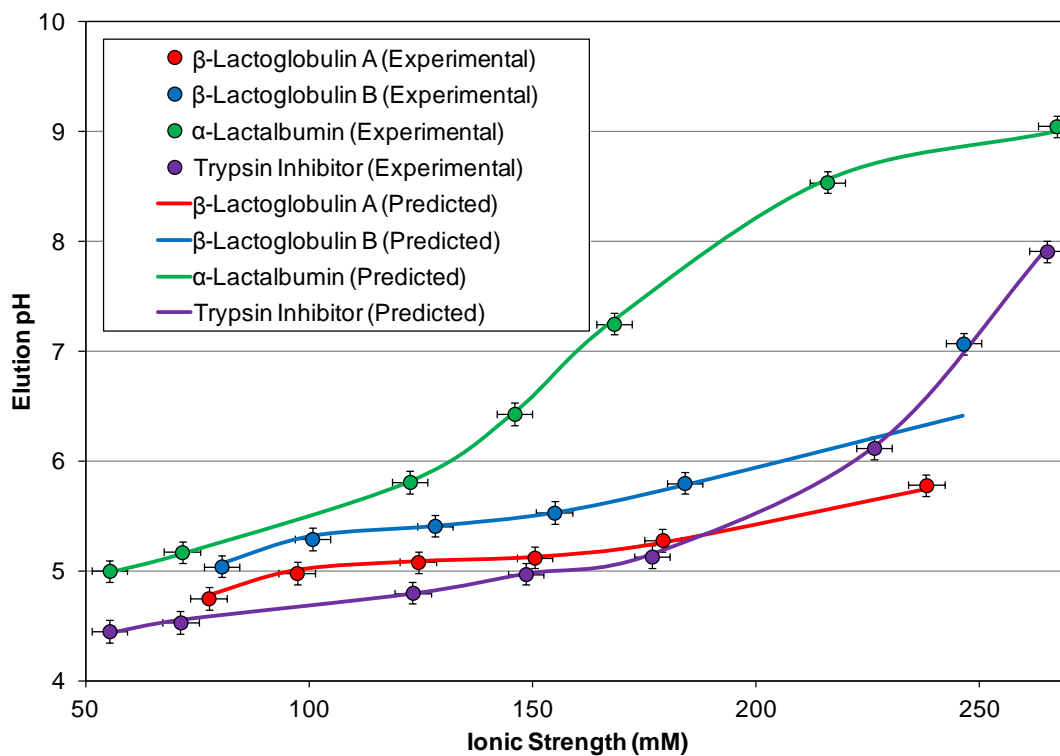


Figure 4.6: Predicted elution pH vs. conductivity for β -lactoglobulin A (red), β -lactoglobulin B (blue), α -lactalbumin (green) and trypsin inhibitor (purple) compared to experimental results for ICF on the Mono Q HR10/10 strong anion exchange column at 25 °C.

As a final validation of the model, Figure 4.6 reports model-estimated elution pH values (solid lines) for four different globular proteins (α -lactalbumin, β -lactoglobulins A and B, and trypsin inhibitor) subjected to a set of different gradient formulations. For all four proteins, model results are in good agreement with the corresponding experimental data.

4.5.3 Model-based interpretation of the isoelectric chromatofocusing of proteins

The ability of the model to capture the basic retention and elution behavior of proteins permitted its application to a broader, more qualitative study aimed at better understanding fundamental behavior in this complex mixed-mode separation. For example, protein chromatofocusing data on the Mono Q column show that an increase in ionic strength alters elution bandwidth (V_W). The elution volume (V_R) normalized bandwidth, given by V_W/V_R , tends to narrow as the ionic strength of the mobile phase is lowered to a value near that where the protein elutes at its pI (Figure 4.7); as shown in Figure 4.1, this is also the I where Gouy-Chapman and Donnan effects are balanced. Experimentally, a small increase in V_W/V_R is then typically observed as I is decreased further. This reveals that the two additional and opposing separation modes operating during chromatofocusing can serve to diminish both the focusing effect and separation quality. In particular, when only Gouy-Chapman and isoelectric focusing contributions are considered (Donnan contributions ignored), the model predicts that normalized bandwidths of eluted proteins will progressively narrow with decreasing I due to the fact that specific charge-based interactions between the protein and matrix are strongest at lower I . However, the Donnan terms of the model predict that the absolute difference in $pH_{surface} - pH_{bulk}$ will increase with decreasing I . This difference can lead to heterogeneity

in the titration states of bound proteins, resulting in different binding affinities and band broadening. Together these two effects produce a minimum in V_w/V_R , with more significant band broadening observed when retention and elution are dominated by the Gouy-Chapman effect (Figure 4.7).

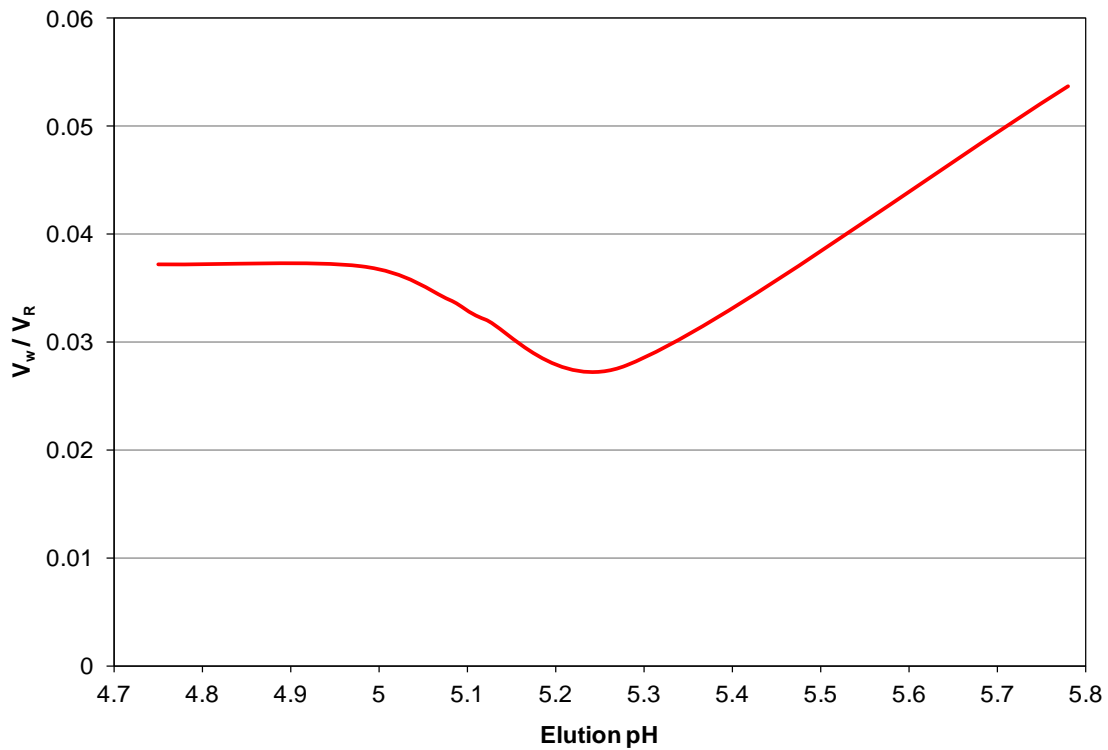


Figure 4.7: Reduced peak width (V_w / V_R) vs. elution pH for β -lactoglobulin A resolved by ICF on a Mono Q HR10/10 strong anion exchange column at 25 °C.

The model also predicts that the influence of the Gouy-Chapman effect on analyte elution becomes stronger with decreasing size of the macro-ion. This result is predicted in large part because the binding strength is related to the characteristic charge (equation 4.6), which typically decreases with decreasing size of the macro-ion. As an example of this

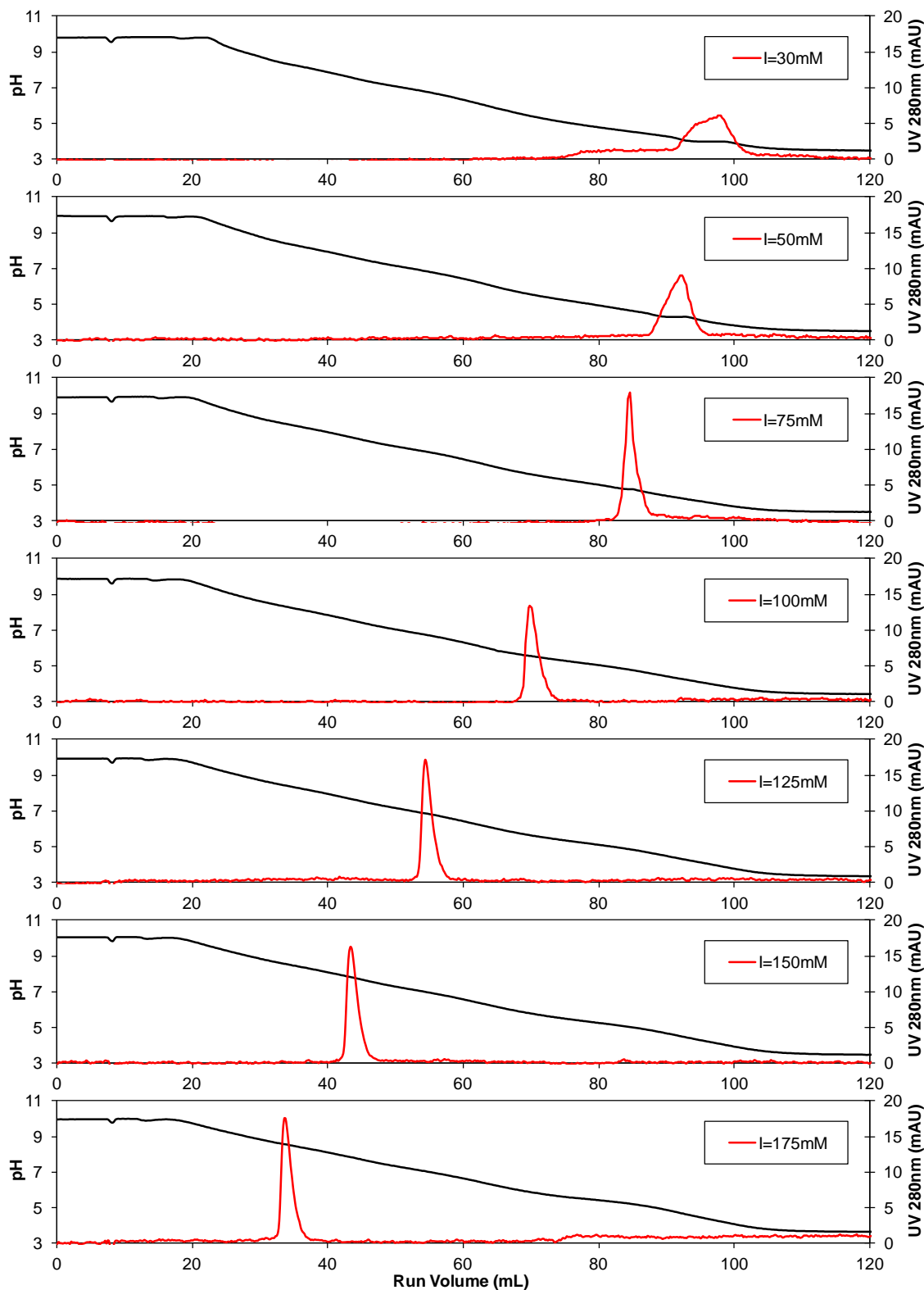


Figure 4.8: Comparison of elution chromatograms generated using buffer formulation 0203 adjusted to ionic strengths of 30 mM, 50 mM, 75 mM, 100mM, 125 mM, 150 mM and 175 mM to generate a pH gradient from 10.0 to 3.5 to elute 0.2 mg mL⁻¹ FLAG[®] Peptide injected as a 500 μ L pulse onto a Mono Q HR10/10 column at 25°C and a mobile phase flow rate of 1 mL min⁻¹.

model-predicted effect, elution volumes for the short FLAG[®] peptide, which has the amino acid sequence DYKDDDK, were measured using pH gradients from 10 to 3.5 generated with buffer formulation 0203 adjusted to various ionic strengths (Figure 4.8). The FLAG[®] peptide has a *pI* of 4.0, and elutes at this *pI* when the ionic strength is approximately 30 - 50 mM. Due to the low buffer concentrations required to achieve the required ionic strength, the macro-ion exhibits buffering capacity at its *pI*, resulting in a plateau effect on the pH gradient and significant band broadening. However, the key finding here is the fact that the decrease in elution volume with increasing *I* is significantly more pronounced for the weaker-binding FLAG[®] peptide than for any proteins studied in this work, with the data for β -lactoglobulins A and B (Figure 4.2) providing a useful representative example.

The dependence of the magnitude of the elution volume shift on ionic strength can be exploited to improve separation performance. For example, trypsin inhibitor (*pI* = 4.5) has an approximate molecular mass of 20 kDa, and contains a total of 51 charged amino acids, of which 30 are acidic residues, while α -lactalbumin (*pI* = 4.3) has an approximate molecular mass of 14 kDa and contains a total of 36 charged amino acids, of which 20 are acidic residues. Thus, though α -lactalbumin has the lower *pI*, the model predicts that it can elute earlier than the larger trypsin inhibitor and show a larger dependence on *I* due to its smaller size and lower charge state. Results in Figure 4.9 support this model prediction, as α -lactalbumin indeed elutes first and exhibits a larger shift in elution pH with increasing ionic strength.

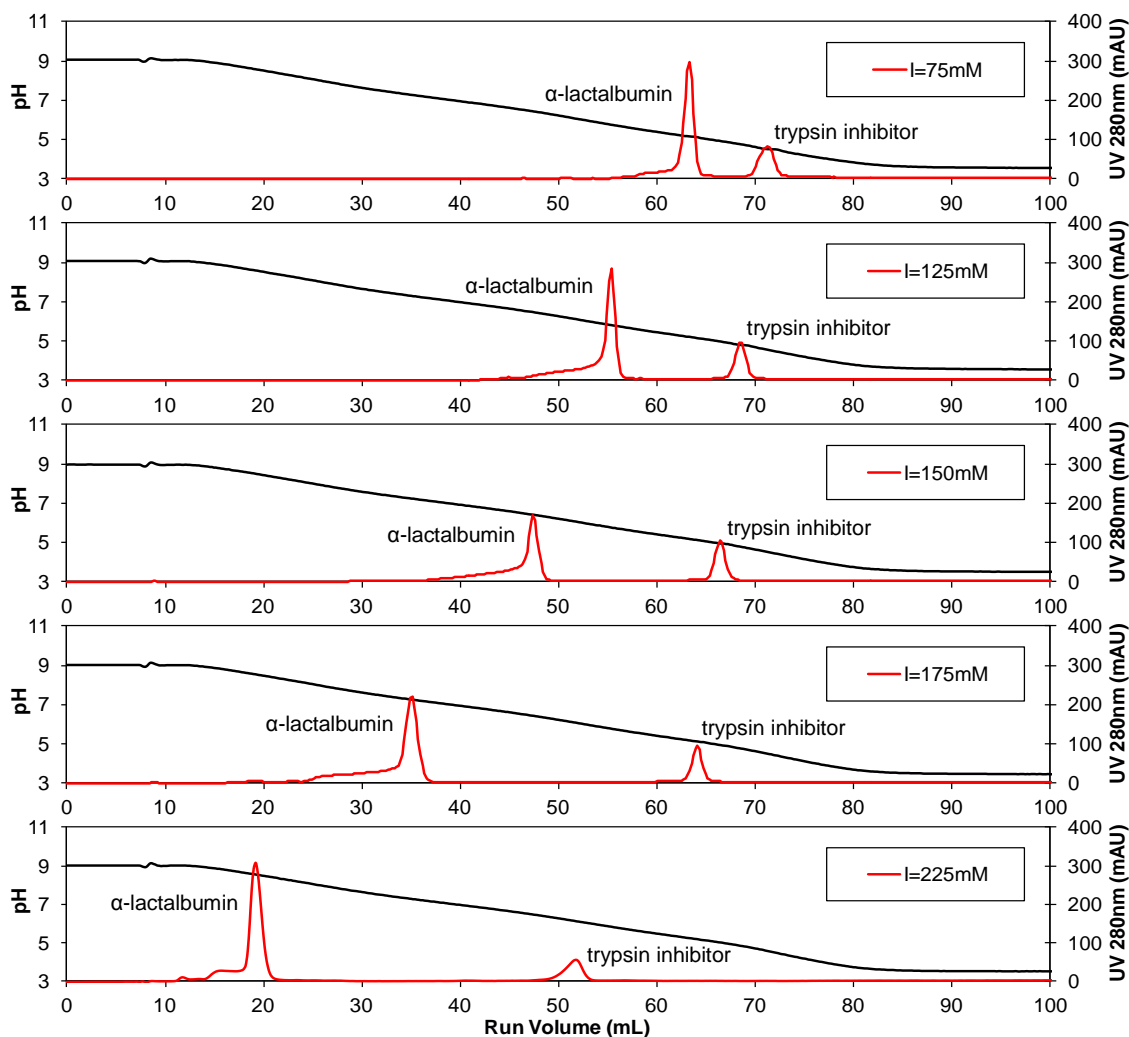


Figure 4.9: Comparison of elution chromatograms generated using buffer formulation 1093 adjusted to ionic strengths of 75 mM, 125 mM, 150 mM, 175 mM and 225 mM. The resulting linear pH gradient from 9.0 to 3.5 is used to resolve a mixture of 2.5 mg mL^{-1} α -lactalbumin and 2.5 mg mL^{-1} of trypsin inhibitor injected as a $500 \text{ }\mu\text{L}$ pulse onto a Mono Q HR10/10 column at 25°C and a mobile phase flow rate of 1 mL min^{-1} .

4.5.4 Ion-displacement effects on protein retention and resolution

In the ICF systems studied here, the anion of the added salt, in this case the chloride ion, serves as the dominant matrix counter-ion in the system. However, as reported in Chapter 2, acetate and lactate ions are also present. Both compete with the chloride ion and protein macro-ions for binding sites on the positively charged sorbent surface, and

the affinity of each for the stationary phase is greater than that of the chloride ion. The relative affinity of a protein for the Mono Q matrix will therefore decrease when larger concentrations of lactate and acetate ions are introduced during elution. An increase in ionic strength will likewise reduce protein affinity. By tracking both chemical equilibria in solution and adsorption equilibria at the stationary phase, the model captures these two effects and predicts that the separation of proteins having similar pI values can be improved, in some cases dramatically, through the tailoring of the acetate/chloride and lactate/chloride ratios, as well as the total ionic strength of the mobile phase (Figure 4.10). For a mixture of β -lactoglobulins A and B, a significant improvement in resolution and peak capacity (width) is achieved through a 4-fold increase in lactate and acetate concentration in buffer B, and a concomitant greater than 3-fold increase in I . At high buffer concentrations (formulation 4093), significant amounts of the two weak acids bind to the matrix during the introduction of elution buffer B. As the mobile-phase pH approaches their pK values, acetate and lactate desorb from the matrix, generating the UV 280 nm response (red trace) seen near the very end of the gradient. However, at pH values above those pK values, acetate and lactate both compete with each protein for binding sites. That competition reduces protein elution volumes and sharpens elution peaks, with the latter trend predicted to be a direct and specific consequence of ion displacement effects. This is seen by comparing the chromatograms in Figure 4.2, where I is increased without change in the acetate and lactate concentrations, with those in Figure 4.10, where the concentrations of both weak acids have been increased significantly. The results indeed show that an increase in ionic strength alone leads to greater peak separation, but also broadens the peaks, as reported in section 4.5.3. As

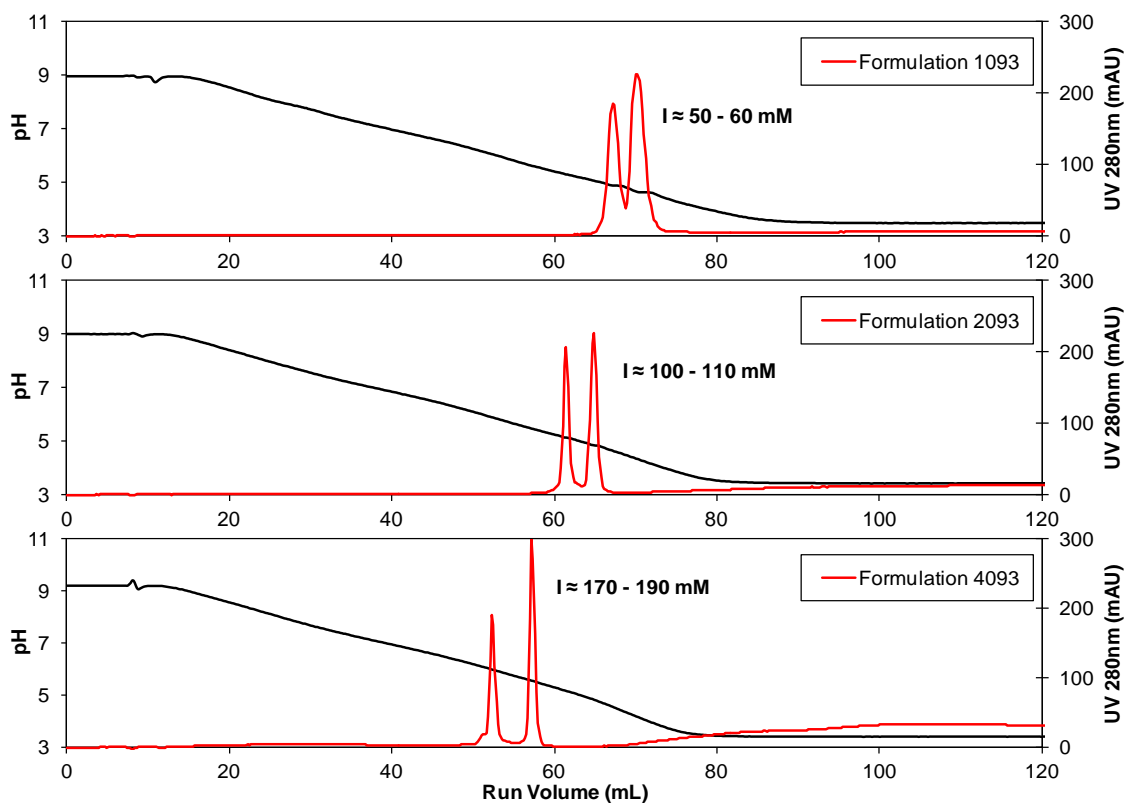


Figure 4.10: Comparison of elution chromatograms generated using buffer formulations 1093, 2093 and 4093. Each linear pH gradient from 9.0 to 3.5 is used to resolve a mixture of 2.5 mg mL^{-1} β -lactoglobulin A and 2.5 mg mL^{-1} of β -lactoglobulin B injected as a $500 \mu\text{L}$ pulse onto a Mono Q HR10/10 column at 25°C and a mobile phase flow rate of 1 mL min^{-1} . The range of ionic strength at which the two proteins elute is indicated.

shown in Figure 4.10, that peak broadening can be eliminated in favor of peak sharpening through modulation of ion displacement effects. A significantly improved separation is thereby realized.

4.6 Concluding Remarks

A model defining and quantifying the dominant contributions to protein retention and elution in ion exchange columns operated in chromatofocusing mode is presented and used to obtain an improved fundamental understanding of this potentially powerful separation method. Verified through comparison to a series of experiments, the model treats chromatofocusing as a mixed-mode separation where protein elution is defined not only by the protein's pI , but also by Donnan effects, Gouy-Chapman effects and ion displacement at the Stern layer. The model provides insights into how changes in ionic strength and buffer species concentrations can be used to modulate the strength of macro-ion retention so as to improve separation of proteins with similar isoelectric points; important elution characteristics including elution volumes, peak widths and resolution can be altered with a large degree of freedom to achieve desired separations. The model therefore provides a powerful tool for predicting protein elution profiles in ICF, and when used together with the previously described method to design custom elution pH profiles, offers the potential for the rational optimization of separation characteristics, which should make the technique more attractive for suitable analytical and preparative applications.

Chapter 5

Chromatofocusing Design for Preparative Isocratic Purification of Proteins: Separating Isoforms of the N-Lobe of Human Transferrin Produced in Recombinant *Pichia Pastoris*

A strategy is described for defining suitable operating conditions for isoelectric chromatofocusing using preparative strong (an)ion-exchange media and isocratic elution. The method involves mapping elution pH as a function of ionic strength and using this information in conjunction with the model presented in Chapter 2 to custom-design, within the limits of a two-solvent system, appropriate mobile phases for isocratic elution. The strategy is designed to offer a practical recipe for optimizing ICF purification of protein products from a fermentation broth when detailed physicochemical and binding information for the target protein and contaminants, or model parameters required for predicting elution behavior, are not available. The value of the method is demonstrated through application to the purification of an isoform of the recombinant N-lobe of human transferrin produced by the methylotrophic yeast *Pichia pastoris*.

5.1 Background

Ion exchange remains the most popular mode of chromatography for the large-scale purification of proteins in part because it uses relatively inexpensive, high capacity

stationary phases that can operate at high linear velocities. However, though powerful, standard ion exchange chromatography is not always capable of achieving desired product purities and yields. Isoelectric chromatofocusing (ICF), an alternate separation mode that utilizes ion exchange media and therefore enjoys the same column-derived benefits, can achieve outstanding peak capacities and resolving power when designed properly. Nevertheless, the method has not found significant use as a means of purifying protein products at preparative scales. For that to change, the current requirement to use proprietary polyampholyte buffers would need to be eliminated [65, 66] in favor of simpler, less expensive buffering methods that can be made compatible with preparative stationary phases. Gradient elution may need to be replaced with an operationally simpler step change from loading to elution phase (isocratic elution) that produces a pH and ionic strength profile capable of achieving the desired separation. Load and elution buffers would need to be optimized so as to operate the column at elution pH values and salt conditions where column loading is dictated by the dynamic binding capacity and not by product or contaminant solubility limits. In particular, product elution should occur away from the product protein's pI , where its solubility is typically lowest, to avoid both irreversible column fouling and excessive band broadening.

In this chapter, a simple method is described that permits one to define an ICF gradient shape (including pH and ionic strength changes) generated by an isocratic elution process that provides robust and rapid purification of a target protein or protein isoform from a complex clarified feedstock. The method leverages the capabilities of the model presented in Chapter 2 to custom-design elution pH profiles, in this case through a step

change between two isocratic solvent states. It likewise exploits the capacity of the model presented in Chapter 4 to provide basic insights into protein elution behavior during chromatofocusing. However, it does not attempt to use that model to predict elution times. While the local equilibrium approximation applied in that model is appropriate for the relatively slow changes in pH and ionic strength, and thus gradual changes in bound protein amounts, generated during gradient elution, it is not proven in this work to be valid under step elution conditions. Here, the elution behaviors of the target protein and key contaminants are therefore characterized experimentally using a defined set of linear gradient elutions. Those data are combined with mechanistic insights drawn from the protein elution model described in Chapter 4 to identify a desired shape and span to the elution pH/ionic strength profiles. The model described in Chapter 2 is then used to custom-design the loading (buffer A) and elution (buffer B) phases required to generate the desired gradient using a step change between isocratic solvent states. Moreover, by using the model to also set desired and/or acceptable changes in eluent ionic strength, target-protein elution can be tailored to occur away from the protein's *pI*. The method is demonstrated through its application to the purification of a desired isoform of the recombinant N-lobe of human transferrin (hTf/2N) produced by cultures of the methylotrophic yeast *Pichia pastoris*.

5.2 Experimental

5.2.1 Materials for analytical studies

DL-dithiothreitol (Cat No. D9163) and iodoacetamide (Cat No. I6125) were obtained from Sigma. NuPAGE LDS Sample Buffer 4X (Cat No. NP0007), SeeBlue Plus2 Pre-Stained Standard (Cat No. LC5925), NuPAGE 4-12% Bis-Tris Gel 1.0 mm x 12 well (Cat. No. NP0322), NuPAGE MES SDS Running Buffer 20X (Cat No. NP0002), Simply Blue SafeStain (Cat No. LC6060) and Gel-Dry Drying Solution (Cat No. LC4025) were purchased from Invitrogen. Trypsin Gold (Cat. No. V5280) was obtained from Promega.

5.2.2 Materials for preparative ICF studies

1,3 Diaminopropane (Cat. No. D23602), diethanolamine (Cat. No. D83303), imidazole (Cat. No. I0125), bis-tris (Cat. No. 156663), piperazine (Cat. No. P7003) and lactic acid (Cat. No. L6661) were obtained from Sigma. Tris (Cat No. BP152), glacial acetic acid (Cat. No. A38P), hydrochloric acid (Cat. No. A144) and sodium chloride (Cat. No. S271) were obtained from Fisher. Buffer formulations are shown in Table 5.1.

Table 5.1: pH, ionic strength (mM) and buffer species concentrations (mM) in model-sculpted formulations of buffer A/buffer B pairs used for ICF separation of recombinant *Pichia pastoris* supernatants

Formulation		pH	I	DAP	DEA	TRS	IMI	BTS	PIP	ACE	LAC
1003	Starting	10.0	12	10	10	10	10	10	10	0	0
	Elution	3.5	102	10	10	10	10	10	10	10	10
1005C	Starting	10.0	1	1	1	1	20	20	1	0	0
	Elution	5.0	56	1	1	1	20	20	1	0	0

Abbreviations: I – ionic strength; DAP – 1,3 diaminopropane; DEA – diethanolamine; TRS – tris; IMI – imidazole; BTS – bis-Tris; PIP – piperazine; ACE – acetic acid; LAC – lactic acid

All buffer solutions used as mobile phases for column equilibration and sample loading/elution were prepared with nanopure water, adjusted to the desired pH with concentrated HCl and the desired ionic strength with NaCl, and then filtered through a 0.22 μm membrane and vacuum degassed. Q Ceramic HyperD 20 strong anion exchange media was kindly provided by Pall Life Sciences. An empty HR10/10 column (Cat No. 19-7464-01, 18-1541-01, 18-1542-01) was obtained from GE Healthcare Life Sciences. The MidGee Cross Flow Cartridge 0.2 μm (Cat No. CFP-2-E-MM01A) and Kwick Start 10 kDa Select Cassette (Cat No. 11-0006-04) were obtained from GE Healthcare Life Sciences.

5.2.3 Fermentations

All fermentations were carried out using the recombinant *Pichia pastoris* Mut^S construct producing hTf/2N described by Mason *et al.* [124]. Inoculums were cultured overnight at 30 °C and under continuous shaking at 200 RPM in 2 L baffled flasks containing 250 mL of BMGY medium; 60 mL of that culture was then used to inoculate 1 L of media contained in a 3 L Applikon bioreactor with temperature, pH, and dissolved oxygen (DO) maintained at specified set points of 30 °C, pH 4.5, and 40% (v/v) saturation DO, respectively. The basal salt medium used contained (per litre) 26.7 mL of 85% phosphoric acid, 0.93 g of calcium sulfate:2H₂O, 18.2 g of potassium sulfate, 14.9 g of magnesium sulfate:7H₂O, 4.13 g potassium hydroxide, 40 g of glycerol and 1 mL of antifoam 204. A solution of 50% (w/v) glycerol and 12 mL L⁻¹ trace salts (PTM₁ from Invitrogen) was fed at 18 mL h⁻¹ 6 hours after inoculation. At approximately 24 hours after inoculation, the culture was induced with methanol and the methanol concentration

was maintained at 1.0% (v/v) through a controlled feed of 12 mL L⁻¹ of PTM₁ trace salts in 100% methanol; the feed of 50% (w/v) glycerol and 12 mL L⁻¹ PTM₁ salts was continued at a reduced rate of 11 mL h⁻¹ after induction. Fermentations were terminated and harvested 67 hours after inoculation.

5.2.4 Sample preparation for chromatography

Clarified supernatant was produced from fermentation broths by chilling to 4 °C and then centrifuging on a Beckman J2-21 centrifuge operating at 5000 RPM (JA-14 rotor) for 60 minutes. An AKTAcrossflow (GE Healthcare Life Sciences), controlled using the Unicorn 5.11 (Build 407) software, was then used to further clarify the feedstock by microfiltration using a 0.2 µm MidGee Cross Flow Cartridge (GE Healthcare Life Sciences) operating at a tangential flow rate of 200 mL min⁻¹ and a trans-membrane pressure of 0.8 bar. The filtered samples were concentrated 10-fold and buffer-exchanged by diafiltration into the appropriate starting buffer for ICF using a Kwick Start 10 kDa Select Cassette (GE Healthcare Life Sciences) operating at a tangential flow rate of 50 mL min⁻¹ and a trans-membrane pressure of 1.5 bar. Both the semi-clarified feedstock and the clarified, concentrated feedstock were stored at -80 °C.

5.2.5 pH electrode calibration

Buffer pH values were measured with a pH/Ion Analyzer 350 from Corning, calibrated with standard buffers of pH 4.00 (Cat No. B00765), 7.00 (Cat No. B00813) and 10.00 (Cat No. B00801) from Radiometer Analytical. To eliminate observed flow effects on measured pH values, the pH electrode in the AKTAexplorer100 was adjusted at a flow of

25 mL min⁻¹ within the column-free system to the static pH values of the starting and elution buffers measured off-line using the calibrated pH/Ion Analyzer.

5.2.6 Chromatography

The AKTAexplorer100 (GE Healthcare Life Sciences), an integrated FPLC system consisting of two LC pumps, a pH flow cell, 3-channel UV detector, conductivity detector, and fraction collector (FRAC-950) was used for all chromatofocusing studies. The system was controlled using the Unicorn 4.12 (Build 213) software. Q Ceramic HyperD 20 media, washed and suspended in the packing mobile phase (0.1 M potassium phosphate and 0.5 M sodium chloride at pH 6.8), was loaded into a HR10/10 column up to a bed height of 10 cm at a constant pressure of 2.0 MPa, followed by 10 CVs of packing mobile phase.

Proteins were manually injected using a 10 mL sample loop and detected upon elution at 280 nm at a path length of 2 mm. A 2 mL mixing chamber was used for the mixing of the two buffers A (the column equilibration and sample loading buffer) and B (the buffer required for isocratic or gradient elution). The column was first equilibrated with 7 CVs of buffer A. All runs were performed at a flow rate of 25 mL min⁻¹. For gradient elutions, the sample contained in the sample loop was injected in a 15 mL injection cycle at a flow rate of 10 mL min⁻¹, followed by a 60 mL gradient from 0% (v/v) to 100% (v/v) of buffer B and 60 mL of 100% (v/v) buffer B (gradient elution). For isocratic elutions, sample was loaded in a 15 mL injection cycle at a flow rate of buffer A of 25 mL min⁻¹, washed in 2 CVs of buffer A, then eluted in 60 mL of 100% (v/v) of buffer B, again at a

flow rate of 25 mL min⁻¹. After each run, the column was washed with 12.5 mL of 1 M NaCl followed by 5 CVs of 20% (v/v) ethanol at a flow rate of either 10 mL min⁻¹ or 25 mL min⁻¹.

5.2.7 Gel electrophoresis

The Novex Mini-Cell electrophoresis unit from Invitrogen was used to perform SDS-PAGE runs. Sample buffer was comprised of 50% (v/v) NuPAGE LDS buffer, 20% (v/v) 0.5 M DTT and 30% (v/v) nanopure water. Protein samples were diluted 2-fold in sample buffer, and heated in a water bath at 80 °C for 10 minutes. Each lane was loaded with either 20 µL of a protein sample or 10 µL of SeeBlue Plus2 pre-stained standard. Electrophoresis was performed at 200 V on a FB300 power supply from Fisher Biotech until appropriate band migration across the entire length of the gel was achieved. The gel was rinsed with nanopure water and stained with SimplyBlueTM SafeStain (Invitrogen) at room temperature for 1 hour under constant shaking; the stained gel was then destained overnight with nanopure water and dried in cellophane prior to visualization.

5.2.8 Mass spectrometry

Mass spectrometry was completed in collaboration with the University of British Columbia (UBC) Biomedical Research Centre (BRC) Multi-user Facility for Functional Proteomics (MFFP). Protein fractions collected from isoelectric chromatofocusing were directly used for mass analysis without desalting. Intact protein mass analysis was performed on a 4700 MALDI-TOF/TOF from Applied Biosystems. Peptide fragment

identification was performed by mass analysis on a QStar XL Q-TOF from Applied Biosystems following reduction, alkylation and tryptic digestion.

5.3 Results and Discussion

5.3.1 Recombinant protein production

Representative data for recombinant *Pichia pastoris* growth and induction, as well as extracellular titres of the recombinant N-lobe of human transferrin (hTf/2N), are reported

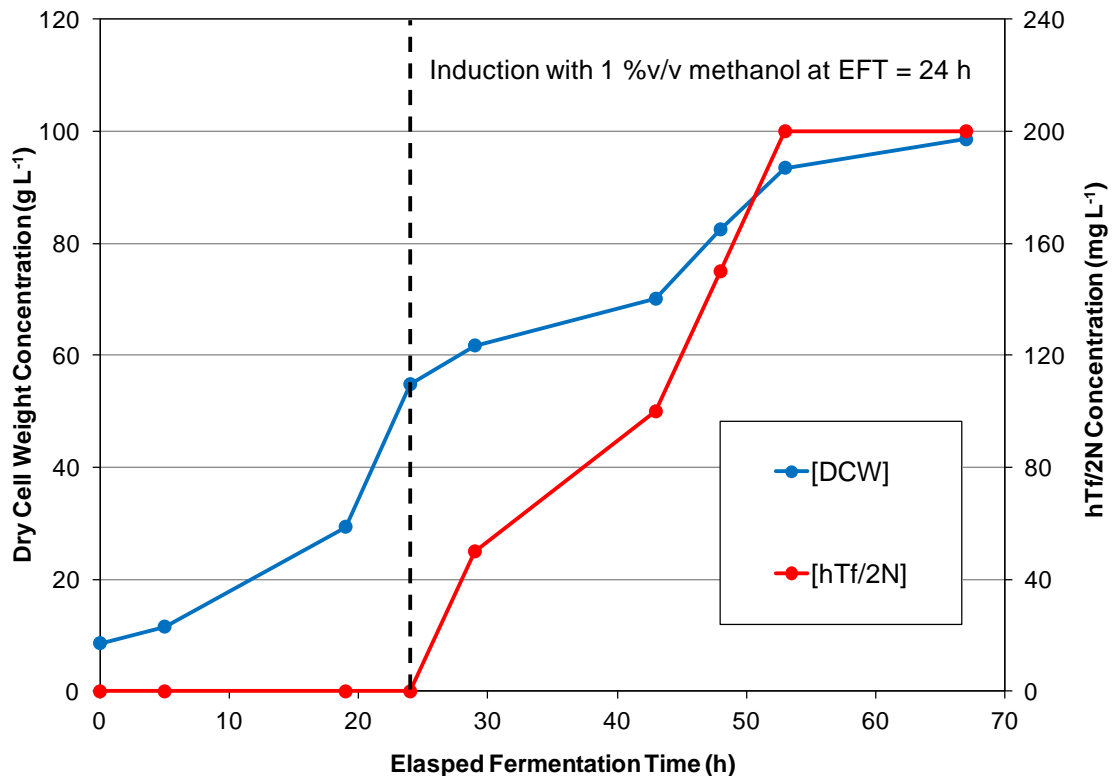


Figure 5.1: Changes in dry cell weight and hTf/2N concentrations throughout fermentation of recombinant *Pichia pastoris* Mut^S at 30 °C, 40% (v/v) of saturation DO concentration, pH 4.5, and 1% (v/v) methanol. Induction was initiated 24 hours after culture inoculation (batch fermentation from 0 h < Elapsed Fermentation Time (EFT) < 6 h; culture was batch-fed with 50% (w/v) glycerol at 18 mL h⁻¹ from 6 h < EFT < 24 h; then fed with 50% (w/v) glycerol at 11 mL h⁻¹ from 24h < EFT < 67 h).

in Figure 5.1. Cell densities between 55 g and 65 g (dry cell weight) L⁻¹ were typically achieved prior to induction, resulting in the secretion of hTf/2N to titres at or near 0.2 g L⁻¹ following induction. As noted in Chapter 2, hTf/2N is recombinantly produced in this host as four dominant isoforms distinguished by differences in their molecular mass possibly resulting from variations in post-translational processing [124].

5.3.2 Comparing gradient and isocratic isoelectric chromatofocusing

Isoelectric chromatofocusing of the clarified supernatant using a 60 mL programmed linear pH gradient results in a chromatogram comprised of four peaks eluting between pH 8.5 and 6.5, and two additional broader peaks eluting below pH 6 (Figure 5.2A). Intact and tryptic mass spectrometry of each peak confirms that the four peaks eluting between pH 8.5 and 6.5 comprise the four dominant isoforms of recombinant hTf/2N produced in *P. pastoris*, while the two late eluting peaks are found to contain no hTf/2N, and are likely comprised of secreted host cell proteins (HCPs) that serve to contaminate the supernatant. The loading and elution buffer (buffer formulation 1003) used here was designed using the model described in Chapter 2 (Table 2.4) and produces a linear elution pH gradient on the Q Ceramic HyperD 20 HR10/10 column. Good removal of supernatant HCPs is achieved in the gradient separation conducted on this preparative stationary phase. Moreover, the 36701 Da hTf/2N isoform (hTf/2N-4), which has been shown by others [124] to exhibit the strongest binding to the transferrin receptor (a carrier protein for transferrin needed to import iron into the cell and to regulate intracellular iron abundance), is well isolated from less active isomers despite the very high mobile phase flow rate used (25 mL min⁻¹). Thus, ICF conducted on preparative matrices can yield

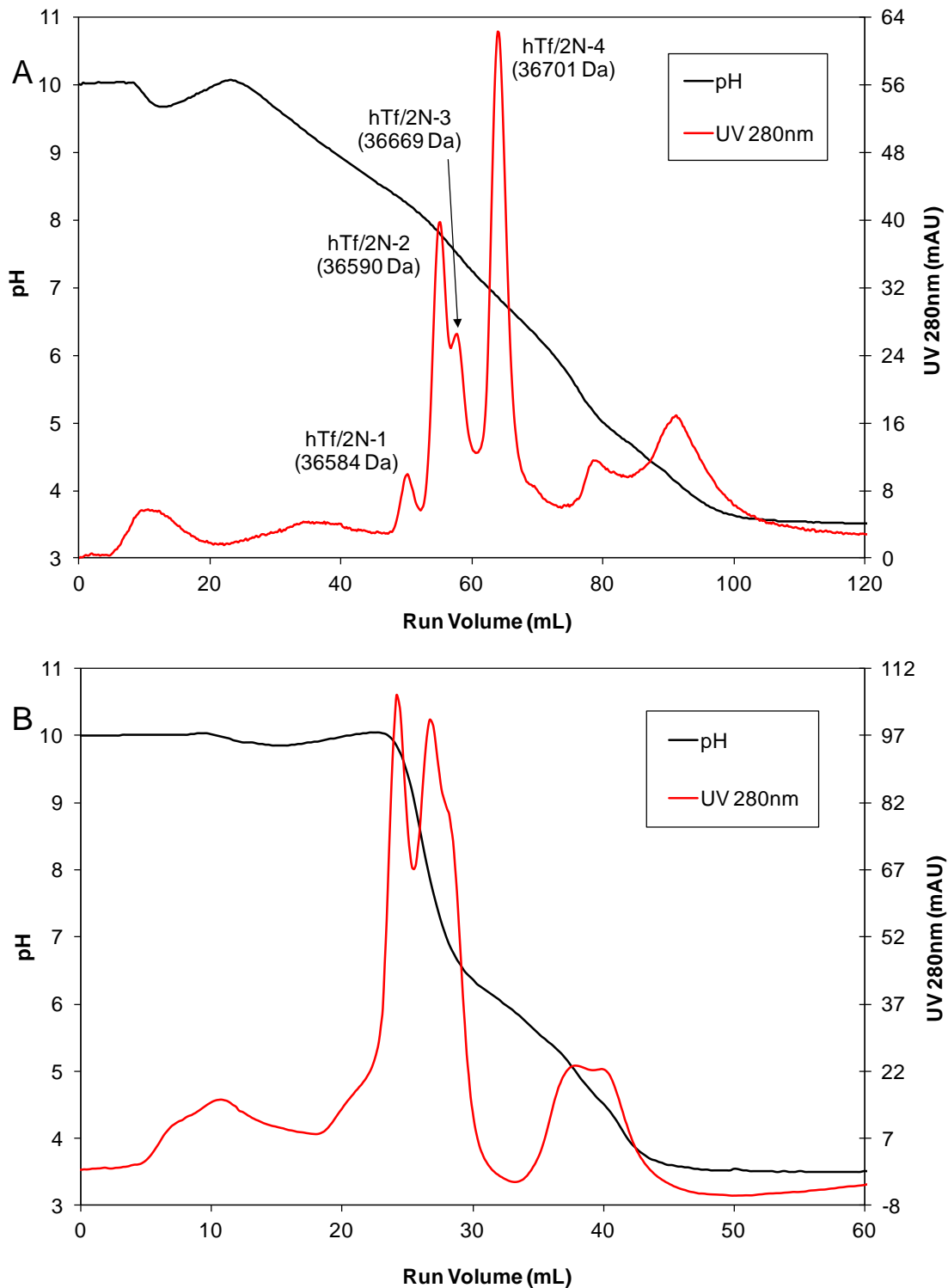


Figure 5.2: Comparison of A) gradient isoelectric chromatofocusing (labeled with the intact masses of four distinguishable hTf/2N isoforms) and B) isocratic isoelectric chromatofocusing of recombinant *Pichia pastoris* Mut^S fermentation broth on a Q Ceramic HyperD 20 HR10/10 strong anion exchange column at a mobile phase (buffer formulation 1003) flow rate of 25 mL min⁻¹ at 25 °C.

exceptional separation factors when an appropriate gradient elution strategy is applied. The goal here, however, was to define a corresponding strategy by which an isocratic elution process can be designed and applied to effectively purify the hTf/2N-4 isoform from culture supernatant.

Baseline separation of hTf/2N-4 cannot be achieved in an isocratic elution mode (Figure 5.2B) when the same buffer formulation (1003), which was specifically designed in Chapter 2 for linear gradient elution on a Mono Q column, is applied. Mono Q and Q Ceramic HyperD 20 are both strong anion exchange media and therefore provide no intrinsic buffering capacity to the system. Thus, although formulation 1003 is custom designed using the model to produce a linear pH profile on Mono Q when operated under programmed gradient elution, it should also and does produce a linear pH profile on Q Ceramic HyperD 20 when operated under the same solvent gradient program. However, buffer formulation 1003 does not yield a linear pH profile in either column when applied in an isocratic elution mode and very little resolution of hTf/2N isoforms is achieved (Figure 5.2B).

5.3.3 Simple strategy for optimizing ICF operating under isocratic elution

The ICF model developed in Chapter 4 to describe protein retention predicts that elution time depends on the pI of the protein and decreases nonlinearly with increasing ionic strength. In the absence of model parameters, the precise relationship between the elution pH of a particular protein and ionic strength is unknown, but can be estimated by 1) performing a set of programmed linear-gradient ICF separations that cover a range of

ionic strengths; 2) aligning trends observed in the data set with the mechanisms of elution and their dependence on ionic strength as encoded in the model; and 3) narrowing options based on the properties of the target protein and limitations in the types of gradients that can be generated by two-solvent isocratic elution. Together, this information can be used to sculpt a desired isocratic elution gradient by designing the required load and elution buffers using the model reported in Chapter 2.

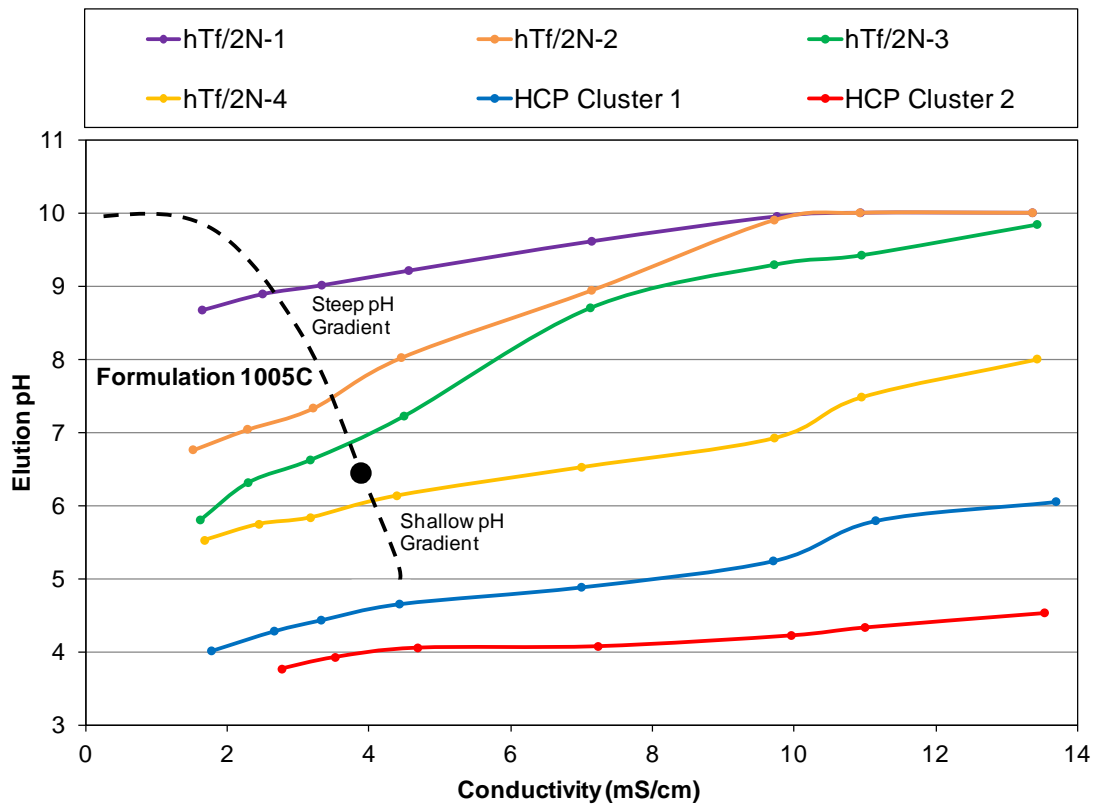


Figure 5.3: Elution pH vs. conductivity for major protein components resolved using ICF on the Q Ceramic HyperD 20 HR10/10 strong anion exchange column. Dotted black line represents approximate changes in ionic strength during ICF separations with buffer formulation 1005C.

To test this isocratic-elution design strategy, clarified supernatant from a recombinant *P. pastoris* fermentation was fractionated by programmed linear-gradient ICF at eight different ionic strengths (20 mM, 30 mM, 40 mM, 50 mM, 55 mM, 75 mM, 105 mM and 125 mM) using NaCl. From that study, measured elution pH values for each of the six major protein components in the sample are plotted against mobile phase conductivity in Figure 5.3. The data define the dependence of protein elution on both mobile phase pH and ionic strength. As predicted by the ICF elution model, the elution pH of each component in the supernatant increases with increasing ionic strength, with the magnitude of that dependence being protein and protein-isoform dependent.

The data in Figure 5.3 also reveal that the desired hTf/2N-4 isoform can be most easily separated from both HCP contaminants and other hTf/2N isoforms in the clarified supernatant through the application of a linear elution pH gradient at a relatively high conductivity of *ca.* 10 mS cm⁻¹. While buffer formulations could be designed to approximate that gradient by step elution between two isocratic solvents, it is not an ideal approach in practice. Firstly, the cost of preparative ICF separations increases with increasing ionic strength, and the approach negates one of the key processing advantages of ICF: namely the ability to both load and elute at relatively low ionic strengths to ease integration with subsequent downstream operations (*e.g.* avoid costly diafiltration). Secondly, elution at or near a conductivity of 10 mS cm⁻¹ would cause hTf/2N-4 to elute at high ionic strength and a pH very near its *pI* (~ 6.9), resulting in solubility concerns and the undesired possibility of needing to reduce feedstock concentrations to avoid precipitation of the eluting target protein.

A more desirable strategy is therefore to design an isocratic elution to recover pure hTf/2N-4 at conductivities near 4 mS cm^{-1} . The elution pH of hTf/2N-4 is then a pH unit below the protein's pI , and buffer usage is likely reduced. The data in Figure 5.3 indicate that this is a considerably tougher separation, as the elution pH values of hTf/2N-2, hTf/2N-3 and hTf/2N-4 under a linear gradient are much closer at low conductivities. But the data also reveal that the separation can be achieved by an isocratic elution in which the pH gradient is steep and negative from the load pH to about pH 6.6, and is then made much shallower in slope from pH 6.6 to 5.0 (dashed line in Figure 5.3). The data also show that the required pH profile can be accompanied by a modest increase in ionic strength (conductivity) since the elution pH of hTf/2N-4 diverges from that of the other isoforms with increasing ionic strength. Using this protocol, the elution pH of hTf/2N-4 is expected to be *ca.* 6 and therefore sufficiently removed from the protein's pI to avoid solubility concerns.

Using the model described in Chapter 2, buffer formulation 1005C (Table 5.1) was designed to generate the desired pH gradient between pH 10.0 and 5.0, including a shallow gradient region between pH 6.6 and 5.4, using isocratic elution (Figure 5.4). Based on predictions of the elution model reported in Chapter 4, a modest increase in ionic strength was also introduced in the elution gradient to improve peak separation, promote complete elution of proteins and reduce peak tailing. As fixing the desired shape of the pH gradient was the goal (the elution pH of hTf/2N-4 depends rather weakly on I), and pH and ionic strength changes cannot be sculpted independently when a step-change between solvent states is applied, this increase in ionic strength is nonlinear with

elution volume and fluctuates somewhat due to protein-matrix interactions and changes in buffer speciation (see Chapters 2 and 4).

Using this model-aided strategy, near-baseline separation of hTf/2N-4 from other isoforms is achieved. Contaminating isoforms are eluted in the first column volume of eluent, then the desired hTf/2N isoform is eluted at a pH of *ca.* 6, as expected (Figure 5.3); finally, contaminating HCPs are removed using a final high ionic strength wash (Figure 5.4). The custom-designed gradient permits exceptionally high flow rates (25 mL min^{-1}) to be employed, so that purification of the desired hTf/2N-4 isoform is achieved in approximately 1 minute, with a total column cycle time of less than 5 minutes.

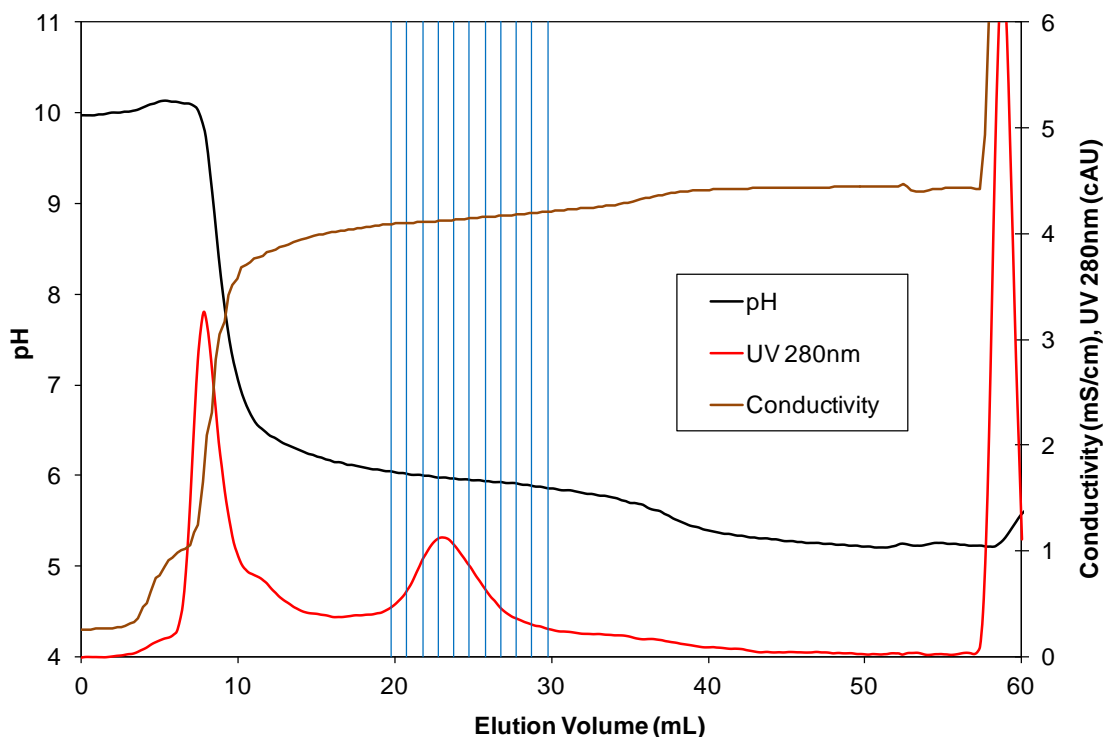


Figure 5.4: Customized isocratic elution and pH gradient applied to the isolation of the desired hTf/2N isoform (collected in eight 1 mL fractions) from HCP and three undesired isoforms using the Q Ceramic HyperD 20 HR10/10 strong anion exchange column at a mobile phase (buffer formulation 1005C) flow rate of 25 mL min^{-1} at $25 \text{ }^\circ\text{C}$.

The peak containing the desired isoform was collected in a series of 1 mL fractions, each of which was analyzed using SDS-PAGE and found to align with the most intense band in the lane loaded with clarified culture supernatant (Figure 5.5). The fractions were also subjected directly (without desalting) to intact protein mass spectrometry to confirm pure hTf/2N-4 (36701 Da) in each fraction of the product peak.

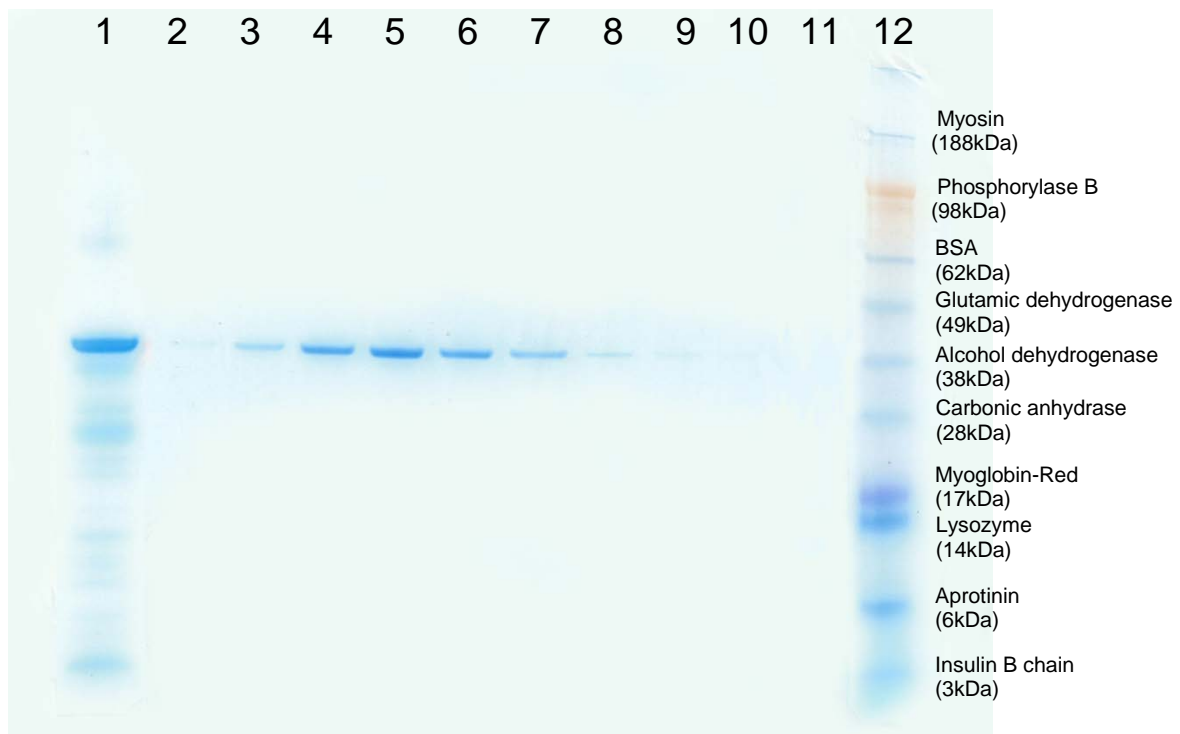


Figure 5.5: SDS-PAGE gel separation of raw culture supernatant (Lane 1), isometrically pure transferrin peak collected from ICF (Lanes 2 to 9) and SeeBlue Plus2 Pre-Stained Standard (Lane 12)

Though applied here to a difficult separation on preparative media, the isocratic gradient sculpting method described should be equally applicable to the improvement of separations at analytical scales by shifting the elution pH of the various components in the sample to desired values. In that case, custom linear and non-linear gradients in both

pH and ionic strength can be generated by isocratically introducing a third buffer of high ionic strength. In the absence of detailed binding and physicochemical data for the feedstock components, the simple empirical strategy described can serve to design optimal pH and ionic strength gradients for ICF, and for conventional IEC.

5.4 Concluding Remarks

A simple method for designing effective load and elution gradients in ICF is devised using a step change between isocratic solvents. The technique uses a limited set of linear-gradient elution data, simple low-molecular-weight buffering species, and a preparative strong ion exchange column as the design inputs, and is shown to yield purified proteins in low-ionic-strength solvents that can be directly subjected to mass spectrometric analysis without desalting. On columns packed with a preparative matrix, very high mobile phase flow rates can be employed without compromising separation quality due to the focusing effect exploited in ICF. The method therefore improves the potential of custom isocratic ICF to be implemented in manufacturing processes and associated preparative purifications.

Chapter 6

Application of Custom Gradient Chromatofocusing to Detection and Identification of O-GlcNAc Modified Proteins in Differentiated C2C12 Mouse Myoblasts

A liquid chromatography-based separation platform for the isolation and analysis of protein post-translational modifications (PTMs) from complex proteomes has been developed. The platform involves initial fractionation of the proteome using isoelectric chromatofocusing (ICF) at low ionic strength, followed by parallel antibody-based selection of proteins with or likely to possess the modification of interest via western blotting and sodium dodecyl sulfate-polyacrylamide gel electrophoresis (SDS-PAGE) separation, the latter of which yields gel-band samples that can be subjected to sequence analysis by mass spectrometry. This technique is demonstrated through the investigation of the O-linked N-acetylglucosamine (O-GlcNAc) PTM within the cell-lysate proteome of the C2C12 mouse myoblast cell line. The novel ICF-based fractionation platform, when used in conjunction with mass spectrometry data for protein identification, is shown to result in the detection of a number of putative O-GlcNAc-modified proteins within the proteome of differentiated C2C12 mouse myoblasts.

6.1 Background

Most eukaryotic proteins undergo some form of modification following translation. These post-translational modifications (PTMs), which may include glycosylation, phosphorylation and sulfation (to name but a few), serve many functions. As a result, the analysis of proteins and their post-translational modifications is integral to the study of diseases where multiple genes are known to be involved, such as heart disease, cancer and diabetes. Analysis of PTMs is aided by the fact that they result in modification-specific changes in chemistry that may be detected using antibody base screens, and in mass that may be detected by mass spectrometry provided the modified protein(s) are sufficiently pure and enriched.

Examples of the central role PTMs play in mediating the biological activities of many families of proteins include function altering conformational changes in blackfin tuna myoglobin induced by S-nitrosylation [125], phosphorylation of the S6 kinase within mTOR (the mammalian target of rapamycin) that regulates cell growth and motility [126], and O-linked N-acetylglucosamine (O-GlcNAc) modification of the insulin receptor substrate proteins IRS-1/2 that leads to attenuated insulin signaling [127]. In general such modifications are dynamically regulated and rapidly changing, making their study difficult and highlighting the need for reliable methods to detect and identify across a wide dynamic range proteins bearing specific PTMs within a proteomic sample.

Among the many methods used to study PTMs within complex proteomes, the most commonly used include antibody-based methods that enrich and detect modified proteins [128, 129], chemical-modification-based methods that serve to ease or enhance detection [130], and two-dimensional gel electrophoresis (2DGE) based separation to permit detection and quantification by an appropriate mass spectrometric method [131]. Each has its own advantages and disadvantages, and all typically target a single modification of interest to reduce the complexity of the analysis. A very common workflow involves pre-fractionating a proteomic sample using two-dimensional (2D) western blotting employing a PTM-specific antibody. The general intent of this type of study is to identify a library of proteins likely to carry the PTM, each of which can subsequently be purified to homogeneity and subjected to further assays to confirm the presence of the PTM. In a 2D western blot, protein spots are matched to corresponding locations on a parallel Coomassie-stained 2D SDS-PAGE gel. In principle, this permits intact proteins of interest to be visualized and then excised for mass spectrometric analysis. Although this general workflow has proven useful, the method is known to suffer from poor reproducibility and, in particular, low throughput due to the reliance on parallel 2DGE procedures and gel-band matching. Poor sensitivity is another problem: western blotting is usually capable of identifying a spot or band containing 1 ng or more of protein. Since the maximum protein load on an immobilized pH gradient (IPG) strip used for 2DGE is of the order of several hundred micrograms, a 2D western blot typically offers a dynamic range of no more than five orders of magnitude, and that range can be and often is much lower due to the poor efficiency in extracting proteins from the gel, a particular problem for larger proteins.

Prior to the size-based separation of a proteome within a 2D gel, isoelectric focusing (IEF) gel electrophoresis is used to pre-fractionate the proteome along the IPG within the gel. That IEF fractionation step is conducted at voltages significantly higher than the redox potential of water. As a result, (non-biological) chemical modifications of proteins during the IEF step have been widely reported [94] and are known to be greatly enhanced by the presence of even small amounts of salt(s) in the sample [56]. Other unwanted chemical modifications of proteins during IEF have also been reported [95-99], some of which can be minimized through sample reduction and alkylation prior to loading. Nevertheless, IEF exposes proteins to harsh conditions that are conducive to undesired modifications or denaturation.

The goal of this work is to develop an alternate, milder chromatography-based strategy to pre-fractionate a library of proteins likely to bear a PTM of interest. To be applicable, the separation performance should approach that of the traditional 2DGE/western blotting, and a few studies suggest this may be possible when highly efficient modes of HPLC are applied [132, 133]. Though liquid chromatography does not generally achieve the degree of resolution attainable by electrophoresis, that prior work shows it can approach it or even exceed it in certain cases, while also offering superior reproducibility and flexibility. In the platform proposed here, fractions collected from the chromatography step are then further fractionated on a simple 1D western gel and, in parallel, a 1D SDS-PAGE gel. One challenge to this approach is the fact that many traditional modes of chromatography show limited compatibility with either 2D western blotting or 1D western gels. Reversed phase chromatography denatures intact proteins, while conventional ion exchange and

hydrophobic interaction chromatography use high ionic strength elution conditions that interfere with gel electrophoresis. In contrast, isoelectric chromatofocusing (ICF) is directly compatible with western analysis and 1D SDS-PAGE, provided that polyampholyte buffers are not employed for elution gradient generation [65, 66]. As shown in previous chapters of this thesis, ICF can use simple monoprotic and diprotic buffers to achieve nondenaturing separations at low ionic strength. That approach might therefore permit fractionation of a complex proteome prior to the selection of a post-translational modification of interest via parallel 1D western and SDS-PAGE gels. ICF fractionates proteins under very mild conditions when compared to IEF, eliminating the need for pre-alkylation or reduction of the sample to reduce the occurrence of unwanted modifications or degradation.

Here, gradient-sculpting methods are used to enhance the resolution of ICF when used to pre-fractionate the clarified lysate of a complex proteome. The separation achieved is shown to enable identification of candidate proteins bearing a specific PTM by parallel western and 1D SDS-PAGE gels followed by mass spectrometry. Since to a first approximation ICF separates proteins based on their isoelectric point (pI), the platform is analogous to the separation achieved by the traditional 2DGE method. By using ICF as the first dimension, sufficient amounts of sample can be loaded and fractionated in a single separation step to provide enough pre-fractionated proteins in native form for multiple second-dimension processes; these can potentially include several different western analyses directed against different PTM targets, replicate analyses, as well as any other protein-specific analyses that require native protein samples. Higher loads can

likewise serve to increase the dynamic range of the method. Here, as a proof of concept, the platform is applied to the isolation and sequence identification of proteins in the clarified-lysate proteome of differentiated C2C12 mouse myoblasts (C2C12 mouse myoblasts differentiate into myotubes (skeletal muscle cells) and myofibers) that are likely to be post-translationally modified with O-linked N-acetylglucosamine.

The O-GlcNAc modification, first reported in 1984 by Torres and Hart [134], is found on transcription factors, nuclear pore proteins, RNA-binding proteins, cytoskeletal proteins, stress induced proteins and other proteins involved in various cellular processes [135]. The diversity of the types of proteins modified with this PTM has made clear the fact that the O-GlcNAc modification plays a significant role in the regulation of cellular processes. It is integral in carbon nutrient sensing, and glucose uptake and metabolism [136], while emerging science suggests that its dysregulation could be of significance in the pathology of type 2 diabetes mellitus. A relevant nutrient-sensing pathway involved in glucose metabolism is the hexosamine biosynthesis pathway (HBP), which has been linked to a hallmark symptom of diabetes, insulin resistance [137], and also releases as its end product uridine diphosphate N-acetylglucosamine (UDP-GlcNAc). Within the HBP, fructose-6-phosphate conversion to glucosamine-6-phosphate by glutamine-fructose-6-phosphate amido-transferase (GFAT) dictates cellular levels of UDP-GlcNAc [138].

UDP-GlcNAc levels are increased in skeletal muscles of diabetic mice [139]. Enhanced activity of GFAT is also observed in the skeletal muscles of type 2 diabetic patients [140], and that finding has suggested that stimulation of the HBP could mediate

hyperglycemia-induced insulin resistance in skeletal muscles of type 2 diabetic mice [141] since GFAT controls the flux of glucose into the HBP, and insulin resistance is known to result from a combination of high glucose, insulin and glutamine [137, 138].

As UDP-GlcNAc is also the primary substrate for the O-GlcNAc modification of proteins, changes in its intracellular abundance caused by hyperglycemia-induced insulin resistance and associated changes in GFAT activity should alter the number and total abundance of intracellular O-GlcNAc modifications. Indeed, diabetes-associated proteins, including IRS-1 [35], eNOS [142] and Sp1 [143], have all been shown to have their degree of O-GlcNAc modification affected by either insulin stimulation or resistance.

Detecting changes in the rate of occurrence of O-GlcNAc PTMs upon stimulating muscle cells with insulin and glucose to induce hyperglycemia therefore represents a biologically relevant model for testing the performance of the novel proteomics platform proposed. Here, the C2C12 mouse myoblast cells are differentiated into primary muscle fibers and then treated with insulin, streptozotocin (STZ) and glucose to induce hyperglycemia. The platform is then used to scout proteins that become O-GlcNAc modified as a result of that treatment. Here, the intent is not to report new findings related to the biology of hyperglycemia-induced insulin resistance, but rather to show that the platform is capable of isolating and identifying candidate O-GlcNAc modified proteins in this medically relevant and complex model system.

Although not the model system adopted for this work, the majority of proteins implicated in or associated with Alzheimer's disease are also O-GlcNAc modified. Important examples include tau [103] and the beta-amyloid precursor protein [144]. The formation of tau tangles associated with the disease is the result of a reduction in the O-GlcNAc modification of tau and the subsequent hyperphosphorylation of tau [145]. The severity of Alzheimer's disease has also been correlated to glucose metabolism, where decreased metabolism results in increased symptoms of the disease [146]. Over-expression of O-GlcNAc transferase increases the amount of O-GlcNAc modification while decreasing phosphorylation of tau [145]. Levels of O-GlcNAc modified tau are therefore tightly associated with the susceptibility to and development of Alzheimer's disease.

6.2 Experimental

6.2.1 Cell culture

C2C12 mouse myoblast cells, kindly provided by Dr. Fabio Rossi (University of British Columbia Biomedical Research Centre), were cultured in DMEM (Invitrogen) supplemented with 2% penicillin/streptomycin and 10% fetal bovine serum at 37 °C and 5% CO₂. Cultured cells were either passaged at 70% confluence or differentiated at 90% confluence with differentiation medium MEM α (Invitrogen) supplemented with 5% heat-inactivated horse serum (Invitrogen) and 20% penicillin/streptomycin. Cells were differentiated for three days before being subjected to various treatments.

6.2.1.1 Insulin/streptozotocin/glucose treatment

Differentiated cells were washed two times with PBS (137 mM NaCl, 10 mM phosphate, 2.7 mM KCl pH 7.4) and serum starved overnight in MEM α media at 37 °C and 5% CO₂. Insulin (10 nM), streptozotocin (STZ) (2 mM), and glucose (12 g L⁻¹) were added, and the cells were incubated for 24 hours at 37 °C and 5% CO₂. Cells were then lysed with 200 μ L/dish of lysis buffer (50 mM Tris pH 7.5, 150 mM NaCl, 5 mM MgCl₂ and 0.1% (v/v) NP40) containing a protease inhibitor cocktail (Roche, Laval, QC). The resulting whole cell lysates were centrifuged at 14000 RPM for 15 minutes to remove cell debris.

6.2.1.2 Untreated and alloxan treatment

Differentiated cells were washed two times with PBS (137 mM NaCl, 10 mM phosphate 2.7 mM KCl pH 7.4) and serum starved overnight in MEM α at 37 °C and 5% CO₂ and either left untreated or treated with alloxan (4 mM) for 4 hours. Cells were lysed with 200 μ L / dish of lysis buffer (50 mM Tris pH 7.5, 400 mM NaCl and 5 mM MgCl₂) plus a protease inhibitor cocktail (Roche, Laval, QC). Whole cell lysates were then centrifuged at 14000 RPM for 15 minutes to remove cell debris.

6.2.2 Sample preparation for chromatography

Samples were buffer exchanged into the selected ICF loading buffer by applying 16 mg of clarified lysate onto a PD-10 desalting column (GE Healthcare Life Sciences) according to manufacturer's instructions. Following desalting, samples were concentrated to a final volume of 10 mL using a 50 mL Millipore centrifugal device (Millipore) with a 10 kDa protein cutoff membrane. Following concentration, samples

were passed through a 0.45 μm syringe filter (Pall) to remove large particulates, then passed through a 0.22 μm syringe filter (Pall) to remove any remaining particulate matter.

6.2.3 Isoelectric chromatofocusing

1,3 Diaminopropane (Cat. No. D23602), diethanolamine (Cat. No. D83303), imidazole (Cat. No. I0125), bis-tris (Cat. No. 156663), piperazine (Cat. No. P7003), lactic acid (Cat. No. L6661), DL-dithiothreitol (Cat No. D9163) and iodoacetamide (Cat No. I6125) were purchased from Sigma. Tris (Cat No. BP152), glacial acetic acid (Cat. No. A38P) and hydrochloric acid (Cat. No. A144) were obtained from Fisher. Relevant buffer formulations designed and used are reported in Table 6.1. All buffer solutions used as mobile phases for column equilibration and sample loading/elution were prepared with nanopure water, adjusted to the desired pH with concentrated HCl, and then filtered through a 0.22 μm membrane and vacuum degassed. Buffer pH values were measured with a pH/Ion Analyzer 350 from Corning, calibrated with standard pH buffers 4.00 (Cat No. B00765), 7.00 (Cat No. B00813) and 10.00 (Cat No. B00801) from Radiometer Analytical. All buffer solutions were prepared with nanopure water, filtered through a

Table 6.1: pH, ionic strength (mM) and buffer species concentrations (mM) in model-sculpted formulations of buffer A/buffer B pairs used for ICF fractionation of differentiated C2C12 mouse myoblast samples

Formulation		pH	I	DAP	DEA	TRS	IMI	BTS	PIP	ACE	LAC
1003	Starting	10.0	12	10	10	10	10	10	10	0	0
	Elution	3.5	102	10	10	10	10	10	10	10	10
03CC	Starting	10.0	6	5	5	5	5	5	5	5	5
	Elution	3.5	468	50	50	50	50	50	50	50	50

Abbreviations: I – ionic strength; DAP – 1,3 diaminopropane; DEA – diethanolamine; TRS – tris; IMI – imidazole; BTS – bis-Tris; PIP – piperazine; ACE – acetic acid; LAC – lactic acid

0.22 μm membrane Durapore[®] PVDF membrane (Millipore) and vacuum degassed.

The Mono Q HR10/10 strong anion exchange column was purchased from GE Healthcare Life Sciences. The AKTAexplorer100 (GE Healthcare Life Sciences) was used and was controlled by the Unicorn 4.12 (Build 213) software implementing a 3D kit control strategy. Samples were manually injected into a 10 mL sample loop and detected at 280 nm. To eliminate flow effects on pH, the pH electrode in the AKTAexplorer was calibrated to the adjusted pH values of the loading and elution buffers while pumping at 1 mL min⁻¹ without a column. A 2 mL mixing chamber was used for the mixing of buffers A and B. The column was first equilibrated with five column volumes of starting buffer at a flow rate of 0.5 mL min⁻¹. The sample contained in the sample loop was then injected in a 15 mL injection cycle at a flow rate of 1 mL min⁻¹, followed by a 60 mL gradient from 0% (v/v) to 100% (v/v) of buffer B and 60 mL of 100% (v/v) buffer B. After each run, the column was washed with 12.5 mL of 1M NaCl followed by 5 CVs of 20% (v/v) ethanol at a flow rate of 0.5 mL min⁻¹. Eluting samples were collected in 1 mL 96-deep-well plates using a FRAC-950 fraction collector (GE Healthcare Life Sciences).

6.2.4 Initial dot-blot screen

For platform development and as an initial screen, individual fractions were analyzed for presence of the O-GlcNAc modification by direct immuno-dot-blotting. 12 μL of each ICF fraction were spotted onto a pre-wetted PVDF membrane and blocked with 5% BSA overnight at 4 °C. The loaded membrane was incubated with the primary antibody CTD110.6 (1:5000 dilution in PBS-T; Covance) under gentle rocking for 1 hour at room

temperature, and then rinsed 5 times for 5 minutes in PBS-T. Each membrane was then incubated with horseradish-peroxidase coupled goat anti-mouse IgM secondary antibody (1:5000) (Sigma) for 1 hour under gentle rocking at room temperature. The membrane was again washed 5 times for 5 minutes in PBS-T. The sample and antibody loaded membranes were developed using an enhanced chemiluminescence (ECL) (GE Healthcare Life Science) kit and subsequently visualized with high performance chemiluminescence film (GE Healthcare Life Sciences) for 10 seconds, 30 seconds, 1 minute or overnight.

6.2.5 Electrophoresis

ICF/dot-blot fractions of interest were transferred into 1.5 mL Eppendorf tubes and reduced to 40 μ L using a vacuum centrifuge (Thermo) at 60 $^{\circ}$ C; 10 μ L of 5X Laemmli's sample buffer (10% SDS, 50% glycerol, 200 mM Tris, 752 mM 2-mercaptoethanol and bromophenol blue) were added. Samples were then boiled for 10 minutes prior to being split in a 60:20:20 volume ratio for separate loading onto three independent gels: the first (1D SDS-PAGE) used for Coomassie staining, the second (1D western gel) for O-GlcNAc immune-detection, and the third (1D western gel) for a secondary-antibody-only control.

On each 10% tris-glycine polyacrylamide (PAGE) gel, samples were co-loaded with See-Blue Plus2 pre-stained marker (Invitrogen) and then separated in 1X running buffer (25 mM Tris, 192 mM Glycine and 0.1 M SDS) at 70 V until the dye front passed the stacking gel. The voltage was then increased to 90 V until the dye front reached the bottom of the gel. The gel was stained with Coomassie Blue (0.1% (v/v) Coomassie

Brilliant Blue R250, 40% (v/v) methanol and 1% (v/v) acetic acid) for 1 hour and then destained with 10% (v/v) acetic acid until the gel background was clear.

6.2.6 Western gels

Resolved proteins on a gel loaded with 20% (v/v) of the sample were transferred at 23 V for 1 hour onto a PVDF membrane (Pall) in a 1X semi-dry transfer buffer (48 mM Tris, 39 mM Glycine, 13 mM SDS and 20% (v/v) methanol) using a semi-dry transfer apparatus (Bio-Rad). Following transfer, the membranes were blocked overnight at 4 °C with a 5% BSA solution in PBS-T. Blocked membranes were probed with the CTD110.6 antibody (1:5000 dilution in PBS-T; Covance) for 1 hour at room temperature. They were then washed 5 times, each for 5 minutes, with PBS-T, and probed with anti-mouse IgM-HRP for 1 hour at room temperature. The final antibody-stained gels were developed with ECL and exposed to film (GE Healthcare Life Sciences) for 10 seconds, 30 seconds, 1 minute or overnight.

6.2.7 In-gel digestion and mass spectrometric analysis

Gel bands were excised and cut into 1 mm cubes that were then washed with water and desolvated with acetonitrile. Dessicated gel bands were swollen in 10 mM dithiothreitol/0.1 M ammonium bicarbonate and incubated at 56 °C for 30 minutes to reduce any remaining disulphide bonds. Following reduction, gel particles were desolvated with acetonitrile and resolvated with 55 mM iodoacetamine/0.1 M ammonium bicarbonate. The gel particles were then incubated in iodoacetamide for 30 minutes at room temperature in the dark to alkylate proteins in the gel bands. Following alkylation,

gel particles were washed with 0.1 M ammonium bicarbonate prior to being treated again with acetonitrile. To those gel bands, trypsin (Promega, Madison, WI) suspended in 50 mM ammonium bicarbonate was added at a concentration of 0.1 µg / band. That mixture was incubated overnight at 37 °C.

Digestion liquid was collected in separate tubes and the gel particles were then washed with 20 µL of 25 mM ammonium bicarbonate for 15 minutes at 37 °C with shaking. Following washing, 80 µL of acetonitrile was added and the mixture was incubated at 37 °C for 15 minutes. The acetonitrile/ammonium bicarbonate mixture was then removed and transferred to a separate tube, into which 40 µL of 5% formic acid was added to the gel particles, and the mixture was incubated at 37 °C for 15 minutes. After the addition of 100 µL of acetonitrile, the mixture was incubated for 15 minutes, and the liquid in the tubes was pooled with the previously-collected liquids and dried in a vacuum centrifuge at 55 °C. These extracted and dried peptides were reconstituted in 7 µL of 5% formic acid.

Reconstituted peptide samples were analyzed by LC-MS/MS using a Q-Star (Applied Biosystems) hybrid quadrupole time of flight (TOF) instrument. Peptides were separated by reversed phase chromatography using a Famos/Ultimate LC system (Dionex) with the following gradient conditions: buffer A - 0.1% trifluoroacetic acid 5% acetonitrile; buffer B - 0.1% trifluoroacetic acid 80% acetonitrile. Column operation at a flow rate of 0.2 µL min⁻¹ consisted of sample loading in buffer A, a wash in 2% (v/v) buffer B for 10 minutes, elution from 2% (v/v) to 20% (v/v) buffer B for 50 minutes, an increase buffer B

to 90% (v/v) over 5 minutes, and a (regeneration) hold at 90% (v/v) buffer B for 5 minutes. Eluted samples were analyzed by the mass spectrometer using a nanospray source. The MS/MS sequencing results were matched to theoretical sequencing data using the MASCOT database with a peptide tolerance of ± 0.15 Da, MS/MS tolerance of ± 0.5 Da, 1 missed cleavage site allowed, and taking carbamidomethyl as a fixed modification and oxidation as a variable modification. Taken together, peptide mass data and O-GlcNAc activity detection on the western gel were used to assign proteins likely to bear the O-GlcNAc modification. A higher MASCOT score in general indicates an increased likelihood that the protein is present in the analyte (excised band from the given lane). However, as the sequenced and mass-analyzed peptides were not assayed in their homogeneous states, proteins identified in treated and untreated samples in this study are classified as being likely to carry the modification, with the understanding that further analysis is required to make a definitive assignment.

6.3 Results and Discussion

6.3.1 ICF of lysate-derived proteomes of differentiated C2C12 mouse myoblasts

Trial ICF separations of the lysate-derived proteomes of differentiated C2C12 mouse myoblasts that were treated with insulin/STZ/glucose to induce hyperglycemia were conducted to identify a model-designed (Chapter 2) gradient elution formulation that provides high peak capacities and relatively even peak distribution over the entire elution chromatogram. Convex, concave, and various linear gradients were designed and tested. Nonlinear gradients generally did not yield the desired uniform distribution of

fractionated proteins within the elution chromatogram (Figure 6.1A). Dot-blot screens of these fractions therefore revealed clustering of all GlcNAc modified proteins in fractions collected either early (concave gradient) or late (convex gradient) in the chromatogram (data not shown). Linear gradients with very shallow slopes (Figure 6.1B) achieved higher separation resolutions, but diluted protein concentrations in collected fraction such that a reduction in dynamic range was observed; moreover, that approach increased the total number of fractions that must be analyzed by western/SDS-PAGE/MS/MS.

In contrast, very good resolution and distinct peaks across the entire elution chromatogram are achieved using a custom moderately-steep linear-gradient formulation (buffer formulation 1003 in Table 6.1) with a slope of *ca.* -0.1 pH mL^{-1} in which the total ionic strength is designed to increase from 12 to 102 mM across the gradient (Figure 6.2). Sample dilution is greatly reduced and the chromatograms and gradients generated are highly reproducible. For comparison, the chromatograms produced using this formulation on proteomic samples from differentiated cells that were either untreated, treated with insulin/STZ/glucose to induce hyperglycemia, or treated with alloxan (negative control) to inhibit O-GlcNAc modification are overlaid in Figure 6.2 for comparison. The data show all three samples fractionate in a similar fashion, indicating that the addition O-GlcNAc does not greatly affect the isoelectric points or β values (see Chapter 4) of the proteins; maxima of major peaks in all three separations are closely aligned. To permit sufficient mass loading of a proteomic sample, the separation was performed on an 8 mL Mono Q HR10/10 column operated at moderate pressure. If required, resolution could likely be improved by conducting the fractionation on an

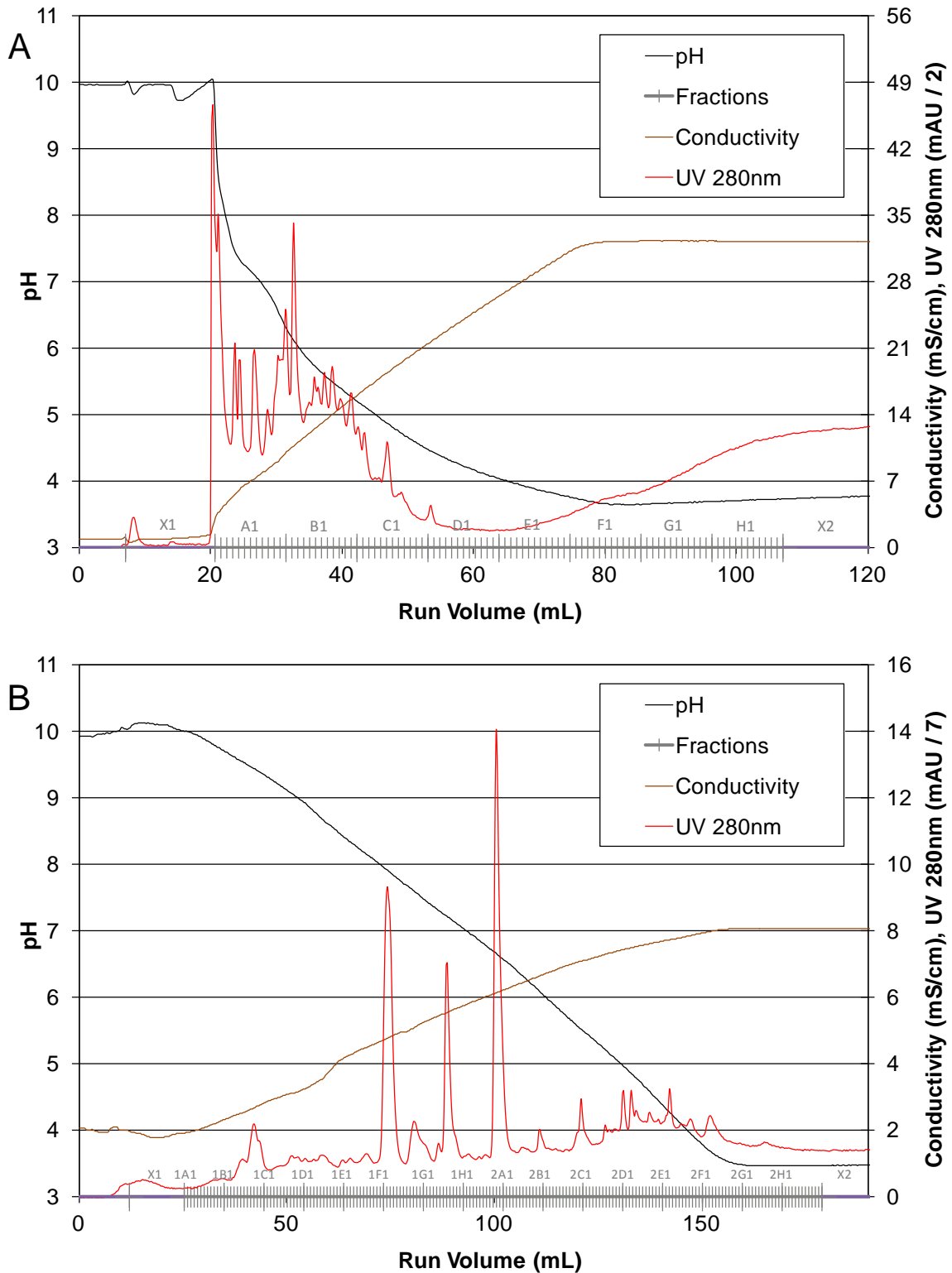


Figure 6.1: A) Concave pH gradient (buffer formulation 03CC) and B) shallow pH gradient (buffer formulation 1003, linear gradient at -0.05 pH mL^{-1}) ICF fractionation of the proteome (16 mg) of insulin/STZ/glucose treated differentiated C2C12 mouse myoblast cell lysate loaded as a 10 mL pulse onto a Mono Q HR10/10 strong anion exchange column at a mobile phase flow rate of 1 mL min^{-1} at $25 \text{ }^\circ\text{C}$; $900 \text{ } \mu\text{L}$ eluent fractions were collected.

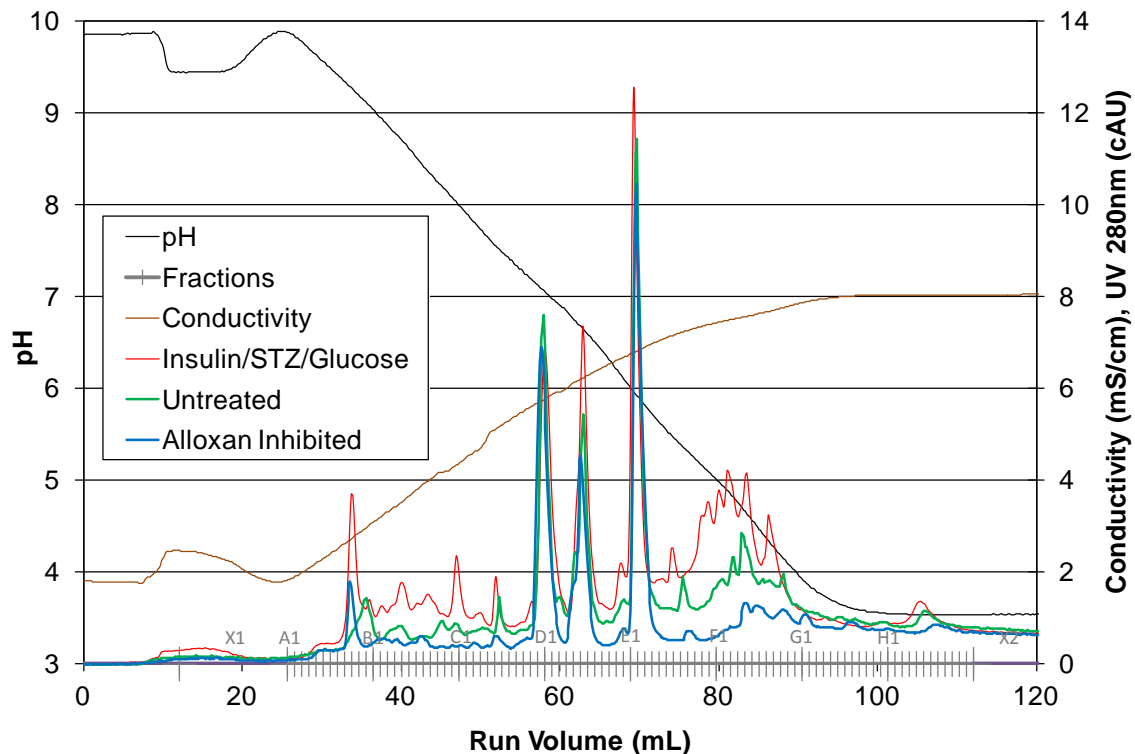


Figure 6.2: Overlay of chromatograms of linear gradient ICF fractionations of the proteomes of insulin/STZ/glucose treated (red), untreated (green) and alloxan-inhibited (blue) differentiated C2C12 mouse myoblast cell lysate samples loaded as a 10 mL pulse onto a Mono Q HR10/10 strong anion exchange column at a mobile phase flow rate of 1 mL min⁻¹ at 25 °C; 900µL eluent fractions were collected.

analytical-grade strong anion exchange column operating at high pressure (at the expense of load capacity), but the customized ICF separation system used here was found to provide more than enough resolving power for adequate reduction of sample complexity while preserving sufficient amounts of each fractionated protein to permit detection and analysis by western gels and mass spectrometry.

Each fraction collected from the ICF separation was first examined by a simple dot-blot method using the CTD110.6 antibody, which specifically targets the O-GlcNAc modification (Figure 6.3). In the sample treated with insulin/STZ/glucose, strong

O-GlcNAc reactivity was found in fractions E7 to F1, while fractions C3 to C11, D4 to E6 and F2 to F5 were found to exhibit moderate reactivity, and all other fractions showed relatively weak reactivity (Figure 6.3A). The dot blot of the untreated sample fractions showed almost no O-GlcNAc reactivity (Figure 6.3B), while the alloxan treated sample, a negative control for the O-GlcNAc modification, showed no significant reactivity across all fractions collected (Figure 6.3C). The results show that O-GlcNAc modification activity is strongly upregulated in slow muscle tissue by induction of hyperglycemia.

The absence of O-GlcNAc activity was verified by subjecting those ICF fractions of the alloxan-treated sample corresponding to O-GlcNAc positive dot-blot fractions in the treated sample to a full western gel, which provides considerably more sensitive detection of O-GlcNAc activity. As before, absolutely no reactivity to the O-GlcNAc modification was observed in the alloxan-treated samples (data not shown). 1D SDS-PAGE gels for the alloxan-treated sample confirm that proteins within the proteome are indeed well-distributed across the entire chromatogram (Figure 6.4). Bands of different intensity in the Coomassie-stained 1D SDS-PAGE gels were excised, subjected to enzymatic digestion, and then analyzed by tandem mass spectrometry to identify benchmark proteins of the differentiated cell proteome based on their peptide mass fingerprints and associated searching of the MASCOT database (Table 6.2). These benchmarks were used in this study to normalize the loadings of proteomic material in the platform, thereby allowing relative changes in the abundance of proteins of interest to be detected.

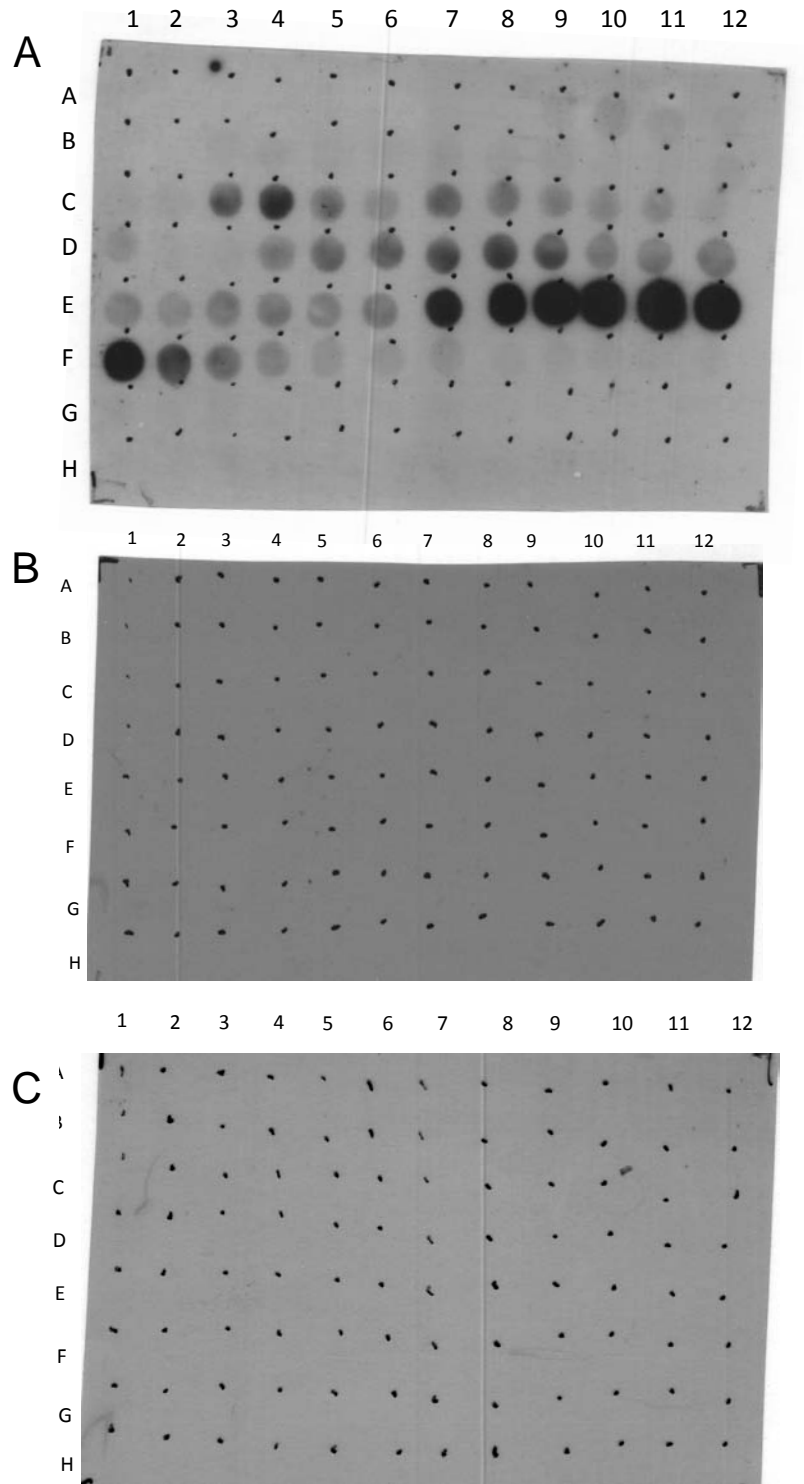


Figure 6.3: Dot-blots (12 μ L) of each fraction collected by linear gradient ICF (Figure 6.2) of the proteomes of A) insulin/STZ/glucose treated, B) untreated, and C) alloxan-inhibited differentiated C1C12 mouse myoblasts on a PVDF membrane blocked with a 5% BSA solution and probed with CTD110.6.

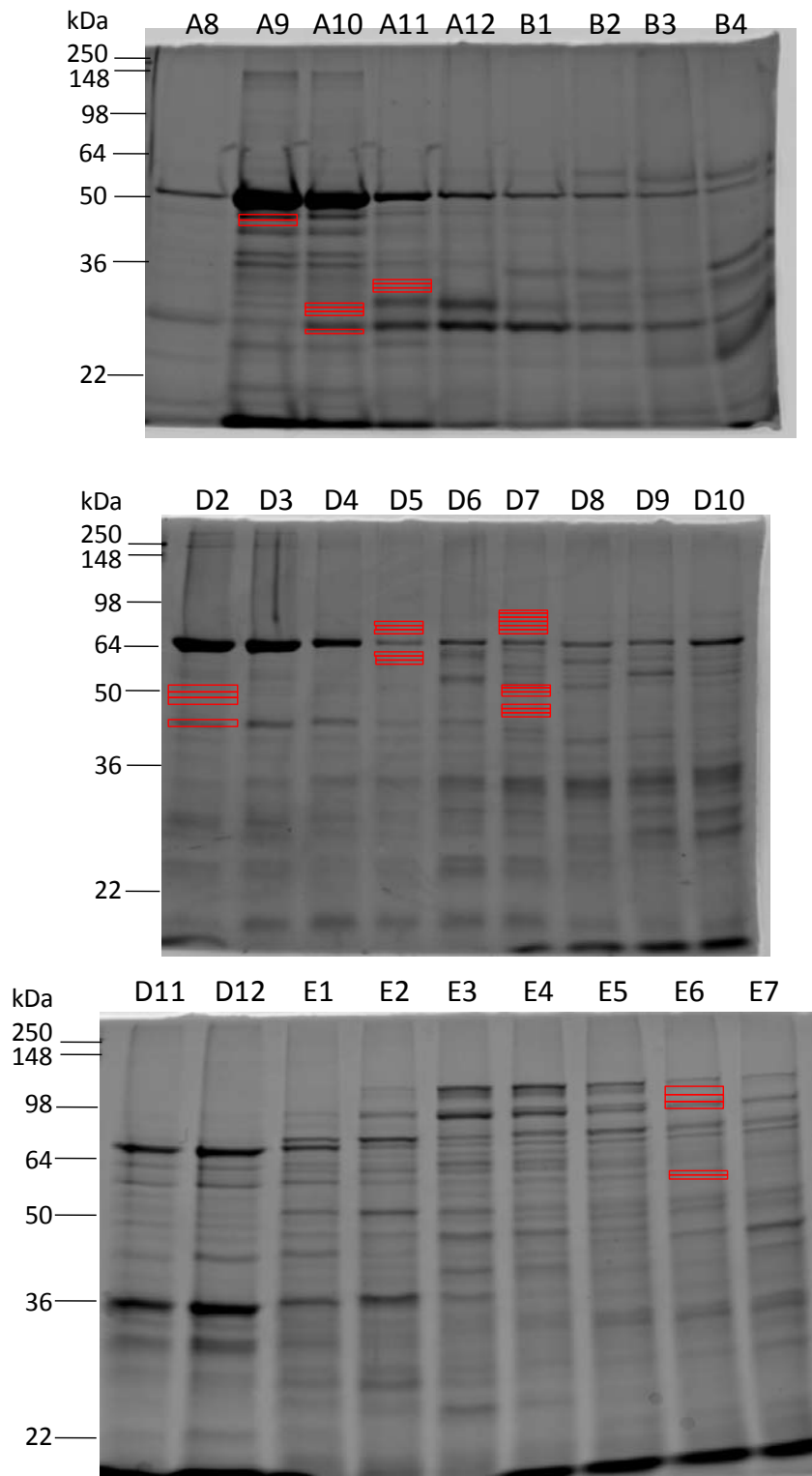


Figure 6.4: SDS-PAGE (10%) gel separation of selected fractions from ICF separation of the proteome of alloxan-inhibited differentiated C2C12 mouse myoblast cell lysate; red outlined bands on the SDS-PAGE gel were excised for mass analysis.

Table 6.2: Benchmark proteins identified in selected SDS-PAGE bands derived from alloxan-inhibited differentiated C2C12 mouse myoblast samples

Band	Protein ID	Accession Number	MW	pI	Elution pH	Mascot Score	Peptide Match
A9-1	Glucose 6 Phosphate Isomerase	P06745	62.9	8.18	9.4	1010	160
A9-2	Glucose 6 Phosphate Isomerase	P06745	62.9	8.18	9.4	128	16
A10-1	Glucose 6 Phosphate Isomerase	P06745	62.9	8.18	9.4	63	5
A10-3	Carbonic Anhydrase 3	P16015	29.63	6.97	9.3	131	17
A11-1	Carbonic Anhydrase 3	P16015	29.63	6.97	9.2	217	468
A11-2	Glucose 6 Phosphate Isomerase	P06745	62.9	8.18	9.2	257	40
D2-1	Moesin	P26041	67.8	6.24	7.0	245	26
D2-2	Keratin Type II Cytoskeletal 8	P11679	54.5	5.70	7.0	179	22
D2-3	Moesin	P26041	67.8	6.24	7.0	124	15
D2-4	Adenosylhomocysteinase	P50247	48.1	6.08	7.0	383	47
D5-3	Moesin	P26041	67.8	6.24	6.8	102	6
E6-1	Vinculin	Q64727	117.2	5.77	5.8	54	2
E6-2	Vinculin	Q64727	117.2	5.77	5.8	125	10
E6-3	Elongation Factor 2	P58252	96.2	6.42	5.8	253	29

6.3.2 Insulin/streptozotocin/glucose treated sample

Western gels and corresponding SDS-PAGE gels were run on those ICF fractions of the insulin/STZ/glucose treated sample that showed reactivity in the dot-blot screen. After the ICF separation each selected fraction contains a number of proteins, but the complexity of the fractions is sufficiently reduced to allow distinct protein bands to be obtained and excised from the subsequent western-aligned 1D SDS-PAGE gel (Figure 6.5A). Images of the western gels collected over short exposure times (10 seconds to 1 minute) show that bands containing O-GlcNAc modified proteins tend to elute over about three fractions (Figure 6.5B), which corresponds to a peak width of approximately 2.7 mL; this is consistent with peak widths observed in the chromatograms. Candidate O-GlcNAc modified proteins are found in fractions showing both strong and weak dot-blot-screen reactivity, and strong bands on the western gel often align with regions of the Coomassie-stained gel exhibiting relatively low total protein loads.

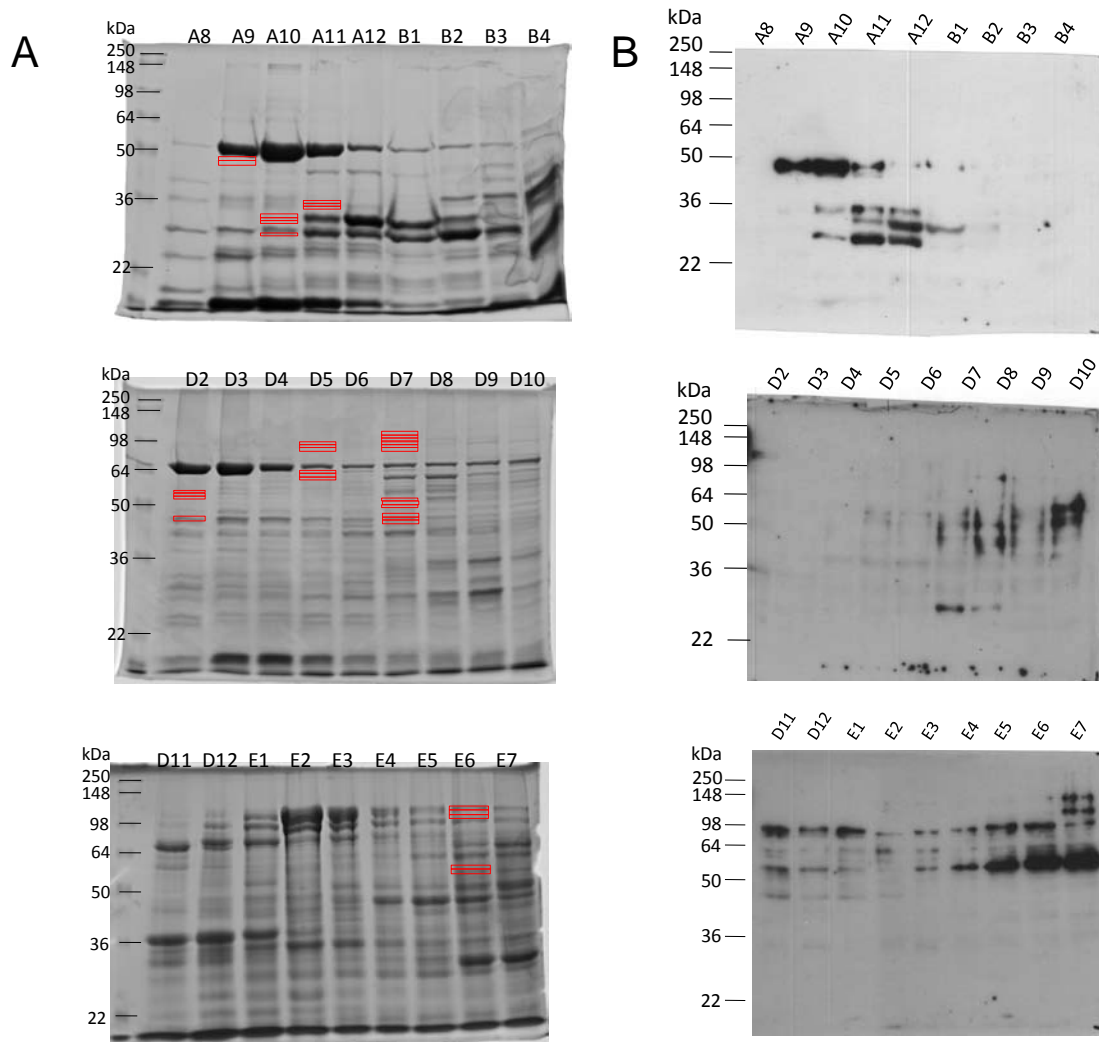


Figure 6.5: A) SDS-PAGE (10%) gel separation of selected fractions from ICF separation of the proteome of insulin/STZ/glucose treated differentiated C2C12 mouse myoblast cell lysate and B) western gel of the corresponding fractions probed with the CTD110.6 antibody; outlined bands on the SDS-PAGE gel were excised for mass analysis.

As reviewed by Love and Hanover, the largest percentage of proteins in the known O-GlcNAc proteome are involved in transcription and translation [135]. Transcription factors are low abundance modulators within the cell, and usually require a concentration step for detection in subsequent analyses [147, 148]. This likely accounts for the observed disconnect between protein abundances recorded in the Coomassie-stained gel

and the intensity of antibody reactivity recorded in the corresponding lanes of the western gel. From the perspective of evaluating the merits of the proposed platform, the higher initial loads permitted in the ICF fractionation result in a wide range of western signal intensities being observed in a large number of fractions, which itself is an indirect indicator of good dynamic range.

The western gel was used as a guide to identify O-GlcNAc active regions/bands on the corresponding Coomassie-stained gel that were then excised and subjected to enzymatic digestion and mass spectrometric analysis. Putative O-GlcNAc-modified proteins in each band were then identified using their peptide mass fingerprints and the MASCOT database (Table 6.3). Proteins known to carry an O-GlcNAc modification based on previous studies [103, 149-161] are marked with a “ * ”. Some of these, including vinculin and cytokeratin, are known to be involved in the phosphorylation-dependent reversible bridging of the cytoskeleton to the cell membrane, where the O-GlcNAc modification is thought to help mediate protein-protein interactions involved in the organization of the cytoskeleton [162].

In addition, several candidate O-GlcNAc modified proteins not identified in previous studies were discovered using this new platform, illustrating the potential power of custom-gradient ICF as a pre-fractionation step for proteome-wide PTM analysis. Of particular interest is the putative discovery of O-GlcNAc modification of a number of enzymes involved in sugars uptake and metabolism, including glucose- and fructose-6-phosphate isomerase, GTP:AMP phosphotransferase, and GTP binding protein [163].

Table 6.3: Proteins identified as O-GlcNAc positive in aligned western/SDS-PAGE gels derived from insulin/STZ/glucose treated differentiated C2C12 mouse myoblasts[§]

Band	Protein ID	Accession Number	MW	pI	Elution pH	Mascot Score	Peptide Match
A9-1	Glucose 6 Phosphate Isomerase	P06745	62.9	8.18	9.4	275	24
A9-2	Glutathione S-transferase P1 *	P19157	23.7	8.13	9.4	110	6
	Keratin Type I Cytoskeletal (18)*	P05784	47.5	5.22		88	3
A10-1	Four and a Half LIM Domains Protein 1	P97447	33.8	8.76	9.3	418	29
A10-2	Four and a Half LIM Domains Protein 1	P97447	33.8	8.76	9.3	148	8
A10-3	Carbonic Anhydrase 3	P16015	29.6	6.97	9.3	268	30
	GTP:AMP Phosphotransferase	Q9WTP7	25.4	8.88		150	11
	Peptidyl-prolyl Cis-trans Isomerase A	P17742	18.1	7.88		133	8
	FK506-binding Protein 3	Q62446	25.1	9.29		124	7
A11-1	Malate Dehydrogenase (mitochondrial precursor)	P08249	36.0	8.55	9.2	581	39
	Annexin A2*	P07356	38.9	7.53		306	14
A11-2	Annexin A2*	P07256	38.9	7.53	9.2	882	79
	Malate Dehydrogenase (mitochondrial precursor)	P08249	36.0	8.55		117	4
A11-3	Annexin A2*	P07356	38.9	7.53	9.2	348	12
D2-1	Cytosol Aminopeptidase*	Q9CPY7	56.5	7.61	7.0	217	7
D2-2	Cytosol Aminopeptidase*	Q9CPY7	56.5	7.61	7.0	798	54
	Fructose 6 Phosphate Isomerase	P06745	62.9	8.18		216	11
	Moesin	P26041	67.8	6.24		144	10
D2-4	Adenosylhomocysteinase*	P50247	48.1	6.08	7.0	1150	134
	Putative GTP-binding Protein 9	Q9CZ30	44.7	7.64		418	31
D5-5	Moesin	P26041	67.8	6.24	6.8	356	20
D5-6	Phosphoglucosmutase-1	Q9D0F9	61.7	6.32	6.8	413	22
	Moesin	P26041	67.8	6.32		411	21
D7-11	Adenosylhomocysteinase*	P50247	48.1	6.08	6.8	427	15
D7-12	Adenosylhomocysteinase*	P50247	48.1	6.08	6.8	294	10
E6-1	Vinculin*	Q64727	117.2	5.77	5.8	1905	68
	Elongation Factor 2	P58252	96.2	6.42		128	6
E6-2	Vinculin*	Q64727	117.2	5.77	5.8	1269	39
	Elongation Factor 2	P58252	96.2	6.42		775	30
E6-3	Elongation Factor 2	P58252	96.2	6.42	5.8	1196	56
	Vinculin*	Q64727	117.2	5.77		706	26
	Glycogen Phosphorylase	Q9WUB3	97.68	6.65		174	10
E6-4	T-complex Protein 1 Subunit Beta	P80314	57.7	5.98	5.8	779	25
	Cytosol Aminopeptidase*	Q9CPY7	56.5	7.61		433	14
	T-complex Protein 1 Subunit Eta	P80313	60.1	7.95		408	16
E6-5	T-complex Protein 1 Subunit Beta	P80314	57.7	5.98	5.8	779	25
	RuvB-Like 1	P60122	50.5	6.02		246	10
	Septin 11	Q8C1B7	50.0	6.26		237	8

§ Proteins identified in previous studies to be O-GlcNAc modified are marked with an “ * ”; proteins detected as O-GlcNAc positive and found in similar fractions in both the treated and untreated samples are in **bold**

6.3.2 Untreated sample

1D SDS-PAGE gels for ICF fractions of the untreated sample (Figure 6.6A) show band patterns very similar to those in gels for the corresponding fractions of the insulin/STZ/glucose treated sample (Figure 6.5A). This result is consistent with the ICF chromatograms (Figure 6.2) and indicates both that the insulin/STZ/glucose treatment does not grossly alter protein expression patterns, and that the O-GlcNAc modification does not grossly affect protein *pI*.

1D western gels of ICF fractions collected from the untreated differentiated C2C12 mouse myoblasts were imaged for much longer time periods (overnight) to permit detection of very low abundance O-GlcNAc activity (Figures 6.6B and 6.3B) as compared to that observed in the treated samples (Figures 6.5B and 6.3A). Regions on the Coomassie-stained gels identified in the untreated and insulin/STZ/glucose treated sample as O-GlcNAc positive were excised and subjected to enzymatic digestion and mass spectrometric analysis to yield peptide mass fingerprints and protein IDs (Table 6.4). A number of proteins (shown in **bold** in Tables 6.3 and 6.4), such as cytosol aminopeptidase in band D2-2, were identified in both the treated and untreated samples. For each such protein, the difference in western gel exposure times (< 1 minute for the treated sample versus overnight for the untreated sample), as well as the dot-blot data (Figure 6.3), provides strong qualitative evidence that induction of hyperglycemia in slow smooth muscle cells results in a significant increase in the extent of the O-GlcNAc modification to their proteins..

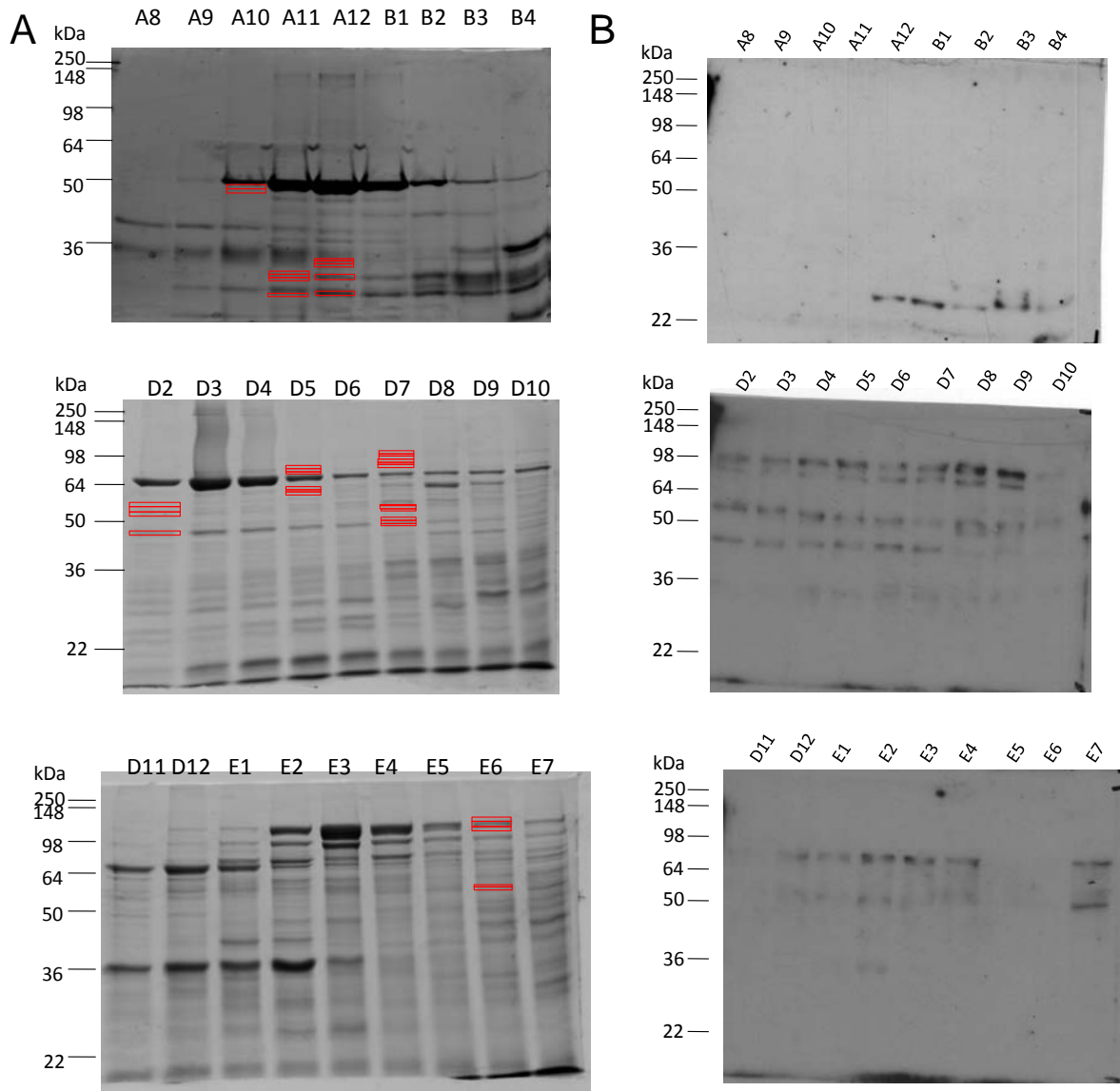


Figure 6.6: A) SDS-PAGE (10%) gel separation of selected fractions from ICF separation of the proteome of untreated differentiated C2C12 mouse myoblast cell lysate, and B) western gel of the corresponding fractions probed with the CTD110.6 antibody; red outlined bands on the SDS-PAGE gel were excised for mass analysis.

Table 6.4: Proteins identified as O-GlcNAc positive in aligned western/SDS-PAGE gels derived from untreated differentiated C2C12 mouse myoblasts[§]

Band	Protein ID	Accession Number	MW	pI	Elution pH	Mascot Score	Peptide Match
A9-2	Keratin Type I Cytoskeletal*	P02535	57.9	5.04	9.4	234	6
	Keratin Type I Cytoskeletal*	Q61414	49.2	4.79		112	4
A10-1	Keratin Type I Cytoskeletal*	Q61414	49.2	4.79	9.3	159	4
A11-1	Malate Dehydrogenase	P14152	36.0	8.55	9.2	116	4
D2-1	Moesin	P26041	67.8	6.24	7.0	80	5
D2-2	Cytosol Aminopeptidase*	Q9CPY7	56.5	7.61	7.0	222	8
D2-3	Glutathione Reductase	P47791	54.2	6.99	7.0	89	3
D2-4	Adenosylhomocysteinase*	P50247	48.1	6.08	7.0	726	27
	Putative GTP-binding Protein 9	Q9CZ30	44.7	7.64		202	5
D5-1	Moesin	P26041	67.8	6.24	6.9	78	3
D5-2	Moesin	P26041	67.8	6.24	6.9	273	20
D5-3	Moesin	P26041	67.8	6.24	6.9	390	34
	Ezrin	P26040	69.5	5.83		144	16
D5-4	Moesin	P26041	67.8	6.24	6.9	78	5
D5-5	Phosphoglucomutase-1	Q9D0F9	61.7	6.32	6.9	221	16
D5-6	Phosphoglucomutase-1	Q9D0F9	61.7	6.32	6.9	169	14
D7-1	Leukotriene A-4 Hydrolase	P24527	69.6	5.98	6.8		
D7-3	Elongation Factor 2	P58252	96.2	6.42	6.8	110	4
D7-4	Ras-specific Guanine Nucleotide-releasing Factor 1	P27671	145.2	6.74	6.8	29	3
D7-6	Collagen Alpha-1(XXV) Chain	Q99MQ5	65.8	8.70	6.8	32	2
D7-7	6-phosphogluconate dehydrogenase	Q9DCD0	53.7	6.88	6.8	205	9
D7-8	Adenosylhomocysteinase*	P50247	48.1	6.08	6.8	539	24
D7-9	Adenosylhomocysteinase*	P50247	48.1	6.08	6.8	155	7
D7-11	Adenosylhomocysteinase*	P50247	48.1	6.08	6.8	630	51
D7-12	Adenosylhomocysteinase*	P50247	48.1	6.08	6.8	132	11
E6-1	Vinculin*	Q64727	117.2	5.77	5.7	450	31
E6-2	Vinculin*	Q64727	117.2	5.77	5.7	2225	370
	Elongation Factor 2	P58252	96.2	6.42		78	8
E6-3	Vinculin*	Q64727	117.2	5.77	5.7	1551	188
	Elongation Factor 2	P58252	96.2	6.42		238	16
E6-4	Septin 11	Q8C1B7	50.05	6.26	5.7	249	25
	Elongation Factor 2	P58252	96.2	6.42		82	6
E6-5	Septin 11	Q8C1B7	50.05	6.26	5.7	555	98
	Septin 8	Q8CHH9	50.1	5.68		196	51
	Moesin	P26041	67.8	6.24		140	10
	GDP-fucose Protein O-fucosyltransferase 2 Precursor	Q8VHI3	49.7	5.95		135	15

§ Proteins identified in previous studies to be O-GlcNAc modified are marked with an “ * ”; proteins detected as O-GlcNAc positive and found in similar fractions in both the treated and untreated samples are in **bold**

Only a small number of proteins (*e.g.* glycogen phosphorylase) showing O-GlcNAc reactivity in the treated sample were not also detected as having a basal level of O-GlcNAc activity in the untreated sample. The results therefore suggest that induced hyperglycemia leads to a pronounced increase in the O-GlcNAc modification of those proteins for which a fraction is modified in the normal state, but does not result in extensive O-GlcNAc modification of proteins that are otherwise not likely to carry that PTM.

Less can be inferred in the reverse direction due to the nature of the experiment conducted which permitted detection of very low O-GlcNAc activity in the untreated fractions, but high O-GlcNAc activity in the treated fractions. As a result, some proteins found to be O-GlcNAc positive in the untreated sample were not observed in the treated sample (*e.g.*, 6-phosphogluconate dehydrogenase), suggesting that their levels of O-GlcNAc modification did not increase significantly in response to induced hyperglycemia. However, a proteomics study specifically designed to address that question would be required to confirm that observation.

6.3.4 Using proteomics data to validate proposed ICF elution mechanisms

In Chapter 4, a comprehensive model of protein transport and binding in ICF was derived. It treats protein elution in ICF as a mixed-mode separation that includes Donnan, Gouy-Chapman and ion-displacement contributions. In addition to serving as a demonstration of the utility of custom ICF, the proteomic and associated chromatograms

presented in this chapter provide a large and potentially useful data set for further validation of that model.

Relative to their pI , proteins are predicted by the model to elute earlier in the chromatogram as the ionic strength is increased. This is because at a fixed mobile phase ionic strength, the magnitude of the difference between the elution pH and the pI is inversely related to K_{bi} , the SMA-type equilibrium constant for the binding of protein i to the charged stationary phase. Equation 4.7, derived from Gouy-Chapman theory, finds that K_{bi} increases with the exponential of m , the characteristic charge. As noted in Chapter 4, m is expected to increase with protein molecular weight. Thus, the model predicts that the magnitude of the difference between the elution pH and the pI should increase with decreasing protein molecular weight (MW). The combined ICF and proteomics data for the benchmark alloxan-treated sample show that this is indeed the case (Figure 6.7). Moreover, the logarithmic form of the data suggests that to a first approximation m can be taken to depend linearly on protein MW. The small degree of scatter in the correlation is in line with model findings that non-coulombic contributions to protein binding (*i.e.* protein surface hydrophobic) may also affect K_{bi} through their contributions to β .

Tables 6.3 and 6.4 report pI and elution pH for additional C2C12 mouse myoblast derived proteins fractionated by ICF on a Mono Q strong anion exchange column. The elution gradient included changes in mobile-phase conductivity ranging from 2 mS cm⁻¹ to 8 mS cm⁻¹. Under these ICF separation conditions, the proteins generally elute at a pH

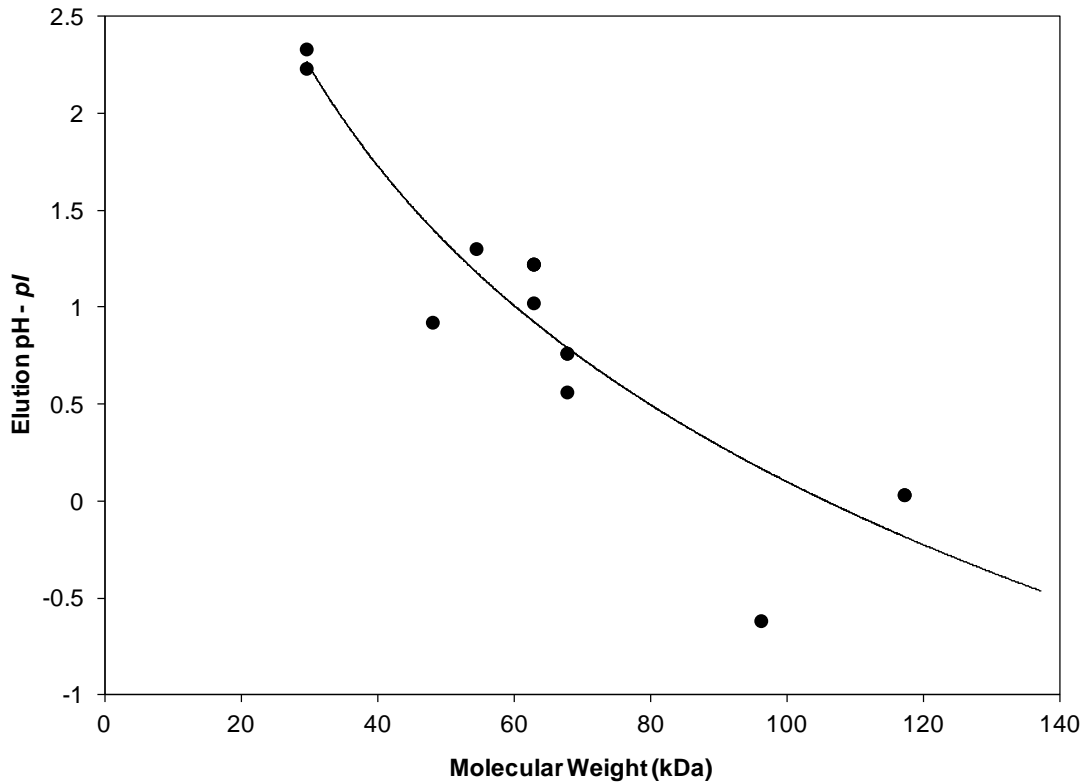


Figure 6.7: Difference between elution pH and pI plotted against the molecular weight of benchmark C2C12 mouse myoblast cell lysate proteins reveals a roughly logarithmically inverse relationship.

that is either roughly equal to or higher than their pI . Again, larger proteins (> 50 kDa) elute at a pH relatively close to their pI , while smaller proteins in general elute at pH values further from their pI . For example, carbonic anhydrase 3 has a pI of 6.97 and a MW of 29.6 kDa: it elutes at pH 9.3 due to its small size that results in fewer charged groups interacting favorably with the strong ion exchange matrix, making it more sensitive to the Gouy-Chapman and ion-displacement effects.

One apparent outlier in this analysis is glutathione S-transferase P1: it has a *pI* of 8.13 and, in its monomeric state, a MW of 23.7 kDa. It elutes at pH 9.4, a value that is closer to the protein's *pI* than suggested by the Gouy-Chapman effect encoded in the model. However, glutathione S-transferase P1 has been identified in previous studies to be O-GlcNAc modified and, more importantly, to exist as a stable dimer in solution [155]. While its theoretical mass is 23.7 kDa, glutathione S-transferase P1 therefore runs as a near 50 kDa protein on a gel, which likely explains the decreased sensitivity of its elution pH to ionic strength.

These results further demonstrate the validity of the mixed-mode model developed in Chapter 4 to describe protein elution in ICF. Calculation of the exact difference between elution pH and the *pI* of a protein requires specific information about the protein's characteristic charge as a function of pH and its β value. However, the data collected here certainly support the importance of the various elution mechanisms embodied in the model and their dependence on ionic strength.

6.4 Concluding Remarks

A custom ICF platform has been developed to efficiently pre-fractionate complex proteomes in a manner that permits the detection and analysis of the O-GlcNAc PTM on proteins found in the cell lysate of differentiated C2C12 mouse myoblasts. Sufficient amounts of sample can be obtained from the first-dimension ICF separation to perform a 1D western on each collected fraction, as well as a 1D SDS-PAGE separation from which

O-GlcNAc positive protein bands can be excised and analyzed by tandem mass spectrometry. By tuning elution conditions to maximize peak capacities, the platform reveals a number of candidate proteins that become O-GlcNAc modified or show increased O-GlcNAc activity when the cells become hyperglycemic. In addition to its use as a PTM discovery tool, the platform is also shown to be useful as a means to better understand mechanisms that govern protein elution in ICF.

Chapter 7

Conclusions and Recommendations for Future Work

7.1 Motivation for and Advances Provided by this Work

Although an extremely powerful mode of chromatography when applied to protein mixtures, chromatofocusing has not been widely used since its debut in 1978. This is in part due to disadvantages associated with the use of polyampholyte buffers, which are expensive to manufacture, have unpredictable buffering characteristics, and are incompatible with many downstream processes [65, 66]. A lack of fundamental understanding of ICF elution mechanisms also contributes to the poor acceptance of the technology. During chromatofocusing, proteins often elute at pH values far removed from their isoelectric points defined by IEF gel electrophoresis, which to date has hampered efforts to interpret ICF data and design ICF separations.

Some of these concerns have been addressed through the replacement of polyampholyte buffers with mobile phases comprised of simple low molecular weight buffers commonly used for pH regulation in conventional ion exchange [65, 66, 69-79]. Some progress has also been made toward understanding protein elution in chromatofocusing [76, 79, 91, 100]. However, the most advanced model to date is only valid for cases where the elution pH is near the expected pI of the protein [100]. Moreover, most of the simple

buffer formulations available rely on the use of specific weak ion exchangers for buffering capacity [66, 68, 74-77], which restricts the flexibility in applying those reagents to preparative separations. Finally, no attempt has been made to resolve the problem associated with reduced capacity caused by poor solubility of the target protein near its *pI* during chromatofocusing. These limitations must all be addressed before scientists and engineers will adopt the use of chromatofocusing and begin to take advantage of the potential increases in separation performance it offers.

The work presented in this thesis is expected to advance chromatofocusing technology towards maturity by addressing a number of practical issues that previously hindered the widespread use of the technique. Mobile phase formulations containing simple buffers are developed to generate stable pH gradients over much larger ranges: spanning pH 10.0 to 3.5 in anion exchange columns (Chapter 2) and spanning pH 2.0 to 11.0 in cation exchange columns (Chapter 3). Those spans are the widest ever reported by a considerable margin. Large pH gradient spans are then shown to be useful, particularly for the analytical separation of complex proteomes containing hundreds to thousands of distinct proteins, including as the first dimension in a multidimensional fractionation platform. Moreover, the components of these mobile phases are selected and shown to be compatible with analytical techniques required for protein and proteomics studies, including UV absorption, circular dichroism, gel electrophoresis and mass spectrometry implementing either ESI or MALDI ionization.

Advanced models are developed to permit custom-design of programmed elution pH gradients on cation or anion exchange media. Those models may also be used to design buffer formulations for isocratic elution schemes applied to either analytical or preparative media. Using these models, pH gradient profiles may be sculpted according to the specific composition and properties of the sample in order to improve separation performance. Demonstrations of the utility of this approach were provided through separations of the human blood plasma proteome, where the use of a custom pH gradient profile resulted in a *ca.* 2X increase in peak capacity over that achieved by a linear pH gradient operating over the same separation time (Chapter 2); of the clarified supernatant of recombinant *P. pastoris* cultures, where homogeneous isolation of a desired isoform of hTf/2N was achieved (Chapter 5); and of the lysate-derived proteomes of differentiated C2C12 mouse myoblasts, where the method successfully isolated and identified proteins exhibiting enhanced O-GlcNAc PTM activity when the differentiated cell population is in a hyperglycemic state (Chapter 6).

In Chapter 4, a comprehensive model of protein transport and binding in ICF is developed and used to show that protein elution is influenced by a combination of mechanisms that includes Donnan, Gouy-Chapman and ion-displacement effects. The elution pH of any protein can therefore be shifted by changing the mobile phase ionic strength, which is shown to be useful for optimizing the separation of protein orthologs differing by as little as a single charged amino acid, or protein isoforms having identical sequence and similar conformations. Changes in the elution behavior due to variations in mobile-phase ionic strength are predicted by the model and used to improve the

separation of β -lactoglobulin orthologs by AEICF and cytochrome C isoforms by CEICF. By accounting for all speciation in the system and all factors affecting protein-matrix interactions, the model is shown to accurately predict protein elution times. In addition, a simple, more empirical method is developed which exploits the quantitative capabilities of the pH-sculpting model (Chapters 2 and 3) and the basic findings of the elution model (Chapter 4) to speed and simplify optimization of ICF separations when the required parameters for the elution model are not available (Chapter 5).

7.2 Recommendations for Future Work

While the mobile phases comprised of mixtures of simple buffers developed in this work are more complex (and hence are expected to be more costly) than those used in conventional ion exchange chromatography, they may be applied in ICF at low ionic strengths, which is expected to translate into significant reduction in the load on downstream desalting processes such as diafiltration. Moreover, the ability to custom-design elution gradients can be used to minimize separation time/volume, thereby minimizing total mobile phase solvent consumption. Nevertheless, further studies into the economics of ICF as a replacement for more traditional modes of preparative chromatography are required to show that any increases in cost associated with running ICF (instead of say IEC) can be offset by savings elsewhere in the process pipeline.

The model developed in Chapter 4 is capable of accurately predicting the first moments of elution peaks during AEICF. In the future, the model can also be applied to the

prediction of elution times during CEICF by accounting for the association of protons to the cation exchange matrix and its effects on the equilibrium binding isotherm and the stationary phase surface pH. Extension of the model to predict peak shapes (higher moments) by including all contributions to mass transfer and band focusing/broadening during protein isoelectric chromatofocusing is possible, but challenging, and would represent a significant and useful advance. Complete accounting of the band focusing effect requires the consideration of both attractive and repulsive interactions between the protein and the matrix. Essentially all reliable characteristic charge data available in the literature are limited to m values where the protein is attracted to the stationary phase matrix, in part because traditional ion exchange chromatography is operated at pH conditions where the protein always carries a net charge opposite to that of the matrix. The development of an experimental and/or computational method to determine/estimate m on both sides of the protein's pI would be of tremendous use, as that knowledge is required in the model to predict elution peak shapes.

Prediction of protein elution times likewise requires a value for β , which defines the protein's hypothetical non-coulombic affinity for the matrix. The value of β depends on specific physicochemical properties of the protein, such as the presence/absence of areas of strong surface hydrophobicity, but the exact nature of those dependencies is unknown. A potential method to estimate the value of β is to empirically correlate β with protein structure descriptors using methods such as quantitative structure-activity relationship (QSAR) modeling. This method, which generates useful quantitative structure-retention relationships (QSRR), has proven very effective when applied to understanding the

chromatographic behavior of small molecules, including peptides, and simple low molecular weight proteins. The method has shown great value when applied to either reversed phase or ion exchange chromatography, particularly in the hands of the Cramer lab [164-168] and other leading labs [169-175]. Using QSAR, it may therefore be possible to define relationships between a relevant set of protein and matrix physicochemical property descriptors and the value of β . In turn, this could allow *in silico* prediction of β and the corresponding elution time of a protein.

References

1. Tswett, M., *Solubility of chlorophyllin and a new method of isolation of it*. Berichte Der Deutschen Chemischen Gesellschaft, 1911. **44**: p. 1124-1127.
2. Carta, G. and A. Jungbauer, *Protein Chromatography: Process Development and Scale-Up*. 2010, Weinheim: Wiley-VCH.
3. Cowan, G.H., et al., *Physical and mathematical modeling to aid scale-up of liquid chromatography*. Journal of Chromatography A, 1986. **363**(1): p. 31-36.
4. Ganetsos, G. and P.E. Barker, *Preparative and production scale chromatography*. 1993: Marcel Dekker Inc.
5. Gu, T., *Mathematical modeling and scale-up of liquid chromatography*. 1995, New York: Springer.
6. Rathore, A. and A. Velayudhan, eds. *Scale-Up and Optimization in Preparative Chromatography: Principles and Biopharmaceutical Applications*. 2002, CRC Press.
7. Kastner, M., *Protein liquid chromatography*. 2000, Amsterdam: Elsevier.
8. Ladisch, M.R., *Bioseparations Engineering: Principles, Practice, and Economics*. 2001, New York, NY: John Wiley & Sons, Inc.
9. Schmidt-Traub, H., M. Schulte, and A. Seidel-Morgenstern, eds. *Preparative Chromatography*. 2nd ed. 2012, Wiley-VCH: Weinheim.
10. Lathe, G.H. and C.R.J. Ruthven, *Separation of Substances and Estimation of Their Relative Molecular Sizes by the Use of Columns of Starch in Water*. Biochemical Journal, 1956. **62**(4): p. 665-674.
11. Porath, J. and P. Flodin, *Gel Filtration - Method for Desalting and Group Separation*. Nature, 1959. **183**(4676): p. 1657-1659.
12. Mori, S. and H.G. Barth, *Size Exclusion Chromatography*. 1999: Springer.
13. Wu, C.-S., *Column handbook for size exclusion chromatography*. 1999, London: Academic Press.
14. Parris, N.A., *Instrumental Liquid Chromatography: A Practical Manual on High Performance LIiquid Chromatographic Methods*. Journal of Chromatography Library. Vol. 5. 1976, Amsterdam: Elsevier.
15. Molnar, I. and C. Horvath, *Reverse-Phase Chromatography of Polar Biological Substances - Separation of Catechol Compounds by High-Performance Liquid-Chromatography*. Clinical Chemistry, 1976. **22**(9): p. 1497-1502.
16. Gad, S.C., ed. *Handbook of Pharmaceutical Biotechnology*. 2007, Wiley: Hoboken.
17. Linden, J.C. and C.L. Lawhead, *Liquid-Chromatography of Saccharides*. Journal of Chromatography, 1975. **105**(1): p. 125-133.
18. Wang, P.G. and W. He, eds. *Hydrophilic Interaction Liquid Chromatography (HILIC) and Advanced Applications*. Chromatographic Science Series. 2011, CRC Press.

19. Scopes, R.K., *Protein Purification: Principles and Practice*. 3rd ed. 1994: Springer.
20. Determan.H and K. Lampert, *Hydrophobic Interaction in Gel Adsorption Chromatography*. *Journal of Chromatography*, 1972. **69**(1): p. 123-&.
21. Heftmann, E., ed. *Chromatography: Fundamentals and applications of chromatography and related differential migration methods*. 6th ed. *Journal of Chromatography Library*. Vol. 69B. 2004, Elsevier: Amsterdam.
22. Cuatrecasas, P., M. Wilchek, and C.B. Anfinsen, *Selective Enzyme Purification by Affinity Chromatography*. *Proceedings of the National Academy of Sciences of the United States of America*, 1968. **61**(2): p. 636-&.
23. Zachariou, M., ed. *Affinity Chromatography: Methods and Protocols*. 2nd ed. *Methods in Molecular Biology*. Vol. 421. 2008, Humana Press: Totowa.
24. Heftmann, E., ed. *Chromatography: Fundamentals and applications of chromatography and related differential migration methods*. 6th ed. *Journal of Chromatography Library*. Vol. 69A. 2004, Elsevier: Amsterdam.
25. Spedding, F.H., et al., *The Separation of Rare Earths by Ion Exchange .3. Pilot Plant Scale Separations*. *Journal of the American Chemical Society*, 1947. **69**(11): p. 2812-2818.
26. Spedding, F.H., et al., *The Separation of Rare Earths by Ion Exchange .1. Cerium and Yttrium*. *Journal of the American Chemical Society*, 1947. **69**(11): p. 2777-2781.
27. Spedding, F.H., et al., *The Separation of Rare Earths by Ion Exchange .2. Neodymium and Praseodymium*. *Journal of the American Chemical Society*, 1947. **69**(11): p. 2786-2792.
28. Spedding, R.H., et al., *Improved Ion Exchange Method for Separating Rare Earths in Macro Quantities*. *Journal of the American Chemical Society*, 1948. **70**(4): p. 1671-1672.
29. Hostettmann, K., A. Marston, and M. Hostettmann, *Preparative Chromatography Techniques: Applications in Natural Product Isolation*. 2nd ed. 1998: Springer.
30. Janson, J.-C., ed. *Protein Purification: Principles, High Resolution Methods, and Applications*. 3rd ed. *Methods of Biochemical Analysis*. Vol. 54. 2011, Wiley: Hoboken.
31. Necina, R., K. Amatschek, and A. Jungbauer, *Capture of human monoclonal antibodies from cell culture supernatant by ion exchange media exhibiting high charge density*. *Biotechnology and Bioengineering*, 1998. **60**(6): p. 689-698.
32. Shukla, A.A., et al., *Downstream processing of monoclonal antibodies—Application of platform approaches*. *Journal of Chromatography B-Polyclonal and Monoclonal Antibody Production, Purification, Process and Product Analytics*, 2007. **848**(1): p. 28-39.
33. Subramanian, G., ed. *Biopharmaceutical Production Technology*. Vol. 1. 2012, Wiley.
34. Baumgartner, P., et al., *Large-scale production, purification, and characterisation of recombinant Phaseolus vulgaris phytohemagglutinin E-form expressed in the methylotrophic yeast Pichia pastoris*. *Protein Expression and Purification*, 2002. **26**(3): p. 394-405.

35. Byrne, M.P., et al., *Fermentation, Purification, and Efficacy of a Recombinant Vaccine Candidate against Botulinum Neurotoxin Type F from Pichia pastoris*. Protein Expression and Purification, 2000. **18**(3): p. 327.
36. Li, L., et al., *High level expression, purification, and characterization of the shrimp antimicrobial peptide, Ch-penaeidin, in Pichia pastoris*. Protein Expression and Purification, 2005. **39**(2): p. 144-151.
37. Minning, S., et al., *Optimization of the high-level production of Rhizopus oryzae lipase in Pichia pastoris*. Journal of Biotechnology, 2001. **86**(1): p. 59-70.
38. Murphy Jr., K.P., et al., *Expression of Human Interleukin-17 in Pichia pastoris: Purification and Characterization*. Protein Expression and Purification, 1998. **12**(2): p. 208-214.
39. Goldberg, R.N., N. Kishore, and R.M. Lennen, *Thermodynamic quantities for the ionization reactions of buffers*. 2002, Gaithersburg, MD, United States of America: Biotechnology Division, National Institute of Standards and Technology.
40. *Instructions 71-5017-89 AE: Mono Q 10/100GL and Mono S 10/100GL Ion Exchange Columns*. 2006, Uppsala, Sweden: GE Healthcare Bio-sciences AB.
41. Christiansen, M., et al., *Protein chemical characterization of Gc globulin (vitamin D-binding protein) isoforms; Gc-1f, Gc-1s and Gc-2*. Biochimica et Biophysica Acta - Proteins and Proteomics, 2007. **1774**(4): p. 481-492.
42. Yamamoto, S. and I. Takashi, *Ion-exchange chromatography of proteins near the isoelectric points*. Journal of Chromatography A, 1999. **852**(1): p. 31-36.
43. Barnthouse, K.A., et al., *Cation-exchange displacement chromatography for the purification of recombinant protein therapeutics from variants*. Journal of Biotechnology, 1998. **66**(2-3): p. 125-136.
44. Cramer, S.M., *Displacement Chromatography*. Nature, 1991. **351**(6323): p. 251-252.
45. Cramer, S.M. and G. Subramanian, *Recent Advances in the Theory and Practice of Displacement Chromatography*. Separation and Purification Reviews, 1990. **19**(1): p. 31-91.
46. Jayaraman, G., S.D. Gadam, and S.M. Cramer, *Ion-exchange displacement chromatography of proteins: Dextran-based polyelectrolytes as high affinity displacers*. Journal of Chromatography A, 1993. **630**(1-2): p. 53-68.
47. Jayaraman, G., et al., *Ion-exchange displacement chromatography of proteins Dendritic polymers as novel displacers*. Journal of Chromatography A, 1995. **702**(1-2): p. 143-155.
48. Kundu, A., K.A. Barnthouse, and S.M. Cramer, *Selective displacement chromatography of proteins*. Biotechnology and Bioengineering, 1997. **56**(2): p. 119-129.
49. Kundu, A. and S.M. Cramer, *Low-Molecular-Weight Displacers for High-Resolution Protein Separations*. Analytical Biochemistry, 1997. **248**(1): p. 111-116.
50. Kundu, A., S. Vunnum, and S.M. Cramer, *Antibiotics as low-molecular-mass displacers in ion-exchange displacement chromatography*. Journal of Chromatography A, 1995. **707**(1): p. 57-67.

51. Nihal, T., et al., *Displacement chromatography of anti-sense oligonucleotide and proteins using saccharin as a non-toxic displacer*. Reactive and Functional Polymers, 2003. **54**(1-3): p. 37-47.
52. Shukla, A.A., et al., *Purification of an Antigenic Vaccine Protein by Selective Displacement Chromatography*. Biotechnology Progress, 1998. **14**(1): p. 92-101.
53. Subramanian, G. and S.M. Cramer, *Displacement Chromatography of Proteins Under Elevated Flow Rate and Crossing Isotherm Conditions*. Biotechnology Progress, 1989. **5**(3): p. 92-97.
54. Subramanian, G., M.W. Phillips, and S.M. Cramer, *Displacement chromatography of biomolecules*. Journal of Chromatography A, 1988. **439**(2): p. 341-351.
55. Subramanian, G., et al., *Displacement chromatography of biomolecules with large particle diameter systems*. Journal of Chromatography A, 1989. **484**: p. 225-236.
56. Curtis, S., et al., *Generic/matrix evaluation of SV40 clearance by anion exchange chromatography in flow-through mode*. Biotechnology and Bioengineering, 2003. **84**(2): p. 179-186.
57. Knudsen, H.L., et al., *Membrane ion-exchange chromatography for process-scale antibody purification*. Journal of Chromatography A, 2001. **907**(1-2): p. 145-154.
58. Sluyterman, L.A.A. and O. Elgersma, *Chromatofocusing - Isoelectric-Focusing on Ion-Exchange Columns .1. General Principles*. Journal of Chromatography, 1978. **150**(1): p. 17-30.
59. Sluyterman, L.A.A. and J. Wijdenes, *Chromatofocusing - Isoelectric-Focusing on Ion-Exchange Columns .2. Experimental-Verification*. Journal of Chromatography, 1978. **150**(1): p. 31-44.
60. Sluyterman, L.A.A., *Chromatofocusing, a New Protein-Separation Method*. Philips Technical Review, 1980. **39**(5): p. 125-129.
61. Sluyterman, L.A.A. and J. Wijdenes, *Chromatofocusing .4. Properties of an Agarose Polyethyleneimine Ion-Exchanger and Its Suitability for Protein Separations*. Journal of Chromatography, 1981. **206**(3): p. 441-447.
62. Sluyterman, L.A.A. and J. Wijdenes, *Chromatofocusing .3. The Properties of a Deae-Agarose Anion-Exchanger and Its Suitability for Protein Separations*. Journal of Chromatography, 1981. **206**(3): p. 429-440.
63. Sluyterman, L.A.E., *Chromatofocusing - a Preparative Protein Separation Method*. Trends in Biochemical Sciences, 1982. **7**(5): p. 168-170.
64. Sluyterman, L.A.A. and C. Kooistra, *10 Years of Chromatofocusing - a Discussion*. Journal of Chromatography, 1989. **470**(2): p. 317-326.
65. Liu, Y.S. and D.J. Anderson, *Gradient chromatofocusing high-performance liquid chromatography .1. Practical aspects*. Journal of Chromatography A, 1997. **762**(1-2): p. 207-217.
66. Bates, R.C. and D.D. Frey, *Quasi-linear pH gradients for chromatofocusing using simple buffer mixtures: local equilibrium theory and experimental verification*. Journal of Chromatography A, 1998. **814**(1-2): p. 43-54.
67. Soderberg, J.L., *Ampholyte and its use in separation processes*, U.S.P.a.T. Office, Editor. 1982, Pharmacia Fine Chemicals AB (Uppsala, SE): United States of America.

68. Wall, D.B., D.M. Lubman, and T. Barder, *Three dimensional protein mapping*, U.S.P.a.T. Office, Editor. 2005, Regents of the University of Michigan (Ann Arbor, MI): United States of America.
69. Frey, D.D., *Local-equilibrium behavior of retained pH and ionic strength gradients in preparative chromatography*. Biotechnology Progress, 1996. **12**(1): p. 65-72.
70. Frey, D.D., A. Barnes, and J. Strong, *Numerical-Studies of Multicomponent Chromatography Using Ph Gradients*. Aiche Journal, 1995. **41**(5): p. 1171-1183.
71. Frey, D.D. and A.E. Rodrigues, *Explicit Calculation of Multicomponent Equilibria for Ideal Absorbed Solutions*. Aiche Journal, 1994. **40**(1): p. 182-186.
72. Narahari, C.R., J.C. Strong, and D.D. Frey, *Displacement chromatography of proteins using a self-sharpening pH front formed by adsorbed buffering species as the displacer*. Journal of Chromatography A, 1998. **825**(2): p. 115-126.
73. Strong, J.C. and D.D. Frey, *Experimental and numerical studies of the chromatofocusing of dilute proteins using retained pH gradients formed on a strong-base anion-exchange column*. Journal of Chromatography A, 1997. **769**(2): p. 129-143.
74. Bates, R.C., X.Z. Kang, and D.D. Frey, *High-performance chromatofocusing using linear and concave pH gradients formed with simple buffer mixtures I. Effect of buffer composition on the gradient shape*. Journal of Chromatography A, 2000. **890**(1): p. 25-36.
75. Kang, X.Z. and D.D. Frey, *Chromatofocusing using micropellicular column packings with computer-aided design of the elution buffer composition*. Analytical Chemistry, 2002. **74**(5): p. 1038-1045.
76. Kang, X.Z., R.C. Bates, and D.D. Frey, *High-performance chromatofocusing using linear and concave pH gradients formed with simple buffer mixtures II. Separation of proteins*. Journal of Chromatography A, 2000. **890**(1): p. 37-43.
77. Logan, K.A., I. Lagerlund, and S.M. Chamow, *A simple, two-component buffer enhances use of chromatofocusing for processing of therapeutic proteins*. Biotechnology and Bioengineering, 1999. **62**(2): p. 208-215.
78. Liu, Y.S. and D.J. Anderson, *Gradient chromatofocusing high-performance liquid chromatography .2. Theoretical aspects*. Journal of Chromatography A, 1997. **762**(1-2): p. 47-54.
79. Shan, L. and D.J. Anderson, *Gradient chromatofocusing. Versatile pH gradient separation of proteins in ion-exchange HPLC: Characterization studies*. Analytical Chemistry, 2002. **74**(21): p. 5641-5649.
80. Liu, Y. and D.J. Anderson, *Anion-exchange HPLC of fibrinogen and fibrinogen degradation products using pH gradients*. Journal of Liquid Chromatography & Related Technologies, 1999. **22**(5): p. 681-694.
81. Pepaj, M., et al., *Two-dimensional capillary liquid chromatography: pH Gradient ion exchange and reversed phase chromatography for rapid separation of proteins*. Journal of Chromatography A, 2006. **1120**(1-2): p. 132-141.
82. Pepaj, M., et al., *Fractionation and separation of human salivary proteins by pH-gradient ion exchange and reversed phase chromatography coupled to mass spectrometry*. Journal of Separation Science, 2006. **29**(4): p. 519-528.

83. Pepaj, M., E. Lundanes, and T. Greibrokk, *Separation of apolipoprotein A-I from human plasma by on-line two dimensional liquid chromatography*. Journal of Liquid Chromatography & Related Technologies, 2007. **30**(13-16): p. 1879-1894.
84. Tran, B.Q., et al., *The behaviour of reduced, alkylated and native proteins in a pH-gradient LC system*. Chromatographia, 2007. **66**(9-10): p. 709-715.
85. Tran, B.Q., et al., *On-line method for identification of native proteins using pH-gradient SAX chromatography and reversed phase chromatography-mass spectrometry of tryptic peptides*. Journal of Liquid Chromatography & Related Technologies, 2008. **31**(10): p. 1387-1411.
86. Francina, A., et al., *Chromatofocusing of Human Hemoglobins - Application to the Quantitation of Hemoglobin-a2*. Journal of Chromatography, 1982. **228**(Mar): p. 177-185.
87. Hearn, M.T.W. and D.J. Lyttle, *Buffer-Focusing Chromatography Using Multicomponent Electrolyte Elution Systems*. Journal of Chromatography, 1981. **218**(1-3): p. 483-495.
88. Kang, X.Z. and D.D. Frey, *High-performance cation-exchange chromatofocusing of proteins*. Journal of Chromatography A, 2003. **991**(1): p. 117-128.
89. Kang, X.Z. and D.D. Frey, *Chromatofocusing of peptides and proteins using linear pH gradients formed on strong ion-exchange adsorbents*. Biotechnology and Bioengineering, 2004. **87**(3): p. 376-387.
90. Frey, D.D., C.R. Narahari, and C.D. Butler, *General local-equilibrium chromatographic theory for eluents containing adsorbing buffers*. Aiche Journal, 2002. **48**(3): p. 561-571.
91. Shan, L. and D.J. Anderson, *Effect of buffer concentration on gradient chromatofocusing performance separating proteins on a high-performance DEAE column*. Journal of Chromatography A, 2001. **909**(2): p. 191-205.
92. Zhu, K., et al., *Protein pl shifts due to posttranslational modifications in the separation and characterization of proteins*. Analytical Chemistry, 2005. **77**(9): p. 2745-2755.
93. Rosell, F.I., J.C. Ferrer, and A.G. Mauk, *Proton-linked protein conformational switching: Definition of the alkaline conformational transition of yeast iso-1-ferricytochrome c*. Journal of the American Chemical Society, 1998. **120**(44): p. 11234-11245.
94. Righetti, P.G., *Isoelectric focusing: theory, methodology and applications*. Laboratory Techniques in Biochemistry and Molecular Biology, ed. E. Work and T.S. Work. Vol. 11. 1983, Amsterdam: Elsevier Publishers B.V.
95. Herbert, B., et al., *Reduction and alkylation of proteins in preparation of two-dimensional map analysis: Why, when, and how?* Electrophoresis, 2001. **22**(10): p. 2046-2057.
96. Herbert, B., et al., *beta-elimination: An unexpected artefact in proteome analysis*. Proteomics, 2003. **3**(6): p. 826-831.
97. McCarthy, J., et al., *Carbamylation of proteins in 2-D electrophoresis - Myth or reality?* Journal of Proteome Research, 2003. **2**(3): p. 239-242.
98. Righetti, P.G., *Real and imaginary artefacts in proteome analysis via two-dimensional maps*. Journal of Chromatography B-Analytical Technologies in the Biomedical and Life Sciences, 2006. **841**(1-2): p. 14-22.

99. Righetti, P.G., M. Chiari, and C. Gelfi, *Immobilized Ph Gradients - Effect of Salts, Added Carrier Ampholytes and Voltage Gradients on Protein-Patterns*. Electrophoresis, 1988. **9**(2): p. 65-73.
100. Shen, H. and D.D. Frey, *Charge regulation in protein ion-exchange chromatography: Development and experimental evaluation of a theory based on hydrogen ion Donnan equilibrium*. Journal of Chromatography A, 2004. **1034**(1-2): p. 55-68.
101. Chong, B.E., et al., *Chromatofocusing nonporous reversed-phase high-performance liquid chromatography/electrospray ionization time-of-flight mass spectrometry of proteins from human breast cancer whole cell lysates: a novel two-dimensional liquid chromatography/mass spectrometry method*. Rapid Communications in Mass Spectrometry, 2001. **15**(4): p. 291-296.
102. Qin, S.Z., et al., *Chromatofocusing fractionation and two-dimensional difference gel electrophoresis for low abundance serum proteins*. Proteomics, 2005. **5**(12): p. 3183-3192.
103. Hart, G.W., et al., *O-GlcNAcylation of key nuclear and cytoskeletal proteins: reciprocity with O-phosphorylation and putative roles in protein multimerization*. Glycobiology, 1996. **6**(7): p. 711-716.
104. Hutchens, T.W., *Chromatofocusing*. Protein Purification, ed. J.J.a.R. L. 1989, New York: VCH. 149-174.
105. Frey, D.D. and J. Strong, *Theory and Application of Improved Methods for Protein-Purification Using Chromatofocusing*. Abstracts of Papers of the American Chemical Society, 1995. **209**: p. 62-Btec.
106. Frey, D.D., J. Strong, and R. Bates, *Protein separation and purification using novel chromatofocusing methods*. Abstracts of Papers of the American Chemical Society, 1996. **211**: p. 173-BIOT.
107. Frey, D.D., J. Strong, and R. Bates, *Chromatofocusing of proteins*. Abstracts of Papers of the American Chemical Society, 1997. **213**: p. 149-IEC.
108. Andersen, T., et al., *Isoelectric point separation of proteins by capillary pH-gradient ion-exchange chromatography*. Journal of Chromatography A, 2004. **1025**(2): p. 217-226.
109. Robinson, R.A. and R.H. Stokes, *Electrolyte solutions*. 1959, New York: Academic Press.
110. Van't Hoff, J.H., *Études de dynamique chimique*. 1884, Amsterdam: Frederik Muller.
111. Guggenheim, E.A. and J.C. Turgeon, *Specific interaction of ions*. Transactions of the Faraday Society, 1955. **51**: p. 747-761.
112. Davies, C.W., *Ion Association*. 1962, London: Butterworth Press.
113. Cramer, S.M. and C.A. Brooks, *Steric mass-action ion exchange: Displacement profiles and induced salt gradients*. Aiche Journal, 1992. **38**(12): p. 1969-1978.
114. Serjeant, E.P. and B. Dempsey, *Ionization Constants of Organic Acids in Aqueous Solution*. 1979, Pergamon: Oxford.
115. Putnam, F.W., *The Plasma Proteins*. 2 ed. Vol. 4. 1984, New York: Academic Press.
116. Stern, O., *Zur Theorie der elektrolytischen Doppelschicht*. Zeitschrift für Elektrochemie und Angewandte Physikalische Chemie, 1924. **30**: p. 508-516.

117. Chapman, D.L., *A contribution to the theory of Electro-Capillarity*. Philosophical Magazine, 1913. **25**(6): p. 475-481.
118. Gouy, L.G., *Sur la constitution de la charge électrique a la surface d'un électrolyte*. Journal of Physics, 1910. **9**(4): p. 457-468.
119. Tsonev, L.I. and A.G. Hirsh, *Theory and applications of a novel ion exchange chromatographic technology using controlled pH gradients for separating proteins on anionic and cationic stationary phases*. Journal of Chromatography A, 2008. **1200**(2): p. 166-182.
120. Velayudhan, A. and C. Horvath, *Preparative chromatography of proteins: Analysis of the multivalent ion-exchange formalism*. Journal of Chromatography A, 1988. **443**: p. 13-29.
121. Atkins, P.W., *Physical Chemistry*. Second ed. 1982: Oxford University Press.
122. Donnan, F.G., *Theorie der Membrangleichgewichte und Membranpotentiale bei Vorhandensein von nicht dialysierenden Elektrolyten*. Zeitschrift für Elektrochemie und angewandte physikalische Chemie, 1911. **17**(14): p. 572-581.
123. Grahame, D.C., *The electrical double layer and the theory of electrocapillarity*. Chemical Reviews, 1947. **41**(3): p. 441-501.
124. Mason, A.B., et al., *Production and isolation of the recombinant N-lobe of human serum transferrin from the methylotrophic yeast Pichia pastoris*. Protein Expression and Purification, 1996. **8**(1): p. 119-125.
125. Schreiter, E.R., et al., *S-Nitrosylation-induced Conformational Change in Blackfin Tuna Myoglobin*. Journal of Biological Chemistry, 2007. **282**(27): p. 19773-19780.
126. Yang, Q. and K.-L. Guan, *Expanding mTOR signaling*. Cell Research, 2007. **17**(8): p. 666-681.
127. Federici, M., et al., *Insulin-Dependent Activation of Endothelial Nitric Oxide Synthase Is Impaired by O-Linked Glycosylation Modification of Signaling Proteins in Human Coronary Endothelial Cells*. Circulation, 2002. **106**(4): p. 466-472.
128. Rush, J., et al., *Immunoaffinity profiling of tyrosine phosphorylation in cancer cells*. Nature Biotechnology, 2005. **23**(1): p. 94-101.
129. Li, S.G., et al., *Tyrosine phosphorylation of Grb2 by Bcr/Abl and epidermal growth factor receptor: a novel regulatory mechanism for tyrosine kinase signaling*. Embo Journal, 2001. **20**(23): p. 6793-6804.
130. Collins, M.O., L. Yu, and J.S. Choudhary, *Analysis of protein phosphorylation on a proteome-scale*. Proteomics, 2007. **7**(16): p. 2751-2768.
131. Metodiev, M.V., A. Timanova, and D.E. Stone, *Differential phosphoproteome profiling by affinity capture and tandem matrix-assisted laser desorption/ionization mass spectrometry*. Proteomics, 2004. **4**(5): p. 1433-1438.
132. Vanrobaeys, F., et al., *Profiling of myelin proteins by 2D-gel electrophoresis and multidimensional liquid chromatography coupled to MALDI TOF-TOF mass spectrometry*. Journal of Proteome Research, 2005. **4**(6): p. 2283-2293.
133. Lookhart, G.L., L.D. Albers, and J.A. Bietz, *Comparison of polyacrylamide gel electrophoresis and high-performance liquid chromatography analyses of gliadin polymorphism in the wheat cultivar newton*. Cereal Chemistry, 1986. **63**(6): p. 497-500.

134. Torres, C.R. and G.W. Hart, *Topography and polypeptide distribution of terminal N-acetylglucosamine residues on the surfaces of intact lymphocytes. Evidence for O-linked GlcNAc*. J. Biol. Chem., 1984. **259**(5): p. 3308-3317.
135. Love, D.C. and J.A. Hanover, *The Hexosamine Signaling Pathway: Deciphering the "O-GlcNAc Code"*. Sci. STKE, 2005. **2005**(312): p. re13-.
136. Slawson, C., R.J. Copeland, and G.W. Hart, *O-GlcNAc signaling: a metabolic link between diabetes and cancer?* Trends in Biochemical Sciences, 2010. **35**(10): p. 547-555.
137. Marshall, S., V. Bacote, and R.R. Traxinger, *Discovery of a metabolic pathway mediating glucose-induced desensitization of the glucose transport system. Role of hexosamine biosynthesis in the induction of insulin resistance*. J. Biol. Chem., 1991. **266**(8): p. 4706-4712.
138. Buse, M.G., *Hexosamines, insulin resistance, and the complications of diabetes: current status*. American Journal of Physiology - Endocrinology and Metabolism, 2006. **290**(1): p. E1-E8.
139. Buse, M.G., et al., *Increased activity of the hexosamine synthesis pathway in muscles of insulin-resistant ob/ob mice*. American Journal of Physiology, 1997. **272**(6): p. E1080-E1088.
140. Yki-Järvinen, H., et al., *Increased glutamine:fructose-6-phosphate amidotransferase activity in skeletal muscle of patients with NIDDM*. Diabetes, 1996. **45**(3): p. 302-307.
141. McClain, D.A., *Hexosamines as mediators of nutrient sensing and regulation in diabetes*. Journal of Diabetes and its Complications, 2002. **16**(1): p. 72-80.
142. Du, X.L., et al., *Hyperglycemia inhibits endothelial nitric oxide synthase activity by posttranslational modification at the Akt site*. J Clin Invest, 2001. **108**(9): p. 1341-8.
143. Walgren, J.L.E., et al., *High glucose and insulin promote O-GlcNAc modification of proteins, including alpha -tubulin*. Am J Physiol Endocrinol Metab, 2003. **284**(2): p. 424-434.
144. Griffith, L.S., M. Mathes, and B. Schmitz, *Beta-amyloid precursor protein is modified with O-linked N-acetylglucosamine*. J Neurosci Res, 1995. **41**(2): p. 270-8.
145. Robertson, L.A., K.L. Moya, and K.C. Breen, *The potential role of tau protein O-glycosylation in Alzheimer's disease*. J Alzheimers Dis, 2004. **6**(5): p. 489-95.
146. Alexander, G.E., et al., *Longitudinal PET Evaluation of Cerebral Metabolic Decline in Dementia: A Potential Outcome Measure in Alzheimer's Disease Treatment Studies*. Am J Psychiatry, 2002. **159**(5): p. 738-745.
147. Forde, C.E. and S.L. McCutchen-Maloney, *Characterization of transcription factors by mass spectrometry and the role of SELDI-MS*. Mass Spectrometry Reviews, 2002. **21**(6): p. 419-439.
148. Gadgil, H., L.A. Jurado, and H.W. Jarrett, *DNA Affinity Chromatography of Transcription Factors*. Analytical Biochemistry, 2001. **290**(2): p. 147-178.
149. Chou, C.F., A.J. Smith, and M.B. Omary, *Characterization and dynamics of O-linked glycosylation of human cytokeratin 8 and 18*. Journal of Biological Chemistry, 1992. **267**(6): p. 3901-3906.

150. Cieniewski-Bernard, C., et al., *Identification of O-linked N-Acetylglucosamine Proteins in Rat Skeletal Muscle Using Two-dimensional Gel Electrophoresis and Mass Spectrometry*. *Molecular and Cellular Proteomics*, 2004. **3**(6): p. 577-585.
151. Gurcel, C., et al., *Identification of new O-GlcNAc modified proteins using a click-chemistry-based tagging*. *Analytical and Bioanalytical Chemistry*, 2008. **390**(8): p. 2089-2097.
152. Haltiwanger, R.S., G.D. Holt, and G.W. Hart, *Enzymatic addition of O-GlcNAc to nuclear and cytoplasmic proteins. Identification of a uridine diphospho-N-acetylglucosamine:peptide beta-N-acetylglucosaminyltransferase*. *Journal of Biological Chemistry*, 1990. **265**(5): p. 2563-2568.
153. Hart, G.W., *Dynamic O-linked glycosylation of nuclear and cytoskeletal proteins*. *Annual Review of Biochemistry*, 1997. **66**(1): p. 315-335.
154. Hedou, J., et al., *O-Linked N-Acetylglucosamylation Is Involved in the Ca²⁺ Activation Properties of Rat Skeletal Muscle*. *Journal of Biological Chemistry*, 2007. **282**(14): p. 10360-10369.
155. Housley, M.P., et al., *O-GlcNAc Regulates FoxO Activation in Response to Glucose*. *Journal of Biological Chemistry*, 2008. **283**(24): p. 16283-16292.
156. Jung, E., et al., *Rules for the addition of O-linked N-acetylglucosamine to secreted proteins in Dictyostelium discoideum*. *European Journal of Biochemistry*, 2001. **253**(2): p. 517-524.
157. Sprung, R., et al., *Tagging-via-Substrate Strategy for Probing O-GlcNAc Modified Proteins*. *Journal of Proteome Research*, 2005. **4**(3): p. 950-957.
158. Vostal, J.G. and D.M. Krasnewich, *Dynamic O-linked N-acetylglucosamine glycosylation of platelet vinculin*. *Molecular Biology of the Cell*, 1994. **5**(S): p. 263a.
159. Wells, L., S.A. Whelan, and G.W. Hart, *O-GlcNAc: a regulatory post-translational modification*. *Biochemical and Biophysical Research Communications*, 2003. **302**(3): p. 435-441.
160. Zachara, N.E. and G.W. Hart, *Cell signaling, the essential role of O-GlcNAc!* *Biochimica et Biophysica Acta (BBA) - Molecular and Cell Biology of Lipids*, 2006. **1761**(5-6): p. 599-617.
161. Dehennaut, V., et al., *Identification of structural and functional O-linked N-acetylglucosamine-bearing proteins in xenopus laevis oocyte*. *Molecular and Cellular Proteomics*, 2008. **7**(11): p. 2229-2245.
162. Varki, A., et al., eds. *Essentials in Glycobiology*. 2nd ed. 2009, Cold Spring Harbor Laboratory Press: New York.
163. Shaw, R.J., *Glucose metabolism and cancer*. *Current Opinion in Cell Biology*, 2006. **18**(6): p. 598-608.
164. Ladiwala, A., et al., *Prediction of protein affinity in hydrophobic interaction chromatography using quantitative structure-retention relationship (QSRR) models*. *Abstracts of Papers of the American Chemical Society*, 2004. **227**: p. U1020-U1020.
165. Ladiwala, A., et al., *Investigation of mobile phase salt type effects on protein retention and selectivity in cation-exchange systems using quantitative structure retention relationship models*. *Langmuir*, 2003. **19**(20): p. 8443-8454.

166. Ladiwala, A., et al., *Prediction of protein affinity in cation-exchange chromatography using quantitative structure-retention relationship (QSRR) models*. Abstracts of Papers of the American Chemical Society, 2003. **225**: p. U782-U782.
167. Mazza, C.B., et al., *Prediction of protein retention in ion-exchange systems using molecular descriptors obtained from crystal structure*. Analytical Chemistry, 2001. **73**(22): p. 5457-5461.
168. Song, M.H., et al., *Prediction of protein retention times in anion-exchange chromatography systems using support vector regression*. Journal of Chemical Information and Computer Sciences, 2002. **42**(6): p. 1347-1357.
169. Baczek, T., et al., *Prediction of peptide retention at different HPLC conditions from multiple linear regression models*. Journal of Proteome Research, 2005. **4**(2): p. 555-563.
170. Beaudry, F., M. Coutu, and N.K. Brown, *Determination of drug-plasma protein binding using human serum albumin chromatographic column and multiple linear regression model*. Biomedical Chromatography, 1999. **13**(6): p. 401-406.
171. Kaliszan, R., *Chromatography and capillary electrophoresis in modelling the basic processes of drug action*. Trac-Trends in Analytical Chemistry, 1999. **18**(6): p. 400-410.
172. Kaliszan, R., et al., *Prediction of high-performance liquid chromatography retention of peptides with the use of quantitative structure-retention relationships*. Proteomics, 2005. **5**(2): p. 409-415.
173. Kaliszan, R., A. Nasal, and M. Turowski, *Quantitative structure-retention relationships in the examination of the topography of the binding site of antihistamine drugs on alpha(1)-acid glycoprotein*. Journal of Chromatography A, 1996. **722**(1-2): p. 25-32.
174. Markuszewski, M. and R. Kaliszan, *Quantitative structure-retention relationships in affinity high-performance liquid chromatography*. Journal of Chromatography B-Analytical Technologies in the Biomedical and Life Sciences, 2002. **768**(1): p. 55-66.
175. Nasal, A., et al., *Quantitative Relationships between the Structure of Beta-Adrenolytic and Antihistamine Drugs and Their Retention on an Alpha(1)-Acid Glycoprotein Hplc Column*. Biomedical Chromatography, 1994. **8**(3): p. 125-129.

Appendices

Appendix A: Description of the Program for Sculpting Buffer Compositions through the Calculation of pH and Ionic Strength Profiles in an Anion Exchange Column

All programs are written for use on MATLAB 6.1. The main program script file “ICFM.m” contains model parameters entered by the user and equations responsible for executing the primary finite difference iterations based on the continuity equation of chromatography. Two functions, “C01solve.m” and “Qsolve.m”, are called during the iteration. The following table lists all species tracked by the program and nomenclature used to represent them:

Table A-1: List of species tracked by MATLAB script file “ICFM.m” for the calculation of pH and ionic strength profiles during AEICF

Nomenclature	Species	Description
01	H ⁺	proton
10	DAP	unprotonated 1,3 diaminopropane
11	DAP-H ⁺	monoprotonated 1,3 diaminopropane
12	DAP-2H ²⁺	diprotonated 1,3 diaminopropane
20	DEA	unprotonated diethanolamine
21	DEA-H ⁺	monoprotonated diethanolamine
30	TRS	unprotonated tris
31	TRS-H ⁺	monoprotonated tris
40	IMI	unprotonated imidazole
41	IMI-H ⁺	monoprotonated imidazole
50	BTS	unprotonated bis-tris
51	BTS-H ⁺	monoprotonated bis-tris
60	PIP	unprotonated piperazine
61	PIP-H ⁺	monoprotonated piperazine
62	PIP-2H ²⁺	diprotonated piperazine
70	ACE ⁻	unprotonated acetate
71	ACE-H	monoprotonated acetate
80	LAC ⁻	unprotonated lactate
81	LAC-H	monoprotonated lactate
90	Cl ⁻	chloride ion
A0	Na ⁺	sodium ion
Y0	Y	unprotonated buffer “Y”
Y1	Y-H ⁺	monoprotonated buffer “Y”
Z0	Z	unprotonated buffer “Z”
Z1	Z-H ⁺	monoprotonated buffer “Z”

Buffers “Y” and “Z” in table A-1 are fictitious buffering species used to evaluate the impact of additional buffering capacity on the predicted pH and ionic strength profiles. During the simulation of actual profiles generated on the column, the concentrations of these buffers are set to zero.

The total mobile phase concentrations of all species in the column are tracked using the continuity equation of chromatography. Species that do not associate with the stationary phase regardless of their protonation states (DAP, DEA, TRS, BTS, buffer “Y” and buffer “Z”) are tracked by the following simplified form of the continuity equation:

$$\frac{\partial TC_i}{\partial t} = D_{axi} \frac{\partial^2 TC_i}{\partial z^2} - \left(\frac{u}{\varepsilon} \right) \frac{\partial TC_i}{\partial z} \quad (\text{A-1})$$

The total mobile phase concentration of species i (TC_i) can be used to write the mobile phase concentration of the protonated forms of each of these species as a function of the free proton concentration (C_{01}):

$$C_{11} = \frac{10^{K_{11}^*} C_{01} TC_1}{C_{01}^2 10^{K_{11}^*} 10^{K_{12}^*} + C_{01} 10^{K_{11}^*} + 1} \quad (\text{A-2})$$

$$C_{12} = \frac{10^{K_{11}^*} 10^{K_{12}^*} C_{01}^2 TC_1}{C_{01}^2 10^{K_{11}^*} 10^{K_{12}^*} + C_{01} 10^{K_{11}^*} + 1} \quad (\text{A-3})$$

$$C_{21} = \frac{10^{K_{21}^*} C_{01} TC_2}{C_{01} 10^{K_{21}^*} + 1} \quad (\text{A-4})$$

$$C_{31} = \frac{10^{K_{31}^*} C_{01} TC_3}{C_{01} 10^{K_{31}^*} + 1} \quad (\text{A-5})$$

$$C_{51} = \frac{10^{K_{51}^*} C_{01} TC_5}{C_{01} 10^{K_{51}^*} + 1} \quad (\text{A-6})$$

$$C_{Y1} = \frac{10^{K_{Y1}^*} C_{01} TC_Y}{C_{01} 10^{K_{Y1}^*} + 1} \quad (\text{A-7})$$

$$C_{Z1} = \frac{10^{K_{Z1}^*} C_{01} TC_Z}{C_{01} 10^{K_{Z1}^*} + 1} \quad (\text{A-8})$$

Species that associate non-specifically with the stationary phase (IMI and PIP) are tracked by the following equations:

$$\frac{\partial TC_4}{\partial t} = D_{ax4} \frac{\partial^2 TC_4}{\partial z^2} - \left(\frac{u}{\varepsilon} \right) \frac{\partial TC_4}{\partial z} - \left(\frac{1-\varepsilon}{\varepsilon} \right) \frac{\partial Q_{40}}{\partial t} \quad (\text{A-9})$$

$$\frac{\partial TC_6}{\partial t} = D_{ax6} \frac{\partial^2 TC_6}{\partial z^2} - \left(\frac{u}{\varepsilon} \right) \frac{\partial TC_6}{\partial z} - \left(\frac{1-\varepsilon}{\varepsilon} \right) \left(\frac{\partial Q_{60}}{\partial t} + \frac{\partial Q_{61}}{\partial t} \right) \quad (\text{A-10})$$

where the stationary phase concentrations Q_{40} , Q_{60} , and Q_{61} are described by the following binding isotherm relationships:

$$Q_{40} = (Q_{40}^{\max} K_{40}) C_{40} \quad (\text{A-11})$$

$$Q_{60} = (Q_{60}^{\max} K_{60}) C_{60} \quad (\text{A-12})$$

$$Q_{61} = (Q_{61}^{\max} K_{61}) C_{61} \quad (\text{A-13})$$

The total mobile phase concentration of these species derived from equations A-9 and A-10 can be used to write the mobile phase concentration of the protonated forms of each of these species as a function of the free proton concentration (C_{01}):

$$C_{41} = \frac{10^{K_{41}^*} C_{01} TC_4}{C_{01} 10^{K_{41}^*} + 1} \quad (\text{A-14})$$

$$C_{61} = \frac{10^{K_{61}^*} C_{01} TC_6}{C_{01}^2 10^{K_{61}^*} 10^{K_{62}^*} + C_{01} 10^{K_{61}^*} + 1} \quad (\text{A-15})$$

$$C_{62} = \frac{10^{K_{61}^*} 10^{K_{62}^*} C_{01}^2 TC_6}{C_{01}^2 10^{K_{61}^*} 10^{K_{62}^*} + C_{01} 10^{K_{61}^*} + 1} \quad (\text{A-16})$$

Species that associate specifically with the stationary phase (ACE and LAC) are tracked by the following equations:

$$\frac{\partial TC_7}{\partial t} = D_{ax7} \frac{\partial^2 TC_7}{\partial z^2} - \left(\frac{u}{\varepsilon} \right) \frac{\partial TC_7}{\partial z} - \left(\frac{1 - \varepsilon}{\varepsilon} \right) \frac{\partial Q_{70}}{\partial t} \quad (\text{A-17})$$

$$\frac{\partial TC_8}{\partial t} = D_{ax8} \frac{\partial^2 TC_8}{\partial z^2} - \left(\frac{u}{\varepsilon} \right) \frac{\partial TC_8}{\partial z} - \left(\frac{1 - \varepsilon}{\varepsilon} \right) \frac{\partial Q_{80}}{\partial t} \quad (\text{A-18})$$

where the stationary phase concentrations Q_{70} and Q_{80} are described by the following binding isotherm relationships:

$$Q_{70} = \frac{Q_{70}^{\max} K_{70} C_{70}}{C_{90} + K_{70} C_{70} + K_{80} C_{80}} \quad (\text{A-19})$$

$$Q_{80} = \frac{Q_{80}^{\max} K_{80} C_{80}}{C_{90} + K_{70} C_{70} + K_{80} C_{80}} \quad (\text{A-20})$$

The total mobile phase concentration of these species derived from equations A-17 and A-18 can be used to write the mobile phase concentration of the protonated forms of each of these species as a function of the free proton concentration (C_{01}):

$$C_{71} = \frac{10^{K_{71}^*} C_{01} TC_7}{C_{01} 10^{K_{71}^*} + 1} \quad (\text{A-21})$$

$$C_{81} = \frac{10^{K_{81}^*} C_{01} TC_8}{C_{01} 10^{K_{81}^*} + 1} \quad (\text{A-22})$$

The mobile phase proton concentration (TC_0) is defined by the following:

$$(\text{A-23})$$

$$TC_0 = C_{01} + C_{11} + 2C_{12} + C_{21} + C_{31} + C_{41} + C_{51} + C_{61} + 2C_{62} + C_{71} + C_{81} + C_{Y1} + C_{Z1}$$

which is tracked by the following continuity equation:

$$\frac{\partial TC_0}{\partial t} = D_{ax0} \frac{\partial^2 TC_0}{\partial z^2} - \left(\frac{u}{\varepsilon} \right) \frac{\partial TC_0}{\partial z} \quad (\text{A-24})$$

Substituting equations A-2, A-3, A-4, A-5, A-6, A-7, A-8, A-14, A-15, A-16, A-21 and A-22 into equation A-23, C_{0i} can be solved based on the total mobile phase proton concentration derived from equation A-24.

The bulk mobile phase pH and ionic strength can be calculated using the following equations:

$$pH = -\log^{C_{0i}} \quad (A-25)$$

$$I = 0.5(C_{0i} + C_{1i} + 2^2 C_{12} + C_{2i} + C_{3i} + C_{4i} + C_{5i} + C_{6i} + 2^2 C_{62} + C_{7i} + C_{8i} + C_{Yi} + C_{Zi}) \quad (A-26)$$

Calculated pH and ionic strength values at each column position and run time node are stored in variables “pHM” and “IM”, respectively. End-of-column pH and ionic strength is plotted against run time to generate predicted profiles. The MATLAB code for the solution is shown below.

```
%Script m-file "ICFM.m" that uses an explicit scheme finite difference
%method to solve the continuity equations required for predicting the
%free proton concentration and hence the shape of the pH gradient
%generated at the exit of the Mono Q HR10/10 strong anion exchange
%column.
```

```
clear
tic
```

```
%Column and Run Constants
```

```
Qmax=320;      %Ionic Binding Capacity (mol/m^3)
Rp=5e-6;      %Resin Particle Radius (m)
ep=0.64;      %Resin Particle Voidage
L=0.085;      %Column Length (m)
R=0.005;      %Column Radius (m)
e=0.36;      %Column Voidage
et=e+(1-e)*ep; %Total Voidage
f=1/1e6;      %Mobile Phase Flow Rate (m^3/min)
u=f/(pi*R^2); %Superficial Mobile Phase Velocity (m/min)
G=60/1e6;     %Gradient (0-100% Elution Buffer) Length (m^3)
T=120/1e6;    %Total Run Length (m^3)
pHS=10;      %Starting Buffer pH
pHE=3.5;     %Elution Buffer pH
pHSU=11.357;  %Starting Buffer pH (Unadjusted)
pHEU=9.722;   %Elution Buffer pH (Unadjusted)
Gt=G/f;      %Gradient Run Time (min)
Tt=T/f;      %Total Run Time (min)
```

```
%Axial Dispersion Coefficients
```

```
Dax0=0e-7;    %Total Proton (Includes all protonated species)
Dax1=0e-7;    %DAP
Dax2=0e-7;    %DEA
Dax3=0e-7;    %Tris
Dax4=0e-7;    %Imidazole
Dax5=0e-7;    %Bis-Tris
Dax6=0e-7;    %Piperazine
Dax7=0e-7;    %Acetate
Dax8=0e-7;    %Lactate
Dax9=0e-7;    %Chloride
DaxA=0e-7;    %Sodium
DaxY=0e-7;    %Buffer Y
DaxZ=0e-7;    %Buffer Z
```

```
%Binding Constants for Binding Species
```

```
k70=3.42e0;   %Acetate
k80=1.28e0;   %Lactate
k90=1.00e0;   %Chloride

Qk40=0.70e1;  %Imidazole (m^3/mol)
Qk60=0.11e1;  %Piperazine (m^3/mol)
Qk61=0.52e1;  %PiperazineH (m^3/mol)
```

```
%Equilibrium Constants for Protontation
```

```
K110=10.62;   %First Protontation of DAP (M)
K120=8.640;   %Second Protontation of DAP (M)
K210=8.883;   %First Protontation of DEA (M)
```

```

K310=8.072;      %First Protonation of Tris (M)
K410=6.993;      %First Protonation of Imidazole (M)
K510=6.484;      %First Protonation of Bis-Tris (M)
K610=9.731;      %First Protonation of Piperazine (M)
K620=5.333;      %Second Protonation of Piperazine (M)
K710=4.756;      %First Protonation of Acetate (M)
K810=3.860;      %First Protonation of Lactate (M)
KY10=12.000;     %First Protonation of Buffer Y (M)
KZ10=2.500;      %First Protonation of Buffer Z (M)
i=0;             %Ionic strength (M)
K11=K110+0.509*(1+i)*(i^0.5/(1+i^0.5)-0.2*i);
K12=K120+0.509*(2+i)*(i^0.5/(1+i^0.5)-0.2*i);
K21=K210+0.509*(1+i)*(i^0.5/(1+i^0.5)-0.2*i);
K31=K310+0.509*(1+i)*(i^0.5/(1+i^0.5)-0.2*i);
K41=K410+0.509*(1+i)*(i^0.5/(1+i^0.5)-0.2*i);
K51=K510+0.509*(1+i)*(i^0.5/(1+i^0.5)-0.2*i);
K61=K610+0.509*(1+i)*(i^0.5/(1+i^0.5)-0.2*i);
K62=K620+0.509*(2+i)*(i^0.5/(1+i^0.5)-0.2*i);
K71=K710+0.509*(0+i)*(i^0.5/(1+i^0.5)-0.2*i);
K81=K810+0.509*(0+i)*(i^0.5/(1+i^0.5)-0.2*i);
KY1=KY10+0.509*(0+i)*(i^0.5/(1+i^0.5)-0.2*i);
KZ1=KZ10+0.509*(0+i)*(i^0.5/(1+i^0.5)-0.2*i);

%Equilibrium Constants for Protontation
K11=K11-3;      %First Protonation of DAP (mol/m^3)
K12=K12-3;      %Second Protonation of DAP (mol/m^3)
K21=K21-3;      %First Protonation of DEA (mol/m^3)
K31=K31-3;      %First Protonation of Tris (mol/m^3)
K41=K41-3;      %First Protonation of Imidazole (mol/m^3)
K51=K51-3;      %First Protonation of Bis-Tris (mol/m^3)
K61=K61-3;      %First Protonation of Piperazine (mol/m^3)
K62=K62-3;      %Second Protonation of Piperazine (mol/m^3)
K71=K71-3;      %First Protonation of Acetate (mol/m^3)
K81=K81-3;      %First Protonation of Lactate (mol/m^3)
KY1=KY1-3;      %First Protonation of Pseudo Buffer Y (mol/m^3)
KZ1=KZ1-3;      %First Protonation of Pseudo Buffer Z (mol/m^3)

%Total Species Concentrations Added to Starting Buffer
TC1S=10;        %DAP (mol/m^3)
TC2S=10;        %DEA (mol/m^3)
TC3S=10;        %Tris (mol/m^3)
TC4S=10;        %Imidazole (mol/m^3)
TC5S=10;        %Bis-Tris (mol/m^3)
TC6S=10;        %Piperazine (mol/m^3)
TC7S=0;         %Acetic Acid (mol/m^3)
TC8S=0;         %Lactic Acid (mol/m^3)
TC9S=0;         %Chloride (mol/m^3)
TCAS=0;         %Sodium (mol/m^3)
TCYS=0;         %Buffer Y (mol/m^3)
TCZS=0;         %Buffer Z (mol/m^3)

%Total Species Concentrations Added to Elution Buffer
TC1E=10;        %DAP (mol/m^3)
TC2E=10;        %DEA (mol/m^3)
TC3E=10;        %Tris (mol/m^3)
TC4E=10;        %Imidazole (mol/m^3)
TC5E=10;        %Bis-Tris (mol/m^3)

```

```

TC6E=10;          %Piperazine (mol/m^3)
TC7E=10;          %Acetic Acid (mol/m^3)
TC8E=10;          %Lactic Acid (mol/m^3)
TC9E=0;           %Chloride (mol/m^3)
TCAE=0;           %Sodium (mol/m^3)
TCYE=0;           %Buffer Y (mol/m^3)
TCZE=0;           %Buffer Z (mol/m^3)

```

%Species Concentrations in Unadjusted Starting Buffer

```

C01SU=10^(-pHSU)*1e3;          %Free Proton (mol/m^3)
C10SU=TC1S/(C01SU^2*10^K11*10^K12+C01SU*10^K11+1); %DAP (mol/m^3)
C11SU=10^K11*C01SU*C10SU;     %DAPH (mol/m^3)
C12SU=10^K12*C01SU*C11SU;     %DAPHH (mol/m^3)
C20SU=TC2S/(C01SU*10^K21+1);  %DEA (mol/m^3)
C21SU=10^K21*C01SU*C20SU;     %DEAH (mol/m^3)
C30SU=TC3S/(C01SU*10^K31+1);  %Tris (mol/m^3)
C31SU=10^K31*C01SU*C30SU;     %TrisH (mol/m^3)
C40SU=TC4S/(C01SU*10^K41+1);  %Imidazole (mol/m^3)
C41SU=10^K41*C01SU*C40SU;     %ImidazoleH (mol/m^3)
C50SU=TC5S/(C01SU*10^K51+1);  %Bis-Tris (mol/m^3)
C51SU=10^K51*C01SU*C50SU;     %Bis-TrisH (mol/m^3)
C60SU=TC6S/(C01SU^2*10^K61*10^K62+C01SU*10^K61+1); %Piperazine (mol/m^3)
C61SU=10^K61*C01SU*C60SU;     %PiperazineH (mol/m^3)
C62SU=10^K62*C01SU*C61SU;     %PiperazineHH (mol/m^3)
C70SU=TC7S/(C01SU*10^K71+1);  %Acetate (mol/m^3)
C71SU=10^K71*C01SU*C70SU;     %Acetic Acid (mol/m^3)
C80SU=TC8S/(C01SU*10^K81+1);  %Lactate (mol/m^3)
C81SU=10^K81*C01SU*C80SU;     %Lactic Acid (mol/m^3)
CY0SU=TCYS/(C01SU*10^KY1+1);  %Buffer Y (mol/m^3)
CY1SU=10^KY1*C01SU*CY0SU;     %Buffer YH (mol/m^3)
CZ0SU=TCZS/(C01SU*10^KZ1+1);  %Buffer Z (mol/m^3)
CZ1SU=10^KZ1*C01SU*CZ0SU;     %Buffer ZH (mol/m^3)
TC0SU=C01SU+C11SU+2*C12SU+C21SU+C31SU+C41SU+C51SU+C61SU+2*C62SU+C71SU+...
C81SU+CY1SU+CZ1SU;            %Total Proton (mol/m^3)
C90SU=TC9S;                    %Chloride (mol/m^3)
CA0SU=TCAS;                     %Sodium (mol/m^3)

```

%Species Concentrations in Unadjusted Elution Buffer

```

C01EU=10^(-pHEU)*1e3;          %Free Proton (mol/m^3)
C10EU=TC1E/(C01EU^2*10^K11*10^K12+C01EU*10^K11+1); %DAP (mol/m^3)
C11EU=10^K11*C01EU*C10EU;     %DAPH (mol/m^3)
C12EU=10^K12*C01EU*C11EU;     %DAPHH (mol/m^3)
C20EU=TC2E/(C01EU*10^K21+1);  %DEA (mol/m^3)
C21EU=10^K21*C01EU*C20EU;     %DEAH (mol/m^3)
C30EU=TC3E/(C01EU*10^K31+1);  %Tris (mol/m^3)
C31EU=10^K31*C01EU*C30EU;     %TrisH (mol/m^3)
C40EU=TC4E/(C01EU*10^K41+1);  %Imidazole (mol/m^3)
C41EU=10^K41*C01EU*C40EU;     %ImidazoleH (mol/m^3)
C50EU=TC5E/(C01EU*10^K51+1);  %Bis-Tris (mol/m^3)
C51EU=10^K51*C01EU*C50EU;     %Bis-TrisH (mol/m^3)
C60EU=TC6E/(C01EU^2*10^K61*10^K62+C01EU*10^K61+1); %Piperazine (mol/m^3)
C61EU=10^K61*C01EU*C60EU;     %PiperazineH (mol/m^3)
C62EU=10^K62*C01EU*C61EU;     %PiperazineHH (mol/m^3)
C70EU=TC7E/(C01EU*10^K71+1);  %Acetate (mol/m^3)
C71EU=10^K71*C01EU*C70EU;     %Acetic Acid (mol/m^3)
C80EU=TC8E/(C01EU*10^K81+1);  %Lactate (mol/m^3)
C81EU=10^K81*C01EU*C80EU;     %Lactic Acid (mol/m^3)

```

```

CY0EU=TCYE/(C01EU*10^KY1+1); %Buffer Y (mol/m^3)
CY1EU=10^KY1*C01EU*CY0EU; %Buffer YH (mol/m^3)
CZ0EU=TCZE/(C01EU*10^KZ1+1); %Buffer Z (mol/m^3)
CZ1EU=10^KZ1*C01EU*CZ0EU; %Buffer ZH (mol/m^3)
TC0EU=C01EU+C11EU+2*C12EU+C21EU+C31EU+C41EU+C51EU+C61EU+2*C62EU+C71EU+...
C81EU+CY1EU+CZ1EU; %Total Proton (mol/m^3)
C90EU=TC9E; %Chloride (mol/m^3)
CA0EU=TCAE; %Sodium (mol/m^3)

```

%Species Concentrations in Starting Buffer

```

C01S=10^(-pHS)*1e3; %Free Proton (mol/m^3)
C10S=TC1S/(C01S^2*10^K11*10^K12+C01S*10^K11+1); %DAP (mol/m^3)
C11S=10^K11*C01S*C10S; %DAPH (mol/m^3)
C12S=10^K12*C01S*C11S; %DAPHH (mol/m^3)
C20S=TC2S/(C01S*10^K21+1); %DEA (mol/m^3)
C21S=10^K21*C01S*C20S; %DEAH (mol/m^3)
C30S=TC3S/(C01S*10^K31+1); %Tris (mol/m^3)
C31S=10^K31*C01S*C30S; %TrisH (mol/m^3)
C40S=TC4S/(C01S*10^K41+1); %Imidazole (mol/m^3)
C41S=10^K41*C01S*C40S; %ImidazoleH (mol/m^3)
C50S=TC5S/(C01S*10^K51+1); %Bis-Tris (mol/m^3)
C51S=10^K51*C01S*C50S; %Bis-TrisH (mol/m^3)
C60S=TC6S/(C01S^2*10^K61*10^K62+C01S*10^K61+1); %Piperazine (mol/m^3)
C61S=10^K61*C01S*C60S; %PiperazineH (mol/m^3)
C62S=10^K62*C01S*C61S; %PiperazineHH (mol/m^3)
C70S=TC7S/(C01S*10^K71+1); %Acetate (mol/m^3)
C71S=10^K71*C01S*C70S; %Acetic Acid (mol/m^3)
C80S=TC8S/(C01S*10^K81+1); %Lactate (mol/m^3)
C81S=10^K81*C01S*C80S; %Lactic Acid (mol/m^3)
CY0S=TCYS/(C01S*10^KY1+1); %Buffer Y (mol/m^3)
CY1S=10^KY1*C01S*CY0S; %Buffer YH (mol/m^3)
CZ0S=TCZS/(C01S*10^KZ1+1); %Buffer Z (mol/m^3)
CZ1S=10^KZ1*C01S*CZ0S; %Buffer ZH (mol/m^3)
TC0S=C01S+C11S+2*C12S+C21S+C31S+C41S+C51S+C61S+2*C62S+C71S+C81S+CY1S+...
CZ1S; %Total Proton (mol/m^3)
C90S=TC0S-TC0SU+C90SU; %Chloride (mol/m^3)
CA0S=CA0SU; %Sodium (mol/m^3)
IS=0.5*(C01S+C11S+C12S*2^2+C21S+C31S+C41S+C51S+C61S+C62S*2^2+C70S+C80S...
+C90S+CA0S) %Start Buffer Ionic Strength (mol/m^3)

```

%Species Concentrations in Elution Buffer

```

C01E=10^(-pHE)*1e3; %Free Proton (mol/m^3)
C10E=TC1E/(C01E^2*10^K11*10^K12+C01E*10^K11+1); %DAP (mol/m^3)
C11E=10^K11*C01E*C10E; %DAPH (mol/m^3)
C12E=10^K12*C01E*C11E; %DAPHH (mol/m^3)
C20E=TC2E/(C01E*10^K21+1); %DEA (mol/m^3)
C21E=10^K21*C01E*C20E; %DEAH (mol/m^3)
C30E=TC3E/(C01E*10^K31+1); %Tris (mol/m^3)
C31E=10^K31*C01E*C30E; %TrisH (mol/m^3)
C40E=TC4E/(C01E*10^K41+1); %Imidazole (mol/m^3)
C41E=10^K41*C01E*C40E; %ImidazoleH (mol/m^3)
C50E=TC5E/(C01E*10^K51+1); %Bis-Tris (mol/m^3)
C51E=10^K51*C01E*C50E; %Bis-TrisH (mol/m^3)
C60E=TC6E/(C01E^2*10^K61*10^K62+C01E*10^K61+1); %Piperazine (mol/m^3)
C61E=10^K61*C01E*C60E; %PiperazineH (mol/m^3)
C62E=10^K62*C01E*C61E; %PiperazineHH (mol/m^3)
C70E=TC7E/(C01E*10^K71+1); %Acetate (mol/m^3)

```

```

C71E=10^K71*C01E*C70E; %Acetic Acid (mol/m^3)
C80E=TC8E/(C01E*10^K81+1); %Lactate (mol/m^3)
C81E=10^K81*C01E*C80E; %Lactic Acid (mol/m^3)
CY0E=TCYE/(C01E*10^KY1+1); %Buffer Y (mol/m^3)
CY1E=10^KY1*C01E*CY0E; %Buffer YH (mol/m^3)
CZ0E=TCZE/(C01E*10^KZ1+1); %Buffer Z (mol/m^3)
CZ1E=10^KZ1*C01E*CZ0E; %Buffer ZH (mol/m^3)
TC0E=C01E+C11E+2*C12E+C21E+C31E+C41E+C51E+C61E+2*C62E+C71E+C81E+CY1E+...
CZ1E; %Total Proton (mol/m^3)
C90E=TC0E-TC0EU+C90EU; %Chloride (mol/m^3)
CA0E=CA0EU; %Sodium (mol/m^3)
IE=0.5*(C01E+C11E+C12E*2^2+C21E+C31E+C41E+C51E+C61E+C62E*2^2+C70E+C80E...
+C90E+CA0E) %Elution Buffer Ionic Strength (mol/m^3)

```

%Programming Information

```

n=1000; %Number of Time Steps Used 626
k=20; %Number of Distance Steps Used
dt=Tt/n; %Time Step (min)
dz=L/k; %Distance Step (m)
dz2=dz^2; %Distance Step Squared (m^2)
tol=1e-4; %C01 Iteration Tolerance
pHSp=pHS+0.5; %C01 Iteration Starting pH
pHEm=pHE-0.5; %C01 Iteration Ending pH

```

%Calculate Number of Nodes (Column Beginning and End Counts as Nodes)

```

nG=Gt/dt+1; %Number of Time Nodes During Gradient
nT=Tt/dt+1; %Total Number of Time Nodes
k=L/dz+1; %Total Number of Distance Nodes
kp=k+1; %k+1 (For indexing of extra point outside end of column)

```

%Calculate PDE Constants

```

A0=Dax0*dt/dz2; %Constant for Diffusion Term for Total Proton
A1=Dax1*dt/dz2; %Constant for Diffusion Term for DAP
A2=Dax2*dt/dz2; %Constant for Diffusion Term for DEA
A3=Dax3*dt/dz2; %Constant for Diffusion Term for Tris
A4=Dax4*dt/dz2; %Constant for Diffusion Term for Imidazole
A5=Dax5*dt/dz2; %Constant for Diffusion Term for Bis-Tris
A6=Dax6*dt/dz2; %Constant for Diffusion Term for Piperazine
A7=Dax7*dt/dz2; %Constant for Diffusion Term for Acetate
A8=Dax8*dt/dz2; %Constant for Diffusion Term for Lactate
A9=Dax9*dt/dz2; %Constant for Diffusion Term for Chloride
AA=DaxA*dt/dz2; %Constant for Diffusion Term for Sodium
AY=DaxY*dt/dz2; %Constant for Diffusion Term for Buffer Y
AZ=DaxZ*dt/dz2; %Constant for Diffusion Term for Buffer Z
B=u*dt/et/dz; %Constant for Flow Term
C=(1-et)/et; %Constant for Binding Term

```

%Boundary Conditions for TC0(t) at z=0

```

TC0I=(0:dt:Gt)*(TC0E-TC0S)/Gt+TC0S;
TC0I(1,nG:nT)=TC0E;

```

%Boundary Conditions for TC1(t) at z=0

```

TC1I=((0:dt:Gt)*(TC1E-TC1S)/Gt+TC1S);
TC1I(1,nG:nT)=TC1E;

```

%Boundary Conditions for TC2(t) at z=0

```

TC2I=((0:dt:Gt)*(TC2E-TC2S)/Gt+TC2S);

```

```

TC2I(1,nG:nT)=TC2E;

%Boundary Conditions for TC3(t) at z=0
TC3I=((0:dt:Gt)*(TC3E-TC3S)/Gt+TC3S);
TC3I(1,nG:nT)=TC3E;

%Boundary Conditions for TC4(t) at z=0
TC4I=((0:dt:Gt)*(TC4E-TC4S)/Gt+TC4S);
TC4I(1,nG:nT)=TC4E;

%Boundary Conditions for TC5(t) at z=0
TC5I=((0:dt:Gt)*(TC5E-TC5S)/Gt+TC5S);
TC5I(1,nG:nT)=TC5E;

%Boundary Conditions for TC6(t) at z=0
TC6I=((0:dt:Gt)*(TC6E-TC6S)/Gt+TC6S);
TC6I(1,nG:nT)=TC6E;

%Boundary Conditions for TC7(t) at z=0
TC7I=((0:dt:Gt)*(TC7E-TC7S)/Gt+TC7S);
TC7I(1,nG:nT)=TC7E;

%Boundary Conditions for TC8(t) at z=0
TC8I=((0:dt:Gt)*(TC8E-TC8S)/Gt+TC8S);
TC8I(1,nG:nT)=TC8E;

%Boundary Conditions for C90(t) at z=0
C90I=(0:dt:Gt)*(C90E-C90S)/Gt+C90S;
C90I(1,nG:nT)=C90E;

%Boundary Conditions for CA0(t) at z=0
CA0I=(0:dt:Gt)*(CA0E-CA0S)/Gt+CA0S;
CA0I(1,nG:nT)=CA0E;

%Boundary Conditions for TCY(t) at z=0
TCYI=((0:dt:Gt)*(TCYE-TCYS)/Gt+TCYS);
TCYI(1,nG:nT)=TCYE;

%Boundary Conditions for TCZ(t) at z=0
TCZI=((0:dt:Gt)*(TCZE-TCZS)/Gt+TCZS);
TCZI(1,nG:nT)=TCZE;

%Initial z vectors (t=0)
TC0=ones(1,k)*TC0S; %Total Proton (mol/m^3)
C01=ones(1,k)*C01S; %Free Proton (mol/m^3)
TC1=ones(1,k)*TC1S; %Total DAP (mol/m^3)
TC2=ones(1,k)*TC2S; %Total DEA (mol/m^3)
TC3=ones(1,k)*TC3S; %Total Tris (mol/m^3)
TC4=ones(1,k)*TC4S; %Total Imidazole (mol/m^3)
TC5=ones(1,k)*TC5S; %Total Bis-Tris (mol/m^3)
TC6=ones(1,k)*TC6S; %Total Piperazine (mol/m^3)
TC7=ones(1,k)*TC7S;...
%Total Mobile Phase Acetate and Acetic Acid (mol/m^3)
Q70=ones(1,k)*k70*C70S*Qmax/(k70*C70S+k80*C80S+C90S);...
%Bound Acetate (mol/m^3)
TC8=ones(1,k)*TC8S;...
%Total Mobile Phase Lactate and Lactic Acid (mol/m^3)

```

```

Q80=ones(1,k)*k80*C80S*Qmax/(k70*C70S+k80*C80S+C90S);...
%Bound Lactate (mol/m^3)
C90=ones(1,k)*C90S; %Mobile Phase Chloride (mol/m^3)
Q90=ones(1,k)*Qmax-Q70-Q80; %Bound Chloride (mol/m^3)
T90=C90+Q90; %Total Chloride (mol/m^3)
CA0=ones(1,k)*CA0S; %Sodium (mol/m^3)
TCY=ones(1,k)*TCYS; %Total Buffer Y (mol/m^3)
TCZ=ones(1,k)*TCZS; %Total Buffer Z (mol/m^3)
Q40=ones(1,k)*Qk40*C40S; %Bound Imidazole
Q60=ones(1,k)*Qk60*C60S; %Bound Piperazine
Q61=ones(1,k)*Qk61*C61S; %Bound PiperazineH

%Initial End-of-Column pH and Ionic Strength at First Time Step
pH(1)=pHS;
I(1)=0.5*(C01S+C11S+C12S*2^2+C21S+C31S+C41S+C51S+C61S+C62S*2^2+C70S+...
C80S+C90S+CA0S);

%Initiate "old" variables used to record previous End-of-Column
variables
TC0old=TC0(k); %Total Proton
TC1old=TC1(k); %Total DAP
TC2old=TC2(k); %Total DEA
TC3old=TC3(k); %Total Tris
TC4old=TC4(k); %Total Imidazole
TC5old=TC5(k); %Total Bis-Tris
TC6old=TC6(k); %Total Piperazine
TC7old=TC7(k); %Total Mobile Phase Acetate and Acetic Acid
TC8old=TC8(k); %Total Mobile Phase Lactate and Lactic Acid
C90old=C90(k); %Total Mobile Phase Chloride
T90old=T90(k); %Total Chloride
CA0old=CA0(k); %Sodium
TCYold=TCY(k); %Total Buffer Y
TCZold=TCZ(k); %Total Buffer Z

%Set Bound Species at First Time Step
Q70next=Q70;
Q80next=Q80;
Q90next=Q90;
Q40next=Q40;
Q60next=Q60;
Q61next=Q61;

%Time Loop for Calculation of All Time Nodes (Except Initial Node)
for t=2:nT
    %Set extra point outside end of column to be End-of-Column value
    from previous time step
    TC0(kp)=TC0old;
    TC1(kp)=TC1old;
    TC2(kp)=TC2old;
    TC3(kp)=TC3old;
    TC4(kp)=TC4old;
    TC5(kp)=TC5old;
    TC6(kp)=TC6old;
    TC7(kp)=TC7old;
    TC8(kp)=TC8old;
    C90(kp)=C90old;
    CA0(kp)=CA0old;

```

```

TCY(kp)=TCYold;
TCZ(kp)=TCZold;

%Set Top-of-Column boundary vales for current time step
TC0next(1)=TC0I(t);
TC1next(1)=TC1I(t);
TC2next(1)=TC2I(t);
TC3next(1)=TC3I(t);
TC4next(1)=TC4I(t);
TC5next(1)=TC5I(t);
TC6next(1)=TC6I(t);
TC7next(1)=TC7I(t);
TC8next(1)=TC8I(t);
C90next(1)=C90I(t);
CA0next(1)=CA0I(t);
TCYnext(1)=TCYI(t);
TCZnext(1)=TCZI(t);

%Distance Loop for Calculation of All Distance Nodes (Except
Initial Node)
for z=2:k
    zp=z+1;
    zm=z-1;
    TC0next(z)=TC0(z)+A0*TC0(zp)-(B+2*A0)*TC0(z)+(A0+B)*TC0(zm);
    TC1next(z)=TC1(z)+A1*TC1(zp)-(B+2*A1)*TC1(z)+(A1+B)*TC1(zm);
    TC2next(z)=TC2(z)+A2*TC2(zp)-(B+2*A2)*TC2(z)+(A2+B)*TC2(zm);
    TC3next(z)=TC3(z)+A3*TC3(zp)-(B+2*A3)*TC3(z)+(A3+B)*TC3(zm);
    TC4next(z)=TC4(z)+A4*TC4(zp)-(B+2*A4)*TC4(z)+(A4+B)*TC4(zm)...
    -C*Q40next(z)+C*Q40(z);
    TC5next(z)=TC5(z)+A5*TC5(zp)-(B+2*A5)*TC5(z)+(A5+B)*TC5(zm);
    TC6next(z)=TC6(z)+A6*TC6(zp)-(B+2*A6)*TC6(z)+(A6+B)*TC6(zm)...
    -C*Q60next(z)+C*Q60(z)-C*Q61next(z)+C*Q61(z);
    TCYnext(z)=TCY(z)+AY*TCY(zp)-(B+2*AY)*TCY(z)+(AY+B)*TCY(zm);
    TCZnext(z)=TCZ(z)+AZ*TCZ(zp)-(B+2*AZ)*TCZ(z)+(AZ+B)*TCZ(zm);
    TC7next(z)=TC7(z)+A7*TC7(zp)-(B+2*A7)*TC7(z)+(A7+B)*TC7(zm)...
    -C*Q70next(z)+C*Q70(z);
    TC8next(z)=TC8(z)+A8*TC8(zp)-(B+2*A8)*TC8(z)+(A8+B)*TC8(zm)...
    -C*Q80next(z)+C*Q80(z);
    C90next(z)=C90(z)+A9*C90(zp)-(B+2*A9)*C90(z)+(A9+B)*C90(zm)...
    -C*Q90next(z)+C*Q90(z);
    T7=TC7next(z)+Q70next(z);
    T8=TC8next(z)+Q80next(z);
    T9=C90next(z)+Q90next(z);
    T4=TC4next(z)+Q40next(z);
    T6=TC6next(z)+Q60next(z)+Q61next(z);
    Q70(z)=Q70next(z);
    Q80(z)=Q80next(z);
    Q90(z)=Q90next(z);
    Q40(z)=Q40next(z);
    Q60(z)=Q60next(z);
    Q61(z)=Q61next(z);

    [C01next(z),Q70next(z),Q80next(z),Q90next(z),Q40next(z),...
    Q60next(z),Q61next(z)]=C01solve(TC0next(z),TC1next(z),...
    TC2next(z),TC3next(z),T4,TC5next(z),T6,T7,T8,T9,TCYnext(z),...
    TCZnext(z),Qmax,Qk40,Qk60,Qk61,k70,k80,k90,pHSp,pHEm,tol);

```

```

CA0next(z)=CA0(z)+AA*CA0(zp)-(B+2*AA)*CA0(z)+(AA+B)*CA0(zm);
if TC7next(z) < 0
    error('Negative TC7')
elseif TC8next(z) < 0
    error('Negative TC8')
elseif C90next(z) < 0
    error('Negative C90')
elseif TC3next(z) < 0
    error('Negative TC3')
elseif TC6next(z) < 0
    error('Negative TC6')
end
end

%Update "old" variables used to record previous End-of-Column
variables
TC0old=TC0(k);
TC1old=TC1(k);
TC2old=TC2(k);
TC3old=TC3(k);
TC4old=TC4(k);
TC5old=TC5(k);
TC6old=TC6(k);
TC7old=TC7(k);
TC8old=TC8(k);
C90old=C90(k);
CA0old=CA0(k);
TCYold=TCY(k);
TCZold=TCZ(k);

%Update Vectors
TC0=TC0next;
C01=C01next;
TC1=TC1next;
TC2=TC2next;
TC3=TC3next;
TC4=TC4next;
TC5=TC5next;
TC6=TC6next;
TC7=TC7next;
TC8=TC8next;
C90=C90next;
CA0=CA0next;
TCY=TCYnext;
TCZ=TCZnext;

%Calculate New End-of-Column pH and Ionic Strength
pH(t)=-log10(C01next(k)/1e3);
C11=10^K11*C01next(k)*TC1next(k)/((C01next(k)^2*10^K11*10^K12+...
C01next(k)*10^K11+1);           %DAPH (mol/m^3)
C12=10^K12*C01next(k)*C11;           %DAPHH (mol/m^3)
C21=10^K21*C01next(k)*TC2next(k)/((C01next(k)*10^K21+1);...
%DAAH (mol/m^3)
C31=10^K31*C01next(k)*TC3next(k)/((C01next(k)*10^K31+1);...
%TrisH (mol/m^3)
C41=10^K41*C01next(k)*TC4next(k)/((C01next(k)*10^K41+1);...
%ImidazoleH (mol/m^3)

```

```

C51=10^K51*C01next(k)*TC5next(k)/(C01next(k)*10^K51+1);...
%Bis-TrisH (mol/m^3)
C61=10^K61*C01next(k)*TC6next(k)/(C01next(k)^2*10^K61*10^K62+...
C01next(k)*10^K61+1);
%PiperazineH (mol/m^3)
C62=10^K62*C01next(k)*C61;
%PiperazineHH (mol/m^3)
CY1=10^KY1*C01next(k)*TCYnext(k)/(C01next(k)*10^KY1+1);...
%Buffer YH (mol/m^3)
CZ1=10^KZ1*C01next(k)*TCZnext(k)/(C01next(k)*10^KZ1+1);...
%Pseudo Buffer ZH (mol/m^3)
C70=TC7next(k)/(C01next(k)*10^K71+1); %Acetic Acid (mol/m^3)
C80=TC8next(k)/(C01next(k)*10^K81+1); %Lactic Acid (mol/m^3)
I(t)=0.5*(C01next(k)+C11+C12*2^2+C21+C31+C41+C51+C61+C62*2^2+C70+...
C80+C90next(k)+CA0next(k));

fCl(t)=C90(k);
bCl(t)=Q90(k);
fAc(t)=C70;
fLc(t)=C80;
bAc(t)=Q70(k);
bLc(t)=Q80(k);

%Calculate pH and Ionic Strength Matrices
pHM(t,:)= -log10(C01next/1e3);
C11M=10^K11.*C01next.*TC1next./(C01next.^2*10^K11*10^K12+C01next*...
10^K11+1);
%DAPH (mol/m^3)
C12M=10^K12.*C01next.*C11;
%DAPHH (mol/m^3)
C21M=10^K21.*C01next.*TC2next./(C01next*10^K21+1);...
%DEAH (mol/m^3)
C31M=10^K31.*C01next.*TC3next./(C01next*10^K31+1);...
%TrisH (mol/m^3)
C41M=10^K41.*C01next.*TC4next./(C01next*10^K41+1);...
%ImidazoleH (mol/m^3)
C51M=10^K51.*C01next.*TC5next./(C01next*10^K51+1);...
%Bis-TrisH (mol/m^3)
C61M=10^K61.*C01next.*TC6next./(C01next.^2*10^K61*10^K62+C01next*...
10^K61+1);
%PiperazineH (mol/m^3)
C62M=10^K62.*C01next.*C61;
%PiperazineHH (mol/m^3)
CY1M=10^KY1.*C01next.*TCYnext./(C01next*10^KY1+1);...
%Buffer YH (mol/m^3)
CZ1M=10^KZ1.*C01next.*TCZnext./(C01next*10^KZ1+1);...
%Buffer ZH (mol/m^3)
C70M=TC7next./(C01next*10^K71+1); %Acetic Acid (mol/m^3)
C80M=TC8next./(C01next*10^K81+1); %Lactic Acid (mol/m^3)
IM(t,:)=0.5*(C01next+C11M+C12M*2^2+C21M+C31M+C41M+C51M+C61M+C62M*...
2^2+C70M+C80M+C90next+CA0next);

%Report Current pH and Time Step to User
pH(t)
t
end

%Plot pH and Ionic Strength Results
Delay=13e-6; %Column + Tubing Volume (m^3)
Time=(0:dt:Tt)+Delay/f;
plotyy(Time,pH,Time,I)
xlabel('Run Time (min)')
ylabel('pH')

```

```

title('Mobile phase pH and Ionic Strength Profiles')

%Surface pH Calculation
%Constants
IC=0.00032;           %Resin Ionic Capacity (mol Chloride/mL Resin)
SSA=27;              %Resin Specific Surface Area (m^2/mL Resin)
Temp=298;           %Temperature (K)
E=78.5;             %Dielectric Constant of Water at 298K
Nav=6.02e23;        %Avagadro's Number (Number/mol)
e=1.6022e-19;       %Electron Charge (C)
E0=8.85418782e-12; %Permittivity of Free Space (C^2/Nm^2)
k=1.3807e-23;       %Boltzmann's Constant (J/K)

%Calculate Surface Potential
SP=IC.*Nav.*e./((SSA.*E.*E0.*((2.*e.^2.*Nav.*I./(E.*E0.*k.*Temp)).^0.5))
;

%Calculate Surface pH
SpH=pH+log10(exp(1)).*e.*SP./(k.*Temp);

%Plot Surface pH Results
hold
plot(Time,SpH,'c')
title('Mobile Phase Ionic Strength, pH and Resin Surface pH Profiles')

%Output Program Run Time
fprintf('\nProgram run time: %2.4f seconds\n\n', toc)

```

```
%Function C01solve solves for the free proton concentration C01
%governed by total species concentrations of 8 buffers. Solution is
%obtained using incremental search with step size reduction over an
%initial pH range between pHHigh and pHLow, up to a tolerance specified
%by tol.
```

```
function[C01,Q70,Q80,Q90,Q40,Q60,Q61]=C01solve(TC0,TC1,TC2,TC3,T4,TC5,...
T6,T7,T8,T9,TCY,TCZ,Qmax,Qk40,Qk60,Qk61,k70,k80,k90,pHHigh,pHLow,tol)
```

```
%Equilibrium Constants for Protontation
```

```
K110=10.62;      %First Protontation of DAP (M)
K120=8.640;     %Second Protontation of DAP (M)
K210=8.883;     %First Protontation of DEA (M)
K310=8.072;     %First Protontation of Tris (M)
K410=6.993;     %First Protontation of Imidazole (M)
K510=6.484;     %First Protontation of Bis-Tris (M)
K610=9.731;     %First Protontation of Piperazine (M)
K620=5.333;     %Second Protontation of Piperazine (M)
K710=4.756;     %First Protontation of Acetate (M)
K810=3.860;     %First Protontation of Lactate (M)
KY10=12.000;    %First Protontation of Buffer Y (M)
KZ10=2.500;     %First Protontation of Buffer Z (M)
```

```
i=0.1;          %Ionic Strength (M)
K11=K110+0.509*(1+1)*(i^0.5/(1+i^0.5)-0.2*i);
K12=K120+0.509*(2+1)*(i^0.5/(1+i^0.5)-0.2*i);
K21=K210+0.509*(1+1)*(i^0.5/(1+i^0.5)-0.2*i);
K31=K310+0.509*(1+1)*(i^0.5/(1+i^0.5)-0.2*i);
K41=K410+0.509*(1+1)*(i^0.5/(1+i^0.5)-0.2*i);
K51=K510+0.509*(1+1)*(i^0.5/(1+i^0.5)-0.2*i);
K61=K610+0.509*(1+1)*(i^0.5/(1+i^0.5)-0.2*i);
K62=K620+0.509*(2+1)*(i^0.5/(1+i^0.5)-0.2*i);
K71=K710+0.509*(0+1)*(i^0.5/(1+i^0.5)-0.2*i);
K81=K810+0.509*(0+1)*(i^0.5/(1+i^0.5)-0.2*i);
KY1=KY10+0.509*(0+1)*(i^0.5/(1+i^0.5)-0.2*i);
KZ1=KZ10+0.509*(0+1)*(i^0.5/(1+i^0.5)-0.2*i);
```

```
%Equilibrium Constants for Protontation
```

```
K11=K11-3;      %First Protontation of DAP (mol/m^3)
K12=K12-3;     %Second Protontation of DAP (mol/m^3)
K21=K21-3;     %First Protontation of DEA (mol/m^3)
K31=K31-3;     %First Protontation of Tris (mol/m^3)
K41=K41-3;     %First Protontation of Imidazole (mol/m^3)
K51=K51-3;     %First Protontation of Bis-Tris (mol/m^3)
K61=K61-3;     %First Protontation of Piperazine (mol/m^3)
K62=K62-3;     %Second Protontation of Piperazine (mol/m^3)
K71=K71-3;     %First Protontation of Acetate (mol/m^3)
K81=K81-3;     %First Protontation of Lactate (mol/m^3)
KY1=KY1-3;     %First Protontation of Pseudo Buffer Y (mol/m^3)
KZ1=KZ1-3;     %First Protontation of Pseudo Buffer Z (mol/m^3)
```

```
%Set diff to two times tolerance to initiate while loop
diff=2*tol;
```

```
%Set Starting pH for Iteration
pH=pHHigh;
```

```
%Set Initial Step Size
```

```

dpH=(pHHigh-pHLow)/10;

%Set diffold to be equal to diff to satisfy if statement
diffold=diff;

while abs(diff) > tol
    if diffold/diff > 0      %Not at Solution, continue with time step
        diffold=diff;
        pHold=pH;
        pH=pH-dpH;
        C01=10^-pH*1000;
        C11=(10^K11*C01*TC1/(C01^2*10^K11*10^K12+C01*10^K11+1));
        C12=(10^K12*10^K11*C01^2*TC1/(C01^2*10^K11*10^K12+C01*10^K11+...
        1));
        C21=(10^K21*C01*TC2/(C01*10^K21+1));
        C31=(10^K31*C01*TC3/(C01*10^K31+1));
        C40=T4/(10^K41*C01+1+Qk40);
        C41=10^K41*C01*C40;
        C51=(10^K51*C01*TC5/(C01*10^K51+1));
        C60=T6/(C01^2*10^K61*10^K62+C01*10^K61+1+Qk60+C01*10^K61*Qk61);
        C61=10^K61*C01*C60;
        C62=10^K62*C01*C61;
        CY1=(10^KY1*C01*TCY/(C01*10^KY1+1));
        CZ1=(10^KZ1*C01*TCZ/(C01*10^KZ1+1));
        Q=Qsolve(C01,T7,T8,T9,Qmax,k70,k80,k90,tol);
        C70=T7/(10^K71*C01+1+k70*Q);
        C80=T8/(10^K81*C01+1+k80*Q);
        C90=T9/(1+k90*Q);
        C71=10^K71*C01*C70;
        C81=10^K81*C01*C80;
        diff=(TC0-(C01+C11+2*C12+C21+C31+C41+C51+C61+2*C62+CY1+CZ1+...
        C71+C81));
    else %Passed Solution, return to previous step and reduce step size
        pH=pH+dpH;
        dpH=dpH/10;
        pH=pH-dpH;
        C01=10^-pH*1000;
        C11=(10^K11*C01*TC1/(C01^2*10^K11*10^K12+C01*10^K11+1));
        C12=(10^K12*10^K11*C01^2*TC1/(C01^2*10^K11*10^K12+C01*10^K11+...
        1));
        C21=(10^K21*C01*TC2/(C01*10^K21+1));
        C31=(10^K31*C01*TC3/(C01*10^K31+1));
        C40=T4/(10^K41*C01+1+Qk40);
        C41=10^K41*C01*C40;
        C51=(10^K51*C01*TC5/(C01*10^K51+1));
        C60=T6/(C01^2*10^K61*10^K62+C01*10^K61+1+Qk60+C01*10^K61*Qk61);
        C61=10^K61*C01*C60;
        C62=10^K62*C01*C61;
        CY1=(10^KY1*C01*TCY/(C01*10^KY1+1));
        CZ1=(10^KZ1*C01*TCZ/(C01*10^KZ1+1));
        Q=Qsolve(C01,T7,T8,T9,Qmax,k70,k80,k90,tol);
        C70=T7/(10^K71*C01+1+k70*Q);
        C80=T8/(10^K81*C01+1+k80*Q);
        C90=T9/(1+k90*Q);
        C71=10^K71*C01*C70;
        C81=10^K81*C01*C80;
        diff=(TC0-(C01+C11+2*C12+C21+C31+C41+C51+C61+2*C62+CY1+CZ1+...

```

```

        C71+C81));
    end
end

%Calculates Free Proton Concentration in mol/m^3
C01=10^-pH*1e3;

%Calculates Bound Species Concentrations
Q70=k70*C70*Q;      %Bound Acetate
Q80=k80*C80*Q;      %Bound Lactate
Q90=k90*C90*Q;      %Bound Chloride
Q40=Qk40*C40;       %Bound Imidazole
Q60=Qk60*C60;       %Bound Piperazine
Q61=Qk61*C61;       %Bound PiperazineH

```

```

%Function Qsolve solves for the free resin concentration Q given the
%free proton concentration C01

function Q=Qsolve(C01,T7,T8,T9,Qmax,k70,k80,k90,tol)

%Equilibrium Constants for Protontation
K71=4.756;      %First Protonation of Acetate (M)
K81=3.860;      %First Protonation of Lactate (M)
i=0.1;         %Ionic Strength (M)
K71=K71+0.509*(0+1)*(i^0.5/(1+i^0.5)-0.2*i);
K81=K81+0.509*(0+1)*(i^0.5/(1+i^0.5)-0.2*i);

%Equilibrium Constants for Protontation
K71=K71-3;      %First Protonation of Acetate (mol/m^3)
K81=K81-3;      %First Protonation of Lactate (mol/m^3)

%Set diff to two times tolerance to initial while loop
diff=2*tol;

%Set Initial Step Size
dQ=1;

%Set Starting Q for Iteration
Q=0-dQ;

%Set diffold to be equal to diff to satisfy if statement
diffold=diff;

while abs(diff) > tol
    if diffold/diff > 0      %Not at Solution, continue with time step
        diffold=diff;
        Qold=Q;
        Q=Q+dQ;
        diff=Qmax-(k70*Q*(T7/(10^K71*C01+1+k70*Q))+k80*Q*(T8/(10^K81*...
            C01+1+k80*Q))+k90*Q*(T9/(1+k90*Q)));
    else %Passed Solution, return to previous step and reduce step size
        Q=Q-dQ;
        dQ=dQ/10;
        Q=Q+dQ;
        diff=Qmax-(k70*Q*(T7/(10^K71*C01+1+k70*Q))+k80*Q*(T8/(10^K81*...
            C01+1+k80*Q))+k90*Q*(T9/(1+k90*Q)));
    end
end
end

```

Appendix B: Description of the Program for Sculpting Buffer Compositions through the Calculation of pH and Ionic Strength Profiles in a Cation Exchange Column

All programs are written for use on MATLAB 6.1. The main program script file “ICFM.m” contains model parameters entered by the user and equations responsible for executing the primary finite difference iterations based on the continuity equation of chromatography. Two functions, “C01solve.m” and “Qsolve.m”, are called during the iteration. The following table lists all species tracked by the program and nomenclature used to represent them:

Table B-1: List species tracked by MATLAB script file “ICFM.m” for the calculation of pH and ionic strength profiles during CEICF

Nomenclature	Species	Description
01 H ⁺	H ⁺	proton
10 Malonate ²⁻	MAL ²⁻	unprotonated malonate
11 MalonateH	MAL-H ⁻	monoprotonated malonate
12 MalonateHH	MAL-2H	diprotonated malonate
20 Formate ⁻	FOR ⁻	unprotonated formate
21 FormateH	FOR-H	monoprotonated formate
30 Acetate ⁻	ACE ⁻	unprotonated acetate
31 AcetateH	ACE-H	monoprotonated acetate
40 MES ⁻	MES ⁻	unprotonated MES
41 MESH	MES-H	monoprotonated MES
50 MOPSO ⁻	MSO ⁻	unprotonated MOPSO
51 MOPSOH	MSO-H	monoprotonated MOPSO
52 MOPSOHH ⁺	MSO-2H ⁺	diprotonated MOPSO
60 HEPES ⁻	HPS ⁻	unprotonated HEPES
61 HEPESH	HPS-H	monoprotonated HEPES
62 HEPESHH ⁺	HPS-2H ⁺	diprotonated HEPES
70 BICINE ⁻	BCN ⁻	unprotonated BICINE
71 BICINEH	BCN-H	monoprotonated BICINE
72 BICINEHH ⁺	BCN-2H ⁺	diprotonated BICINE
80 CHES ⁻	CHS ⁻	unprotonated CHES
81 CHESH	CHS-H	monoprotonated CHES
90 CAPS ⁻	CPS ⁻	unprotonated CAPS
91 CAPSH	CPS-H	monoprotonated CAPS
A0 Cl ⁻	Cl ⁻	chloride ion
B0 Na ⁺	Na ⁺	sodium ion

The total mobile phase concentrations of all species in the column are tracked using the continuity equation of chromatography. Species that do not associate with the stationary phase regardless of their protonation states (MAL, FOR, ACE, MES, CHS and CPS) are tracked by the following simplified form of the continuity equation:

$$\frac{\partial TC_i}{\partial t} = D_{axi} \frac{\partial^2 TC_i}{\partial z^2} - \left(\frac{u}{\varepsilon} \right) \frac{\partial TC_i}{\partial z} \quad (\text{B-1})$$

The total mobile phase concentration of species i (TC_i) can be used to write the mobile phase concentration of the protonated forms of each of these species as a function of the free proton concentration (C_{01}):

$$C_{11} = \frac{10^{K_{11}^*} C_{01} TC_1}{C_{01}^2 10^{K_{11}^*} 10^{K_{12}^*} + C_{01} 10^{K_{11}^*} + 1} \quad (\text{B-2})$$

$$C_{12} = \frac{10^{K_{11}^*} 10^{K_{12}^*} C_{01}^2 TC_1}{C_{01}^2 10^{K_{11}^*} 10^{K_{12}^*} + C_{01} 10^{K_{11}^*} + 1} \quad (\text{B-3})$$

$$C_{21} = \frac{10^{K_{21}^*} C_{01} TC_2}{C_{01} 10^{K_{21}^*} + 1} \quad (\text{B-4})$$

$$C_{31} = \frac{10^{K_{31}^*} C_{01} TC_3}{C_{01} 10^{K_{31}^*} + 1} \quad (\text{B-5})$$

$$C_{41} = \frac{10^{K_{41}^*} C_{01} TC_4}{C_{01} 10^{K_{41}^*} + 1} \quad (\text{B-6})$$

$$C_{81} = \frac{10^{K_{81}^*} C_{01} TC_8}{C_{01} 10^{K_{81}^*} + 1} \quad (\text{B-7})$$

$$C_{91} = \frac{10^{K_{91}^*} C_{01} TC_9}{C_{01} 10^{K_{91}^*} + 1} \quad (\text{B-8})$$

Buffering species that associate with the stationary phase (MSO, HPS and BCN) are tracked by the following equations:

$$\frac{\partial TC_5}{\partial t} = D_{ax5} \frac{\partial^2 TC_5}{\partial z^2} - \left(\frac{u}{\varepsilon} \right) \frac{\partial TC_5}{\partial z} - \left(\frac{1-\varepsilon}{\varepsilon} \right) \frac{\partial Q_{52}}{\partial t} \quad (\text{B-9})$$

$$\frac{\partial TC_6}{\partial t} = D_{ax6} \frac{\partial^2 TC_6}{\partial z^2} - \left(\frac{u}{\varepsilon} \right) \frac{\partial TC_6}{\partial z} - \left(\frac{1-\varepsilon}{\varepsilon} \right) \frac{\partial Q_{62}}{\partial t} \quad (\text{B-10})$$

$$\frac{\partial TC_7}{\partial t} = D_{ax7} \frac{\partial^2 TC_7}{\partial z^2} - \left(\frac{u}{\varepsilon} \right) \frac{\partial TC_7}{\partial z} - \left(\frac{1-\varepsilon}{\varepsilon} \right) \frac{\partial Q_{72}}{\partial t} \quad (\text{B-11})$$

where the stationary phase concentrations Q_{52} , Q_{62} , and Q_{72} are described by the following binding isotherm relationships:

$$Q_{52} = \frac{Q_{52}^{\max} K_{52} C_{52}}{C_{B0} + K_{01} C_{01} + K_{52} C_{52} + K_{62} C_{62} + K_{72} C_{72}} \quad (\text{B-12})$$

$$Q_{62} = \frac{Q_{62}^{\max} K_{62} C_{62}}{C_{B0} + K_{01} C_{01} + K_{52} C_{52} + K_{62} C_{62} + K_{72} C_{72}} \quad (\text{B-13})$$

$$Q_{72} = \frac{Q_{72}^{\max} K_{72} C_{72}}{C_{B0} + K_{01} C_{01} + K_{52} C_{52} + K_{62} C_{62} + K_{72} C_{72}} \quad (\text{B-14})$$

The total mobile phase concentration of these species derived from equations B-9, B-10 and B-11 can be used to write the mobile phase concentration of the protonated forms of each of these species as a function of the free proton concentration (C_{01}):

$$C_{51} = \frac{10^{K_{51}^*} C_{01} TC_5}{C_{01}^2 10^{K_{51}^*} 10^{K_{52}^*} + C_{01} 10^{K_{51}^*} + 1} \quad (\text{B-15})$$

$$C_{52} = \frac{10^{K_{51}^*} 10^{K_{52}^*} C_{01}^2 TC_5}{C_{01}^2 10^{K_{51}^*} 10^{K_{52}^*} + C_{01} 10^{K_{51}^*} + 1} \quad (\text{B-16})$$

$$C_{61} = \frac{10^{K_{61}^*} C_{01} TC_6}{C_{01}^2 10^{K_{61}^*} 10^{K_{62}^*} + C_{01} 10^{K_{61}^*} + 1} \quad (\text{B-17})$$

$$C_{62} = \frac{10^{K_{61}^*} 10^{K_{62}^*} C_{01}^2 TC_6}{C_{01}^2 10^{K_{61}^*} 10^{K_{62}^*} + C_{01} 10^{K_{61}^*} + 1} \quad (\text{B-18})$$

$$C_{71} = \frac{10^{K_{71}^*} C_{01} TC_7}{C_{01}^2 10^{K_{71}^*} 10^{K_{72}^*} + C_{01} 10^{K_{71}^*} + 1} \quad (\text{B-19})$$

$$C_{72} = \frac{10^{K_{71}^*} 10^{K_{72}^*} C_{01}^2 TC_7}{C_{01}^2 10^{K_{71}^*} 10^{K_{72}^*} + C_{01} 10^{K_{71}^*} + 1} \quad (\text{B-20})$$

The mobile phase proton concentration (TC_0) is defined by the following:

$$TC_0 = C_{01} + C_{11} + C_{21} + C_{31} + 2C_{32} + C_{41} + C_{51} + 2C_{52} + C_{61} + 2C_{62} + C_{71} + 2C_{72} + C_{81} + C_{91} \quad (\text{B-21})$$

which is tracked by the following continuity equation:

$$\frac{\partial TC_0}{\partial t} = D_{ax0} \frac{\partial^2 TC_0}{\partial z^2} - \left(\frac{u}{\varepsilon} \right) \frac{\partial TC_0}{\partial z} - \left(\frac{1-\varepsilon}{\varepsilon} \right) \frac{\partial Q_{01}}{\partial t} \quad (\text{B-22})$$

where the stationary phase proton concentration Q_{01} is described by the following binding isotherm relationship:

$$Q_{01} = \frac{Q_{01}^{\max} K_{01} C_{01}}{C_{B0} + K_{01} C_{01} + K_{52} C_{52} + K_{62} C_{62} + K_{72} C_{72}} \quad (\text{B-23})$$

Substituting equations B-2, B-3, B-4, B-5, B-6, B-7, B-8, B-15, B-16, B-17, B-18, B-19 and B-20 into equation B-21, C_{01} can be solved based on the total mobile phase proton concentration derived from equation B-22.

The bulk mobile phase pH and ionic strength can be calculated using the following equations:

$$pH = -\log^{C_{01}} \quad (\text{B-24})$$

$$I = 0.5 \left(C_{01} + C_{11} + C_{21} + C_{31} + 2^2 C_{32} + C_{41} + C_{51} + 2^2 C_{52} + C_{61} + 2^2 C_{62} + C_{71} + 2^2 C_{72} + C_{81} + C_{91} \right) \quad (\text{B-25})$$

Calculated pH and ionic strength values at each column position and run time node are stored in variables “pHM” and “IM”, respectively. End-of-column pH and ionic strength is plotted against run time to generate predicted profiles. The MATLAB code for the solution is shown below.

```
%Script m-file "ICFM.m" that uses an explicit scheme finite difference
%method to solve the continuity equations required for predicting the
%free proton concentration and hence the shape of the pH gradient
%generated at the exit of the Mono S HR10/10 strong cation exchange
%column.
```

```
clear
tic
```

```
%Column and Run Constants
```

```
Qmax=135;      %Binding Capacity (mol/m^3)
Rp=5e-6;      %Resin Particle Radius (m)
ep=0.64;      %Resin Particle Voidage
L=0.10;       %Column Length (m)
R=0.005;      %Column Radius (m)
e=0.36;       %Column Voidage
et=e+(1-e)*ep; %Total Voidage
f=1/1e6;      %Mobile Phase Flow Rate (m^3/min)
u=f/(pi*R^2); %Superficial Mobile Phase Velocity (m/min)
G=60/1e6;     %Gradient (0-100% Elution Buffer) Length (m^3)
T=120/1e6;    %Total Run Length (m^3)
pHS=2;        %Starting Buffer pH
pHE=11;       %Elution Buffer pH
pHSU=2.3;     %Starting Buffer pH (Unadjusted)
pHEU=2.3;     %Elution Buffer pH (Unadjusted)
Gt=G/f;       %Gradient Run Time (min)
Tt=T/f;       %Total Run Time (min)
```

```
%Axial Dispersion Coefficients
```

```
Dax0=0e-7;    %Total Proton (Includes all protonated species)
Dax1=0e-7;    %Malonic
Dax2=0e-7;    %Formate
Dax3=0e-7;    %Acetate
Dax4=0e-7;    %MES
Dax5=0e-7;    %MOPSO
Dax6=0e-7;    %HEPES
Dax7=0e-7;    %BICINE
Dax8=0e-7;    %CHES
Dax9=0e-7;    %CAPS
DaxA=0e-7;    %Chrloride
DaxB=0e-7;    %Sodium
```

```
%Binding Constants for Binding Species
```

```
k01=1;        %Hydrogen
kB0=1;        %Sodium
k52=0;        %MOPSOHH
k62=1.14;     %HEPESHH
k72=1.21;     %BICINEHH
```

```
Qk31=0;       %Acetic Acid (m^3/mol)
Qk41=0;       %MESH (m^3/mol)
Qk81=5;       %CHESH (m^3/mol)
Qk91=15;      %CAPSH (m^3/mol)
```

```
%Equilibrium Constants for Protontation
```

```
K110=5.690;   %First Protontation of Malonate (M)
```

```

K120=2.830;      %Second Protonation of Malonate (M)
K210=3.750;      %First Protonation of Formate (M)
K310=4.756;      %First Protonation of Acetate (M)
K410=6.270;      %First Protonation of MES (M)
K510=6.900;      %First Protonation of MOPSO (M)
K520=0.060;      %Second Protonation of MOPSO (M)
K610=7.564;      %First Protonation of HEPES (M)
K620=3.000;      %Second Protonation of HEPES (M)
K710=8.334;      %First Protonation of BICINE (M)
K720=2.000;      %Second Protonation of BICINE (M)
K810=9.394;      %First Protonation of CHES (M)
K910=10.499;     %First Protonation of CAPS (M)
i=0.3;
K11=K110+0.509*(-2+1)*(i^0.5/(1+i^0.5)-0.2*i)
K12=K120+0.509*(0+1)*(i^0.5/(1+i^0.5)-0.2*i);
K21=K210+0.509*(0+1)*(i^0.5/(1+i^0.5)-0.2*i);
K31=K310+0.509*(0+1)*(i^0.5/(1+i^0.5)-0.2*i);
K41=K410+0.509*(0+1)*(i^0.5/(1+i^0.5)-0.2*i);
K51=K510+0.509*(0+1)*(i^0.5/(1+i^0.5)-0.2*i);
K52=K520+0.509*(2+1)*(i^0.5/(1+i^0.5)-0.2*i);
K61=K610+0.509*(0+1)*(i^0.5/(1+i^0.5)-0.2*i);
K62=K620+0.509*(2+1)*(i^0.5/(1+i^0.5)-0.2*i);
K71=K710+0.509*(0+1)*(i^0.5/(1+i^0.5)-0.2*i);
K72=K720+0.509*(2+1)*(i^0.5/(1+i^0.5)-0.2*i);
K81=K810+0.509*(0+1)*(i^0.5/(1+i^0.5)-0.2*i);
K91=K910+0.509*(0+1)*(i^0.5/(1+i^0.5)-0.2*i);

```

%Equilibrium Constants for Protontation

```

K11=K11-3;      %First Protonation of Malonic Acid (mol/m^3)
K12=K12-3;      %Second Protonation of Malonic Acid (mol/m^3)
K21=K21-3;      %First Protonation of Formic Acid (mol/m^3)
K31=K31-3;      %First Protonation of Acetic Acid (mol/m^3)
K41=K41-3;      %First Protonation of MES (mol/m^3)
K51=K51-3;      %First Protonation of MOPSO (mol/m^3)
K52=K52-3;      %Second Protonation of MOPSO (mol/m^3)
K61=K61-3;      %First Protonation of HEPES (mol/m^3)
K62=K62-3;      %Second Protonation of HEPES (mol/m^3)
K71=K71-3;      %First Protonation of BICINE (mol/m^3)
K72=K72-3;      %Second Protonation of BICINE (mol/m^3)
K81=K81-3;      %First Protonation of CHES (mol/m^3)
K91=K91-3;      %First Protonation of CAPS (mol/m^3)

```

%Total Species Concentrations Added to Starting Buffer

```

TC1S=10;        %Malonic Acid (mol/m^3)
TC2S=10;        %Formic Acid (mol/m^3)
TC3S=10;        %Acetic Acid (mol/m^3)
TC4S=10;        %MES (mol/m^3)
TC5S=10;        %MOPSO (mol/m^3)
TC6S=10;        %HEPES (mol/m^3)
TC7S=10;        %BICINE (mol/m^3)
TC8S=10;        %CHES (mol/m^3)
TC9S=10;        %CAPS (mol/m^3)
TCAS=150;       %Chloride (mol/m^3)
TCBS=150;       %Sodium (mol/m^3)

```

%Total Species Concentrations Added to Elution Buffer

```

TC1E=10;          %Malonic Acid (mol/m^3)
TC2E=10;          %Formic Acid (mol/m^3)
TC3E=10;          %Acetic Acid (mol/m^3)
TC4E=10;          %MES (mol/m^3)
TC5E=10;          %MOPSO (mol/m^3)
TC6E=10;          %HEPES (mol/m^3)
TC7E=10;          %BICINE (mol/m^3)
TC8E=10;          %CHES (mol/m^3) 15
TC9E=10;          %CAPS (mol/m^3) 20
TCAE=50;          %Chloride (mol/m^3)
TCBE=50;          %Sodium (mol/m^3)

%Important Species Concentrations in Unadjusted Starting Buffer
C01SU=10^(-pHSU)*1e3;          %Free Proton (mol/m^3)
C10SU=TC1S/(C01SU^2*10^K11*10^K12+C01SU*10^K11+1); %Malonate (mol/m^3)
C11SU=10^K11*C01SU*C10SU;          %MalonateH (mol/m^3)
C12SU=10^K12*C01SU*C11SU;          %MalonateHH (mol/m^3)
C20SU=TC2S/(C01SU*10^K21+1);          %Formate (mol/m^3)
C21SU=10^K21*C01SU*C20SU;          %FormateH (mol/m^3)
C30SU=TC3S/(C01SU*10^K31+1);          %Acetate (mol/m^3)
C31SU=10^K31*C01SU*C30SU;          %AcetateH (mol/m^3)
C40SU=TC4S/(C01SU*10^K41+1);          %MES (mol/m^3)
C41SU=10^K41*C01SU*C40SU;          %MESH (mol/m^3)
C50SU=TC5S/(C01SU^2*10^K51*10^K52+C01SU*10^K51+1); %MOPSO (mol/m^3)
C51SU=10^K51*C01SU*C50SU;          %MOPSOH (mol/m^3)
C52SU=10^K52*C01SU*C51SU;          %MOPSOHH (mol/m^3)
C60SU=TC6S/(C01SU^2*10^K61*10^K62+C01SU*10^K61+1); %HEPES (mol/m^3)
C61SU=10^K61*C01SU*C60SU;          %HEPESH (mol/m^3)
C62SU=10^K62*C01SU*C61SU;          %HEPESHH (mol/m^3)
C70SU=TC7S/(C01SU^2*10^K71*10^K72+C01SU*10^K71+1); %BICINE (mol/m^3)
C71SU=10^K71*C01SU*C70SU;          %BICINEH (mol/m^3)
C72SU=10^K72*C01SU*C71SU;          %BICINEHH (mol/m^3)
C80SU=TC8S/(C01SU*10^K81+1);          %CHES (mol/m^3)
C81SU=10^K81*C01SU*C80SU;          %CHESH (mol/m^3)
C90SU=TC9S/(C01SU*10^K91+1);          %CAPS (mol/m^3)
C91SU=10^K91*C01SU*C90SU;          %CAPSH (mol/m^3)
TC0SU=C01SU+C11SU+2*C12SU+C21SU+C31SU+C41SU+C51SU+2*C52SU+C61SU+2*...
C62SU+C71SU+2*C72SU+C81SU+C91SU;          %Total Proton (mol/m^3)
CA0SU=TCAS;          %Chloride (mol/m^3)
CB0SU=TCBS;          %Sodium (mol/m^3)

%Important Species Concentrations in Unadjusted Elution Buffer
C01EU=10^(-pHEU)*1e3;          %Free Proton (mol/m^3)
C10EU=TC1E/(C01EU^2*10^K11*10^K12+C01EU*10^K11+1); %Malonate (mol/m^3)
C11EU=10^K11*C01EU*C10EU;          %MalonateH (mol/m^3)
C12EU=10^K12*C01EU*C11EU;          %MalonateHH (mol/m^3)
C20EU=TC2E/(C01EU*10^K21+1);          %Formate (mol/m^3)
C21EU=10^K21*C01EU*C20EU;          %FormateH (mol/m^3)
C30EU=TC3E/(C01EU*10^K31+1);          %Acetate (mol/m^3)
C31EU=10^K31*C01EU*C30EU;          %AcetateH (mol/m^3)
C40EU=TC4E/(C01EU*10^K41+1);          %MES (mol/m^3)
C41EU=10^K41*C01EU*C40EU;          %MESH (mol/m^3)
C50EU=TC5E/(C01EU^2*10^K51*10^K52+C01EU*10^K51+1); %MOPSO (mol/m^3)
C51EU=10^K51*C01EU*C50EU;          %MOPSOH (mol/m^3)
C52EU=10^K52*C01EU*C51EU;          %MOPSOHH (mol/m^3)
C60EU=TC6E/(C01EU^2*10^K61*10^K62+C01EU*10^K61+1); %HEPES (mol/m^3)

```

```

C61EU=10^K61*C01EU*C60EU; %HEPESH (mol/m^3)
C62EU=10^K62*C01EU*C61EU; %HEPESHH (mol/m^3)
C70EU=TC7E/(C01EU^2*10^K71*10^K72+C01EU*10^K71+1); %BICINE (mol/m^3)
C71EU=10^K71*C01EU*C70EU; %BICINEH (mol/m^3)
C72EU=10^K72*C01EU*C71EU; %BICINEHH (mol/m^3)
C80EU=TC8E/(C01EU*10^K81+1); %CHES (mol/m^3)
C81EU=10^K81*C01EU*C80EU; %CHESH (mol/m^3)
C90EU=TC9E/(C01EU*10^K91+1); %CAPS (mol/m^3)
C91EU=10^K91*C01EU*C90EU; %CAPSH (mol/m^3)
TC0EU=C01EU+C11EU+2*C12EU+C21EU+C31EU+C41EU+C51EU+2*C52EU+C61EU+2*...
C62EU+C71EU+2*C72EU+C81EU+C91EU; %Total Proton (mol/m^3)
CA0EU=TCAE; %Chloride (mol/m^3)
CB0EU=TCBE; %Sodium (mol/m^3)

```

%Important Species Concentrations in Starting Buffer

```

C01S=10^(-pHS)*1e3; %Free Proton (mol/m^3)
C10S=TC1S/(C01S^2*10^K11*10^K12+C01S*10^K11+1); %Malonate (mol/m^3)
C11S=10^K11*C01S*C10S; %MalonateH (mol/m^3)
C12S=10^K12*C01S*C11S; %MalonateHH (mol/m^3)
C20S=TC2S/(C01S*10^K21+1); %Formate (mol/m^3)
C21S=10^K21*C01S*C20S; %FormateH (mol/m^3)
C30S=TC3S/(C01S*10^K31+1); %Acetate (mol/m^3)
C31S=10^K31*C01S*C30S; %AcetateH (mol/m^3)
C40S=TC4S/(C01S*10^K41+1); %MES (mol/m^3)
C41S=10^K41*C01S*C40S; %MESH (mol/m^3)
C50S=TC5S/(C01S^2*10^K51*10^K52+C01S*10^K51+1); %MOPSO (mol/m^3)
C51S=10^K51*C01S*C50S; %MOPSOH (mol/m^3)
C52S=10^K52*C01S*C51S; %MOPSOHH (mol/m^3)
C60S=TC6S/(C01S^2*10^K61*10^K62+C01S*10^K61+1); %HEPES (mol/m^3)
C61S=10^K61*C01S*C60S; %HEPESH (mol/m^3)
C62S=10^K62*C01S*C61S; %HEPESHH (mol/m^3)
C70S=TC7S/(C01S^2*10^K71*10^K72+C01S*10^K71+1); %BICINE (mol/m^3)
C71S=10^K71*C01S*C70S; %BICINEH (mol/m^3)
C72S=10^K72*C01S*C71S; %BICINEHH (mol/m^3)
C80S=TC8S/(C01S*10^K81+1); %CHES (mol/m^3)
C81S=10^K81*C01S*C80S; %CHESH (mol/m^3)
C90S=TC9S/(C01S*10^K91+1); %CAPS (mol/m^3)
C91S=10^K91*C01S*C90S; %CAPSH (mol/m^3)
TC0S=C01S+C11S+2*C12S+C21S+C31S+C41S+C51S+2*C52S+C61S+2*C62S+C71S+2*...
C72S+C81S+C91S %Total Proton (mol/m^3)
CA0S=TC0S-TC0SU+CA0SU; %Chloride (mol/m^3)
CB0S=CB0SU; %Sodium (mol/m^3)
IS=0.5*(C01S+C10S*2^2+C11S+C20S+C30S+C40S+C50S+C52S+C60S+C62S+C70S+...
C72S+C80S+C90S+CA0S+CB0S); %Start Buffer Ionic Strength (mol/m^3)

```

%Important Species Concentrations in Elution Buffer

```

C01E=10^(-pHE)*1e3; %Free Proton (mol/m^3)
C10E=TC1E/(C01E^2*10^K11*10^K12+C01E*10^K11+1); %Malonate (mol/m^3)
C11E=10^K11*C01E*C10E; %MalonateH (mol/m^3)
C12E=10^K12*C01E*C11E; %MalonateHH (mol/m^3)
C20E=TC2E/(C01E*10^K21+1); %Formate (mol/m^3)
C21E=10^K21*C01E*C20E; %FormateH (mol/m^3)
C30E=TC3E/(C01E*10^K31+1); %Acetate (mol/m^3)
C31E=10^K31*C01E*C30E; %AcetateH (mol/m^3)
C40E=TC4E/(C01E*10^K41+1); %MES (mol/m^3)
C41E=10^K41*C01E*C40E; %MESH (mol/m^3)

```

```

C50E=TC5E/(C01E^2*10^K51*10^K52+C01E*10^K51+1); %MOPSO (mol/m^3)
C51E=10^K51*C01E*C50E; %MOPSOH (mol/m^3)
C52E=10^K52*C01E*C51E; %MOPSOHH (mol/m^3)
C60E=TC6E/(C01E^2*10^K61*10^K62+C01E*10^K61+1); %HEPES (mol/m^3)
C61E=10^K61*C01E*C60E; %HEPESH (mol/m^3)
C62E=10^K62*C01E*C61E; %HEPESHH (mol/m^3)
C70E=TC7E/(C01E^2*10^K71*10^K72+C01E*10^K71+1); %BICINE (mol/m^3)
C71E=10^K71*C01E*C70E; %BICINEH (mol/m^3)
C72E=10^K72*C01E*C71E; %BICINEHH (mol/m^3)
C80E=TC8E/(C01E*10^K81+1); %CHES (mol/m^3)
C81E=10^K81*C01E*C80E; %CHESH (mol/m^3)
C90E=TC9E/(C01E*10^K91+1); %CAPS (mol/m^3)
C91E=10^K91*C01E*C90E; %CAPSH (mol/m^3)
TC0E=C01E+C11E+2*C12E+C21E+C31E+C41E+C51E+2*C52E+C61E+2*C62E+C71E+2*...
C72E+C81E+C91E %Total Proton (mol/m^3)
CA0E=CA0EU; %Chloride (mol/m^3)
CB0E=TC0EU-TC0E+CB0EU; %Sodium (mol/m^3)
IE=0.5*(C01E+C10E*2^2+C11E+C20E+C30E+C40E+C50E+C52E+C60E+C62E+C70E+...
C72E+C80E+C90E+CA0E+CB0E); %Elution Buffer Ionic Strength (mol/m^3)

```

%Programming Information

```

n=1000; %Number of Time Steps Used
k=20; %Number of Distance Steps Used
dt=Tt/n; %Time Step (min)
dz=L/k; %Distance Step (m)
dz2=dz^2; %Distance Step Squared (m^2)
tol=1e-8; %C01 Iteration Tolerance
pHSm=pHS-1; %C01 Iteration Starting pH
pHEp=pHE+1; %C01 Iteration Ending pH

```

%Calculate Number of Nodes (Column Beginning and End Counts as Nodes)

```

nG=Gt/dt+1; %Number of Time Nodes During Gradient
nT=Tt/dt+1; %Total Number of Time Nodes
k=L/dz+1; %Total Number of Distance Nodes
kp=k+1; %k+1 (For indexing of extra point outside end of column)

```

%Calculate PDE Constants

```

A0=Dax0*dt/dz2; %Constant for Diffusion Term for Total Proton
A1=Dax1*dt/dz2; %Constant for Diffusion Term for Chloroacetate
A2=Dax2*dt/dz2; %Constant for Diffusion Term for Formate
A3=Dax3*dt/dz2; %Constant for Diffusion Term for Pimelate
A4=Dax4*dt/dz2; %Constant for Diffusion Term for MES
A5=Dax5*dt/dz2; %Constant for Diffusion Term for MOPSO
A6=Dax6*dt/dz2; %Constant for Diffusion Term for HEPES
A7=Dax7*dt/dz2; %Constant for Diffusion Term for BICINE
A8=Dax8*dt/dz2; %Constant for Diffusion Term for CHES
A9=Dax9*dt/dz2; %Constant for Diffusion Term for CAPS
AA=DaxA*dt/dz2; %Constant for Diffusion Term for Chloride
AB=DaxB*dt/dz2; %Constant for Diffusion Term for Sodium
B=u*dt/et/dz; %Constant for Flow Term
C=(1-et)/et; %Constant for Binding Term

```

%Boundary Conditions for TC0(t) at z=0

```

TC0I=(0:dt:Gt)*(TC0E-TC0S)/Gt+TC0S;
TC0I(1,nG:nT)=TC0E;

```

```

%Boundary Conditions for TC1(t) at z=0
TC1I=((0:dt:Gt)*(TC1E-TC1S)/Gt+TC1S);
TC1I(1,nG:nT)=TC1E;

%Boundary Conditions for TC2(t) at z=0
TC2I=((0:dt:Gt)*(TC2E-TC2S)/Gt+TC2S);
TC2I(1,nG:nT)=TC2E;

%Boundary Conditions for TC3(t) at z=0
TC3I=((0:dt:Gt)*(TC3E-TC3S)/Gt+TC3S);
TC3I(1,nG:nT)=TC3E;

%Boundary Conditions for TC4(t) at z=0
TC4I=((0:dt:Gt)*(TC4E-TC4S)/Gt+TC4S);
TC4I(1,nG:nT)=TC4E;

%Boundary Conditions for TC5(t) at z=0
TC5I=((0:dt:Gt)*(TC5E-TC5S)/Gt+TC5S);
TC5I(1,nG:nT)=TC5E;

%Boundary Conditions for TC6(t) at z=0
TC6I=((0:dt:Gt)*(TC6E-TC6S)/Gt+TC6S);
TC6I(1,nG:nT)=TC6E;

%Boundary Conditions for TC7(t) at z=0
TC7I=((0:dt:Gt)*(TC7E-TC7S)/Gt+TC7S);
TC7I(1,nG:nT)=TC7E;

%Boundary Conditions for TC8(t) at z=0
TC8I=((0:dt:Gt)*(TC8E-TC8S)/Gt+TC8S);
TC8I(1,nG:nT)=TC8E;

%Boundary Conditions for C90(t) at z=0
TC9I=((0:dt:Gt)*(TC9E-TC9S)/Gt+TC9S);
TC9I(1,nG:nT)=TC9E;

%Boundary Conditions for CA0(t) at z=0
CA0I=((0:dt:Gt)*(CA0E-CA0S)/Gt+CA0S);
CA0I(1,nG:nT)=CA0E;

%Boundary Conditions for CB0(t) at z=0
CB0I=((0:dt:Gt)*(CB0E-CB0S)/Gt+CB0S);
CB0I(1,nG:nT)=CB0E;

%Initial z vectors (t=0)
TC0=ones(1,k)*TC0S;
C01=ones(1,k)*C01S;
Q01=ones(1,k)*k01*C01S*Qmax/(k01*C01S+k52*C52S+k62*C62S+k72*C72S+kB0*...
CB0S);
T01=TC0+C01+Q01;
TC1=ones(1,k)*TC1S;
TC2=ones(1,k)*TC2S;
TC3=ones(1,k)*TC3S;
Q31=ones(1,k)*Qk31*C31S;
TC4=ones(1,k)*TC4S;

%Total Mobile Phase Proton (mol/m^3)
%Free Proton (mol/m^3)
%Bound Proton (mol/m^3)
%Total Proton (mol/m^3)
%Total Malonic Acid (mol/m^3)
%Total Formic Acid (mol/m^3)
%Total Acetic Acid (mol/m^3)
%Bound Acetic Acid (mol/m^3)
%Total MES (mol/m^3)

```

```

Q41=ones(1,k)*Qk41*C41S;           %Bound MESH (mol/m^3)
TC5=ones(1,k)*TC5S;                 %Total MOPSO (mol/m^3)
Q52=ones(1,k)*k52*C52S*Qmax/(k01*C01S+k52*C52S+k62*C62S+k72*C72S+kB0*...
CB0S);                               %Bound MOPSOHH (mol/m^3)
TC6=ones(1,k)*TC6S;                 %Total HEPES (mol/m^3)
Q62=ones(1,k)*k62*C62S*Qmax/(k01*C01S+k52*C52S+k62*C62S+k72*C72S+kB0*...
CB0S);                               %Bound MOPSOHH (mol/m^3)
TC7=ones(1,k)*TC7S;                 %Total BICINE (mol/m^3)
Q72=ones(1,k)*k72*C72S*Qmax/(k01*C01S+k52*C52S+k62*C62S+k72*C72S+kB0*...
CB0S);                               %Bound MOPSOHH (mol/m^3)
TC8=ones(1,k)*TC8S;                 %Total CHES (mol/m^3)
Q81=ones(1,k)*Qk81*C81S;           %Bound CHESH (mol/m^3)
TC9=ones(1,k)*TC9S;                 %Total CAPS (mol/m^3)
Q91=ones(1,k)*Qk91*C91S;           %Bound CAPSH (mol/m^3)
CA0=ones(1,k)*CA0S;                 %Total Chloride (mol/m^3)
CB0=ones(1,k)*CB0S;                 %Mobile Phase Sodium (mol/m^3)
QB0=ones(1,k)*kB0*CB0S*Qmax/(k01*C01S+k52*C52S+k62*C62S+k72*C72S+kB0*...
CB0S);                               %Bound Sodium (mol/m^3)
TB0=CB0+QB0;                       %Total Sodium (mol/m^3)

```

```
%Initial End-of-Column pH and Ionic Strength at First Time Step
```

```

pH(1)=pHS;
I(1)=0.5*(C01S+C10S*2^2+C11S+C20S+C30S+C40S+C50S+C52S+C60S+C62S+C70S+...
C72S+C80S+C90S+CA0S+CB0S);

```

```
%Initiate "old" variables used to record previous End-of-Column
variables
```

```

TC0old=TC0(k);           %Total Mobile Phase Proton
T01old=T01(k);           %Total Proton
TC1old=TC1(k);           %Total Malonic Acid
TC2old=TC2(k);           %Total Formic Acid
TC3old=TC3(k);           %Total Acetic Acid
TC4old=TC4(k);           %Total MES
TC5old=TC5(k);           %Total MOPSO
TC6old=TC6(k);           %Total HEPES
TC7old=TC7(k);           %Total BICINE
TC8old=TC8(k);           %Total CHES
TC9old=TC9(k);           %Total CAPS
CA0old=CA0(k);           %Chloride
CB0old=CB0(k);           %Total Mobile Phase Sodium
TB0old=TB0(k);           %Total Sodium

```

```
%Set Bound Species at First Time Step
```

```

Q01next=Q01;
Q52next=Q52;
Q62next=Q62;
Q72next=Q72;
Q31next=Q31;
Q41next=Q41;
Q81next=Q81;
Q91next=Q91;
QB0next=QB0;

```

```
%Time Loop for Calculation of All Time Nodes (Except Initial Node)
```

```
for t=2:nT
```

```

%Calculate pK
i=I(t-1)/1000;
K11=K110+0.509*(-2+1)*(i^0.5/(1+i^0.5)-0.2*i)-3;
K12=K120+0.509*(0+1)*(i^0.5/(1+i^0.5)-0.2*i)-3;
K21=K210+0.509*(0+1)*(i^0.5/(1+i^0.5)-0.2*i)-3;
K31=K310+0.509*(0+1)*(i^0.5/(1+i^0.5)-0.2*i)-3;
K41=K410+0.509*(0+1)*(i^0.5/(1+i^0.5)-0.2*i)-3;
K51=K510+0.509*(0+1)*(i^0.5/(1+i^0.5)-0.2*i)-3;
K52=K520+0.509*(2+1)*(i^0.5/(1+i^0.5)-0.2*i)-3;
K61=K610+0.509*(0+1)*(i^0.5/(1+i^0.5)-0.2*i)-3;
K62=K620+0.509*(2+1)*(i^0.5/(1+i^0.5)-0.2*i)-3;
K71=K710+0.509*(0+1)*(i^0.5/(1+i^0.5)-0.2*i)-3;
K72=K720+0.509*(2+1)*(i^0.5/(1+i^0.5)-0.2*i)-3;
K81=K810+0.509*(0+1)*(i^0.5/(1+i^0.5)-0.2*i)-3;
K91=K910+0.509*(0+1)*(i^0.5/(1+i^0.5)-0.2*i)-3;

%Set extra point outside end of column to be End-of-Column value
from previous time step
TC0(kp)=TC0old;
TC1(kp)=TC1old;
TC2(kp)=TC2old;
TC3(kp)=TC3old;
TC4(kp)=TC4old;
TC5(kp)=TC5old;
TC6(kp)=TC6old;
TC7(kp)=TC7old;
TC8(kp)=TC8old;
TC9(kp)=TC9old;
CA0(kp)=CA0old;
CB0(kp)=CB0old;

%Set Top-of-Column boundary vales for current time step
TC0next(1)=TC0I(t);
TC1next(1)=TC1I(t);
TC2next(1)=TC2I(t);
TC3next(1)=TC3I(t);
TC4next(1)=TC4I(t);
TC5next(1)=TC5I(t);
TC6next(1)=TC6I(t);
TC7next(1)=TC7I(t);
TC8next(1)=TC8I(t);
TC9next(1)=TC9I(t);
CA0next(1)=CA0I(t);
CB0next(1)=CB0I(t);

%Distance Loop for Calculation of All Distance Nodes (Except
Initial Node)
for z=2:k
    zp=z+1;
    zm=z-1;
    TC0next(z)=TC0(z)+A0*TC0(zp)-(B+2*A0)*TC0(z)+(A0+B)*...
    TC0(zm)-...C*Q01next(z)+C*Q01(z);
    T0=TC0next(z)+Q01next(z);
    TC1next(z)=TC1(z)+A1*TC1(zp)-(B+2*A1)*TC1(z)+(A1+B)*TC1(zm);
    TC2next(z)=TC2(z)+A2*TC2(zp)-(B+2*A2)*TC2(z)+(A2+B)*TC2(zm);
    TC3next(z)=TC3(z)+A3*TC3(zp)-(B+2*A3)*TC3(z)+(A3+B)*...

```

```

TC3(zm)-C*Q31next(z)+C*Q31(z);
TC4next(z)=TC4(z)+A4*TC4(zp)-(B+2*A4)*TC4(z)+(A4+B)*...
TC4(zm)-C*Q41next(z)+C*Q41(z);
TC5next(z)=TC5(z)+A5*TC5(zp)-(B+2*A5)*TC5(z)+(A5+B)*...
TC5(zm)-C*Q52next(z)+C*Q52(z);
TC6next(z)=TC6(z)+A6*TC6(zp)-(B+2*A6)*TC6(z)+(A6+B)*...
TC6(zm)-C*Q62next(z)+C*Q62(z);
TC7next(z)=TC7(z)+A7*TC7(zp)-(B+2*A7)*TC7(z)+(A7+B)*...
TC7(zm)-C*Q72next(z)+C*Q72(z);
TC8next(z)=TC8(z)+A8*TC8(zp)-(B+2*A8)*TC8(z)+(A8+B)*...
TC8(zm)-C*Q81next(z)+C*Q81(z);
TC9next(z)=TC9(z)+A9*TC9(zp)-(B+2*A9)*TC9(z)+(A9+B)*...
TC9(zm)-C*Q91next(z)+C*Q91(z);
CA0next(z)=CA0(z)+AA*CA0(zp)-(B+2*AA)*CA0(z)+(AA+B)*CA0(zm);
CB0next(z)=CB0(z)+AB*CB0(zp)-(B+2*AB)*CB0(z)+(AB+B)*...
CB0(zm)-C*QB0next(z)+C*QB0(z);
T3=TC3next(z)+Q31next(z);
T4=TC4next(z)+Q41next(z);
T5=TC5next(z)+Q52next(z);
T6=TC6next(z)+Q62next(z);
T7=TC7next(z)+Q72next(z);
T8=TC8next(z)+Q81next(z);
T9=TC9next(z)+Q91next(z);
TB=CB0next(z)+QB0next(z);

[C01next(z),Q01next(z),Q31next(z),Q41next(z),Q52next(z),...
Q62next(z),Q72next(z),Q81next(z),Q91next(z),QB0next(z)]=...
C01solve(T0,TC1next(z),TC2next(z),T3,T4,T5,T6,T7,T8,T9,TB,...
Qmax,k01,Qk31,Qk41,k52,k62,k72,Qk81,Qk91,kB0,pHSm,pHEP,i,tol);
if TC0next(z) < 0
    error('Negative TC0')
elseif TC3next(z) < 0
    error('Negative TC3')
elseif TC4next(z) < 0
    error('Negative TC4')
elseif TC5next(z) < 0
    error('Negative TC5')
elseif TC6next(z) < 0
    error('Negative TC6')
elseif TC7next(z) < 0
    error('Negative TC7')
elseif TC8next(z) < 0
    error('Negative TC8')
elseif TC9next(z) < 0
    error('Negative TC9')
elseif CB0next(z) < 0
    error('Negative CB0')
end
end

%Update "old" variables used to record previous End-of-Column
variables
TC0old=TC0(k);
TC1old=TC1(k);
TC2old=TC2(k);
TC3old=TC3(k);
TC4old=TC4(k);

```

```

TC5old=TC5(k);
TC6old=TC6(k);
TC7old=TC7(k);
TC8old=TC8(k);
TC9old=TC9(k);
CA0old=CA0(k);
CB0old=CB0(k);

%Update Vectors
TC0=TC0next;
C01=C01next;
TC1=TC1next;
TC2=TC2next;
TC3=TC3next;
TC4=TC4next;
TC5=TC5next;
TC6=TC6next;
TC7=TC7next;
TC8=TC8next;
TC9=TC9next;
CA0=CA0next;
CB0=CB0next;
Q01=Q01next;
Q31=Q31next;
Q41=Q41next;
Q52=Q52next;
Q62=Q62next;
Q72=Q72next;
Q81=Q81next;
Q91=Q91next;
QB0=QB0next;

%Calculate New End-of-Column pH and Ionic Strength
pH(t)=-log10(C01next(k)/1e3);
C10=TC1next(k)/(C01next(k)^2*10^K11*10^K12+C01next(k)*10^K11+1);...
%Malonate (mol/m^3)
C11=10^K11*C01next(k)*C10; %MalonateH (mol/m^3)
C20=TC2next(k)/(C01next(k)*10^K21+1); %Formate (mol/m^3)
C30=TC3next(k)/(C01next(k)*10^K31+1); %Acetate (mol/m^3)
C40=TC4next(k)/(C01next(k)*10^K41+1); %MES (mol/m^3)
C50=TC5next(k)/(C01next(k)^2*10^K51*10^K52+C01next(k)*10^K51+1);...
%MOPSO (mol/m^3)
C52=10^K52*10^K51*C01next(k)^2*C50; %MOPSOHH (mol/m^3)
C60=TC6next(k)/(C01next(k)^2*10^K61*10^K62+C01next(k)*10^K61+1);...
%HEPES (mol/m^3)
C62=10^K62*10^K61*C01next(k)^2*C60; %HEPESHH (mol/m^3)
C70=TC7next(k)/(C01next(k)^2*10^K71*10^K72+C01next(k)*10^K71+1);...
%BICINE (mol/m^3)
C72=10^K72*10^K71*C01next(k)^2*C70; %BICINEHH (mol/m^3)
C80=TC8next(k)/(C01next(k)*10^K81+1); %CHES (mol/m^3)
C90=TC9next(k)/(C01next(k)*10^K91+1); %CAPS (mol/m^3)
I(t)=0.5*(C01next(k)+C10*2^2+C11+C20+C30+C40+C50+C52+C60+C62+C70+...
C72+C80+C90+CA0next(k)+CB0next(k));

%Report Current pH and Time Step to User
pH(t)

```

```

    t
end

%Plot pH and Ionic Strength Results
Delay=13e-6           %Column + Tubing Volume (m^3)
Time=(0:dt:Tt)+Delay/f;
plotyy(Time,pH,Time,I)
xlabel('Run Time (min)')
ylabel('pH')
title('Mobile phase pH and Ionic Strength Profiles')

%Surface pH Calculation
%Constants
IC=0.00032;          %Resin Ionic Capacity (mol Chloride/mL Resin)
SSA=27;              %Resin Specific Surface Area (m^2/mL Resin)
Temp=298;            %Temperature (K)
E=78.5;              %Dielectric Constant of Water at 298K
Nav=6.02e23;         %Avagadro's Number (Number/mol)
e=1.6022e-19;        %Electron Charge (C)
E0=8.85418782e-12;  %Permittivity of Free Space (C^2/Nm^2)
k=1.3807e-23;        %Boltzmann's Constant (J/K)

%Calculate Surface Potential
SP=IC.*Nav.*e./((SSA.*E.*E0.*((2.*e.^2.*Nav.*I./(E.*E0.*k.*Temp)).^0.5))
;

%Calculate Surface pH
SpH=pH+log10(exp(1)).*e.*SP./(k.*Temp);

%Plot Surface pH Results
hold
plot(Time,SpH,'c')
title('Mobile Phase Ionic Strength, pH and Resin Surface pH Profiles')

%Output Program Run Time
fprintf('\nProgram run time: %2.4f seconds\n\n', toc)

```

```
%Function C01solve solves for the free proton concentration C01
%governed by total species concentrations of 8 buffers. Solution is
%obtained using incremental search with step size reduction over an
%initial pH range between pHHigh and pHLow, up to a tolerance specified
%by tol.
```

```
function[C01,Q01,Q31,Q41,Q52,Q62,Q72,Q81,Q91,QB0]=C01solve(T0,TC1,TC2,...
T3,T4,T5,T6,T7,T8,T9,TB,Qmax,k01,Qk31,Qk41,k52,k62,k72,Qk81,Qk91,kB0,...
pHS,pHE,i,tol)
```

```
%Equilibrium Constants for Protontation
```

```
K110=5.690; %First Protontation of Malonate (M)
K120=2.830; %Second Protontation of Malonate (M)
K210=3.750; %First Protontation of Formate (M)
K310=4.756; %First Protontation of Acetate (M)
K410=6.270; %First Protontation of MES (M)
K510=6.900; %First Protontation of MOPSO (M)
K520=0.060; %Second Protontation of MOPSO (M)
K610=7.564; %First Protontation of HEPES (M)
K620=3.000; %Second Protontation of HEPES (M)
K710=8.334; %First Protontation of BICINE (M)
K720=2.000; %Second Protontation of BICINE (M)
K810=9.394; %First Protontation of CHES (M)
K910=10.499; %First Protontation of CAPS (M)
K11=K110+0.509*(-2+1)*(i^0.5/(1+i^0.5)-0.2*i);
K12=K120+0.509*(0+1)*(i^0.5/(1+i^0.5)-0.2*i);
K21=K210+0.509*(0+1)*(i^0.5/(1+i^0.5)-0.2*i);
K31=K310+0.509*(0+1)*(i^0.5/(1+i^0.5)-0.2*i);
K41=K410+0.509*(0+1)*(i^0.5/(1+i^0.5)-0.2*i);
K51=K510+0.509*(0+1)*(i^0.5/(1+i^0.5)-0.2*i);
K52=K520+0.509*(2+1)*(i^0.5/(1+i^0.5)-0.2*i);
K61=K610+0.509*(0+1)*(i^0.5/(1+i^0.5)-0.2*i);
K62=K620+0.509*(2+1)*(i^0.5/(1+i^0.5)-0.2*i);
K71=K710+0.509*(0+1)*(i^0.5/(1+i^0.5)-0.2*i);
K72=K720+0.509*(2+1)*(i^0.5/(1+i^0.5)-0.2*i);
K81=K810+0.509*(0+1)*(i^0.5/(1+i^0.5)-0.2*i);
K91=K910+0.509*(0+1)*(i^0.5/(1+i^0.5)-0.2*i);
```

```
%Equilibrium Constants for Protontation
```

```
K11=K11-3; %First Protontation of Malonic Acid (mol/m^3)
K12=K12-3; %Second Protontation of Malonic Acid (mol/m^3)
K21=K21-3; %First Protontation of Formic Acid (mol/m^3)
K31=K31-3; %First Protontation of Acetic Acid (mol/m^3)
K41=K41-3; %First Protontation of MES (mol/m^3)
K51=K51-3; %First Protontation of MOPSO (mol/m^3)
K52=K52-3; %Second Protontation of MOPSO (mol/m^3)
K61=K61-3; %First Protontation of HEPES (mol/m^3)
K62=K62-3; %Second Protontation of HEPES (mol/m^3)
K71=K71-3; %First Protontation of BICINE (mol/m^3)
K72=K72-3; %Second Protontation of BICINE (mol/m^3)
K81=K81-3; %First Protontation of CHES (mol/m^3)
K91=K91-3; %First Protontation of CAPS (mol/m^3)
```

```
%Set diff to two times tolerance to initiate while loop
diff=-2*tol;
```

```

%Set Starting pH for Iteration
pH=pHS;

%Set Initial Step Size
dpH=(pHS-pHE)/10;

%Set diffold to be equal to diff to satisfy if statement
diffold=diff;

while abs(diff) > tol
    if diffold/diff > 0      %Not at Solution, continue with time step
        diffold=diff;
        pH=pH-dpH;
        C01=10^-pH*1000;
        C11=(10^K11*C01*TC1/(C01^2*10^K11*10^K12+C01*10^K11+1));
        C12=(10^K12*10^K11*C01^2*TC1/(C01^2*10^K11*10^K12+C01*10^K11+...
        1));
        C21=(10^K21*C01*TC2/(C01*10^K21+1));
        C31=(10^K31*C01*T3/(C01*10^K31+1+C01*10^K31*Qk31));
        C41=(10^K41*C01*T4/(C01*10^K41+1+C01*10^K41*Qk41));
        C81=(10^K81*C01*T8/(C01*10^K81+1+C01*10^K81*Qk81));
        C91=(10^K91*C01*T9/(C01*10^K91+1+C01*10^K91*Qk91));
        Q=Qsolve(C01,T5,T6,T7,TB,Qmax,k01,k52,k62,k72,kB0,i,tol);
        Q01=k01*C01*Q;
        C50=T5/(C01^2*10^K51*10^K52+C01*10^K51+1+C01^2*10^K51*10^K52*...
        k52*Q);
        C51=10^K51*C01*C50;
        C52=10^K52*C01*C51;
        C60=T6/(C01^2*10^K61*10^K62+C01*10^K61+1+C01^2*10^K61*10^K62*...
        k62*Q);
        C61=10^K61*C01*C60;
        C62=10^K62*C01*C61;
        C70=T7/(C01^2*10^K71*10^K72+C01*10^K71+1+C01^2*10^K71*10^K72*...
        k72*Q);
        C71=10^K71*C01*C70;
        C72=10^K72*C01*C71;
        diff=(T0-(C01+C11+2*C12+C21+C31+C41+C51+2*C52+C61+2*C62+C71+...
        2*C72+C81+C91+Q01));
    else %Passed Solution, return to previous step and reduce step size
        pH=pH+dpH;
        dpH=dpH/10;
        pH=pH-dpH;
        C01=10^-pH*1000;
        C11=(10^K11*C01*TC1/(C01^2*10^K11*10^K12+C01*10^K11+1));
        C12=(10^K12*10^K11*C01^2*TC1/(C01^2*10^K11*10^K12+C01*10^K11+...
        1));
        C21=(10^K21*C01*TC2/(C01*10^K21+1));
        C31=(10^K31*C01*T3/(C01*10^K31+1+C01*10^K31*Qk31));
        C41=(10^K41*C01*T4/(C01*10^K41+1+C01*10^K41*Qk41));
        C81=(10^K81*C01*T8/(C01*10^K81+1+C01*10^K81*Qk81));
        C91=(10^K91*C01*T9/(C01*10^K91+1+C01*10^K91*Qk91));
        Q=Qsolve(C01,T5,T6,T7,TB,Qmax,k01,k52,k62,k72,kB0,i,tol);
        Q01=k01*C01*Q;
        C50=T5/(C01^2*10^K51*10^K52+C01*10^K51+1+C01^2*10^K51*10^K52*...
        k52*Q);
        C51=10^K51*C01*C50;

```

```

C52=10^K52*C01*C51;
C60=T6/(C01^2*10^K61*10^K62+C01*10^K61+1+C01^2*10^K61*10^K62*...
k62*Q);
C61=10^K61*C01*C60;
C62=10^K62*C01*C61;
C70=T7/(C01^2*10^K71*10^K72+C01*10^K71+1+C01^2*10^K71*10^K72*...
k72*Q);
C71=10^K71*C01*C70;
C72=10^K72*C01*C71;
diff=(T0-(C01+C11+2*C12+C21+C31+C41+C51+2*C52+C61+2*C62+C71+...
2*C72+C81+C91+Q01));
end
end

```

```

%Calculates Free Proton Concentration in mol/m^3

```

```

C01=10^-pH*1e3;

```

```

%Calculates Bound Species Concentrations

```

```

Q01=k01*C01*Q;           %Bound Hydrogen
Q31=Qk31*C31;           %Bound Acetic Acid
Q41=Qk41*C41;           %Bound MESH
Q52=k52*C52*Q;           %Bound MOPSOHH
Q62=k62*C62*Q;           %Bound MOPSOHH
Q72=k72*C72*Q;           %Bound MOPSOHH
Q81=Qk81*C81;           %Bound CHESH
Q91=Qk91*C91;           %Bound CAPSH
QB0=kB0*Q*TB/(1+kB0*Q); %Bound Sodium

```

```
%Function Qsolve solves for the free resin concentration Q given the
%free proton concentration C01
```

```
function Q=Qsolve(C01,T5,T6,T7,TB,Qmax,k01,k52,k62,k72,kB0,i,tol)
```

```
%Equilibrium Constants for Protontation
```

```
K510=6.900;      %First Protonation of MOPSO (M)
K520=0.060;      %Second Protonation of MOPSO (M)
K610=7.564;      %First Protonation of HEPES (M)
K620=3.000;      %Second Protonation of HEPES (M)
K710=8.334;      %First Protonation of BICINE (M)
K720=2.000;      %Second Protonation of BICINE (M)
K51=K510+0.509*(0+1)*(i^0.5/(1+i^0.5)-0.2*i);
K52=K520+0.509*(2+1)*(i^0.5/(1+i^0.5)-0.2*i);
K61=K610+0.509*(0+1)*(i^0.5/(1+i^0.5)-0.2*i);
K62=K620+0.509*(2+1)*(i^0.5/(1+i^0.5)-0.2*i);
K71=K710+0.509*(0+1)*(i^0.5/(1+i^0.5)-0.2*i);
K72=K720+0.509*(2+1)*(i^0.5/(1+i^0.5)-0.2*i);
```

```
%Equilibrium Constants for Protontation
```

```
K51=K51-3;      %First Protonation of MOPSO (mol/m^3)
K52=K52-3;      %Second Protonation of MOPSO (mol/m^3)
K61=K61-3;      %First Protonation of HEPES (mol/m^3)
K62=K62-3;      %Second Protonation of HEPES (mol/m^3)
K71=K71-3;      %First Protonation of BICINE (mol/m^3)
K72=K72-3;      %Second Protonation of BICINE (mol/m^3)
```

```
%Set diff to two times tolerance to initial while loop
diff=2*tol;
```

```
%Set Initial Step Size
```

```
dQ=1;
```

```
%Set Starting Q for Iteration
```

```
Q=0-dQ;
```

```
%Set diffold to be equal to diff to satisfy if statement
```

```
diffold=diff;
```

```
while abs(diff) > tol
```

```
    if diffold/diff > 0      %Not at Solution, continue with time step
```

```
        diffold=diff;
```

```
        Qold=Q;
```

```
        Q=Q+dQ;
```

```
        diff=Qmax-(k01*Q*C01+k52*Q*10^K52*10^K51*C01^2*(T5/(C01^2*10^...
K51*10^K52+C01*10^K51+1+C01^2*10^K51*10^K52*k52*Q))+k62*Q*10^...
K62*10^K61*C01^2*(T6/(C01^2*10^K61*10^K62+C01*10^K61+1+C01^2*...
10^K61*10^K62*k62*Q))+k72*Q*10^K72*10^K71*C01^2*(T7/(C01^2*10^...
K71*10^K72+C01*10^K71+1+C01^2*10^K71*10^K72*k72*Q))+kB0*Q*(TB/...
(1+kB0*Q)));
```

```
    else %Passed Solution, return to previous step and reduce step size
```

```
        Q=Q-dQ;
```

```
        dQ=dQ/10;
```

```
        Q=Q+dQ;
```

```
        diff=Qmax-(k01*Q*C01+k52*Q*10^K52*10^K51*C01^2*(T5/(C01^2*10^...
```

```
K51*10^K52+C01*10^K51+1+C01^2*10^K51*10^K52*k52*Q))+k62*Q*10^...
K62*10^K61*C01^2*(T6/(C01^2*10^K61*10^K62+C01*10^K61+1+C01^2*...
10^K61*10^K62*k62*Q))+k72*Q*10^K72*10^K71*C01^2*(T7/(C01^2*10^...
K71*10^K72+C01*10^K71+1+C01^2*10^K71*10^K72*k72*Q))+kB0*Q*(TB/...
(1+kB0*Q));
```

```
end
end
```

Appendix C: Description of the Program for the Prediction of Protein Elution from an Anion Exchange Column during Isoelectric Chromatofocusing

All programs are written for use on MATLAB 6.1. The main program script file “solver.m” contains model parameters entered by the user. Input matrices for total anion concentration, pH and ionic strength at each discretized position and time node are calculate using program code described in Appendix A. The function “right.m” defines the continuity equation and the equilibrium binding isotherm and is solved by the MATLAB function ode15s designed to solve ordinary differential equations. The following table lists input data variables and files required by the program:

Table C-1: Input data files and variables used in MATLAB script file “solver.m” for the prediction of protein elution during AEICF

File/Variable	Type	Contents
TCA _n	MATLAB Variable	Total Anion Concentration across column position and run time
pH _M	MATLAB Variable	pH across column position and run time
IM	MATLAB Variable	Ionic Strength across column position and run time
mvspH.xls	Microsoft Excel File	Table of characteristic charge vs. pH values
Chromatogram.xls	Microsoft Excel File	Experimental UV280nm trace
pH.xls	Microsoft Excel File	Experiment pH trace
Conductivity.xls	Microsoft Excel File	Experimental conductivity trace

Variables “TCAn”, “pHM” and “IM” are calculated at the appropriate mobile-phase conditions using program code described in Appendix A. The Microsoft Excel file “mvspH.xls” contains a table of user-input values describing the relationship between pH and the characteristic charge of the target protein on the Mono Q matrix. Microsoft Excel files “Chromatogram.xls”, “pH.xls” and “Conductivity.xls” contains experimental data that is plotted to validate simulation results.

The surface pH of the Mono Q matrix at each position and time node is calculated according to the mobile phase pH and ionic strength according to the Donnan equation:

$$pH_{surf} = pH_{bulk} + 2.303 \left(\frac{e\psi(0)}{kT} \right) \quad (C-1)$$

where bulk mobile-phase pH (pH_{bulk}) values are obtained from the input variable “pHM” and the matrix surface potential ($\psi(0)$) is calculated using ionic strength information contained in the input variable “IM”. The characteristic charge of the target protein is interpolated for the surface pH at each position and time node using data contained in the file “mvspH.xls”. The binding constant at each node is determined by the following equation:

$$K = e^{\frac{\beta m}{\sqrt{I}}} \quad (C-2)$$

The movement of the target protein is tracked using the continuity equation of chromatography:

$$\varepsilon \frac{dc}{dt} + (1 - \varepsilon) \frac{dq}{dt} = u \frac{dc}{dz} + \varepsilon D_{ax} \frac{d^2c}{dz^2} \quad (\text{C-3})$$

Association of the target protein with the matrix is defined by the following binding isotherm:

$$K = \frac{qA^m}{c(S_T - mq - \sigma q)^m} \quad (\text{C-4})$$

where total anion concentration (A) values are obtained from the input variable “TCAn”. Equation C-4 is used to determine the stationary-phase protein concentration (q), with the binding constant (K) calculated using equation C-2 and the characteristic charge (m) at the matrix surface pH derived from equation C-1, to solve equation C-3. Boundary conditions include initial mobile-phase (c) and stationary-phase (q) concentrations in the column, and c at the entrance of the column during the separation. The MATLAB code for the solution is shown below.

```
%Script m-file "solver.m" that uses Matlab function ode15s to solve the
%continuity equation for predicting the elution time of beta-
%lactoglobulin A or B during isoelectric chromatofocusing at varying
%mobile phase conditions on the Mono Q HR10/10 strong anion exchange
%column.
```

```
clear
```

```
global k u d TCAn IC K m Timei c0 t0 e dz
```

```
%Column and Run Constants
```

```
IC=0.32*1000;      %Column Ionic Capacity (mol/m^3)
e=0.36;           %Column Voidage
ep=0.68;          %Resin Particle Voidage
et=e+(1-e)*ep;    %Total Voidage
L=0.10;           %Column Length (m)
R=0.005;          %Column Radius (m)
f=1/1e6;          %Mobile Phase Flow Rate (m^3/min)
u=f/(pi*R^2);     %Superficial Mobile Phase Velocity (m/min)
G=60/1e6;         %Gradient (0-100% Elution Buffer) Length (m^3)
T=120/1e6;        %Total Run Length (m^3)
Gt=G/f;           %Gradient Run Time (min)
Tt=T/f;           %Total Run Time (min)
```

```
%Programming Information
```

```
n=1000;           %Number of Time Nodes
k=100;            %Number of Plates
dt=Tt/n;          %Time Step (min)
dz=L/k;           %Distance Step (m)
dz2=dz^2;         %Distance Step Squared (m^2)
tol=1e-4;         %Iteration Tolerance
```

```
%Parameters
```

```
beta=1.8;
```

```
%Calculate Number of Nodes (Column Beginning and End Counts as Nodes)
```

```
nG=Gt/dt+1;      %Number of Time Nodes During Gradient
nT=Tt/dt+1;      %Total Number of Time Nodes
```

```
%Load Total Anion, pH and Ionic Strength Matrices
```

```
load var105 TCAn pHM IM
```

```
%Indices for Reading Experimental pH Profile
```

```
index1=3;
index2=index1+1;
multiplier=1;
TCurve='mvspH.xls';
```

```
%Set Figure Information
```

```
FigureTitle='Elution of b-Lactoglobulin B';
IonicStrength='I~105mM';
```

```
%Surface pH Calculation Constants
```

```
ICD=IC;           %Resin Ionic Capacity (mol Chloride/m^3 Resin)
SSA=4.3e8;        %Resin Specific Surface Area (m^2/m^3 Resin)
Temp=298;         %Temperature (K)
```

```

E=78.5;           %Dielectric Constant of Water at 298K
Nav=6.02e23;     %Avagadro's Number (Number/mol)
ec=1.6022e-19;  %Electron Charge (C)
E0=8.85418782e-12; %Permittivity of Free Space (C^2/Nm^2)
kB=1.3807e-23;  %Boltzmann's Constant (J/K)

%Calculate Surface Potential
SP=ICD.*Nav.*ec./((SSA.*E.*E0.*((2.*ec.^2.*Nav.*IM./(E.*E0.*kB.*Temp)).^
0.5)));

%Calculate Surface pH
pHM=pHM+log10(exp(1)).*ec.*SP./(kB.*Temp);

%Read Characteristic Charge Curve
xls=xlsread(TCurve);
TpH=xls(:,1);
Tcharge=xls(:,2);

%Calculate characteristic charge and binding constant matrices
m=interp1(TpH,Tcharge,pHM);
K=exp(beta.*m./IM.^0.5);
Time=transpose(0:dt:Tt); %Time Vector
Timei=transpose(0:Tt/200:Tt); %Time Vector for Interpolation

TCAn(:,1)=[];
m(:,1)=[];
K(:,1)=[];

multiple=k/10;
for counter=1:multiple:(k-multiple+1)
    for i=counter:counter+multiple-1
        TCAntemp(:,i)=TCAn(:,(counter-1)/multiple+1);
        mtemp(:,i)=m(:,(counter-1)/multiple+1);
        Ktemp(:,i)=K(:,(counter-1)/multiple+1);
    end
end

TCAn=TCAntemp;
m=mtemp;
K=Ktemp;
d=1*1e-9;
t=120; %Total Simulation Time
c0=0.01; %Concentration at Inlet
t0=1; %Length of Injection Pulse

%Solve
dz=L/k;
y=zeros(2*k,1); %Initial State Vector (Empty Column)

%Mass matrix defines that the first p equations are differential and
%the second p equations are algebraic
M=[eye(k) zeros(k);zeros(k,2*k)];

%ODE solver
[T Y]=ode15s(@right,0:t/n:t,y,odeset('stats','off','Mass',M));

```

```

%Output
G=Y(:,1:k); %Excerpt of g over time and column position
Q=Y(:,k+1:2*k); %Excerpt of q over time and column position
C=1/e*G-(1-e)/e*Q; %Variable Transform

%Plot Elution
xls=xlsread('Chromatogram.xls');
ChromTime=xls(:,index1);
ChromUV=xls(:,index2);
xls=xlsread('pH.xls');
pHTime=xls(:,index1);
pH=xls(:,index2);
xls=xlsread('Conductivity.xls');
CondTime=xls(:,index1);
Cond=xls(:,index2);

ChromUV=ChromUV./max(ChromUV)*7;
C=C./max(C(:,k))*multiplier;

Delay=13e-6; %Column + Tubing Volume (m^3)
Time=(0:dt:Tt)+Delay/f;
plotyy(pHTime,pH,CondTime,Cond)
hold
plot(Time,C(:,k)+3,ChromTime,ChromUV+3)
set(gca,'XLim',[0 80])
set(gca,'YLim',[3 11])
xlabel('Run Time (min)')
ylabel('pH')

```

```

%Function right defines the binding isotherm for beta-lactoglobulin A
%or B, and outputs the right-hand-side of the differential-algebraic
%equation system used by script m-file "solver.m" in the prediction of
%elution time during isoelectric chromatofocusing.

function dy=right(t,y)

global k u d TCAn IC K m Timei c0 t0 e dz

%pH Impact:
as=transpose(interpl(Timei,TCAn,t));
ms=transpose(interpl(Timei,m,t));
Ks=transpose(interpl(Timei,K,t));

%The first k elements of vector define  $g=e*c+(1-e)*q$  at the p knots
g=y(1:k);

%The second k elements of vector define q at the p knots
q=y(k+1:2*k);

c=1/e*g-(1-e)/e*q; %Variable Transform

%Concentrations at left axial knots with special case at column inlet
cl=[(t<t0)*c0;c(1:end-1)];

%Concentrations at right axial knots with special case at column outlet
cr=[c(2:end);c(end)];

%Calculation of Right Hand Side

dc1=(cl-c)/dz; %Finite Difference Approx of 1st z Derivative
dc2=(cl-2*c+cr)/dz^2; %Finite Difference Approx of 2nd z Derivative

dg=u*dc1+e*d*dc2; %Balance Equation

r=c-(q.*as.^ms)./((Ks.*(IC-ms.*q)).^ms); %Isotherm Equation (Implicit)

dy=[dg;r]; %Right Hand Side of Differential-algebraic Equation System

```